EXTREME CLIMATE VARIABILITY AND IMPACTS OF FUTURE CLIMATE CHANGE ON THE STREAMFLOW IN THE SOUTHEAST QUEENSLAND, AUSTRALIA

A Thesis submitted by

Hadis Pakdel
MSc in Eng.

For the award of

Doctor of Philosophy

2024

ABSTRACT

South East Queensland has experienced a series of recent catastrophic climatic events. From December 2010 to January 2011 and in February 2022, heavy rains caused flooding impacting over 2.5 million people and causing approximately 33 deaths. These events challenged the assumption of stationary conditions as no longer viable. The persistent use of this baseline assumption could potentially lead to misestimations in forecasting future floods. The severity and frequency of extremes are escalating; thus, it is necessary to evaluate the impacts of land cover changes and urbanisation, along with climate change. A framework of the trend analysis methods to analyse temporal patterns, spatial analysis techniques utilising the Google Earth Engine (GEE), Generalised Extreme Value (GEV) method, and land cover patterns classification including Random Forest (RF) and Support Vector Machine (SVM) can be useful for hydrometeorological variables extreme events analysis. This research highlights the importance of using spatiotemporal techniques and trend analysis by underscoring the changing frequency and severity of extreme events analysis. The aim of this research is to evaluate extreme events under non-stationary conditions, where the location parameter has a linear function with time. For this study, a unique framework consisting of the hydrological model in line with the Process-informed Non-Stationary Extreme Value Analysis (ProNEVA) GEV model and the ensemble of General Circulation Models (GCMs), mapping land cover patterns using classification methods within the GEE platform, were employed to comprehensively analyse the impacts of climate variability and land cover changes on extreme hydrological events. Runoff was projected under two scenarios for eight GCMs and by incorporating the percentage of each land cover into the hydrological model for two horizons, (2020-2065 and 2066-2085). The outcomes of this study suggest that neglecting non-stationary assumptions of flood frequency can lead to underestimating the magnitude of flooding. This, in turn, can lead to greater and increased risks to infrastructure planning and design. The framework of this research paper is adaptable to various geographical regions for the purposes of estimating extreme conditions; thereby offering valuable insights for infrastructure design, planning, risk assessment, and the sustainable management of future water resources in the context of long-term water management plans.

CERTIFICATION OF THESIS

I, Hadis Pakdel, declare that the PhD Thesis entitled *Extreme Climate Variability and Impacts of Future Climate Change on the Streamflow in the Southeast Queensland, Australia* is not more than 100,000 words in length including quotes and exclusive of tables, figures, appendices, bibliography, references, and footnotes.

This Thesis is the work of Hadis Pakdel except where otherwise acknowledged, with the majority of the contribution to the papers presented as a Thesis by Publication undertaken by the student. The work is original and has not previously been submitted for any other award, except where acknowledged.

Date: 09 Jul 2024

Endorsed by:

Dr Sreeni Chadalavada
Principal Supervisor

Dr Md Jahangir Alam
Associate Supervisor

Dr Dev Raj Paudyal
Associate Supervisor

Student and supervisors' signatures of endorsement are held at the University.

STATEMENT OF CONTRIBUTION

Paper 1:

Pakdel, H.; Vazifedoust, M.; Paudyal, D.R.; Chadalavada, S.; Alam, M.J. Google Earth Engine as Multi-Sensor Open-Source Tool for Monitoring Stream Flow in the Transboundary River Basin: Doosti River Dam. *ISPRS International Journal of Geo-Information* **2022**, *11*, 535. ***(Published**). https://doi.org/10.3390/ijgi11110535.*

Hadis Pakdel contributed 80% to this paper. Collectively, Sreeni Chadalavada, Md Jahangir Alam and Dev Raj Paudyal contributed the remainder.

Paper 2:

Pakdel, H.; Paudyal, D.R.; Chadalavada, S.; Alam, M.J.; Vazifedoust, M. A Multi-Framework of Google Earth Engine and GEV for Spatial Analysis of Extremes in Non-Stationary Condition in Southeast Queensland, Australia. ISPRS International Journal of Geo-Information **2023**, 12, 370. ***(Published**).* https://doi.org/10.3390/ijgi12090370.

Hadis Pakdel contributed 80% to this paper. Collectively, Sreeni Chadalavada, Md Jahangir Alam and Dev Raj Paudyal contributed the remainder.

Paper 3:

Pakdel, H.; Chadalavada, S.; Alam, M.J.; Paudyal, D.R.; Vazifedoust, M. Variability of Extreme Climate Events and Prediction of Land Cover Change and Future Climate Change Effects on the Streamflow in Southeast Queensland, Australia. ISPRS International Journal of Geo-Information **2024**, 13, 123. ***(Published).*** https://doi.org/10.3390/ijgi13040123.

Hadis Pakdel contributed 80% to this paper. Collectively, Sreeni Chadalavada, Md Jahangir Alam and Dev Raj Paudyal contributed the remainder.

Paper 4:

Chowdhury, R.; Chadalavada, S.; **Pakdel, H.;** McDougall, K. Extreme Temperatures and Temperature-Duration-Frequency (TDF) Relationship in Varying Climatic Zones Across Australia (Submitted to Urban Climate Journal).

Hadis Pakdel contributed 50% to this paper. Hadis Pakdel contributed significantly to the modelling for non-stationary GEV analysis using the Non-stationary Extreme Value Analysis (NEVA) model and conducted some of the statistical tests for trend and step change. Collectively, Sreeni Chadalavada, Rezaul Chowdhury (R.I.P) and Kevin McDougall contributed the remainder.

The overall contribution of Hadis Pakdel is 80% to the theoretical, statistical and model development, analysis and revising of the final submission. Dr Sreeni Chadalavada, Dr Md Jahangir Alam and Dr Dev Paudyal contributed to the remaining 20% of the study's theoretical development, structure, analysis, and editing.

ACKNOWLEDGEMENTS

Firstly, I would like to acknowledge the financial support provided by the Graduate Research School, University of Southern Queensland.

Secondly, I would like to express gratitude to my supervisors, Dr Sreeni Chadalavada, Dr Dev Raj Paudyal, and Dr Md Jahangir Alam for their guidance and support throughout my research. Their consistent involvement and input were instrumental in helping me complete my research within the allocated time.

Furthermore, I would like to acknowledge my husband, Soroush Ziafatdoost for his unwavering support, and understanding throughout this journey. His encouragement, patience, and belief in me have made this PhD research not only possible but also meaningful.

In conclusion, I want to honour Dr Rezaul Chowdhury, whose untimely passing occurred before I started my PhD thesis. His invaluable assistance was instrumental in guiding me to receive the scholarship and I hope this thesis is something he would have been proud to be associated with.

I would like to acknowledge the financial support provided by the University of Southern Queensland through the UniSQ International Fees Research Scholarship and International Stipend Research Scholarship.

TABLE OF CONTENTS

ABSTRACT i
CERTIFICATION OF THESIS ii
STATEMENT OF CONTRIBUTION iii
ACKNOWLEDGEMENTS v
LIST OF TABLES ix
LIST OF FIGURES x
ABBREVIATIONS xi
CHAPTER 1: INTRODUCTION 1
1.1. Background to research 1
1.2. Research aim and objectives 6
1.3. Thesis structure 9
1.4. Research scope and limitations 13
1.5. Conclusions 13
CHAPTER 2: LITERATURE REVIEW 14
2.1. Overview 14
2.2. Significance of Research Problems 14
2.3. Stationary and Non-stationary assumptions in hydrology 14
2.3.1. Stationary assumptions 15
2.3.2. Non-stationary assumptions 15
2.3.3. Stationary and non-stationary assumptions in NEVA & ProNEVA 16
2.4. Applying machine learning for the classification and projection of landcover changes 16
2.5. Hydrologic modelling 17
2.6. Future climate projections and scenarios 18
2.7. Conclusions 20
CHAPTER 3: METHODS 21
3.1. Research methodology overview 21
3.1.1. Overview 21
3.1.2. Data 21

3.1.3. Mann-Kendall trend and Sen's slope test 24
3.1.4. Google Earth Engine application: The geeSEBAL algorithm 25
3.1.5. Classification and projection of land cover changes 26
3.1.6. Landcover changes projection 26
3.1.7. Hydrological model 26
3.1.8. Future climate projections and greenhouse gas emissions scenarios 27
3.1.9. Assessing extremes in a non-stationary approach using the GEV model 27
CHAPTER 4: PAPER 1 – GOOGLE EARTH ENGINE AS A MULTI-SENSOR OPEN-SOURCE TOOL FOR MONITORING STREAM FLOW IN THE TRANSBOUNDARY RIVER BASIN: DOOSTI RIVER DAM 29
4.1. Introduction 29
4.2. Published paper 29
4.3. Links and implications 58
4.4. Conclusion 59
CHAPTER 5: PAPER 2 – A MULTI-FRAMEWORK Of GOOGLE EARTH ENGINE AND GEV FOR SPATIAL ANALYSIS OF EXTREMES IN NON-STATIONARY CONDITION IN SOUTHEAST QUEENSLAND, AUSTRALIA 60
5.1. Introduction 60
5.2. Published paper 61
5.3. Links and implications 87
5.4. Conclusions 88
CHAPTER 6: PAPER 3 – VARIABILITY OF EXTREME CLIMATE EVENTS AND PREDICTION OF LAND COVER CHANGE AND FUTURE CLIMATE CHANGE EFFECTS ON THE STREAMFLOW IN SOUTHEAST QUEENSLAND, AUSTRALIA 89
6.1. Introduction 89
6.2. Published paper 90
6.3. Links and implications 112
6.4. Conclusion 113

CHAPTER 7: PAPER 4 – EXTREME TEMPERATURES AND TEMPERATURE-DURATION-FREQUENCY (TDF) RELATIONSHIP IN VARYING CLIMATIC ZONES ACROSS AUSTRALIA 114
7.1. Introduction 114
7.2. Submitted paper 115
7.3. Links and implications..... 139
7.4. Conclusion 139
CHAPTER 8: DISCUSSION AND CONCLUSION 140
8.1. Introduction 140
8.2. Assess and map hydro-climatological trends and their impacts on surface water using GEE. Develop a framework for extreme hydrometeorological events. 140
8.3. Develop a framework for assessing extreme events and land cover impacts using SVM and RF in GEE. Perform hydrological simulations under GCM ensembles, RCPs, and land cover changes. 141
8.4. Determine extreme climate events in the catchment. Assess the effectiveness of GEV models in overcoming climatic model limitations for evaluating extremes..... 142
8.5. Contribution to knowledge..... 143
8.6. Future research direction 144
REFERENCES 145

LIST OF TABLES

Table 3. 1 Source of datasets. 23

LIST OF FIGURES

Figure 1. 1 The study area's geographical position in Australia (left) and hydro-meteorological stations are taken into consideration throughout the catchment (right). 3

Figure 1. 2 Thesis structure 12

Figure 3. 1 Summary of papers of this research..... 24

ABBREVIATIONS

ARR	Australian Rainfall Runoff
AWAP	Australian Water Availability Project
AWBM	Australian Water Balance Model
CMIP	Coupled Model Intercomparison Project
CIMEC	Calibration using Inverse Modelling at Extreme Conditions
DEM	Digital Elevation Model
EVA	Extreme Value Analysis
GCMs	General Circulation Models
GEE	Google Earth Engine
GEV	Generalised Extreme Value
GP	Generalised Pareto
H0	Null Hypothesis
Ha	Alternative Hypothesis
IPCC	Intergovernmental Panel on Climate Change
LP3	Log-Pearson type III
LUCC	Land Use/Cover Change
MK	Mann-Kendall
PET	Potential ET
ProNEVA	Process-informed Nonstationary Extreme Value Analysis
RF	Random Forest
SEBAL	Surface Energy Balance Algorithm for Land
SEQ	Southeast Queensland
SVM	Support Vector Machine
TDF	Temperature Duration Frequency

CHAPTER 1: INTRODUCTION

1.1. Background to research

The Intergovernmental Panel on Climate Change Assessment Report (IPCC) (IPCC, 2007, 2014) indicates that climate change will be accompanied by a rise in the frequency, severity and duration of extreme natural phenomena such as excessive precipitation and extreme air temperature in the twenty-first century. The trends suggest that the frequency and intensity of flood events are likely to rise globally due to climate and land-use/cover changes attributed largely to urbanisation and anthropogenic activities (IPCC, 2014; Wang, et al., 2020).

It is commonly known that there is a great deal of uncertainty in many worldwide areas' climate estimates and scenarios, particularly when it comes to severe occurrences like excessive precipitation (Bloschl & Montanari, 2010), and extreme streamflow. It is imperative to conduct more research on hydrological extremes, particularly in the areas where large climate change effects are known to exist (Salas et al., 2018). The majority of research for Australia specifically addresses climate change and suggests that changes in annual temperature maxima have consequences for non-stationary flood frequency analysis (Wasko et al., 2023).

Southeast Queensland, Australia, faces a myriad of challenges stemming from the increasing frequency and intensity of extreme climate events, exacerbated by the ongoing effects of climate change. The region's vulnerability to such events, including floods from December 2010, to January 2011 and in February 2022 and changes in streamflow patterns, poses significant environmental risks. The interplay between land cover changes, driven by urbanisation and land cover practices, further complicates the dynamics of these hydrological processes. Despite advancements in climate modelling and hydrological analysis, there remains a critical gap in our understanding of the non-stationary nature of extreme climate events and their implications for future streamflow regimes in this region. This research seeks to address this gap by employing a novel non-stationary approach, which incorporates the temporal evolution of flood and streamflow characteristics through the utilisation of a linear function for the location parameter. Neglecting the non-stationary assumption in flood frequency can lead to underestimating the amounts, which can, in turn, lead to more risks for the related hydraulic structures.

Informed by the observations above, this study aims to offer valuable perspectives for the design of infrastructure, planning, risk evaluation, and the sustainable administration of forthcoming water resources within the framework of enduring water management strategies.

The case research location, the Lockyer Catchment, is situated in Southeast Queensland (SEQ), as Figure 1 shows. It is the primary watercourse that flows into the Brisbane River from the east (Sarker et al., 2008). Within the bounds of the Lockyer Valley Regional Council, Toowoomba Regional Council, Somerset Regional Council, and Ipswich Regional Council local governments, the catchment lies west of Brisbane and east of Toowoomba (WetlandInfo, 2022). The importance of this catchment was recognised by the appropriate infrastructure operators and decision-makers, including the Queensland Department of Environment and Science and Seqwater (Kiem et al., 2020). The average annual rainfall for the catchment is between 1000 and 2012 mm, and it extends over 3000 km^2 (Vance et al., 2015).

However, there are notable variations in rainfall over time, leading to rivers that remain dry for the majority of the year. Some of Australia's richest agricultural regions, including lucrative vegetable farming and grazing, are included in the catchment (Sarker et al., 2008). Significant rainfall is observed in both the northern and southern parts of the Lockyer Catchment. However, during recent droughts in Australia, most of the catchments experienced moderate to low precipitation levels (Lockyer Creek wiki 2022). Collectively, they drain around 3000 km^2 of land altogether, or one-fourth of the watershed of the Brisbane River. With a population of more than 35,000, the Lockyer Catchment is significant from an economic, environmental, and social standpoint.

In recent decades, this region has had several unusual climatic events, such as the above-average rainfall that occurred between 1988 and 1989 and between 2000 and 2008 (Van Dijk et al., 2013), in which the region experienced an extensive and severe drought that persisted over an extended period. In 2008, measures were put in place to alleviate the effects of drought. Nonetheless, the area remains subject to repetitive patterns of flood and drought emergencies, occasionally affecting the entire nation for prolonged periods. Considering that prior research has demonstrated that the stationarity assumption is no longer viable, the frequency of flood occurrences, such as the one in 2022, may be misestimated under this assumption. Furthermore, it

has been noted that there is a non-stationary connection between rainfall and runoff in the Lockyer Catchment (Cui et al., 2018; Armstrong et al., 2020).

Thus, to improve the design and supervision of hydraulic structures that minimise future losses in terms of human and financial, it is imperative to create unique approaches to estimate non-stationary flood extremes, rainfall extremes, evapotranspiration extremes, and water storage deficits.

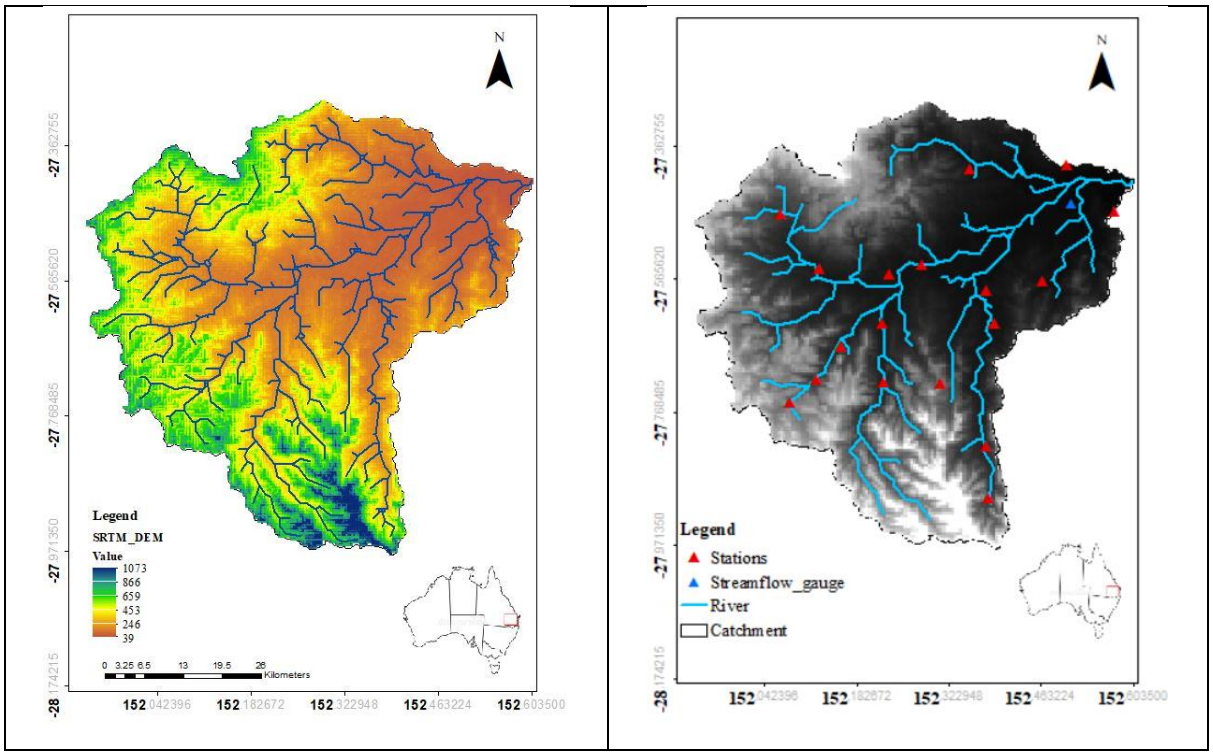

Figure 1. 1 The study area's geographical position in Australia (left) and hydro-meteorological stations are taken into consideration throughout the catchment (right).

In the past, the assumption of stationarity was introduced to make complex statistics easier to understand. Under the assumption of a stationary climate, the conditions of the return level and return duration provide crucial information for planning, making decisions, and evaluating the effects of climatic events.

Typically, this was considered a reasonable assumption because our historical data records were limited, resulting in minimal changes observed over a short time period. Moreover, earlier scholars lacked the computational resources available today and modern researchers have, leading them to rely on simplified assumptions for practicality.

The risks associated with repeatedly presuming stationarity are mostly related to the availability of longer data sets and climate shifts. Static return levels, which

assume that the frequency of extremes does not change over time, have been the foundation of infrastructure design methodologies for a long time (Cheng et al., 2014).

Conversely, the frequency of extreme events has been undergoing alterations and is anticipated to persist in changing over time (IPCC, 2007), recent research has revealed that hydrological data in certain areas exhibit non-stationary characteristics, manifesting in either increasing, decreasing, or mixed patterns. While hydrological parameters were traditionally viewed as stationary, this assumption may no longer hold true due to the influences of climate change and human activities, leading to non-stationary behaviour (Salas et al., 2018).

Given that many extreme events include spatial processes, one area of ongoing research on framework development has been the challenge of including spatial information inside extreme value analysis methodologies (Cooley, 2009; Love et al., 2022). Therefore, models that can take into consideration non-stationary climatic and hydrologic extremes are needed (Cooley, 2013; Salas & Obeysekera, 2014).

Southeast Queensland (SEQ) stands out as among Australia's regions most susceptible to flooding (Abbs et al., 2007). Due to its varied range of climatic regimes and status as the driest inhabited continent in the world, Australia is particularly sensitive to the extreme variations in climate that occur there year over year (Head et al., 2014). Projected changes in climate are anticipated to have noticeable effects on the frequency of hydrological elements such as runoff, rainfall, and evapotranspiration (ET) across various regions (Al-Safi & Sarukkalige, 2017; Ramezani et al., 2023). Distinguishing between the impacts of climate change and land-use changes on observed hydrological shifts is often challenging due to their concurrent occurrence in most regions, both climate change and land-use alterations (Lamichhane & Shakya, 2019; Ramezani et al., 2023). As such, a framework that incorporates land cover patterns and the ensemble of GCMs can be helpful.

Extreme hydrological events are seen to be significantly influenced by climate change (Meaurio et al., 2017) and the land cover changes caused by human activities. It is widely acknowledged that climate projections and scenarios, especially concerning extreme events including extreme precipitation (Bloschl & Montanari, 2010), and extreme streamflow exhibit significant uncertainty across many global regions. Research on hydrological extremes is critically needed, especially for the locations where the consequences of climate change are known to be significant (Salas et al., 2018).

Land use/cover changes (LUCC) have been identified as another influential factor for changing hydrological regimes (Wang et al., 2020). It should be highlighted that the majority of research on land cover is based on historical land-use statistics (Burn et al., 2010) and has given less attention to the combined effects of land cover change and climate change. Therefore, it is important to estimate future land-use scenarios and determine their impacts on extreme hydrological events. In the realm of land cover management and planning, two machine learning algorithm models are employed in Google Earth Engine (GEE): Random Forest (RF) (Gislason et al., 2006) and Support Vector Machine (SVM) (Gualtieri & Cromp, 1999).

Furthermore, the Generalised Extreme Value (GEV) distributions and the Log Pearson Type 3 (LP3) are commonly employed in the frequency analysis of hydroclimatic extremes (Ragno et al., 2019). In hydrology and climate research, these statistical distributions are commonly employed to examine the frequency and intensity of severe occurrences. The GEV distribution was utilised in earlier studies to produce Temperature Duration Frequency (TDF) curves (Ouarda & Charron, 2018; Mazdiyasni et al., 2019). Furthermore, it has been suggested by the Australian Rainfall and Runoff (ARR) guideline (Ball et al., 2019) that the GEV distribution be used to determine design floods and rainfalls.

A Bayesian inference framework that supports both non-stationary and stationary estimations was introduced by (Cheng & AghaKouchak). The concept of non-stationarity is useful in hydroclimatology to analyse extremes since many natural phenomena occur in non-stationary environments. According to their research, the Non-stationary Extreme Value Analysis (NEVA) model (Cheng et al., 2014) provides an efficient way to compute extreme return levels and variables. The economy, infrastructure, agriculture, natural ecosystems, and public health are all negatively impacted by the persistence of hydroclimatic extremes (Huth et al., 2000; Rainham & Smoyer-Tomic, 2003; Khaliq et al., 2005; Jones et al., 2018; Ouarda & Charron, 2018). Process-informed Non-stationary Extreme Value Analysis (ProNEVA) software can be used to undertake a frequency analysis of extremes and examine changes in the extremes' return period to identify design extremes at various recurrence intervals and durations. (Ragno et al., 2019). This model can integrate the changing extremes into intensity and frequency analysis (Cheng & AghaKouchak, 2014).

1.2. Research aim and objectives

This research aims to assess the hydroclimatic variabilities based on stationary and non-stationary assumptions in the Lockyer Catchment in Southeast Queensland by combining the effects of land cover and climate change, and spatial distribution analysis. The geeSEBAL method, which uses meteorological analysis data and Landsat images (Gorelick et al., 2017) to estimate evapotranspiration at regional sizes, was developed utilising GEE infrastructure. The SEBAL algorithm was included in GEE using the JavaScript APIs. To determine the accuracy of geeSEBAL, the results of spatiotemporal distribution of potential evapotranspiration, and rainfall from global climate datasets in comparison with the results of the same variables derived from ground-based observation.

Moreover, The spatiotemporal maps of water storage achieved from a lumped water balance analysis as well as land covers have been evaluated. By developing a multi-framework for assessing the return levels of extremes in the past and future hydrological consequences of climate change, the limitation of the assumption of a stationary climate will be overcome. To the best of my knowledge according to the literature review thus far, there hasn't been a multi-framework with non-stationary assumptions for past and future scenarios for the Lockyer Catchment, and only a few scholars globally have employed this approach. This study has focused on determining the physical system in terms of cause and effect by incorporating land cover projections and GEV distribution. Furthermore, this shows how ignoring the non-stationary assumption in extreme events analysis may lead to inaccurate estimations of design floods (return levels) which will have detrimental effects on infrastructure planning and design.

The Research Objectives are to:

1) Assess and map the spatiotemporal distribution and the overall trends of hydro-climatological data using spatial distribution in the GEE and their impacts on changes in surface water availability.
2) Develop a framework to assess non-stationary conditions in extreme hydrometeorological events such as extreme rainfall, evapotranspiration, and water storage deficit. To evaluate the impacts of land cover changes and urbanisation by applying SVM and RF classification in GEE and climate change.
3) Perform the hydrological simulations for each landcover classification separately under ensembles of General Circulation Models (GCMs) under Representative Concentration Pathways (RCPs) and landcover changes in the baseline, and the near and far future horizons.
4) Analyse the intensity and frequency of projected streamflow extreme events, rainfall extremes, evapotranspiration extremes and water storage deficit extremes under both stationary and non-stationary conditions using the GEV model for the estimation of different return levels.

The key Research Questions investigated in this thesis are:

1) Does the spatial distribution of the remotely sensed dataset can substitute ground-based observations in the sparsely gauged catchments? Does the spatial distribution of global climate datasets agree significantly well with ground-based observations?
2) How can the frequency, intensity, and duration of extreme hydrometeorological events in the catchment be determined? How can an evaluation of the effectiveness of landcover classification methods to generate future landcover be conducted?
3) How do hydrological simulations vary across different land cover classifications when subjected to ensembles of GCMs under different climate and landcover scenarios, considering both baseline conditions and projected land cover changes for near and far future horizons?

4) How can the frequency, intensity, and duration of extreme climate events (flood extremes) in the catchment be determined? Can the limitation of climatic models to evaluate extremes be eliminated using the GEV model?

Thus, in this research, the streamflow is considered based on stationary and non-stationary assumptions. This study assesses the streamflow characteristics in the Lockyer Catchment of Southeast Queensland, Australia, to establish return levels. The study aims to develop a methodology and identify the combined effects of land cover and climate change on extreme events. So, this research presents new insight into extreme events analysis such as flood extremes to explore the methodology that integrates the hydrological model with ensembles of GCMs under RCPs and projected landcover scenarios along with the GEV model to improve extremes predictions under the instantaneous impact of climate change and human activities. The results of the study will help in understanding the spatial variation of the streamflow extreme events at the catchment scale. The investigation of adaptation techniques to handle probable future extremes will be assisted by this new framework for water planners and decision-makers.

The study's findings may help decision-makers better understand extreme events by taking into account both stationary and non-stationary assumptions. This will help them choose the right materials for infrastructure development, emergency response, disaster preparedness, and health care services. This new paradigm will help water planners and decision-makers investigate adaptation strategies to deal with likely future extremes.

The outcomes of the study could be useful in understanding the extreme events by incorporating both stationary and non-stationary assumptions, thereby assisting decision-makers in making informed decisions for emergency response operations, disaster preparedness, health care services and the selection of appropriate materials for infrastructure development. The investigation of adaptation techniques to handle probable future extremes will be assisted by this new framework for water planners and decision-makers.

1.3. Thesis structure

Chapter 1 introduced the research conducted in this thesis by initially offering background on the project's start and the selection of the Lockyer Creek catchment as the studied area. It emphasised the significance of non-stationary assumptions for frequency analysis of return levels of extremes in a changing environment and its implications for extreme events such as flood extremes in the near and distant future.

The significance of the research was emphasised by this foundational work, which also served as a guide for developing the study objectives and preliminary enquiries for this thesis. This chapter outlines the comprehensive methodology employed to accomplish the objectives of all four research papers.

To further understand the hydroclimatological extremes, Chapter 2 covers literature on non-stationary extremes by reviewing the probabilistic methods. The second chapter reviews the examinations of hydrological frequency and intensity. This review helps determine the proper distribution and methodologies for assessing the hydroclimatic extremes in this study. Moreover, an ensemble of GCMs under climate scenarios concepts was incorporated into the extreme analysis. This approach is undertaken as additional concepts for the extreme analysis of future extremes for ensuring sustainability in the face of a changing environment.

The original research conducted as a section of this thesis through publication is presented in Chapters 3 through to Chapter 6. The first research paper in Chapter 3 presents the spatial analysis of hydroclimatic trends in the Doosti dam basin as an ungagged basin with an area of 55141 km^2. The decision to focus on ungagged catchment calibration in Iran provided a unique opportunity to test the applicability of one of their methods in sparsely gauged basins. The feasibility of our research is undertaken in the ungagged basin in the transboundary river basin as the Australian catchments have records of access to high-quality data.

NEVA model employs the Mann-Kendall trend test, allowing users to choose their desired level of significance. This test is utilised to detect trends and non-stationarity in extreme data. To assess the significance of climatic time series trends, the Mann-Kendall statistical test was conducted. The trend analysis methods with spatial pattern distribution were validated in the first paper. The Mann-Kendall test was applied in the second paper by applying the Bayesian approach for estimating GEV parameters under the non-stationary assumption. In this paper, ET_a derived from the geeSEBAL algorithm and *WS* from a lump water balance

The second paper presented in Chapter 4, proposed an integrated framework that combines geeSEBAL, NEVA GEV model and spatial distribution analysis pattern to return the frequency, intensity and return levels of extreme events including extreme evapotranspiration events, extreme rainfall events and extreme water storage deficit.

In the third paper, published here in Chapter 5, it is proposed that an integrated framework for assessing the past and future hydrological consequences of climate change be developed. This framework integrates hydrological models, machine learning method on the GEE platform for landcover changes projection; ProNEVA model and climate projections under different scenarios based on the Generalised Extreme Value (GEV) model in stationary and non-stationary conditions (Pakdel et al., 2023), and explores the impacts of future climate change on the streamflow. The GEV model and spatial distribution of the second paper show the effectiveness of these methods in extreme analysis. This chapter investigates the extreme flood events under land cover changes and RCPs scenarios in the near and far future periods in the Lockyer Catchment.

The fourth paper, published here in Chapter 6 explored annual maximum temperature extremes and durations from one to 15 days using GEV distribution under stationary and non-stationary conditions where the parameters were estimated using the Monte Carlo Bayesian inference approach across Australia. Extreme temperatures pose a significant risk to communities, industry and our natural environment. So, these temperature-duration-frequency (TDF) curves, depicting design temperatures, offer insight into the fluctuation of extreme temperatures in relation to duration and recurrence frequencies.

The main conclusions are reviewed and possibilities for further study are outlined in Chapter 7. Regarding the research articles that were published as part of this study, the major research issues that were first introduced in Chapter 1 are thoroughly addressed. Figure 2 depicts the general thesis structure schematically (see overleaf).

Figure 1. 2 Thesis structure

1.4. Research scope and limitations

The scope of this study is as follows::

- The research focuses on the extreme events analysis in the Lockyer Catchment, Southeast Queensland, with an emphasis on understanding the impacts of climate change and land cover changes.
- Data that was used contains ground-based measurements, remotely sensed data, geospatial data and climate data.
- Methodologies were developed for assessing future land cover changes and simulating hydrological responses under different climate scenarios, with a specific emphasis on extreme event analysis.
- An evaluation was performed into the effectiveness of non-stationary assumptions in extreme event analysis and explored the implications for water resource management and infrastructure development in the region.

This thesis should be interpreted with the following constraints in mind:

- The effectiveness of future land cover projections and hydrological simulations depends on the accuracy of input data and assumptions made in the modelling process.
- There are natural constraints that limit the accuracy of future projections including uncertainties associated with climate projections and scenarios.
- Incorporating different landcover into the conceptual hydrological model was limited to the landcover projections through RF and SVM methods.

1.5. Conclusions

This thesis's first chapter gave a thorough overview of the research background while emphasising its significance and demonstrating its need. Chapter 1 has given the research a distinct direction by outlining the goals and objectives of the study. In Chapter 2, an extensive literature review is presented, focusing on the research aims and objectives to underscore the specific gap in knowledge that this study aims to address.

CHAPTER 2: LITERATURE REVIEW

2.1. Overview

The literature that is relevant to the goals of the research is thoroughly reviewed in the parts that follow, along with additional information on the gap in the literature that this study is trying to address. The examined literature explains why this methodology was chosen for this study.

2.2. Significance of Research Problems

The main research problem addressed in this study is the changing intensity and frequency of extreme events under non-stationary conditions, considering the physical system in terms of cause and effect. This necessitates assessing the impacts of land cover change, urbanisation and climate change. By developing a multi-framework, the study aims to improve the prediction of extreme events, especially flood extremes, by taking into account the direct effects of climate change and human activities. Highlighting the importance of non-stationary conditions is crucial for understanding and managing these evolving extreme events.

2.3. Stationary and Non-stationary assumptions in hydrology

Stationarity and non-stationarity are fundamental concepts in hydrology that profoundly influence the understanding of hydrological processes and the accuracy of predictions. Stationarity refers to the assumption that the statistical properties of hydrological variables, such as streamflow, remain constant over time. In contrast, non-stationarity acknowledges that these properties can change due to various factors, including climate change, landcover alterations, and anthropogenic interventions. The importance of considering stationarity or non-stationarity lies in their implications for hydrological modelling, risk assessment, and water resources management. For example, making assumptions about stationarity when they do not hold might result in inaccurate forecasts of future hydrological conditions and biased assessments of exceptional occurrences.

2.3.1. Stationary assumptions

The conventional methods of developing hydraulic systems that protect against extremes often focus on risk and return period. They assume that the frequency of severe events is independently generated and that they originate from a stationary distribution.

Prior research, as demonstrated by (Pakdel et al., 2023; Pakdel et al., 2024), suggested that stationarity might simplify complicated statistical analyses. Assuming a steady climate, it provided important insights into decision-making, planning, and understanding the impacts of climatic events. However, presuming stationarity is riskier than ever due to longer data sets and a changing environment. Under the presumption of a fixed climate, the terms return period duration and return level provide crucial information for design, decision-making, and evaluation of the significance of unexpected meteorological and climatic events.

It is considered that the data in a stationary model come from a probability distribution function with constant parameters. However, the parameters of the underlying probability distribution function in a non-stationary model vary over time or in reaction to a specific covariate (Sadegh et al., 2015).

As a result, specialists in water resources have been concentrating more on evaluating if conventional methods are appropriate under stationary settings or if new methods are required when non-stationarity is seen. Within the water resources industry, this topic has attracted attention from project planners, governmental authorities, research organisations, and academic institutions worldwide. When developing and evaluating water infrastructure, they are actively looking for novel ways to take the changing hydrological circumstances into account (Salas et al., 2018).

2.3.2. Non-stationary assumptions

In order to "update" design events based on historical data, basic regression techniques for modelling changes in the variance, mean, and skewness are examined. These approaches include mixing such non-stationary moments with different probability distribution functions (pdf). The fundamental ideas, and techniques, as well as the best way to choose a design event in light of non-stationarity and future uncertainty, remain unsettled (Obeysekera & Salas, 2014). In conditions of non-stationarity, the occurrence frequency of extreme events also fluctuates over time.

The rising worry about climate change brought on by a rise in greenhouse gas concentrations in the environment is yet another factor contributing to the growing emphasis on non-stationarity (IPCC, 2007, 2021).

2.3.3. Stationary and non-stationary assumptions in NEVA & ProNEVA

Non-stationary situations arise because the stationary assumption might not be valid for changes brought about by human and climate variables. NEVA uses a Differential Evolution Markov Chain methodology for global optimisation throughout the parameter field to determine the extreme value in a Bayesian way (Cheng et al., 2014). EVT offers two basic distributions to describe extremes: the block maxima approach using the GEV distributions (Morrison & Smith, 2002) or the peaks-over-threshold method using the GPD (Coles et al., 2001; Moisello, 2007; Durocher et al., 2019). NEVA normally consists of two parts: 1. The GEV distribution is utilised for annual maximal evaluation or block maxima. 2. The GPD is employed in the peak-over-threshold (POT) technique to analyse extremes above a particular limit.

ProNEVA allows for non-stationary research using user-defined variables, which can be time or a physical variable. The capacity to include physical constraints in a statistical model is the advantage of performing stationary assessments with covariates connected to the physical component (Ragno et al., 2019).

2.4. Applying machine learning for the classification and projection of landcover changes

The Landsat satellite images (from TM, ETM+ and OLI 1&2 sensors), and ESA global land cover dataset were accessed and used through GEE (Pakdel et al., 2022) for conducting the classifications and modelling of changes in land cover and urban growth. Geospatial datasets of road networks, population density, and Hydrologically Enforced Digital Elevation Model (DEM-H) product with 30m spatial resolution (Mission, 2013) datasets were used as supplementary data inputs during landcover projection analysis. As the distance from roads and population density maps were originally in vector format, both maps were first converted into the raster format and resampled to the 30 m spatial resolution and used for the projection of landcover changes.

SVM was one of the most reliable and widely applied supervised non-parametric statistical machine learning techniques (Cortes & Vapnik, 1995; Esmaeili et al., 2023). To discriminate between various categories, the SVM method translates the training data into two-dimensional space and fits the best hyperplane. The kernel functions, which are non-linear mapping functions, are used to define the optimal hyperplane that divides the classes. The SVM module (Pal & Mather, 2005) is employed for training and classification, utilising a radial basis function (RBF) kernel. Moreover, a radial basis function is characterised by its computational speed and straightforward implementation, involving the tuning of two parameters. These parameters include cost 'sigma(C),' a substantial value used to fine-tune the error associated with misclassifying instances in the training dataset, and 'gamma (γ),' which represents the kernel width.

A non-parametric machine learning method RF (Gislason et al., 2006) was created based on the idea of a learning strategy. To create a single classification, RF combines many tree-based classifiers into an ensemble of decision trees, where each tree provides a vote to choose which class should be assigned to the input data (Briem et al., 2002; Pal & Mather, 2005; Xie & Niculescu, 2021). To project the landcover changes, first, the main land cover types were classified into six classes and following ESA global landcover classification (Zanaga et al., 2022) discriminated from other features in Landsat images for the years 2000, 2010 and 2020 using two supervised classification models including SVM and RF. The Image collection of Landsat images was called for the years 2000, 2010 and 2020 in GEE, separately. The code that was developed in the GEE, was deployed to enable the user to perform the classification using both SVM and RF approaches as two main machine learning models. The user can easily switch between SVM and RF and all statisical indices are produced after running the code.

2.5. Hydrologic modelling

Choosing an appropriate hydrological modelling platform is crucial since incorporating climate projections and scenarios in simulation modelling involves intricate, data-intensive, and perhaps lengthy computations. To analyse the impacts of climate change on runoff at various sizes, ranging from small locations to huge geographic areas, hydrological models have been widely implemented.

The study found that when subjected to the same climate change scenario, other hydrological models that provide acceptable findings for an observable baseline period may behave differently (Gosling & Arnell, 2011; Haddeland et al., 2011).

Moreover, a similar study, by integrating 3 GCMs and different large-scale hydrological models (GHMs) declared that the results of several hydrological models should be used in estimations of climate change impacts as the uncertainty for hydrological change dependant largely on the selection of the hydrological model (Hagemann et al., 2013). The concept of selecting an appropriate hydrological model has been proven by Jahandideh-Tehrani et al. (2019) that in the Australian region, lumped conceptual hydrological models (Petheram et al., 2012) such as AWBM well-suited to use for runoff simulation. AWBM is mostly made up of three basic surface storage configurations.

The depths of these storage tanks are equal to the C1, C2, and C3 (three surface moisture stores) parameters to create the coefficient of runoff simulation. For each time step, the water balance of each partial region is determined (Esmaeili-Gisavandani et al., 2021). As demonstrated by (Ramezani et al., 2023), in this study, runoff from impermeable surfaces was taken into account by recoding and changing the AWBM.

2.6. Future climate projections and scenarios

GCMs project precipitation and evapotranspiration, among other climatic variables, under hypothetical future scenarios or historical trajectories (Jahandideh-Tehrani et al., 2019). Individual CMIP5 models' capability to predict the Australian climate varies depending on whatever part of the modelling process is studied. These models are the most accurate instruments for predicting the reaction of regional climates in the twenty-first century (Kirono et al., 2020). Based on the third and fifth stages of the CMIP, Alexander and Arblaster (2017) conducted detailed evaluations of anticipated changes in extreme climate events over Australia.

Projected runoff by implementing baseline climate data can be estimated or focused on assumptions of climate models (Chiew, 2006; Fu et al., 2007), and another method is applying hydrological models. The best method for estimating the hydrological implications of climate change is to drive a hydrological model with climatic forecasts generated from ensembles of multiple GCMs pushed with different emissions scenarios (Thompson et al., 2013).

Thompson et al. (2013) stated that throughout these climate change hydrological effect evaluations, a number of uncertainties are incorporated. Therefore, selecting well-suited GCMs and RCPs will be a solution to these uncertainties.

In this research, According to the Australian Climate Change Technical Report (CSIRO & BOM, 2015), these 8 climate models have been suggested for investigating climate change impacts on Southeast Queensland.

The definition of stationary may no longer be applicable due to the climatic-related stressors and effects of anthropogenic that create non-stationary conditions (Salas et al., 2018). Recently researchers analysed flood and streamflow under non-stationary assumptions (Strupczewski et al., 2011; Salinas et al., 2014; Debele et al., 2017). The use of generalised extreme value (GEV) distribution to model extreme climate events and their return periods is widely popular (Engeland et al., 2004). As a result, utilising non-stationary data, new methods for analysing the frequency of extremes should be developed.

The stationary assumption is used to estimate the largest instantaneous extremes, and structures are built with this assumption in mind. As the impacts of climate change are growing which means that non-stationary conditions will affect and rise in the world. For instance, natural phenomena recently occurred in Southeast Queensland especially Lockyer Catchment affected by a flood in February 2022 and these extremes occurred in non-stationary assumption. Therefore, it is critical to take a non-stationary approach to these issues.

However, to our knowledge, few studies have used similar methods to analyse extremes of future periods by considering outputs of multi-GCMs after forcing into a hydrological model in a non-stationary and stationary assumption. In Southeast Queensland where extremes are persistently phenomenon, it is indicated that studies of extremes through multi-modelling are crucial for water management in the future.

The outcome of this study from a catchment management perspective, is improving the accuracy of analysis in less time and cost-effective way and might help policymakers in sustainable water resources management. Employing the non-stationary assumption for extreme climate analysis is a novel subject in the rainfall-runoff simulation. This specific study compares hydro-climate variables such as streamflow using different models. Because the research region contains residential and agricultural areas and dams, estimating the return period values of extremes in the future period is critical for water resource management.

This research will help to identify extreme events in the two future periods and the framework of this study can be used in activating emergency response operations to tackle future extremes.

2.7. Conclusions

Chapter 2 of the thesis provides a comprehensive review of the literature that is important to the objectives and aims of the research. This procedure led to the straightforward identification of the research need in Chapter 2 that this study has attempted to solve. Chapter 3 presents the research article that was published as part of this study and discusses how it aligns with Research Objective 1.

CHAPTER 3: METHODS

3.1. Research methodology overview

3.1.1. Overview

This thesis contains a series of four papers that investigate a non-stationary approach by applying a multi-framework. These four research papers explore a dynamic approach to analysing extreme events by employing various methodologies and techniques. This includes trend analysis methods to analyse temporal patterns, and spatial analysis techniques utilising GEE. These mentioned methods were applied to an ungauged catchment at Doosti River Dam to test the feasibility of methods and then applied in the Lockyer Catchment. This framework also includes geeSEBAL, hydrological modelling to simulate water flow dynamics, and climate modelling under two scenarios. Additionally, machine learning techniques are utilised to project changes in land cover within the GEE platform. The GEV model is then employed to assess the frequency and intensity of return levels for hydrometeorological variables. By integrating these diverse approaches, the studies aim to provide a comprehensive understanding of the complex interactions driving extreme events and their implications for hydrological processes. Spatial analysis techniques in GIS including interpolation, and overlay analysis. The approach is summarised in Figure 3 (see overleaf).

3.1.2. Data

A rich time series of spatial analysis and gauge data has been used to gather further details about the scope of this research. Daily meteorological data including minimum and maximum air temperature (°C), minimum and maximum relative humidity (%), wind speed (m/s), surface solar radiation (MJ/m^2), and hydrological data such as evapotranspiration (mm) and rainfall (mm) were sourced from two datasets: ground-based observations and global climate products. The Australian Climate Observations Reference Network – Surface Air Temperature (ACORN-SAT) dataset of the Australian Bureau of Meteorology (BOM) provides daily maximum temperature in degrees Celsius (^oC), which has been developed in order to monitor climate variability and change in the country (Trewin, 2018). The ACORN-SAT data are adjusted, homogenised and peer-reviewed.

The ground-based observations were obtained from SILO, an Australian climate data source (http://www.longpaddock.qld.gov.au/silo) (Jeffrey et al., 2001; CSIRO & BOM, 2015) that covers the period from 1990-2022. The 5 km-grid data achieved through SILO are the most commonly used and most reliable climate data for environmental studies in Australia (Ramezani et al., 2022). Daily streamflow records for 143210B Lockyer Creek at Rifle Range Road station were received from the Queensland Government Water Monitoring Information site (https://water-monitoring.information.qld.gov.au/).

Fourteen SILO meteorological and hydrological stations were applied for this research. First, the Inverse Distance Weighting (IDW) interpolation method was used to interpolate the station data and rasterise the meteorological parameters. To run the geeSEBAL algorithm, daily meteorological ground-based observations and the hourly fifth generation ECMWF reanalysis (ERA5) climate dataset with 9 km spatial resolution were incorporated in GEE and were used separately for running geeSEBAL as well as estimation of water storage. Landuse information was obtained from the Australian government, Geoscience Australia (https://www.ga.gov.au/), for simulation purposes.

The Landsat satellite images (from TM, ETM+ and OLI 1&2 sensors), and the ESA global land cover dataset were accessed and used through GEE (Pakdel et al., 2022) for conducting the classifications and modelling of changes in land cover and urban growth. Geospatial datasets of road networks, population density, and Hydrologically Enforced Digital Elevation Model (DEM-H) product with 30 m spatial resolution (Mission, 2013) dataset were used as supplementary data inputs during landcover projection analysis. Since, the distance from roads and population density maps were originally in vector format, both maps were first converted into the raster format and resampled to the 30 m spatial resolution and used for projection of landcover changes.

The three primary purposes of the geeSEBAL tool are (1) Image: derivation of actual evapotranspiration from a particular image (accessible for JavaScript); (2) ImageCollection: batch method to calculate ET_a provided a date range and (3) Time series: long-term ET_a time series estimate at user-provided locations. All applications and codes are freely accessible at https://github.com/et-brasil/geesebal. Additionally, the Earth Engine programme (https://etbrasil.org/geesebal) offers a graphical user interface version of geeSEBAL (Laipelt et al., 2021; Gonçalves et al., 2022; Kayser et al., 2022). For the purpose of running geeSEBAL, a series of Landsat images with the

highest data quality were used. We used cloud cover filters using the CFMask method (Foga et al., 2017), which generates a bitmask to identify each image's pixels for clouds, clouds with shadows, clouds with confidence and pixels for ice and snow.

Land cover was classified into six types using SVM and RF models. To train the classification models, we mapped the boundaries of more than 200-point features (335) representing six different classes: Tree cover, grassland, cropland, built-up, bare soil/sparse vegetation, and water bodies using ESA global landcover and drawing geometry tools in GEE. The training datasets were split up into groups for training and validation. 70 percent of point features was assigned to the training and 30 percent was used in the validation procedure.

Table 3. 1 Source of datasets.

Raster Dataset	Time coverage	Data Source	Resolution/ format
Landsat 5 TM	2000-2011	Google Earth Engine (LANDSAT/LT05/C02/T1_L2)	30 m
LANDSAT 7 ETM+	1999-2023	Google Earth Engine (LANDSAT/LE07/ C01/ T1_SRLANDSAT/ LE07/C01/T1)	30 m
Landsat 8 OLI/TIRS	2013-2023	Google Earth Engine (LANDSAT/LC08/ C01/ T1_SRLANDSAT/ LC08/C01/T1)	30 m
ESA global land cover	2021	Google Earth Engine (ESA/WorldCover/v100)	10 m
DEM-H: Australian SRTM Hydrologically Enforced Digital Elevation Model	2010	Google Earth Engine (AU/GA/DEM_1SEC/v10/DEM-H)	30 m

Vector Dataset		Source	Data format
Roads	2000 & 2023	Queensland Government	Shapefile (.shp)
Distance from roads	2023	Spatial analysis on road network	Shapefile (.shp)
Population	2023	Australian Bureau of Statistics	Shapefile (.shp)

3.1.3. *Mann-Kendall trend and Sen's slope test*

Using GEE programming, the Mann-Kendall (MK) test and Sen's slope estimator were used to calculate the statistical significance and long-term magnitude of change on hydroclimate datasets. The MK test (Mann, 1945; Kendall, 1975; Zolghadr-Asli et al., 2019) was applied to quantify the significance of trends in meteorological time series (Tabari et al., 2011; Banerjee et al., 2020). Generalised Extreme Value models including the NEVA model use the Mann–Kendall trend test at the user-selected significance level to identify trends and non-stationarity in extremes in data (Cheng et al., 2014). The Mann–Kendall (MK) statistical test (Mann, 1945) was undertaken to calculate the importance of climatic time series trends (Burkey, 2006; Xu et al., 2006; Da Silva et al., 2015; Nyikadzino et al., 2020).

The MK test null hypothesis (H0) states that there is no monotonic trend at the designated level of significance. In this test, the alternative hypothesis (Ha) exhibits a monotonic trend with time. Additional information on Mann-Kendall may be found in (Pakdel et al., 2022).

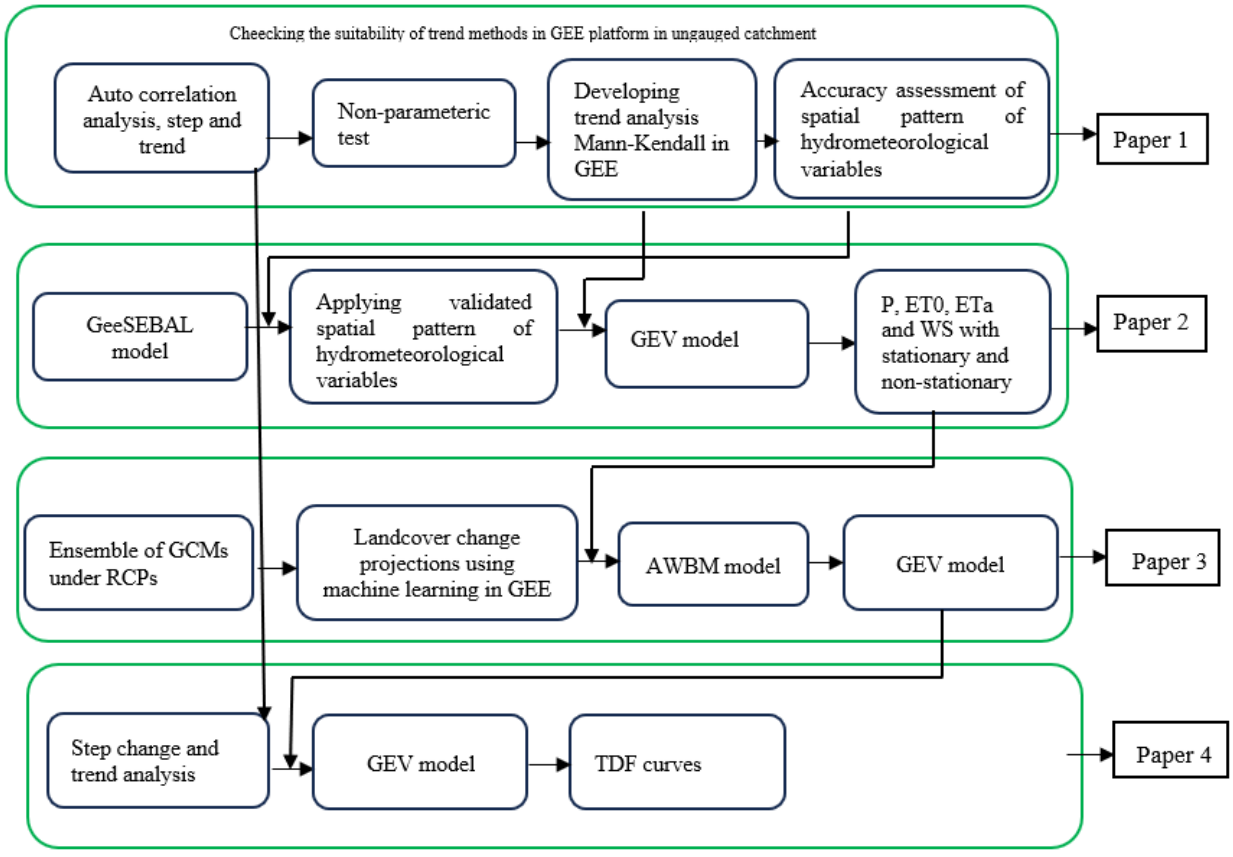

Figure 3. 1 Summary of papers of this research.

3.1.4. Google Earth Engine application: The geeSEBAL algorithm

The development of geeSEBAL marks a significant advancement in the field of hydrological modelling. Leveraging the robust infrastructure of GEE, the geeSEBAL algorithm offers a powerful solution for estimating evapotranspiration at regional scales. By integrating meteorological reanalysis data and Landsat imagery, geeSEBAL provides researchers and practitioners with a comprehensive tool to assess water fluxes and understand ecosystem dynamics. This innovative approach not only enhances our ability to monitor and manage water resources but also contributes to broader efforts in climate change adaptation and sustainable land management.

The geeSEBAL (Laipelt et al., 2021) is based on the original approach developed by Bastiaanssen et al. (Bastiaanssen & al., 1998) is the foundation for which assumes that latent heat flux (LE) (W/m2) can be approximately represented as surface energy balance. Using the geeSEBAL model, ET was automatically estimated and validated against data from ET stations, as ET is a crucial sign of agricultural drought. GeeSEBAL aims to improve understanding of how land cover changes over the last few decades have affected ET. The latest iteration of geeSEBAL employs Landsat imagery and reanalysis data to compute the ETa time series, exhibiting positive results for regional-scale studies carried out in regions with limited data accessibility (Laipelt et al., 2021). The fundamental principle of the Surface Energy Balance Algorithm for Land (SEBAL) involves selecting endmembers representing the hot (dry) and cold (wet) pixels to calculate the near-surface temperature gradient (dT).(Bastiaanssen & al., 1998; Allen et al., 2007).

Previously, the manual identification of hot and cold pixels was standard practice, but technological improvements have made it feasible to automate this procedure. Employing the Normalised Difference Vegetation Index (NDVI) and Ts percentiles, one such method is called Calibration using Inverse Modelling at Extreme Conditions (CIMEC) (Allen et al., 2013), it is used to automatically identify endmembers. In this study, a platform known geeSEBAL (https://github.com/et-brasil/geesebal (accessed on 15 06 2023) was utilised in this study. It integrates the capabilities of GEE with the SEBAL framework (Laipelt et al., 2021). This tool was created to make use of the application programming interface (API) of the GEE platform. It is an effective tool for a variety of remote sensing and evapotranspiration estimating investigations.

3.1.5. Classification and projection of land cover changes

To project the landcover changes, first, the main land cover types were classified into six classes and following ESA global landcover classification (Zanaga et al., 2022) discriminated from other features in Landsat images for the years 2000, 2010 and 2023 using two supervised classification models including SVM and RF. Then, the landcover changes were simulated and projected using RF approaches in the GEE platform.

3.1.6. Landcover changes projection

The probability of transitions from the RF learning procedure is employed in this work to characterise the changes in land cover. The land cover maps for the start year (2000) and the finish year (2010) are included in the model's first phase. After importing the spatial variable factors such as DEM, population density and distance from the road, into the model, a land cover change map is produced, from which the research area's changing pattern between 2000 and 2010 is established. The properties of the explanatory maps are extracted in the same raster format for all datasets, with the exact geographical projected coordinates of EPSG 4326 and with a resolution pixel size of 0.000269495 degrees.

To project the change in land cover, a script was written in GEE to calculate the percentage of area change in a given year. It generates a transition matrix that shows the proportion of pixels shifting from one land cover to another. The code also creates an area change map that shows the change in the land between 2000 and 2010 in all six classes; tree cover, grassland, cropland, built-up, bare soil, and water bodies. The future land cover maps are predicted assuming that existing land cover patterns and dynamics are continuing. Also, based on the classified raster images of 2000 and 2010, land cover transitions are predicted for 2040 and 2060. To model land cover forecast, the RF and SVM classification technique was used to forecast the land cover map.

3.1.7. Hydrological model

Australian Water Balance Model (AWBM) (Boughton, 1993; Boughton, 1995; Boughton, 2004) has been used in other countries and has become one of Australia’s most extensively used hydrological models (Boughton, 2004, 2006; Boughton, 2007). The Rainfall-Runoff Library (RRL) is freely available for users, (further information is

available at :https://toolkit.ewater.org.au/Tools/RRL). Yu and Zhu (2015) indicated that AWBM is better for simulating climate-driven fluctuations in observed streamflow and characterising the consequences of precipitation changes.

The concept of selecting an appropriate hydrological model has been proven by Jahandideh-Tehrani et al. (2019) that in the Australian region, lumped conceptual hydrological models (Petheram et al., 2012) such as AWBM well-suited to use for runoff simulation. For simulation purposes, calibration (60%) and validation (40%) were employed.

The availability of recorded runoff data determined the calibration and validation timeframes for the Lockyer Catchment. So, runoff data were used for the 1990-2002 (calibration period) and 2003-2010 (for validation period). Daily rainfall, potential ET (PET) and daily runoff were derived from SILO and WMIP throughout the catchment respectively.

3.1.8. Future climate projections and greenhouse gas emissions scenarios

Coupled Model Intercomparison Project (CMIP) is the largest intercomparison study, and it serves as a baseline for assessing GCMs' capacity to project observed climate changes. In this study, climate change effects on streamflow in the Lockyer Catchment were assessed using eight GCMs of CMIP5. The recently suggested RCPs provide a broader range of possible futures by taking mitigation techniques and land use changes into account (CSIRO & BOM, 2015). According to the aim of this research study, it is imperative to select appropriate RCP scenarios.

As mentioned in the climate change technical report in Australia (CSIRO & BOM, 2015), the Australian Water Availability Project (AWAP) observed temperature and rainfall data (https://eo-data.csiro.au/projects/awap/) were used to create climatic outputs, which have a resolution of 5 km. In this approach, the model data whose resolution ranged from 100 to 310 km were initially applied to the observed data using interpolation on a 5 km grid. In this research, According to the Australian Climate Change Technical Report (CSIRO & BOM, 2015), these eight climate models have been suggested for investigating climate change impacts on SEQ.

3.1.9. Assessing extremes in a non-stationary approach using the GEV model

Non-stationary situations arise because the stationary assumption might not be valid for changes brought about by human and climate variables. Even with great

progress (Cheng et al., 2014), there is still no complete framework that incorporates the Extreme Value Analysis (EVA) statistical models GEV, Generalised Pareto (GP), and Log-Pearson type III (LP3)) under stationary and non-stationary assumptions (parameters as a function of physical variables or time) (Ragno et al., 2019).

It is critical to recognise that non-stationary situations are becoming more common globally as a result of the escalating effects of climate change. Given that earlier research has shown that the frequency of flood events such as the one in 2022 may be underestimated under a stationarity assumption (Armstrong et al., 2020) and has shown the assumption to no longer be valid. Therefore, adopting a non-stationary perspective on these matters is crucial. To examine non-stationary extremes, the NEVA software package (Cheng et al., 2014) and ProNEVA software (Ragno et al., 2019) were utilised.

Section 1.3 has demonstrated an overview of the research methodology and provided the modelling steps of how the research was carried out to achieve the objectives of the study.

CHAPTER 4: PAPER 1 – GOOGLE EARTH ENGINE AS A MULTI-SENSOR OPEN-SOURCE TOOL FOR MONITORING STREAM FLOW IN THE TRANSBOUNDARY RIVER BASIN: DOOSTI RIVER DAM

4.1. Introduction

Understanding the impacts of global change and human activities on water resources relies heavily on surface water dynamics. A thorough examination of hydroclimatic variations at a regional level is crucial for devising adaptation and mitigation strategies to address the adverse effects of climate change. This research paper investigates the hydroclimatic factors contributing to changes in surface water availability in a specific area using multisensor satellite data from the Google Earth Engine platform. The Mann–Kendall and Sens slope estimator tests were utilised to analyse the spatial and temporal variations of hydroclimate variables. Statistical analyses revealed decreasing trends in temperature and increasing trends in rainfall based on available station data. Additionally, there was observed growth in evapotranspiration and irrigated area development alongside a slight decline in snow cover. The expansion of irrigated areas, particularly during winter growing seasons, suggests a significant diversion of water to support agricultural needs. This study's methodology could be applied to any geographical location to assess hydrological conditions, spatiotemporal changes, and their drivers, including climate change and human activities.

4.2. Published paper

Pakdel et al. (2022), “Google Earth Engine as multi-sensor open-source tool for monitoring stream flow in the transboundary river basin: Doosti River Dam” is published in SPRS International Journal of Geo-Information (2022), Volume 11, Issue 535.

International Journal of Geo-Information

MDPI

Article

Google Earth Engine as Multi-Sensor Open-Source Tool for Monitoring Stream Flow in the Transboundary River Basin: Doosti River Dam

Hadis Pakdel-Khasmakhi [1,2,*], Majid Vazifedoust [3], Dev Raj Paudyal [2], Sreeni Chadalavada [1] and Md Jahangir Alam [1,4]

[1] School of Engineering, The University of Southern Queensland, Springfield Lakes, QLD 4300, Australia
[2] School of Surveying and Built Environment, The University of Southern Queensland, Springfield Lakes, QLD 4300, Australia
[3] Water Engineering Department, University of Guilan, Rasht 4199613776, Iran
[4] Murray-Darling Basin Authority (MDBA), Canberra, ACT 2601, Australia
* Correspondence: hadis.pakdel@usq.edu.au

Abstract: Understanding the effects of global change and human activities on water supplies depends greatly on surface water dynamics. A comprehensive examination of the hydroclimatic variations at the transboundary level is essential for the development of any adaptation or mitigation plans to deal with the negative effects of climate change. This research paper examines the hydroclimatic factors that contribute to the desiccation of the Doosti Dam's basin in the transboundary area using multisensor satellite data from the Google Earth Engine (GEE) platform. The Mann–Kendall and Sens slope estimator test was applied to the satellite datasets to analyse the spatial and temporal variation of the hydroclimate variables and their trend over the transboundary area for 18 years from 2004 to 2021 (as the dam began operating in 2005). Statistical analysis results showed decreasing trends in temperature and an increase in rainfall with respect to station-observed available data. Evapotranspiration and irrigated area development followed the increasing pattern and a slight decrease in snow cover. The results confirmed a large expansion of the irrigated area, especially during the winter growing season. The increase in irrigated cultivated areas during both winter and summer seasons is possibly the main reason for the diversion of water to meet the irrigation requirements of the developed agriculture areas. The approach followed in this study could be applied to any location around the globe to evaluate the hydrological conditions and spatiotemporal changes in response to climate change, trend analysis and human activities.

Keywords: Google Earth Engine; spatiotemporal analysis; cloud-computing platform; Doosti Dam; ungauged or sparsely gauged basin; Landsat; MODIS

check for updates

Citation: Pakdel-Khasmakhi, H.; Vazifedoust, M.; Paudyal, D.R.; Chadalavada, S.; Alam, M.J. Google Earth Engine as Multi-Sensor Open-Source Tool for Monitoring Stream Flow in the Transboundary River Basin: Doosti River Dam. *ISPRS Int. J. Geo-Inf.* **2022**, *11*, 535. https://doi.org/10.3390/ijgi11110535

Academic Editors: Godwin Yeboah and Wolfgang Kainz

Received: 11 August 2022
Accepted: 23 October 2022
Published: 25 October 2022

Publisher's Note: MDPI stays neutral with regard to jurisdictional claims in published maps and institutional affiliations.

1. Introduction

With an increase in human activities, socio-economic and environmental conditions have impacted transboundary river basins [1]. For riparian nations, these increased activities are raising fears about potential flow regime changes due to dam operations and large-scale water withdrawal [2]. Data scarcity and a lack of data-sharing protocols are making transboundary water-sharing management more difficult [3]. The scarce or imbalanced geographical distribution of gauging is also a problem for understanding the hydroclimate patterns and capturing their heterogeneity and spatiotemporal distribution [4]. The situation is dire in ungauged basins, as is the case examined in this paper.

Remote sensing and satellite-based data have solved the data scarcity problem. This study explores the use of multi-sensor open-source tools such as the Google Earth platform to obtain relevant climate and environmental monitoring data for scientific study [5]. The platform provides synoptic coverage for areas which were previously difficult to obtain

due to geographical remoteness [6–8], and allows trend monitoring in real time. Processing remote sensing data is sometimes difficult and very often the acquisition of valuable results necessitates the analysis of large datasets [9]. These problems have been solved with the help of the open source software QGIS (Quantum GIS) [10,11]. QGIS made it possible to analyse remotely sensed data to obtain water levels across a sizable inaccessible area at regular intervals for regional studies [12]. However, there are many challenges with using these data, such as cloud contamination issues and the availability of reliable imagery [13].

For better analysis, Google Earth Engine (GEE) [14] via an internet-based application programming interface (API) and a web-based interactive development environment [15] enables the analysis of global environmental phenomena, changes and trends using satellite pictures, and works with historical series [5,16]. Furthermore, its codes are free to download [14]. It is promoted as the most powerful cloud-based geospatial processing platform in the world, capable of overcoming processing issues experienced by traditional satellite image-processing methods [14].

The growing water scarcity problems in northeastern Iran, and particularly the city of Mashhad which is the second most populated city in Iran, compelled the Iranian government to initiate water diplomacy with the neighboring Turkmen governments. The result of these negotiations was an agreement between Iran and Turkmenistan to jointly build a dam on the river basin called the Iran–Turkmenistan Friendship Dam (or Doosti Dam) in 2004 [17,18]. Although construction of the dam helped water authorities provide part of the drinking water requirements, in recent years, due to several factors such as climate change and excessive harnessing, the water entering the dam has been significantly reduced [19].

Drinking water in Mashhad city has been seriously affected by water shortages that have forced water authorities to investigate the reasons for the reduction of water flow from the Doosti Lake considering climatological and hydrological aspects and agricultural expansion [20]. However, in most cases, realistic climatological data are not readily available, especially in the inaccessible ungauged part of the catchments. Consequently, GEE provides better solutions for the analysis of hydroclimatic variations within the Doosti Lake catchment.

The study found that a number of multi-source remote sensing data with different spatial and temporal resolution are available. Moderate Resolution Imaging Spectrometer (MODIS) [21,22], Landsat Thematic Mapper (TM) [23–25], Synthetic Aperture Radar [13,26] and other passive and active remote sensors with visible and microwave bands have all been employed to estimate inundation areas and delineate water borders. The Deltares Aqua Monitor [27] and GEE [28] were used to examine changes in the Earth's surface water over the last 30 years. Automated systems, however, are not appropriate for a regional scale. The variety of geographical characteristics causes a lack of consistency in the correctness of studies' results. The authors of [12] highlighted that analysis of the driving mechanisms behind regional surface water dynamics and related studies is rare.

As concerns over Doosti Dam's shrinking increase [29], so it is vital that authorities identify the cause/s of shrinkage whether they are climatic or anthropogenic [20]. The research area's available gauge data in Iran and Turkmenistan do not have adequate geographical or temporal coverage [28–31], and this study provides useful information.

This study acknowledges that there are knowledge gaps which can be filled by utilising satellite-based remote sensing systems [20,32] which offer valuable sources of data and observations capable of partially or fully replacing field survey and gauged data. The study aims to determine the suitability of the use of GEE coupled with the QGIS platform to understand the hydroclimatic behaviour and determine stream flow patterns, especially for inaccessible [33–35] and transboundary areas. The specific objectives of this study are:

(1) To propose a novel approach to easily calculate yearly surface water to assist in investigating long-term surface water variation. This will employ nonparametric analysis and the application of the GEE platform [14,15];
(2) To analyse the causes of surface water variation in the Doosti Dam reservoir and identify the trend;

(3) To assess and map spatiotemporal distribution and the overall trends of the hydroclimatological condition using several satellite gridded datasets for the last 20 years and identify the possible factors causing the trend.

To assist decision-making on irrigation growth, techniques that increase irrigation area accuracy are essential. We implemented multi-satellite products in the GEE platform that enable the rapid processing of vast numbers of images and use a spatial method that will help decision makers evaluate the trend of hydroclimate factors and the development of irrigated areas. Previous research on trend and variability analyses of hydroclimatic variables were limited to investigating a small number of observations because Iran lacks a comprehensive record of data of the desirable quality [36]. Additionally, due to data shortage, studies of the spatiotemporal variations of various hydroclimatic variables such as evaporation, snow cover duration, land use and lake reservoir capacity have been limited in the literature, particularly in Iran [37].

We investigated the spatiotemporal variability and trends of key hydroclimatic variables across the Doosti Dam basin from 2004 to 2021. The novel aspects of this research are the selection of superior gridded multi-hydroclimatic satellite variables with non-parametric tests, and the combination of multi-hydroclimatic gridded satellite variables pre-processing with the GEE platform and QGIS. The use of finer spatial resolution data for trend and variability analysis is necessary due to the significant variability of hydroclimatic variables, particularly over location, time and climate zones [37]. Therefore, we implemented the more accurate spatial resolution hydroclimatic datasets in GEE and discovered a relationship between trends of multi-hydroclimatic variables and lake levels that had not been investigated previously. It is anticipated that the findings will aid in the development of future adaptation and mitigation, conservation policies and actions by helping policymakers and water authorities better understand how the Doosti Lake basin is responding to climate change.

2. Materials and Methods

2.1. Study Region

The Doosti Dam's basin (Figure 1) is the biggest transboundary basin between two countries, Iran and Turkmenistan, and is located between latitude 33° N to 36° N and longitude 59° E to 67° E. The basin covers an area of approximately 55,141 km^2, and the climate of this region is semi-arid and the reservoir of the dam is a clear and relatively deep lake with a maximum and mean depth of 35 m and 15 m, respectively [17,18]. The Doosti Dam is important for Iran as the country relies on its role in supplying fresh water to Mashhad, the second-most populous city in Iran with a population of around 3 million. The dam provides drinking water for up to 76% of the population in Mashhad and its principal tributaries, mostly for the purpose of storing water in reservoirs, irrigation for agriculture, and producing electricity.

Mashhad is a great example of a city that depends heavily on outside imports of water and power. Due to the city's fast growth, climate change and severe droughts, and eightfold expansion of the population, Mashhad's local water supplies are under a lot of stress. The city is now considerably more dependent on water from far-off sources as a result [29].

Iran's approach to water management is reactive rather than proactive, putting more emphasis on quick fixes such as expanding the number of wells and dams and transporting water from far-off sources rather than on looking for fresh opportunities and long-term solutions to address any threats or issues before they arise.

2.2. Datasets

2.2.1. Ground Measurements

The daily hydroclimatologic parameters consisting of precipitation and temperature collected from three local stations are presented in Table 1. Because of the lack of field data, remotely sensed data could be a good alternative in this study. Faulty gauge stations can create some gaps in the collection of hydrological time series data. Most often, the

upstream and downstream data exchange between the two riverine countries has not been effective. Data collecting across borders must be independent between nations in order to quickly determine the amount of inundation for emergency response activities [38]. Remote sensors mounted on satellites and aircraft have the capability to provide data [39].

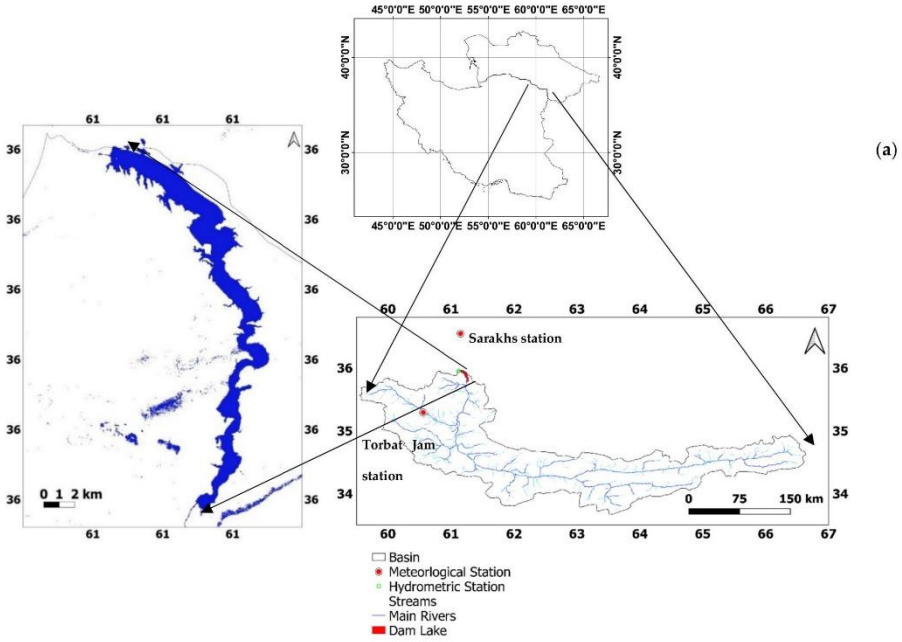

Figure 1. Location of Doosti Dam's river basin drainage system. (**a**) Shows Iran (left) and Turkmenistan (right), (**b**) shows the Doosti reservoir from NDWI Landsat datasets, (**c**) shows Doosti Dam's river basin.

Table 1. Specifications of ground-based data used in evaluation of satellite-based data.

Station	Specifications	Longitude (m)	Latitude (m)	Elevation (m)	Time Scale	Period
Torbat Jam	Meteorology station	60.56	35.29	950	Daily	2001–2020
Sarakhs	Meteorology station	61.15	36.54	278	Daily	2001–2020

2.2.2. Satellite Data

Within each year, surface water varied on a regular basis and, in remote sensing, the use of multispectral satellite data is known to be well suited for trend analysis given its high-spectral correlation with open water surfaces and the accuracy of mapping [40].

We used a rich time series of remote sensing data to gather further details about the scope of this study. The remote sensing data used in this study included the Climate Hazards Group InfraRed Precipitation With Station (CHIRPS) dataset (500 m spatial resolution), MODIS Terra Evapotranspiration (MOD16A2) (500 m spatial resolution), MODIS Terra

snow cover MOD10A1 (500 m spatial resolution), MODIS LST MOD11A1 (1 Km spatial resolution), MODIS NDVI MOD09GQ (250 m), Landsat TM/ETM+/OLI (30 m spatial resolution), SRTM (NASA SRTM Digital Elevation 30 m) were obtained from the online dataset provided by GEE. A framework of this study is presented in Figure 2.

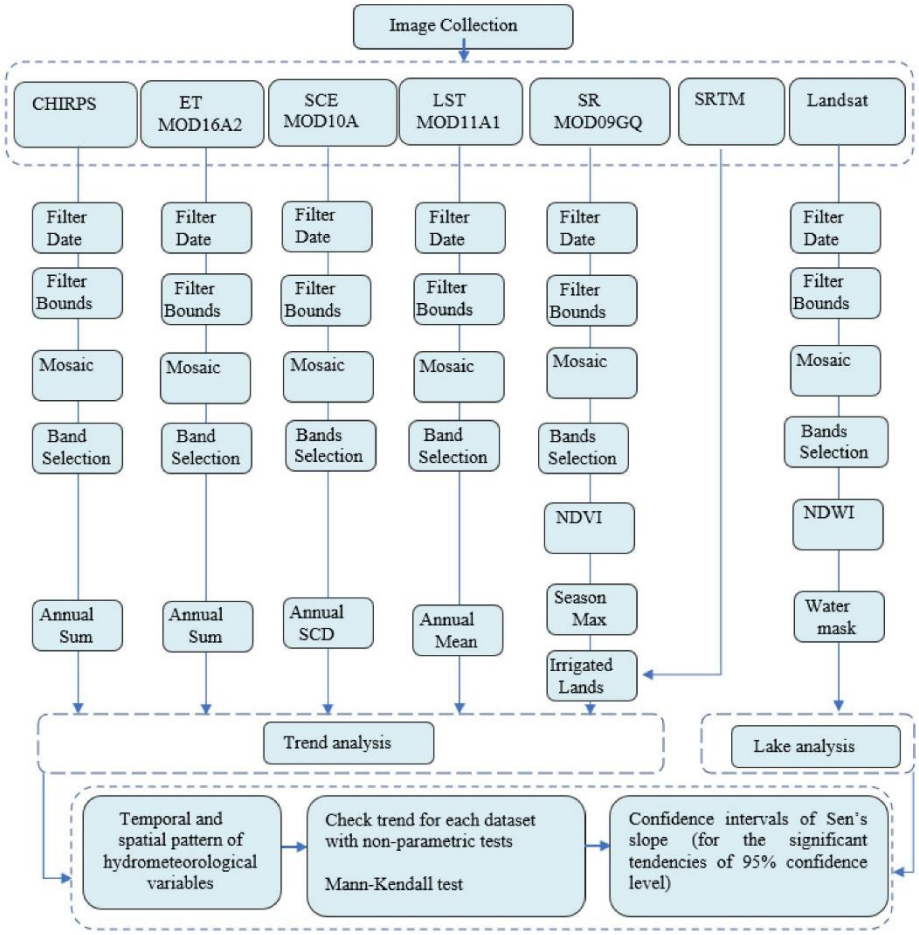

Figure 2. Flowchart of the methods.

In order to assess the effectiveness of the satellite-based rainfall data, different satellite-based rainfall data were examined. Table 2 demonstrates the results of descriptive statistics that show reasonable spatial agreement with gauge and gridded data. All the rainfall satellite datasets overestimated the stations' rainfall, with R^2 and Pearson correlation in the Sarakhs and Torbat-Jam stations varying from 0.71 and 0.85 for CHIRPS to 0.56 and 0.75 for ERA5, and from 0.77 and 0.88 for CHIRPS to 0.71 and 0.84 for GPM, respectively. The minimum RMSE was represented by CHIRPS (5.6 mm) for Sarakhs and CHIRPS (48.57 mm) for Torbat, whereas ERA5 exhibited maximum RMSE (35.59 mm) and (66.16 mm). CHIRPS was chosen for trend analysis as it represents better performance for all the gauge stations (Table 2); and it has a spatial resolution of 5 km which is more accurate compared to other

gridded rainfall data and has low systematic bias. Similarly, Land Surface Temperature (LST) overestimated the stations' temperature with R^2 0.66 and 0.61 and RMSE 9.25 °C and 4.56 °C in Torbat-Jam and Sarakhs stations, respectively.

Table 2. Comparing observed and gridded datasets' (CHIRPS, GPM and ERA5 for rainfall and LST for temperature) spatial similarities using statistical indices for the period from 2001 to 2020.

Statistical Measurements	Rainfall Station (mm), Sarakhs	Rainfall Station (mm), Sarakhs	Rainfall Station (mm), Sarakhs	Rainfall Station (mm), Torbat	Rainfall Station (mm), Torbat	Rainfall Station (mm), Torbat	Temperature Station (°C), Sarakhs	Temperature Station (°C), Torbat
	CHIRPS	**GPM**	**ERA5**	**CHIRPS**	**GPM**	**ERA5**	**LST**	**LST**
R2	0.71	0.74	0.56	0.77	0.71	0.73	0.61	0.66
Pearson's correlation	0.85	0.86	0.75	0.88	0.84	0.85	0.77	0.81
RMSE	25.27	34.28	35.59	48.57	49.23	66.16	4.56	9.25
Bias	5.6	19.7	−2.36	40.40	37.55	59.12	4.44	8.75
MBias	1.02	1.13	0.98	1.31	1.23	1.45	1.16	1.32

Figure 3a–f shows Pearson correlation for both observational and gridded data, revealing strong spatial agreement with CHIRPS. All three gridded datasets were well matched, although CHIRPS had greater agreement with the Sarakhs station (r = 0.85) and Torbat station (0.88) than GPM (0.86) and ERA5 reanalysis (0.75). Figure 3g–h illustrates the similar relationship with the LST datasets. According to the results, LST overestimated temperature for the two stations' data, Sarakhs and Torbat, in the region.

MODIS Data

LST is an extremely important parameter that controls the exchange of longwave radiation and sensible heat flux between the Earth's surface and the atmosphere. Therefore, trend analysis of LST is essential for the study of the hydroclimatology behaviour of basins. Generally, LST products are derived from thermal infrared (TIR) sensors (e.g., AVHRR, MODIS or METEOSAT) [41].

Among the TIR sensors, the LST products of MODIS aboard the Terra and Aqua platforms' data have high quality, global coverage and accurate geolocation [42]. Daily MODIS LST products [43] are retrieved at 1 km pixels by the generalised split-window algorithm. The daily average land surface temperature was extracted from the MODIS [44].

Because of snow's influence on Earth's climate and its role in supplying water resources, in many mountainous areas such as upstream of Doosti Dam, it is necessary to monitor snow cover extent (SCE) and snow properties in both high temporal and spatial resolutions. For more than three decades, optical, infra-red (AVHRR, MODIS) and passive microwave satellite sensors (SSMI/S, AMSR-E) have been used to monitor the extent of snow areas effectively [45]. Although cloud cover often obscures the snow from visible/infra-red spaceborne sensors, due to high spatial and temporal resolution, the MODIS snow products (MOD10A1) [46] with a resolution of 500 m at daily scale are preferred for snow-cover monitoring.

To quantify the vegetation dynamics over space and time and derive the irrigated cultivated lands, MODIS surface reflectance (MODIS/Terra MOD09GQ) [47] with 250 m spatial resolution and daily temporal resolution was implemented from 2001 to 2021. Maximum NDVI maps in the periods of April to June and July to September were used to derive the cultivated areas in the winter and summer agriculture seasons, respectively. A threshold value of 0.5 for NDVI was considered as an indicator of the cultivated agriculture area. Considering the prevalence of surface irrigation in the region, the irrigated cultivated lands were derived by applying a defined elevation range from the river baseline on the DEM map. Topographic information, including the catchment's elevation, was collected

using the Shuttle Radar Topography Mission (SRTM) and digital elevation models (DEMs) 90 m from GEE. For evapotranspiration, MODIS/Terra Net MOD 16A2 evapotranspiration (version 6, 8 day L4 datasets) was launched from 2000 with a pixel resolution of 500 m applied [48].

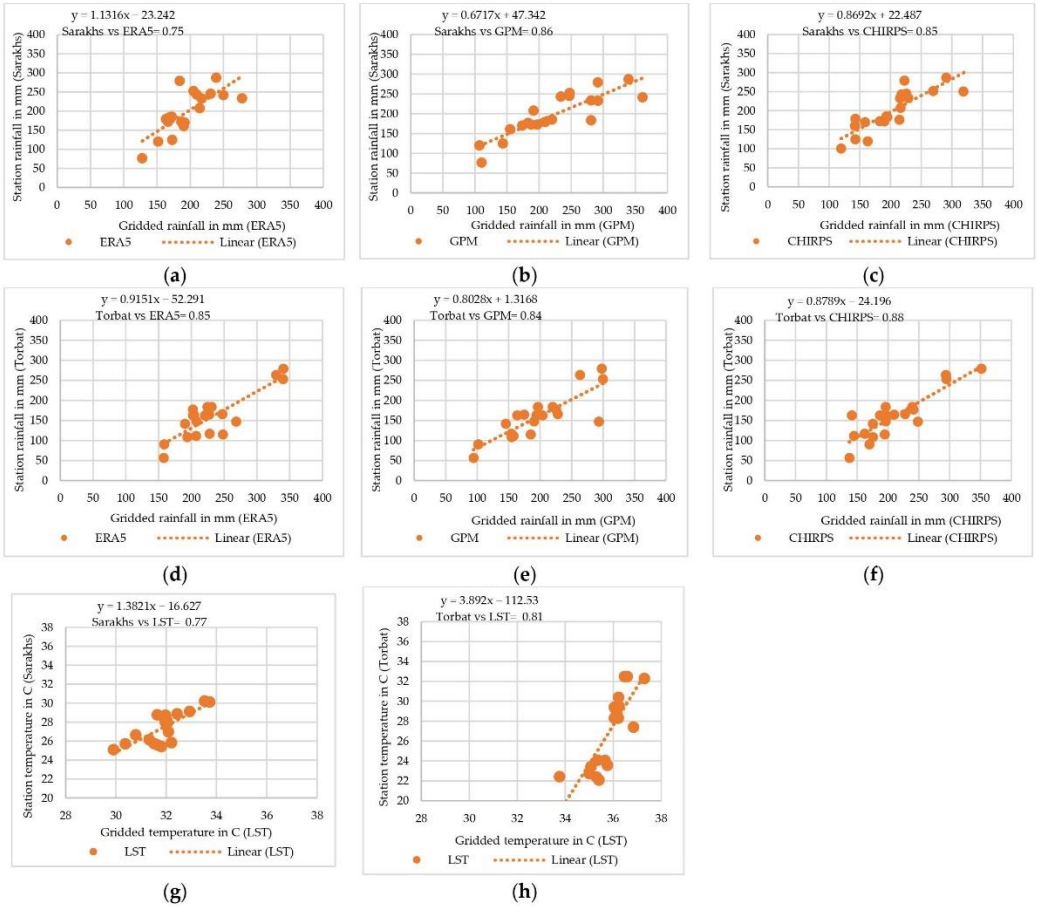

Figure 3. The relationship between gauge datasets and the gridded rainfall (**a**–**f**) and relationship between gauge datasets and LST (**g**–**h**) for the period from 2001 to 2020.

Landsat Images

Water surface areas are regularly determined from optical satellite imagery such as MODIS and Landsat products [49,50]. Changes in lake distribution have been monitored using the MODIS and Landsat datasets [51]. Landsat has a high resolution (30 m), which is its main benefit, but it also has a low repetition frequency [4]. To produce the water mask of the Doosti reservoir, NDWI maps derived from Landsat images from 2001 to 2020 were implemented. Landsat images consisting of ETM+ [52] and OLI data were acquired from GEE. NDWI maps [53,54] were generated based on Green [55] and NIR bands, and the pixels with positive value were assigned as water class. Specifications of all satellite data used in this research are listed in Table 3. A code was developed within the GEE environment to compute the time series of lake area statistics (maximum, minimum, mean and standard deviation) from 2004 to 2021.

Table 3. Specifications of used datasets of satellite imagery available in Google Earth Engine.

Parameters	Temporal Resolution	Product Information	Spatial Resolution	Time Period
CHIRPS	Daily	Climate Hazards Group InfraRed Precipitation with Station Data (Version 2.0 final)	5 km	2001–2021
GPM	Daily	Global Precipitation Measurement (GPM)	10 km	2001–2020
ERA5		European Centre for Medium-Range Weather Forecasts (ECMWF) Climate Reanalysis	25 km	2001–2020
MODIS Terra	Daily Daily Daily 8-Day	Surface reflectance (MOD09Q) Snow cover (MOD10A1) Land Surface Temperature (MOD11A1) Evapotranspiration (MOD16A2)	250 m 500 m 1 km 500 m	2004–2021
Landsat 5 TM	16 days	Level 1	30 m	2004–2021
Landsat 7 ETM	16 days	Level 1	30 m	2004–2021
Landsat 8 OLI	16 days	Level 1	30 m	2013–2021
DEM	1	SRTM	90 m	-

2.3. Methods

The GEE platform contains a substantial amount of satellite data acquired by other missions and it also hosts other ancillary data such as digital elevation models, vector-based datasets, land cover and meteorological data [56]. Since data hosted by GEE is analysis-ready, the need for pre-processing is circumvented as these data have been found to be consistent over time and well-suited for time series analysis and estimating long-term trends [14]. By applying the date filter function to the image collections, the desired time periods (2004–2021) were separated from the whole datasets. The spatial filter function was used to limit the borders to the Doosti Dam watershed. Then, using the trend functions (Mann–Kendall, Sen's slope) in GEE, evaluation of the pixel-based long-term spatiotemporal trend for the gridded datasets was carried out to analyse the trend and its intensity. The Mann–Kendall expression (alpha 0.05 and Z statistics = 1.96, generated from the standard normal table) was used to assess the Sen's slope [57].

2.3.1. Mann–Kendall Trend and Sen's Slope Test

The Mann–Kendall (MK) and Sen's slope estimator was applied using programming in GEE to compute the long-term magnitude of change on hydroclimate datasets and their statistical significance. The MK statistical test [58–60] was used to quantify the significance of trends in meteorological time series [57,61]. The MK test null hypothesis (H0) says that there is no monotonic trend at the specified level of significance. This may be used to detect the monotonic trend in a time series. In this test, the alternative hypothesis (Ha) suggests that the data exhibit a monotonic trend over time that is described by Equation (1):

$$S_{(k,\ l)} = \sum_{i=1}^{n-1} \sum_{j=i+1}^{n} sgn\left(X_{j(k,\ l)} - X_{i(k,\ l)}\right) \quad (1)$$

where n is the number of data points, $X_{i(k,\ l)}$ and $X_{j(k,\ l)}$ are the data values in the time series i and j ($j > i$), respectively, k and l indicate point location in the data matrix and $sgn\left(X_{j(k,\ l)} - X_{i(k,\ l)}\right)$ is the sign function, as illustrated in Equation (2).

$$sgn\left(X_{j(k,\ l)} - X_{i(k,\ l)}\right) = \begin{cases} +1 & if \quad X_{i(k,\ l)} - X_{j(k,\ l)} > 0 \\ 0 & if \quad X_{i(k,\ l)} - X_{j(k,\ l)} = 0 \\ -1 & if \quad X_{i(k,\ l)} - X_{j(k,\ l)} = 0 \end{cases} \quad (2)$$

In cases where the sample size $n > 30$, the standard normal test statistic $Z_{S(l,k)}$ is computed using Equation (3):

$$Zs_{(k,\ l)} = \begin{cases} \frac{S_{(k,\ l)}-1}{\sqrt{Var\left(S_{(k,\ l)}\right)}} & if \quad S_{(k,\ l)} > 0 \\ 0 & if \quad S_{(k,\ l)} = 0 \\ \frac{S_{(k,\ l)}+1}{\sqrt{Var\left(S_{(k,\ l)}\right)}} & if \quad S_{(k,\ l)} < 0 \end{cases} \tag{3}$$

Positive values of $Z_{S(l,k)}$ indicate increasing trends while negative $Z_{S(l,k)}$ values show decreasing trends. A two-tailed test was conducted using the hypothesis test technique at alpha = 50% level of significance, with the null hypothesis being no monotonic trend in time series at the 95% level of significance ($H_0 : \tau = 0$) and the alternative hypothesis being a substantial monotonic trend in time series in the 95% significance level ($H_a : \tau = 0$) [62].

Sen's nonparametric method [63] was used to estimate the magnitude of trends in the time series:

$$T_{i(1,k)} = \frac{X_{j(1,k)} - X_{i(1,k)}}{j - m} \tag{4}$$

In this equation, X_j and X_k represent data values at time j and m, respectively, Consider

$$Q_{i(1,k)} = \begin{cases} T_{(N+1)/2} & N\ is\ odd \\ \frac{1}{2}\left(T_{N/2} + T_{(N+2)/2}\right) & N\ is\ even. \end{cases} . \tag{5}$$

A positive $Q_{i(1,k)}$ value represents an increasing trend and a negative $Q_{i(1,k)}$ value represents a decreasing trend over time.

2.3.2. Descriptive Statistics

To ensure high-quality satellite rainfall data with respect to station observed data, several statistical indices were employed to check the effectiveness and performance of satellite datasets [57]. Statistical measurements [6], including the correlation coefficient (R^2), bias, multiplicative bias root (MBias), mean absolute error (MAE) and root mean square error (RMSE), were performed to assess data distribution and the relative performance of the satellite datasets, thus ensuring high-quality satellite data (rainfall, lake water) with regard to gauge measurements as follows (Equations (6)–(9)):

$$R^2 = \left(\frac{\frac{1\sum_1^n (X_{obs} - X_{obs})(X_{sat} - X_{sat})}{n}}{X_{obs} \times X_{sat}}\right)^2 \tag{6}$$

$$\mathrm{RMSE} = \sqrt{\sum_1^n \frac{(X_{sat} - X_{obs})^2}{n}} \tag{7}$$

$$\mathrm{Bias} = \frac{\sum_1^n (X_{sat} - X_{obs})}{n} \tag{8}$$

$$\mathrm{MBias} = \frac{\sum_1^n (X_{sat})}{\sum_1^n (X_{obs})} \tag{9}$$

In which, X_{obs} and X_{sat} show the gauge and satellite time series, respectively; n is the total number of observations; and $\overline{X}_{obs}$ the average of station values.

3. Results

3.1. Temporal Pattern of Different Hydroclimatic Factors

The underlying structure of the Doosti Dam basin's images, monitored from 2004 to 2021, was investigated (Figure 4). The satellite images reveal a downward trend until 2018.

Figure 4 shows the extent of the Doosti Dam's reservoir in the early spring of the years between 2004 and 2021. As illustrated in Figure 4, the water stored in the dam reservoir has decreased over time from 2013 to 2018, which is a sign of the reduction in water input. During these 18 years, the reservoir has had the lowest area in 2018 and the highest area in the early spring of 2009–10.

3.2. Spatiotemporal Distribution of Rainfall in the Doosti Dam Basin (2004–2021)

To identify the trends of precipitation and provide better insight into how precipitation is distributed over the catchment, the spatial–temporal variation of the annual CHIRPS precipitation [64] for the period of 2004–2021 is displayed in Figure 5. In this figure, the areas with the highest precipitation are shown in red and the areas with the lowest precipitation are colored light orange. Rainfall is highest in the mountainous region southeast of the catchment, located mainly on the Turkmenistan borders, upstream (500 mm) especially in 2009, 2011, 2015, 2019 and 2020. However, in lower elevation areas, the basin downstream experienced the lowest rainfall (100 mm). The annual precipitation varied from 100 mm to approximately 600 mm. The effects of climate change at a local level must be evaluated because it is a global issue and analysing rainfall trends is a necessary first step in determining how climate change may affect the availability of water and food security. The years 2018, 2019 and 2009 experienced the maximum increase (600 mm) in the whole basin, especially the mountainous areas in the west and east. The years 2005, 2008 and 2021 experienced marked minimum rainfall (100 mm). The results also confirm that the mountainous regions of the basin are the wettest regions.

Figure 6 shows the spatial distribution of trends in the annual precipitation based on CHIRPS estimates for the period from 2004 to 2021. The spatial pattern of the MK test shows that precipitation increased in most regions of the Doosti Dam's basin (Figure 6a), and from the statistical point of view, this trend is significant at a 95% level of confidence for annual precipitation. Figure 6b, shows an increasing trend in rainfall in the middle and west regions of the basin with a Sen's slope calculation which varies from 0.00043 (upper limit) to −0.00012 (lower limit) (p-value < 0.05) for upward and downward trends for the significant tendencies at 95% confidence level, respectively. Moreover, a statistically significant increasing tendency was detectable across the center and downstream of the region (+0.00043). The p-value is less than alpha = 0.05, indicating that there was a trend in the time series. So, the results clearly demonstrate that in most parts of basin, especially center to downstream (p-value = 0.5), an upward trend with a 95% confidence level is observed; however, there was no significant trend in the upstream, as illustrated in Figure 6c. In Figure 6b, the Sen's slope and MK test indicate that rainfall trends show climate change has occurred in the basin.

3.3. Spatio-Temporal Distribution of Temperature (LST) in the Doosti Dam Basin (2004–2021)

Temperature extremes are detrimental to agriculture, health, and infrastructure such as hydraulic structures and economic activity. This study investigates the annual temperature distribution and trend of LST from the MODIS Terra (MOD11A1) for the period 2004–2020. As predicted, temperature is strongly influenced by elevation. Figure 7 shows that the highest annual LST (averaging 30.85 °C) occurred at the lowest elevation level surface (Doosti Dam's basin upstream). As shown in this figure, LST follows the topography of the earth, and the highest elevation areas have lower temperatures (Doosti Dam's basin upstream). Most agricultural lands are located alongside the Doosti Dam's river downstream, where higher temperatures were observed. The temperature varied from 26.85 °C to 36.85 °C. There is greater annual spatial variability at the lower elevation area, ranging between 31.85 °C and 41.85 °C. The results also illustrate that the central south area of the basin experienced the highest temperatures for the period 2004 to 2021.

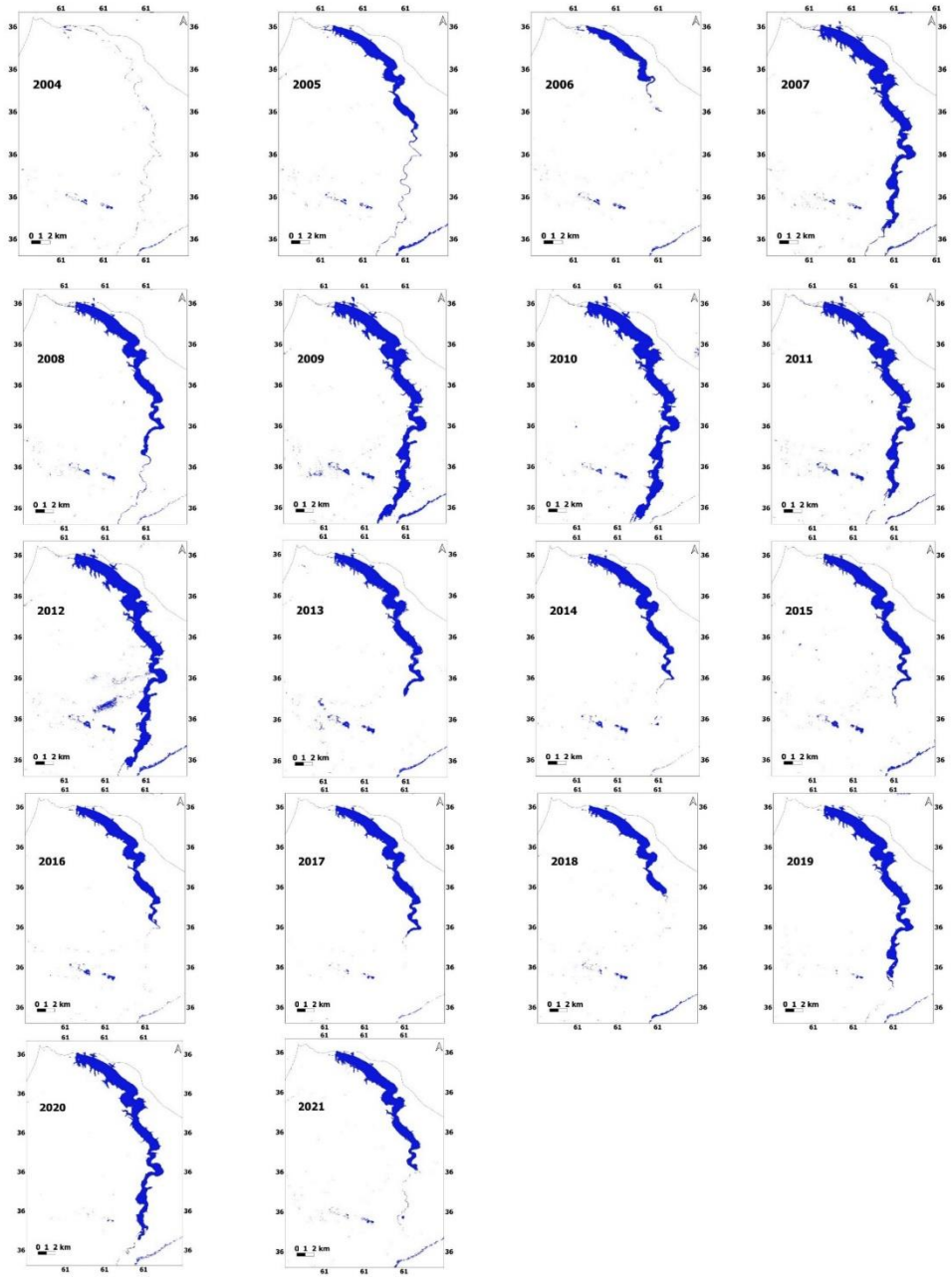

Figure 4. Area of Doosti Dam's reservoir from 2004 to 2021 using GEE.

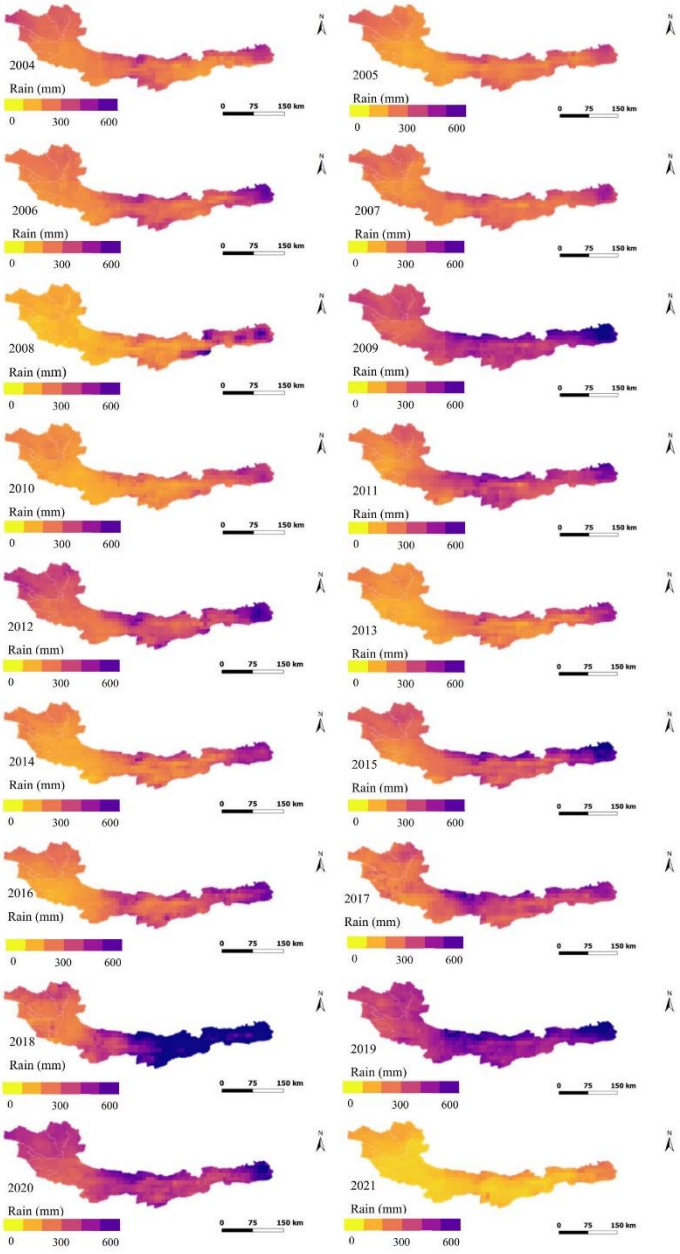

Figure 5. The spatial–temporal distribution of annual rainfall (mm) from the CHIRPS product derived from GEE in the period of 2004–2021.

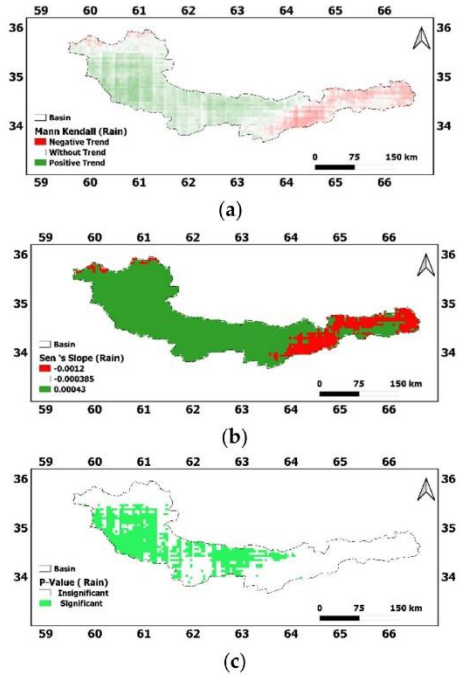

Figure 6. (**a**) Spatial distribution map of trend status of precipitation based on CHIRPS using Kendall estimator, (**b**) spatial distribution of trend intensity of precipitation (mm) using Sen's slope estimator (Z = 1.96 at 95% confidence level), (**c**) spatial distribution of trend significance using p factor, over the 18-year period (2004–2021) at Doosti Dam's basin.

Figure 8a shows the spatial distribution of trends in the annual temperature, based on MODIS (MOD11A1) estimates for the period between 2004 and 2021. The spatial pattern of the Mann–Kendall test showed that temperature decreased in the centre to east of the Doosti Dam's basin (Figure 8a) with a 95 % confidence level, as shown in Figure 8c (p-value < 0.05). The increase in slope of temperature distinguished by Sen's slope is illustrated in Figure 8b. LST exhibits a variation of 29 °C to 31.85 °C, with low annual precipitation varying from 100 mm to 400 mm, indicating that agriculture in these areas is not possible without irrigation.

3.4. Spatio-Temporal Distribution Annual Evapotranspiration from MODIS in the Doosti Dam's Basin (2004–2021)

An analysis of annual distribution and the trend of evapotranspiration offers a more detailed illustration of the increase in water demand causing more water deviation from the river. Figure 9 depicts the importance of evapotranspiration losses which varied from 100 to 200 mm in the basin. From this figure, it can be seen that the periods from 2004 to 2008 had low evaporation loss areas, while the period from 2009 to 2020 experienced high water demand. It also shows that the high elevation areas were underwent higher evapotranspiration (near 200 mm) than the downstream areas (Iranian side). The river line in the center shows the slight and constant evapotranspiration and water demand expanding from the west to the east. Mean annual evapotranspiration (2005–2020) in the Doosti Dam River was observed to be 200 mm across the basin. Interestingly, both precipitation and evapotranspiration have almost identical trends. The precipitation and evapotranspiration exhibited the highest increases in the year 2009 (~500 mm) and (~170 mm), and for year

2019 (~550 mm) and (~200 mm), respectively. This also confirms that the whole basin represents an increasing trend, especially the mountainous areas in the east and alongside the river.

Figure 10 shows the spatial distribution of trends in the annual evapotranspiration based on the MODIS product (MOD16A2) estimates for the period from 2004 to 2021. The spatial pattern of the MK test shows that evapotranspiration is rising in the whole region of the Doosti Dam's basin (Figure 10a), and from the statistical point of view, this increasing trend is significant with the positive trend at a 95% level of confidence for annual evapotranspiration. In Figure 10b, evapotranspiration is observed to have an increasing trend (+0.00043) during the years 2004–2021 in the whole study area.

This figure reveals a rising trend in evapotranspiration in the regions of the basin with a Sen's slope calculation which varies from +0.00043 (upper limit) to −0.0012 (lower limit) for upward and downward trends for the significant tendencies at a 95% confidence level, respectively. Moreover, a statistically significant increasing tendency is detectable across the region (+0.00043). Figure 10c shows that evapotranspiration rose in the whole basin as the *p*-value is less than alpha = 0.05 and with a 95% level of confidence which is significant. This figure also confirms a significant rise in the trend ($p < 0.05$) of evapotranspiration values from 2004 to 2021. The increasing trend in evapotranspiration during the years 2004–2021 is almost identical to the rainfall trend.

3.5. Spatio-Temporal Distribution Annual Snow Cover Duration from MODIS in the Doosti Dam's Basin (2004–2021)

In areas with higher elevations, the MODIS/Terra sensor has ample capability to detect SCD. The MODIS/Terra 8-day snow cover product (MOD10A1) was used to monitor the SCD maps in the Doosti Dam's river basin (Figure 11). The effects of elevation on annual SCD for the period of 2004–2021 was observed in this figure as lower elevation regions experienced less snow cover throughout the period.

The SCD varied from zero to nearer 100 % and followed the topography. Figure 10 indicates the variation of snow pixel numbers (SPN) as an indicator of SCE and in the region and the extent of Doosti Dam's reservoir for the period of 2004 to 2021. Maximum SCD occurred in the high elevated areas (50%). Although statistically insignificant, it indicates that the yearly snow cover generally decreased somewhat at higher elevations and remained constant at lower elevations (approximately 20%). The whole basin (especially the mountainous areas) received the SCD (50%) in the year 2008.

Figure 12 shows the spatial distribution of trends in the annual evapotranspiration based on MOD10A1 estimates for the period from 2004 to 2021. The spatial pattern of the MK test shows that snow cover duration had no significant trend in a large area of the basin (Figure 12a) and in Figure 12c no trend was identified for most of Doosti Dam's basin; however, the significant trend was recognised upstream.

Figure 12b shows a decreasing trend for SCD in the western part of the basin with a Sen's slope calculation of −0.0012 (lower limit) indicating a downward trend for the significant tendencies at a 95% confidence level.

3.6. Spatio-Temporal Distribution for Summer Irrigated Cultivated Areas in the Doosti Dam Basin (2001–2021)

The map presented in Figure 13 shows the irrigated cultivated areas for the summer growing season. Figure 13a demonstrates that irrigated land predominates in the water management region along the Doosti Dam's river. The dominance of the irrigated region supports the fact that irrigation receives most of the freshwater resources available. The irrigated cultivated areas in both the winter and summer growing seasons were extracted by deriving the maximum NDVI maps in the winter (APR–JUN) and summer (JUL–SEP) growing seasons and applying threshold values to the NDVI maps and elevation from Doosti Dam's river basin baseline. It also shows that the downstream and river line in the centre identify irrigated areas.

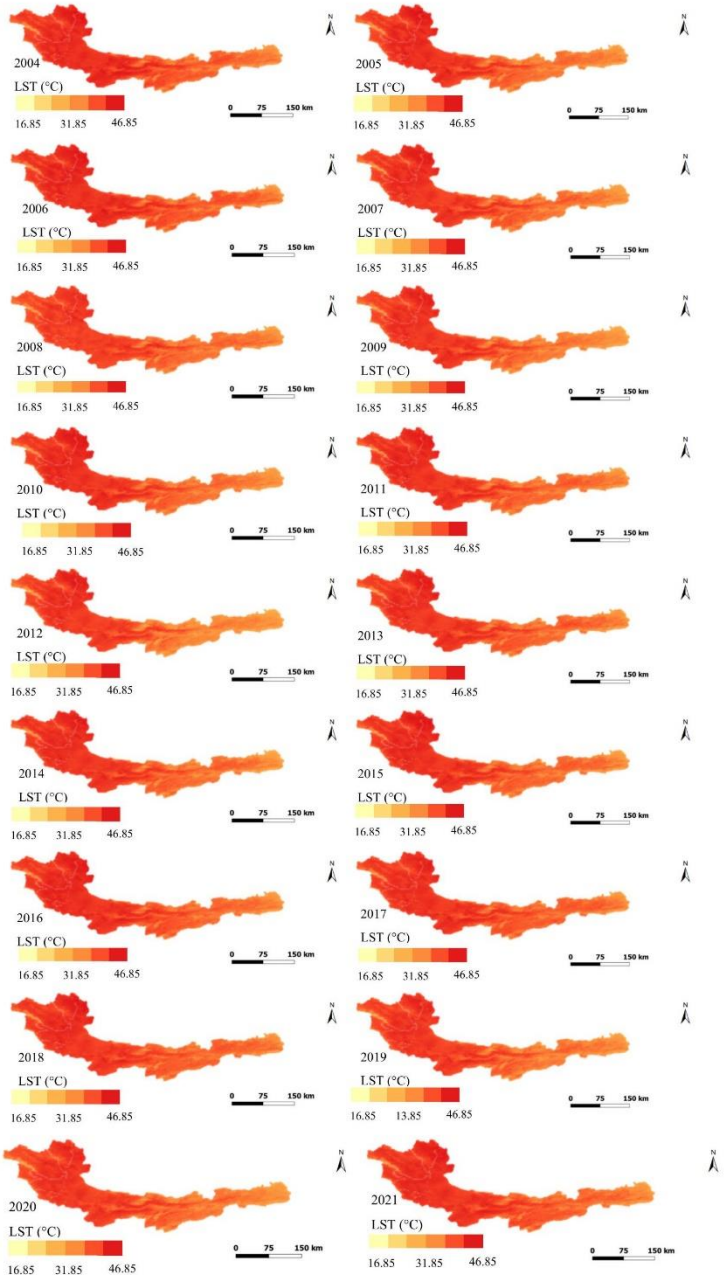

Figure 7. The spatial–temporal distribution of annual land surface temperatures (°C) from the MODIS (MOD11A1) product derived from GEE in the period of 2004–2021.

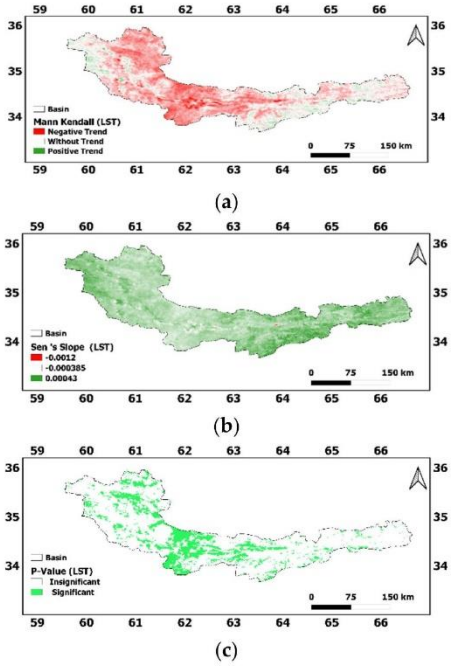

Figure 8. (**a**) Spatial distribution map of trend status of land surface temperature (°C) in the Doosti Dam's basin based on MODIS LST dataset (MOD11) using Kendall estimator, (**b**) spatial distribution of trend intensity of LST (°C) using Sen's Slope Estimator (Z = 1.96 at 95% confidence level), (**c**) spatial distribution of significant trends using p factor, over the 18-year period (2004–2021) in the Doosti Dam's basin.

Figure 13b illustrates the strong correlation between irrigated areas in summer and precipitation. The cultivated areas increased from 451 km^2 to 1029 km^2 as a result of increase in rainfall from 272 mm to 375 mm during 2004 to 2020. This increase does not necessarily indicate a change in the amount of land irrigated; it just indicates that certain agricultural areas that were not irrigated before 2017 were irrigated in 2018. Agriculture's status as a vital industry in the basin, permitting it to continue working throughout the COVID-19 pandemic lockdown period, is the key contributing factor in the increases in the irrigated area in 2020. Since many individuals lost their other means of income during lockdown, agriculture emerged as a substitute.

It is worth mentioning that the cultivated areas ranging from 2001 to 2020 containing three months of data for summer and winter are from January to January, respectively. From Figure 13b, it can be seen that in the periods from 2001 to 2005, the cultivated areas tripled from 200 km^2 to 600 km^2 and between 2006 and 2018, the cultivated areas fluctuated. Between 2006 and 2018, high rainfall in 2009 (343 mm) and 2012 (384 mm) exhibited an increase in the cultivated areas for the basin and subbasin from 320 km^2 to 530 km^2 in 2009 and, 430 km^2 to 630 km^2 in 2012, respectively. Moreover, irrigated areas witnessed a sharp increase for the basin and subbasin which varied from 350 km^2 (2018) to 1029 km^2 (2020) and from 250 km^2 (2018) to 800 km^2 (2020), respectively.

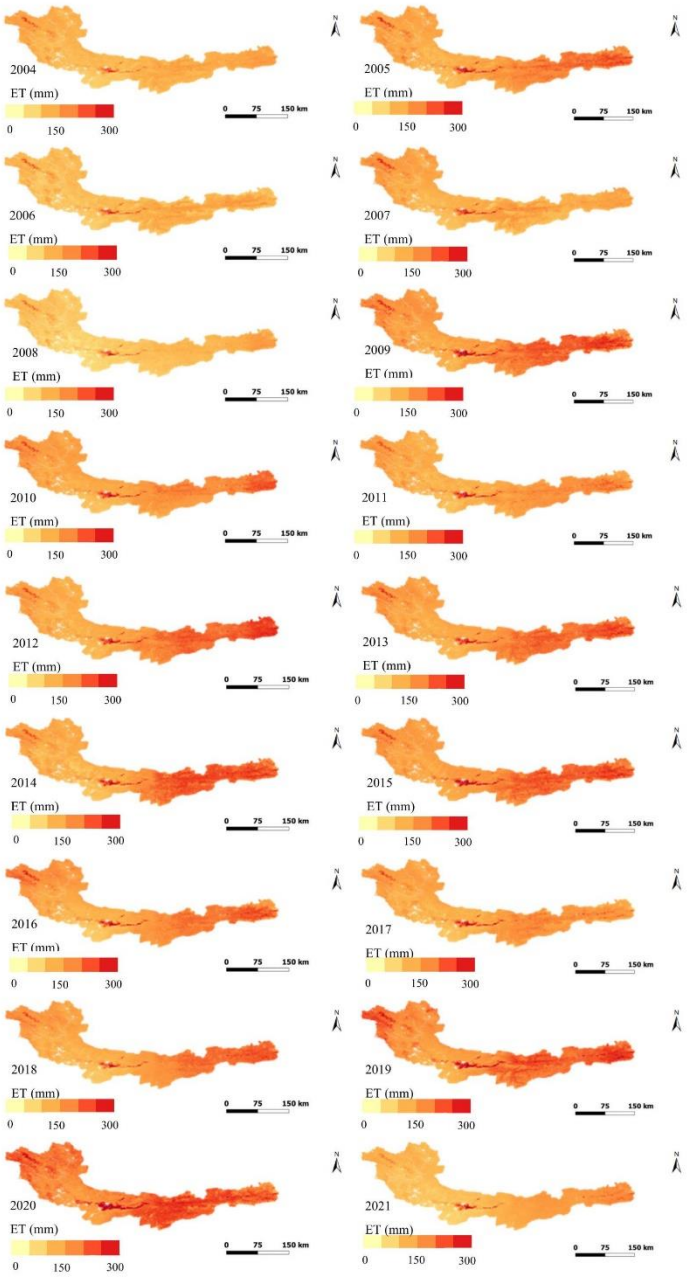

Figure 9. The spatial–temporal distribution of annual evapotranspiration (mm) from the MODIS product (MOD16A2) derived from GEE in the period of 2004–2021.

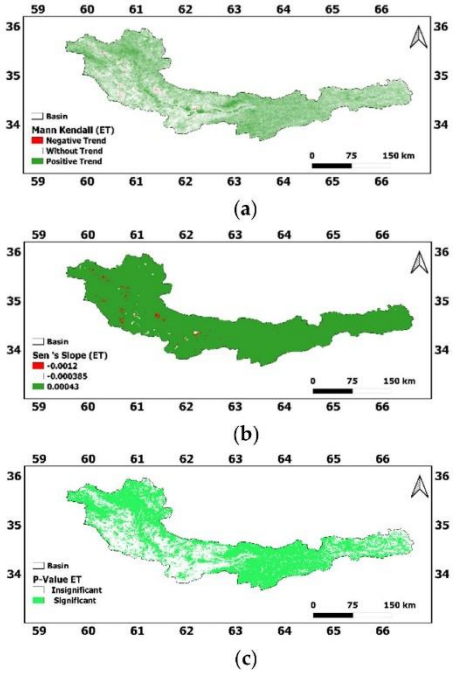

Figure 10. (**a**) Spatial distribution map of trend of annual evapotranspiration (mm) over the Doosti Dam's basin based on MODIS evapotranspiration dataset (MOD16A2) using Kendall estimator, (**b**) spatial distribution of trend intensity of evapotranspiration (mm) using Sen's slope estimator (Z = 1.96 at 95% confidence level), (**c**) spatial distribution of trend significance using p factor, over the 18-year period (2004–2021) for the Doosti Dam's basin.

Figure 13c shows a significant ascending trend in the irrigated areas in the summer season which is an indicator of an increase or densification of vegetation cover in this region. Interestingly, both the irrigated areas and Doosti Dam's Lake showed an identical trend for the highest increase for the year 2006 (320 km^2) and (56 km^2), and the year 2020 (800 km^2) and (45 km^2), respectively. This also confirmed that whole basin experienced an increase in irrigated areas alongside the Doosti Lake.

3.7. Spatio-Temporal Distribution Winter Irrigated Cultivated Areas in the Doosti Dam Basin's (2001–2020)

The map presented in Figure 14 shows the irrigated cultivated areas for the winter growing season. Figure 14a illustrates that irrigated land predominated in the water management region. During the winter season, the cultivated areas increased from 632 km^2 to 1563 km^2 as a result of increased rainfall from 273 mm to 400 mm over the period 2004 to 2020 (Figure 14b). Figure 14c represents a sharp ascending trend in the irrigated areas in the winter season, which is an indicator of an increase in cultivated areas along the Doosti Dam Lake. The irrigated areas and Doosti Dam's Lake showed similar trends with the highest increase in the year 2020 (985 km^2) and (45 km^2) over the 20 years, respectively.

Although the irrigated areas in the winter growing season were significantly higher compared to the summer season, the trend of changes in the cultivated areas from 2011 to 2018 was not significant (Figure 13b and 14b).

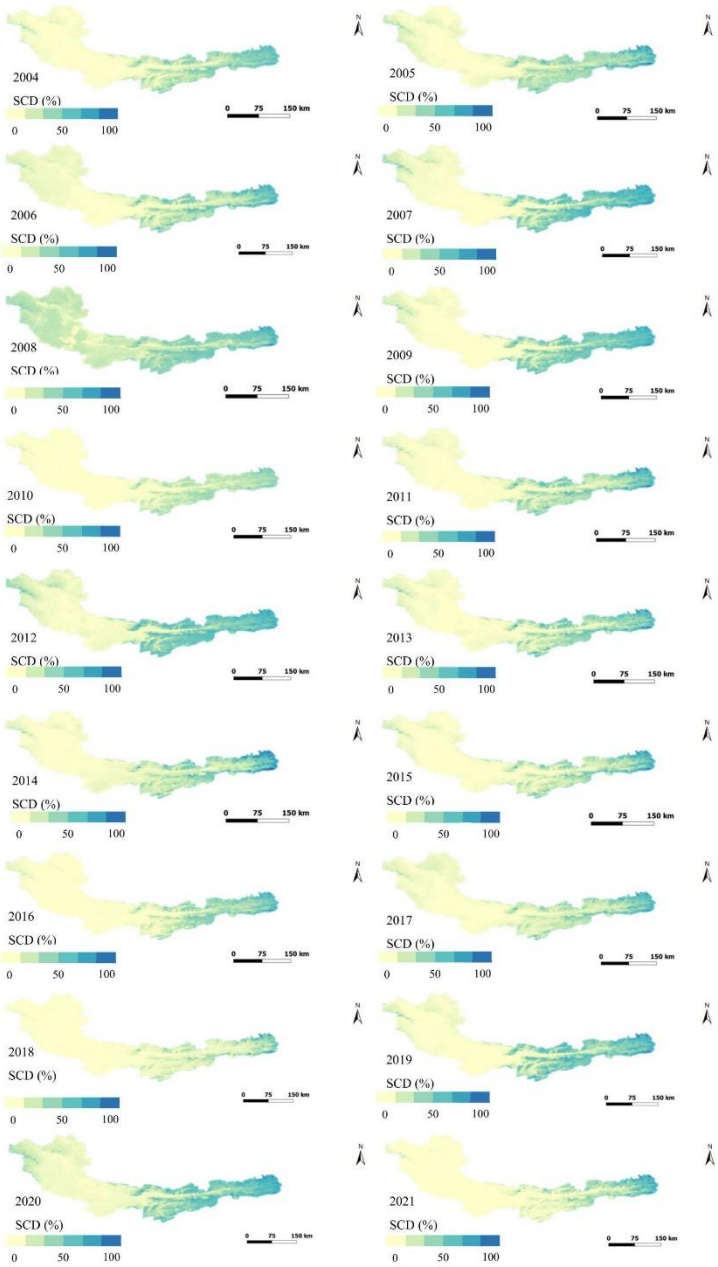

Figure 11. The spatial–temporal distribution of annual snow cover duration (%) from the MODIS (MOD10A1) product derived from GEE in the period of 2004–2021.

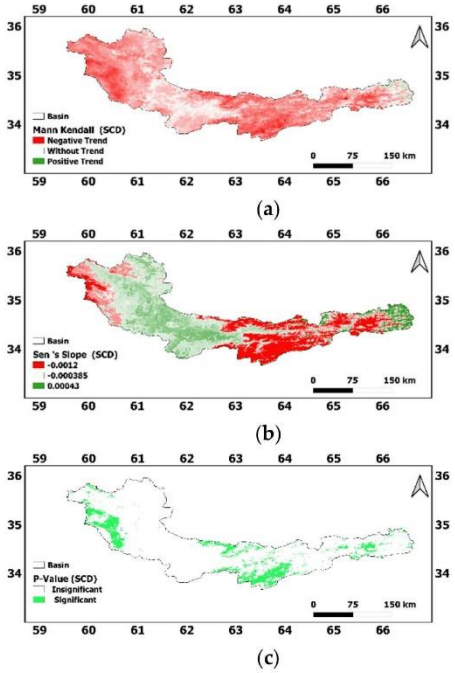

Figure 12. (**a**) Spatial distribution map of trend status of snow cover duration (%) over the Doosti Dam's basin based on the MODIS product (MOD10A1) derived from GEE using Kendall estimator, (**b**) spatial distribution of trend intensity of SCD (%) using Sen's slope estimator (Z = 1.96 at 95% confidence level), (**c**) spatial distribution of trend significance using p factor, over the 18-year period (2004–2021) for the Doosti Dam's basin.

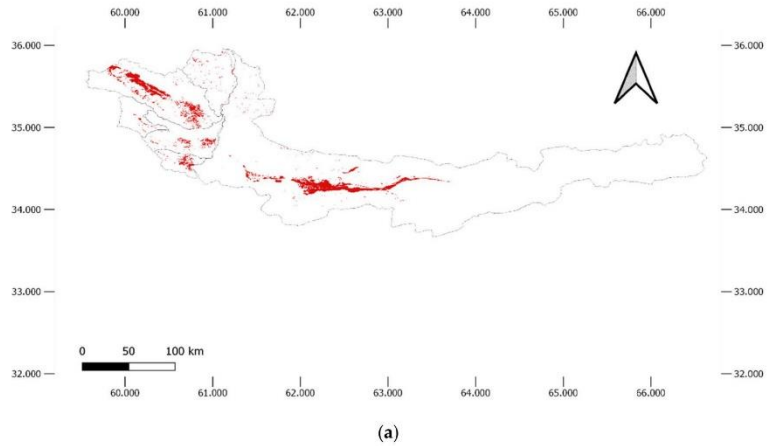

Figure 13. *Cont.*

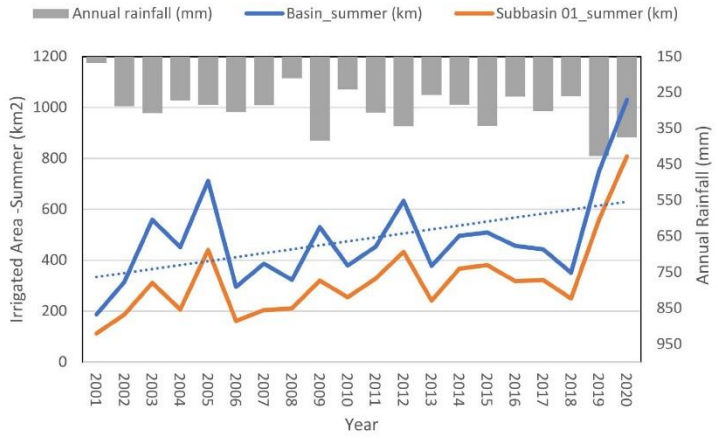

(**b**)

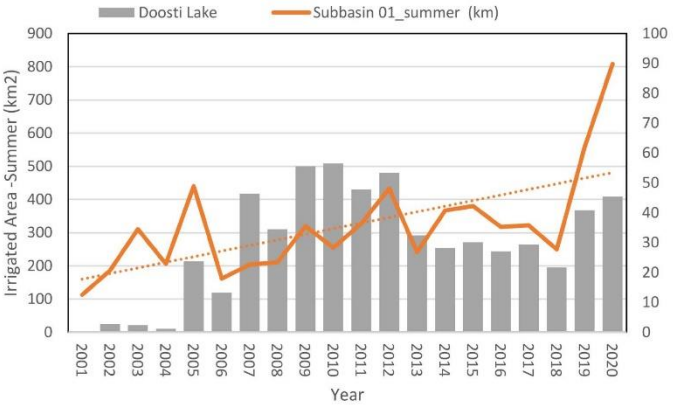

(**c**)

Figure 13. (**a**) Spatial distribution of irrigated cultivated lands in Doosti Dam's basin as well as changes that occurred between 2001 and 2020, (**b**) correlation between rainfall (CHIRPS), irrigated cultivated areas of basin (km^2) in summer growing season based on the MODIS NDVI (MOD09Q) product derived from GEE during 2001–2020 (**c**) Correlation between rainfall time series (CHIRPS), irrigated cultivated areas (km^2) of subbasin in summer growing season and Doosti lake based on Landsat, NDWI index product during 2001–2020.

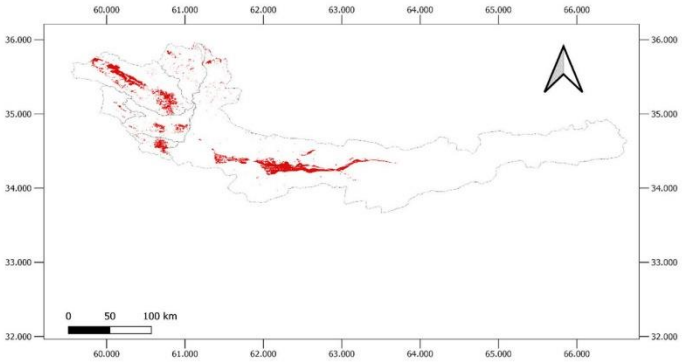

(**a**)

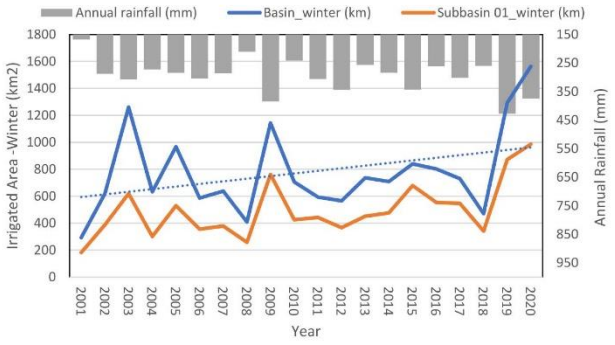

(**b**)

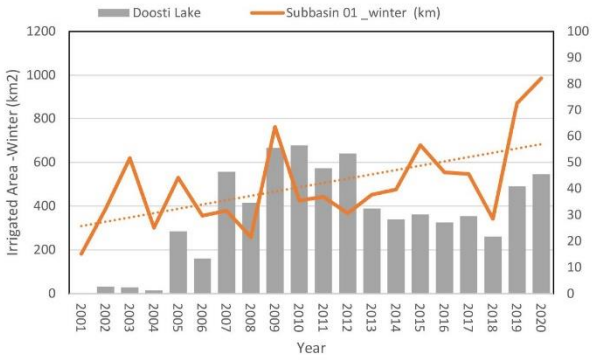

(**c**)

Figure 14. (**a**) Spatial distribution of irrigated cultivated lands in Doosti Dam's basin as well as changes that occurred between 2001 and 2020, (**b**) correlation between rainfall (CHIRPS), irrigated cultivated areas of basin (km^2) in winter growing season based on the MODIS NDVI product (MOD09Q) derived from GEE during 2001–2020, (**c**) correlation between rainfall time series (CHIRPS), irrigated cultivated areas (km^2) of subbasin in winter growing season and Doosti lake based on Landsat, NDWI index product during 2001–2020.

4. Discussion

Using three-gauge measurements and multi-hydroclimatic gridded datasets at various elevation ranges (from 278 m to 4163 m), this study analyses trends and spatiotemporal variability in multi-hydroclimatic variables over the past two decades. A significant increasing trend in precipitation is apparent over the eastern regions of Iran leading to a positive annual trend over the pixels [30]. Unlike the findings of previous studies [37,65], temperature demonstrated a slight decrease, which might be as a result of the different research periods and various precipitation dataset types (point and pixel-based) employed for trend analysis. Indeed, while a satellite product calculates precipitation variables across a region, a rain gauge measures variables at a particular location [30]. The investigation of the trends of evapotranspiration indicated the positive increasing trend over the regions of Iran, confirming the results of a previous study in Iran [66].

Snow cover generally declined slightly over the period 2004–2021, higher elevation areas experienced an increase in SCA alongside a declining temperature trend [67,68]. Land-use changes and the construction of dams, reservoirs and irrigation canals have been identified as the primary anthropogenic activities causing variations in runoff [69]. Irrigated areas in both the winter (APR-JUN) and summer (JUL-SEP) growing seasons increased through the nonparametric tests across the basin. Human activities increased the irrigated areas and so are considered to be the most significant possible driver of the diversion of runoff in the basin [69]. The results also confirmed that the strong correlation between precipitation and irrigated areas and both irrigated areas and the Doosti lake showed an identical trend.

The GEE platform has two advantages: (1) due to data limitations in the inaccessible, sparsely gauged basin, it facilitated data collection in some regions which have few weather stations and (2) it enabled us to process and analyse numerous hydroclimatic variables, including land use, snow cover, lake reservoir, evapotranspiration, integrating the publicly available big geospatial data.

Considering the spatiotemporal variability of numerous hydroclimatic variables in data-sparse regions, this research provides insights for the policy-maker seeking mitigation strategies. On the other hand, the lack of access to long-term data of consistently high quality, missing data and data with inadequate spatial and temporal coverage could have a detrimental impact, leading to poor decision making. The absence of in situ measurements for other hydroclimatic variables, in addition to temperature and precipitation, is another limitation of this study.

As we only covered the trends with the MK and Sen's slope, investigating season–trend fit models such as antileakage least-squares spectral analysis [70–72] or least absolute shrinkage and selection operator (LASSO) [73] is recommended. The Mann–Kendall test's essential requirement is that the data should be independent and mostly applied to an annual-scale time series [30,37,61]. Therefore, before applying the Mann–Kendall test, any positive or negative autocorrelation of the data should be removed [74]. Moreover, in this research, Mann–Kendall was applied to annual-scale time series, so seasonality is not present in annual-scale time series. However, prior to annual trend analysis, the autocorrelation test was applied to ensure that there was no seasonality present and to eliminate any existence of an autocorrelation impact on the data [75]. Furthermore, probable changes in the future are generally studied by general circulation models (GCMs) [76–78] and scenarios [79,80]. However, climate projections are uncertain for the detection of extremes [81]. The probable changes in environmental flow release can be assessed by applying the downscaled outputs of multi-GCMs forced into hydrological models [82] under a non-stationary assumption [83], which can be further studied in the future. Hence, study under non-stationary assumptions to reduce the damage caused by climate change and human activities is suggested.

5. Conclusions

Given the high spatial and temporal variations in hydroclimatic variables in transboundary regions, it is necessary for water resource decision-makers to understand the hydroclimatic behaviours through the analysis of the variables' heterogenicity. This study investigated the spatiotemporal aspects of numerous hydroclimatic variables based on GEE at the transboundary level. The nonparametric statistical tests (MK and Sen's slope) were applied coupled with an advanced web-based cloud computing platform (GEE) to delineate the monotonic trend of data. This study provides a comprehensive understanding of the long-term trend of hydroclimatic variables. The spatial and temporal changes of hydrometeorological temperature (MODIS-Terra), evapotranspiration (MODIS-Terra), snow cover distribution (MODIS-Terra), MODIS Terra NDVI in relation to precipitation (CHIRPS), topography (DEM SRTM) and the LANDSAT NDWI index in the Doosti Dam's basin are presented for the period 2004 to 2021. The key findings of this study are as below:

(1) The study showed how well multisensory satellite data can be used to predict hydrometeorological spatiotemporal trends, especially in transboundary high elevation areas when accessing station-observed data is a major challenge. It demonstrated that, for most variables, these trends largely relied on elevation. This statistically upward trend was seen in rainfall, evapotranspiration, and lower temperature during the years 2004 to 2021, but did not have a remarkable effect on snow cover duration.

(2) This study was focused on understanding how the irrigated cultivated lands responded to different hydroclimatic variables. Because it is a transboundary region, has diverse topography and climate change conditions, the monitoring of the irrigated lands was difficult. Elevation had a significant influence on the climate and the Doosti Dam, situated at a lower elevation, was employed to comprehend the long-term spatiotemporal variability of the irrigated areas and related climatic and hydrological causes. NDVI derived from MODIS indicated the strong correlation between the NDVI and precipitation in the winter.

(3) Additionally, the findings demonstrate that GEE is an effective method for compiling and establishing the spatiotemporal fluctuations in various variables and that remotely sensed data products consistently represent ground observations in remote transboundary areas. It is anticipated that the socio-ecological system in this transboundary area would decline owing to unsustainable water management which will negatively affect the conditions of the residents. It is important to consider the environmental right of the lakes to improve the conditions in the transboundary river basin. GEE's potential has not yet been fully realised, despite the fact that it has gradually evolved into a platform for remote sensing research. With the help of GEE, this study offers a rapid and feasible method for determining spatiotemporal climatic trends. The methodology can be easily applied to other areas with comparable issues when combined with the tools made available by GEE. The results of this study can aid in the management of water resources and the preservation of the ecological environment in the Doosti Dam's basin and other transboundary regions.

(4) In an area characterised by a complicated set of interactions between precipitation, evapotranspiration, temperature, NDVI, snow cover, lake area and discharge, the overall findings of this study could guide water resource management strategies. Future research should take these elements into account in order to provide a full forecast of the spatiotemporal climatic dynamics of transboundary areas, especially in light of the current period of rapid climate change (both natural and anthropogenic).

Author Contributions: Conceptualisation, Hadis Pakdel-Khasmakhi, Majid Vazifedoust, Dev Raj Paudyal, Sreeni Cha-dalavada and Md Jahangir Alam; methodology, Hadis Pakdel-Khasmakhi and Majid Vazifedoust; software, Hadis Pakdel-Khasmakhi and Majid Vazifedoust; validation, Majid Vazifedoust and Hadis Pakdel-Khasmakhi; formal analysis, Hadis Pakdel-Khasmakhi and Majid Vazifedoust; in—vestigation, Hadis Pakdel-Khasmakhi and Majid Vazifedoust; resources, Hadis Pakdel-Khasmakhi; data curation, Hadis Pakdel-Khasmakhi; writing—original draft preparation, Hadis Pakdel-Khasmakhi; writing—review and editing, Dev Raj Paudyal, Sreeni Chadalavada, Md Jahangir Alam and Majid Vazifedoust; visualisation, Hadis Pakdel-Khasmakhi; supervision, Dev Raj Paudyal, Sreeni Chadalavada and Md Jahangir Alam; project administration, Dev Raj Paudyal, Sreeni Chadalavada and Md Jahangir Alam. All authors have read and agreed to the published version of the manuscript.

Funding: This research received no external funding.

Data Availability Statement: The data supporting the findings of this study are available from the first author upon reasonable request.

Acknowledgments: This research has been supported by the Graduate Research School, University of Southern Queensland and this is part of the first author's PhD project entitled "Variability of Extreme Climate Events and Impacts of Future Climate Change on the Streamflow". The authors would like to thank the reviewers and the editors who gave valuable time to review the manuscript.

Conflicts of Interest: The authors declare no conflict of interest. Jahangir Alam works at the MDBA; however, this research has no links with the MDBA.

References

1. Mianabadi, H.; Alioghli, S.; Morid, S. Quantitative evaluation of 'No-harm'rule in international transboundary water law in the Helmand River Basin. *J. Hydrol.* **2021**, *599*, 126368. [CrossRef]
2. Al-Faraj, F.A.; Scholz, M. Assessment of temporal hydrologic anomalies coupled with drought impact for a transboundary river flow regime: The Diyala watershed case study. *J. Hydrol.* **2014**, *517*, 64–73. [CrossRef]
3. Wu, J.; Liu, Z.; Yao, H.; Chen, X.; Chen, X.; Zheng, Y.; He, Y. Impacts of reservoir operations on multi-scale correlations between hydrological drought and meteorological drought. *J. Hydrol.* **2018**, *563*, 726–736. [CrossRef]
4. Gao, H.; Birkett, C.; Lettenmaier, D.P. Global monitoring of large reservoir storage from satellite remote sensing. *Water Resour. Res.* **2012**, *48*, 1–12. [CrossRef]
5. Moreno, M.; Bertolín, C.; Ortiz, P.; Ortiz, R. Satellite product to map drought and extreme precipitation trend in Andalusia, Spain: A novel method to assess heritage landscapes at risk. *Int. J. Appl. Earth Obs. Geoinf.* **2022**, *110*, 102810. [CrossRef]
6. Pakdel Khasmakhi, H.; Vazifedoust, M.; Marofi, S.; Tizro, A.T. Simulation of river discharge in ungauged catchments by forcing GLDAS products to a hydrological model (a case study: Polroud basin, Iran). *Water Supply* **2020**, *20*, 277–286. [CrossRef]
7. Sadeghi Loyeh, N.; Massah Bavani, A. Daily maximum runoff frequency analysis under non-stationary conditions due to climate change in the future period: Case study Ghareh Sou Basin. *J. Water Clim. Chang.* **2021**, *12*, 1910–1929. [CrossRef]
8. Erazo, B.; Bourrel, L.; Frappart, F.; Chimborazo, O.; Labat, D.; Dominguez-Granda, L.; Matamoros, D.; Mejia, R. Validation of satellite estimates (Tropical Rainfall Measuring Mission, TRMM) for rainfall variability over the Pacific slope and Coast of Ecuador. *Water* **2018**, *10*, 213. [CrossRef]
9. Ma, L.; Liu, Y.; Zhang, X.; Ye, Y.; Yin, G.; Johnson, B.A. Deep learning in remote sensing applications: A meta-analysis and review. *ISPRS J. Photogramm. Remote Sens.* **2019**, *152*, 166–177. [CrossRef]
10. Ellsäßer, F.; Röll, A.; Stiegler, C.; Hölscher, D. Introducing QWaterModel, a QGIS plugin for predicting evapotranspiration from land surface temperatures. *Environ. Model. Softw.* **2020**, *130*, 104739. [CrossRef]
11. Zaki, A.; Buchori, I.; Sejati, A.W.; Liu, Y. An object-based image analysis in QGIS for image classification and assessment of coastal spatial planning. *Egypt. J. Remote Sens. Space Sci.* **2022**, *25*, 349–359. [CrossRef]
12. Wang, C.; Jia, M.; Chen, N.; Wang, W. Long-term surface water dynamics analysis based on Landsat imagery and the Google Earth Engine platform: A case study in the middle Yangtze River Basin. *Remote Sens.* **2018**, *10*, 1635. [CrossRef]
13. Dastour, H.; Ghaderpour, E.; Hassan, Q.K. A combined approach for monitoring monthly surface water/ice dynamics of Lesser Slave Lake via Earth observation data. *IEEE J. Sel. Top. Appl. Earth Obs. Remote Sens.* **2022**, *15*, 6402–6417. [CrossRef]
14. Gorelick, N.; Hancher, M.; Dixon, M.; Ilyushchenko, S.; Thau, D.; Moore, R. Google Earth Engine: Planetary-scale geospatial analysis for everyone. *Remote Sens. Environ.* **2017**, *202*, 18–27. [CrossRef]
15. Tamiminia, H.; Salehi, B.; Mahdianpari, M.; Quackenbush, L.; Adeli, S.; Brisco, B. Google Earth Engine for geo-big data applications: A meta-analysis and systematic review. *ISPRS J. Photogramm. Remote Sens.* **2020**, *164*, 152–170. [CrossRef]
16. Google Developers: Get Started with Earth Engine. Available online: https://developers.google.com/earth-engine/getstarted (accessed on 21 September 2022).
17. Mozafari, M.; Raeisi, E.; Zare, M. Water leakage paths in the Doosti Dam, Turkmenistan and Iran. *Environ. Earth Sci.* **2012**, *65*, 103–117. [CrossRef]

18. Majidi, M.; Alizadeh, A.; Farid, A.; Vazifedoust, M. Estimating evaporation from lakes and reservoirs under limited data condition in a semi-arid region. *Water Resour. Manag.* **2015**, *29*, 3711–3733. [CrossRef]
19. Rezaei Sekkeravani, D.; Chenari, S.; Faraji, M.; Dashti, s.F. Study the Iranian hydropolitical challenges in the shared drainage basins with Neighboring Countries. *IOSR J. Humanit. Soc. Sci. IOSR-JHSS* **2018**, *23*, 67–78. [CrossRef]
20. Akbari, M.; Mirchi, A.; Roozbahani, A.; Gafurov, A.; Kløve, B.; Haghighi, A.T. Desiccation of the transboundary Hamun Lakes between Iran and Afghanistan in response to hydro-climatic droughts and anthropogenic activities. *J. Great Lakes Res.* **2022**, *48*, 876–889. [CrossRef]
21. Salomon, J.; Hodges, J.C.; Friedl, M.; Schaaf, C.; Strahler, A.; Gao, F.; Schneider, A.; Zhang, X.; El Saleous, N.; Wolfe, R.E. Global land-water mask derived from MODIS Nadir BRDF-adjusted reflectances (NBAR) and the MODIS land cover algorithm. In Proceedings of the IGARSS 2004. 2004 IEEE International Geoscience and Remote Sensing Symposium, Anchorage, AK, USA, 20–24 September 2004.
22. Li, L.; Vrieling, A.; Skidmore, A.; Wang, T.; Turak, E. Monitoring the dynamics of surface water fraction from MODIS time series in a Mediterranean environment. *Int. J. Appl. Earth Obs. Geoinf.* **2018**, *66*, 135–145. [CrossRef]
23. Carroll, M.; Wooten, M.; DiMiceli, C.; Sohlberg, R.; Kelly, M. Quantifying surface water dynamics at 30 m spatial resolution in the North American high northern latitudes 1991–2011. *Remote Sens.* **2016**, *8*, 622. [CrossRef]
24. Pekel, J.-F.; Cottam, A.; Gorelick, N.; Belward, A.S. High-resolution mapping of global surface water and its long-term changes. *Nature* **2016**, *540*, 418–422. [CrossRef] [PubMed]
25. Tulbure, M.G.; Broich, M.; Stehman, S.V.; Kommareddy, A. Surface water extent dynamics from three decades of seasonally continuous Landsat time series at subcontinental scale in a semi-arid region. *Remote Sens. Environ.* **2016**, *178*, 142–157. [CrossRef]
26. Shen, G.; Fu, W.; Guo, H.; Liao, J. Water Body Mapping Using Long Time Series Sentinel-1 SAR Data in Poyang Lake. *Water* **2022**, *14*, 1902. [CrossRef]
27. Surface Water Changes. (1985–2016). Available online: http://aqua-monitor.deltares.nl (accessed on 21 September 2022).
28. Donchyts, G.; Baart, F.; Winsemius, H.; Gorelick, N.; Kwadijk, J.; Van De Giesen, N. Earth's surface water change over the past 30 years. *Nat. Clim. Chang.* **2016**, *6*, 810–813. [CrossRef]
29. Gholizadeh Sarabi, S.; Rahnama, M.R. From self-sufficient provision of water and energy to regenerative urban development and sustainability: Exploring the potentials in Mashhad City, Iran. *J. Environ. Plan. Manag.* **2021**, *64*, 2459–2480. [CrossRef]
30. Mosaffa, H.; Sadeghi, M.; Hayatbini, N.; Afzali Gorooh, V.; Akbari Asanjan, A.; Nguyen, P.; Sorooshian, S. Spatiotemporal variations of precipitation over Iran using the high-resolution and nearly four decades satellite-based PERSIANN-CDR dataset. *Remote Sens.* **2020**, *12*, 1584. [CrossRef]
31. Raziei, T.; Daryabari, J.; Bordi, I.; Modarres, R.; Pereira, L.S. Spatial patterns and temporal trends of daily precipitation indices in Iran. *Clim. Chang.* **2014**, *124*, 239–253. [CrossRef]
32. Luo, R.; Yuan, Q.; Yue, L.; Shi, X. Monitoring recent lake variations under climate change around the Altai mountains using multimission satellite data. *IEEE J. Sel. Top. Appl. Earth Obs. Remote Sens.* **2020**, *14*, 1374–1388. [CrossRef]
33. Veh, G.; Korup, O.; Roessner, S.; Walz, A. Detecting Himalayan glacial lake outburst floods from Landsat time series. *Remote Sens. Environ.* **2018**, *207*, 84–97. [CrossRef]
34. Ma, Y.; Xu, N.; Sun, J.; Wang, X.H.; Yang, F.; Li, S. Estimating water levels and volumes of lakes dated back to the 1980s using Landsat imagery and photon-counting lidar datasets. *Remote Sens. Environ.* **2019**, *232*, 111287. [CrossRef]
35. Lu, S.; Ouyang, N.; Wu, B.; Wei, Y.; Tesemma, Z. Lake water volume calculation with time series remote-sensing images. *Int. J. Remote Sens.* **2013**, *34*, 7962–7973. [CrossRef]
36. Moghim, S. Impact of climate variation on hydrometeorology in Iran. *Glob. Planet. Chang.* **2018**, *170*, 93–105. [CrossRef]
37. Malaekeh, S.; Safaie, A.; Shiva, L.; Tabari, H. Spatio-temporal variation of hydro-climatic variables and extreme indices over Iran based on reanalysis data. *Stoch. Environ. Res. Risk Assess.* **2022**, 1–28. [CrossRef]
38. Arnell, N.W.; Gosling, S.N. The impacts of climate change on river flow regimes at the global scale. *J. Hydrol.* **2013**, *486*, 351–364. [CrossRef]
39. Blum, J.R.; Eichhorn, A.; Smith, S.; Sterle-Contala, M.; Cooperstock, J.R. Real-time emergency response: Improved management of real-time information during crisis situations. *J. Multimodal User Interfaces* **2014**, *8*, 161–173. [CrossRef]
40. Irwin, K.; Beaulne, D.; Braun, A.; Fotopoulos, G. Fusion of SAR, optical imagery and airborne LiDAR for surface water detection. *Remote Sens.* **2017**, *9*, 890. [CrossRef]
41. Li, Z.-L.; Tang, B.-H.; Wu, H.; Ren, H.; Yan, G.; Wan, Z.; Trigo, I.F.; Sobrino, J.A. Satellite-derived land surface temperature: Current status and perspectives. *Remote Sens. Environ.* **2013**, *131*, 14–37. [CrossRef]
42. Li, S.; Yu, Y.; Sun, D.; Tarpley, D.; Zhan, X.; Chiu, L. Evaluation of 10 year AQUA/MODIS land surface temperature with SURFRAD observations. *Int. J. Remote Sens.* **2014**, *35*, 830–856. [CrossRef]
43. Wan, Z. Collection-5 MODIS Land Surface Temperature Products Users' Guide. ICESS, University of California, Santa Barbara. 2007. Available online: https://www.cen.uni-hamburg.de/en/icdc/data/land/docs-land/modis-lst-products-user-guide-c5.pdf (accessed on 21 September 2022).
44. MOD11A1. Available online: https://developers.google.com/earth-engine/datasets/catalog/MODIS_061_MOD11A1 (accessed on 21 September 2022).
45. Dietz, A.J.; Kuenzer, C.; Gessner, U.; Dech, S. Remote sensing of snow–a review of available methods. *Int. J. Remote Sens.* **2012**, *33*, 4094–4134. [CrossRef]

46. MOD10A1. Available online: https://developers.google.com/earth-engine/datasets/catalog/MODIS_006_MOD10A1 (accessed on 21 September 2022).
47. MOD09GQ. Available online: https://developers.google.com/earth-engine/datasets/catalog/MODIS_061_MOD09GQ (accessed on 21 September 2022).
48. Running, S.; Mu, Q.; Zhao, M. MOD16A2 MODIS/Terra Net Evapotranspiration 8-day L4 global 500m SIN Grid V006 [Data Set]. NASA EOSDIS Land Processes DAAC; 2017. Available online: https://ladsweb.modaps.eosdis.nasa.gov/missions-and-measurements/products/MOD16A2 (accessed on 21 September 2022).
49. Tian, H.; Li, W.; Wu, M.; Huang, N.; Li, G.; Li, X.; Niu, Z. Dynamic monitoring of the largest freshwater lake in China using a new water index derived from high spatiotemporal resolution Sentinel-1A data. *Remote Sens.* **2017**, *9*, 521. [CrossRef]
50. Plug, L.J.; Walls, C.; Scott, B. Tundra lake changes from 1978 to 2001 on the Tuktoyaktuk Peninsula, Western Canadian Arctic. *Geophys. Res. Lett.* **2008**, *35*. [CrossRef]
51. Tao, S.; Fang, J.; Zhao, X.; Zhao, S.; Shen, H.; Hu, H.; Tang, Z.; Wang, Z.; Guo, Q. Rapid loss of lakes on the Mongolian Plateau. *Proc. Natl. Acad. Sci. USA* **2015**, *112*, 2281–2286. [CrossRef] [PubMed]
52. Du, Z.; Bin, L.; Ling, F.; Li, W.; Tian, W.; Wang, H.; Gui, Y.; Sun, B.; Zhang, X. Estimating surface water area changes using time-series Landsat data in the Qingjiang River Basin, China. *J. Appl. Remote Sens.* **2012**, *6*, 063609. [CrossRef]
53. Xu, H. Modification of normalised difference water index (NDWI) to enhance open water features in remotely sensed imagery. *Int. J. Remote Sensing.* **2006**, *27*, 3025–3033. [CrossRef]
54. Pham-Duc, B.; Prigent, C.; Aires, F. Surface water monitoring within Cambodia and the Vietnamese Mekong Delta over a year, with Sentinel-1 SAR observations. *Water* **2017**, *9*, 366. [CrossRef]
55. Li, W.; Du, Z.; Ling, F.; Zhou, D.; Wang, H.; Gui, Y.; Sun, B.; Zhang, X. A comparison of land surface water mapping using the normalized difference water index from TM, ETM+ and ALI. *Remote Sens.* **2013**, *5*, 5530–5549. [CrossRef]
56. Gorelick, N.; Clinton, N. Multitemporal Supervised Classification Using Google Earth Engine. In Proceedings of the AGU Fall Meeting, Washington, DC, USA, 10–14 December 2018.
57. Banerjee, A.; Chen, R.; Meadows, M.E.; Singh, R.; Mal, S.; Sengupta, D. An analysis of long-term rainfall trends and variability in the uttarakhand himalaya using Google Earth Engine. *Remote Sens.* **2020**, *12*, 709. [CrossRef]
58. Mann, H.B. Nonparametric tests against trend. *Econom. J. Econom. Soc.* **1945**, *13*, 245–259. [CrossRef]
59. Kendall, M. *Rank Correlation Methods*, 4th ed.; Charles Griffin: London, UK, 1975.
60. Zolghadr-Asli, B.; Bozorg-Haddad, O.; Sarzaeim, P.; Chu, X. Investigating the variability of GCMs' simulations using time series analysis. *J. Water Clim. Change* **2019**, *10*, 449–463. [CrossRef]
61. Tabari, H.; Marofi, S.; Aeini, A.; Talaee, P.H.; Mohammadi, K. Trend analysis of reference evapotranspiration in the western half of Iran. *Agric. For. Meteorol.* **2011**, *151*, 128–136. [CrossRef]
62. Gholami, H.; Moradi, Y.; Lotfirad, M.; Gandomi, M.A.; Bazgir, N.; Shokrian Hajibehzad, M. Detection of abrupt shift and non-parametric analyses of trends in runoff time series in the Dez river basin. *Water Supply* **2022**, *22*, 1216–1230. [CrossRef]
63. Sen, P.K. Estimates of the regression coefficient based on Kendall's tau. *J. Am. Stat. Assoc.* **1968**, *63*, 1379–1389. [CrossRef]
64. Banerjee, A.; Chen, R.; Meadows, M.E.; Sengupta, D.; Pathak, S.; Xia, Z.; Mal, S. Tracking 21st century climate dynamics of the Third Pole: An analysis of topo-climate impacts on snow cover in the central Himalaya using Google Earth Engine. *Int. J. Appl. Earth Obs. Geoinformation.* **2021**, *103*, 102490. [CrossRef]
65. Tabari, H.; Somee, B.S.; Zadeh, M.R. Testing for long-term trends in climatic variables in Iran. *Atmos. Res.* **2011**, *100*, 132–140. [CrossRef]
66. Alizadeh-Choobari, O.; Najafi, M. Extreme weather events in Iran under a changing climate. *Clim. Dyn.* **2018**, *50*, 249–260. [CrossRef]
67. Bilal, H.; Chamhuri, S.; Mokhtar, M.B.; Kanniah, K.D. Recent snow cover variation in the upper Indus Basin of Gilgit Baltistan, Hindukush Karakoram Himalaya. *J. Mt. Sci.* **2019**, *16*, 296–308. [CrossRef]
68. Azmat, M.; Liaqat, U.W.; Qamar, M.U.; Awan, U.K. Impacts of changing climate and snow cover on the flow regime of Jhelum River, Western Himalayas. *Reg. Environ. Change* **2017**, *17*, 813–825. [CrossRef]
69. Yang, Y.; Tian, F. Abrupt change of runoff and its major driving factors in Haihe River Catchment, China. *J. Hydrol.* **2009**, *374*, 373–383. [CrossRef]
70. Hui, Y.; Pagiatakis, S. Least squares spectral analysis and its application to superconducting gravimeter data analysis. *Geo-Spat. Inf. Sci.* **2004**, *7*, 279–283. [CrossRef]
71. Mathias, A.; Grond, F.; Guardans, R.; Seese, D.; Canela, M.; Diebner, H.H. Algorithms for spectral analysis of irregularly sampled time series. *J. Stat. Softw.* **2004**, *11*, 1–27. [CrossRef]
72. Ghaderpour, E. Multichannel antileakage least-squares spectral analysis for seismic data regularization beyond aliasing. *Acta Geophys.* **2019**, *67*, 1349–1363. [CrossRef]
73. Ghaderpour, E.; Vujadinovic, T.; Hassan, Q.K. Application of the least-squares wavelet software in hydrology: Athabasca River basin. *J. Hydrol. Reg. Stud.* **2021**, *36*, 100847. [CrossRef]
74. Sa'adi, Z.; Shahid, S.; Ismail, T.; Chung, E.-S.; Wang, X.-J. Trends analysis of rainfall and rainfall extremes in Sarawak, Malaysia using Modified Mann–Kendall test. *Meteorol. Atmos. Phys.* **2019**, *131*, 263–277. [CrossRef]
75. Lacombe, G.; Mccartney, M.; Forkuor, G. Drying climate in Ghana over the period 1960–2005: Evidence from the resampling-based Mann-Kendall test at local and regional levels. *Hydrol. Sci. J.* **2012**, *57*, 1594–1609. [CrossRef]

76. Tofiq, F.; Güven, A. Potential changes in inflow design flood under future climate projections for Darbandikhan Dam. *J. Hydrol.* **2015**, *528*, 45–51. [CrossRef]
77. Alfieri, L.; Bisselink, B.; Dottori, F.; Naumann, G.; de Roo, A.; Salamon, P.; Wyser, K.; Feyen, L. Global projections of river flood risk in a warmer world. *Earth's Future* **2017**, *5*, 171–182. [CrossRef]
78. Zolghadr-Asli, B.; Bozorg-Haddad, O.; Enayati, M.; Goharian, E. Developing a robust multi-attribute decision-making framework to evaluate performance of water system design and planning under climate change. *Water Resour. Manag.* **2021**, *35*, 279–298. [CrossRef]
79. Yin, J.; Guo, S.; Yang, Y.; Chen, J.; Gu, L.; Wang, J.; He, S.; Wu, B.; Xiong, J. Projection of droughts and their socioeconomic exposures based on terrestrial water storage anomaly over China. *Sci. China Earth Sci.* **2022**, *65*, 1772–1787. [CrossRef]
80. Zolghadr-Asli, B.; Bozorg-Haddad, O.; Chu, X. Effects of the uncertainties of climate change on the performance of hydropower systems. *J. Water Clim. Chang.* **2019**, *10*, 591–609. [CrossRef]
81. Salas, J.; Obeysekera, J.; Vogel, R. Techniques for assessing water infrastructure for nonstationary extreme events: A review. *Hydrol. Sci. J.* **2018**, *63*, 325–352. [CrossRef]
82. Yin, J.; Guo, S.; Gu, L.; Zeng, Z.; Liu, D.; Chen, J.; Shen, Y.; Xu, C.-Y. Blending multi-satellite, atmospheric reanalysis and gauge precipitation products to facilitate hydrological modelling. *J. Hydrol.* **2021**, *593*, 125878. [CrossRef]
83. Cheng, L.; AghaKouchak, A. Nonstationary precipitation intensity-duration-frequency curves for infrastructure design in a changing climate. *Sci. Rep.* **2014**, *4*, 1. [CrossRef] [PubMed]

4.3. Links and implications

The first paper focused on analysing hydroclimatic variations in the Doosti Dam's basin using multisensor satellite data from the GEE platform. This paper provided a comprehensive understanding of hydroclimatic trends and their implications for water resource management. By engaging in this aspect of the project, it was possible to achieve Research Objective 1: "Assess and map the spatiotemporal distribution and the overall trends of hydro-climatological data using spatial distribution in the GEE."

A powerful web-based cloud computing platform (GEE) was used in conjunction with non-parametric statistical tests (MK and Sen's slope) to explore the spatiotemporal characteristics of various hydroclimatic variables. This allowed the identification of the monotonic trend in the data. An in-depth understanding of the long-term trend of hydroclimatic variables is provided by this study. The first paper demonstrates the effectiveness of using multisensor satellite data, particularly from platforms like GEE, to analyse hydroclimatic trends over large areas. This aligns with the approach taken in the second paper, which also utilises remote sensing techniques, in frequency analysis of extreme events. This paper offers a significant contribution to knowledge in answering the Research Question: *"Can the spatial distribution of remotely sensed dataset substitute ground-based observations in the sparse gauge catchments? Does the spatial distribution of global climate datasets agree significantly well with ground-based observations?".* Both papers underscore the importance of understanding hydroclimatic variability for water resource management and address the impacts of climate change and human activities on water resources. The first paper provides insights into long-term trends and spatial patterns, while the second paper delves into the frequency and severity of extreme events and non-stationary conditions, enhancing our understanding of the dynamic nature of hydroclimatic systems.

This research facilitated the achievement of our research goal by utilising statistical analyses and remote sensing methods to evaluate hydroclimatic patterns, thereby establishing a foundation for methodologies employed in the second paper, including GEV models and spatiotemporal analysis techniques.

4.4. Conclusion

Chapter 3 of this thesis introduced the first paper that was published as a component of this study. This paper established a foundation methodology applied in the second and third papers for extreme analysis through the GEV model. The NEVA model employs the Mann-Kendall trend test, to detect trends in extreme data. Following previous research papers, the second paper is discussed in the subsequent chapter, Chapter 4.

CHAPTER 5: PAPER 2 – A MULTI-FRAMEWORK Of GOOGLE EARTH ENGINE AND GEV FOR SPATIAL ANALYSIS OF EXTREMES IN NON-STATIONARY CONDITION IN SOUTHEAST QUEENSLAND, AUSTRALIA

5.1. Introduction

Extreme precipitation, extreme evapotranspiration, and extreme water storage deficit events are examples of extremes whose frequency and intensity are changing. Therefore, it is imperative to build a framework for estimating non-stationary circumstances. In order to provide a framework that takes into account the cause and effect of the physical system, this chapter used the geeSEBAL platform, Generalised Extreme Value models, and spatiotemporal analytic approaches. Initially, the geeSEBAL platform facilitated the calculation of actual evapotranspiration (ETa) with an unparalleled degree of spatial and temporal precision. Subsequently, the Non-stationary Extreme Value Analysis methodology uses a Differential Evolution Markov Chain technique to apply the Bayesian method and determine the magnitude and frequency of extreme values throughout the parameter space. The study employed station and global climate datasets to examine the rainfall, ETa, reference evapotranspiration (ETo), and water storage variables in the Lockyer Valley, situated in the SEQ region of Australia, both spatially and temporally. A GEV distribution was used to do a frequency analysis of ETa, rainfall, and water storage deficit for 14 sites under both stationary and non-stationary assumptions. The findings show that, in comparison to conclusions generated from station data, global climate databases underestimate the difference between stationary and non-stationary situations. Similar to this, the data show that there is less change in water storage in stationary and non-stationary situations, with a strong variation in rainfall and a moderate variation in evapotranspiration following. The results of this investigation suggest that underestimating the quantities of some hydrometeorological variables might result from disregarding their non-stationary state. This paradigm offers useful insights for disaster management, risk assessment, and infrastructure planning and design, andmay be used to estimate severe situations in any geographic location.

5.2. Published paper

Pakdel et al. (2023), “A Multi-Framework of Google Earth Engine and GEV for Spatial Analysis of Extremes in Non-Stationary Condition in Southeast Queensland, Australia” was published in I*SPRS International Journal of Geo-Information* (2023), Volume 12, Issue 370.

International Journal of Geo-Information

MDPI

Article

A Multi-Framework of Google Earth Engine and GEV for Spatial Analysis of Extremes in Non-Stationary Condition in Southeast Queensland, Australia

Hadis Pakdel [1,*], Dev Raj Paudyal [2], Sreeni Chadalavada [1], Md Jahangir Alam [1,3] and Majid Vazifedoust [4]

[1] School of Engineering, The University of Southern Queensland, Springfield Lakes, QLD 4300, Australia; sreeni.chadalavada@usq.edu.au (S.C.); mdjahangir.alam@usq.edu.au (M.J.A.)
[2] School of Surveying and Built Environment, The University of Southern Queensland, Springfield Lakes, QLD 4300, Australia; devraj.paudyal@usq.edu.au
[3] Murray-Darling Basin Authority (MDBA), Canberra, ACT 2601, Australia
[4] Water Engineering Department, University of Guilan, Rasht 4188958643, Iran; vazifedoust@guilan.ac.ir
* Correspondence: hadis.pakdel@usq.edu.au

Abstract: The frequency and severity of extremes, including extreme precipitation events, extreme evapotranspiration and extreme water storage deficit events, are changing. Thus, the necessity for developing a framework that estimates non-stationary conditions is urgent. The aim of this paper is to develop a framework using the geeSEBAL platform, Generalised Extreme Value (GEV) models and spatiotemporal analysis techniques that incorporate the physical system in terms of cause and effect. Firstly, the geeSEBAL platform has enabled the estimation of actual evapotranspiration (ET_a) with an unprecedented level of spatial-temporal resolution. Following this, the Non-stationary Extreme Value Analysis (NEVA) approach employs the Bayesian method using a Differential Evolution Markov Chain technique to calculate the frequency and magnitude of extreme values across the parameter space. Station and global climate datasets have been used to analyse the spatial and temporal variation of rainfall, reference evapotranspiration (ET_o), ET_a and water storage (WS) variables in the Lockyer Valley located in Southeast Queensland (SEQ), Australia. Frequency analysis of rainfall, ET_a, and water storage deficit for 14 stations were performed using a GEV distribution under stationary and non-stationary assumptions. Comparing the ET_a, ET_o and ERA5 rainfall with station data showed reasonable agreement as follows: Pearson correlation of 0.59–0.75 for ET_a, RMSE of 45.23–58.56 mm for ET_a, Pearson correlation of 0.96–0.97 for ET_o, RMSE of 73.13–87.73 mm for ET_o and Pearson correlation of 0.87–0.92 for rainfall and RMSE of 37.53–57.10 mm for rainfall. The lower and upper uncertainty bounds between stationary and non-stationary conditions for rainfall station data of Gatton varied from 550.98 mm (stationary) to 624.97 mm (non-stationary), and for ERA5 rainfall datasets, 441.30 mm (stationary) to 450.77 mm (non-stationary). The results demonstrate that global climate datasets underestimate the difference between stationary and non-stationary conditions by 9.47 mm compared to results of 73.99 mm derived from station data. Similarly, the results demonstrate less variation between stationary and non-stationary conditions in water storage, followed by a sharp variation in rainfall and moderate variation in evapotranspiration. The findings of this study indicate that neglecting the non-stationary condition in some hydrometeorological variables can lead to underestimating their amounts. This framework can be applied to any geographical area for estimating extreme conditions, providing valuable insights for infrastructure planning and design, risk assessment and disaster management.

Keywords: climate extremes; Google Earth Engine; geeSEBAL; non-stationary; GEV distribution

check for updates

Citation: Pakdel, H.; Paudyal, D.R.; Chadalavada, S.; Alam, M.J.; Vazifedoust, M. A Multi-Framework of Google Earth Engine and GEV for Spatial Analysis of Extremes in Non-Stationary Condition in Southeast Queensland, Australia. *ISPRS Int. J. Geo-Inf.* **2023**, *12*, 370. https://doi.org/10.3390/ijgi12090370

Academic Editors: Wolfgang Kainz and Godwin Yeboah

Received: 20 June 2023
Revised: 31 August 2023
Accepted: 3 September 2023
Published: 6 September 2023

1. Introduction

Stationarity is an assumption that was historically made to simplify the already complex statistics required. The terms of the return period and return level give vital information for designing, decision-making and estimating the implications of climatic occurrences

under the assumption of a stationary climate. This was generally a safe assumption as our data records were shorter in the past; therefore, not much change occurred over that short period of time. Furthermore, researchers of the past did not have the same computational power that we now have, so they relied on simplifying assumptions to make the math manageable. In particular, the availability of longer data records and the changing climate introduce risks in persistently assuming stationarity. For a long time, infrastructure design approaches have depended on stationary return levels which presume that the frequency of extremes does not fluctuate over time [1]. The frequency of extremes, on the other hand, has been shifting and is expected to continue to change in the future [2], and studies have shown that hydrological records in some regions demonstrate non-stationarity in the form of growing or decreasing patterns as well as their combination. Hydrological parameters are considered stationary over time, but the stationary condition may no longer be applicable as climatic and human effects create non-stationary behaviour [3].

The difficulty of incorporating spatial information within extreme value analysis approaches has been one focus of current studies on framework development given that many extreme occurrences involve spatial processes [4,5]. As a result, non-stationary climatic and hydrologic extremes require models that can account for them [6,7]. Southeast Queensland (SEQ) is one of Australia's most flood-prone zones [8] and the Intergovernmental Panel on Climate Change (IPCC) has recognised it as one of the "hotspots" for climate change [2]. According to Mpelasoka et al. [9], the soil-moisture-based drought frequency in SEQ catchments is expected to rise by 80 percent by 2070. In a major catchment in eastern Australia, Zhang, Wang [10] projected that during the next 80 years, real ET will rise significantly while water storage will decline.

This study aims to investigate non-stationary scenarios of rainfall (Rain), actual evapotranspiration (ET_a) and water storage (WS) variables obtained through the global climate datasets and ground-based measurements across various stations in the Lockyer Valley in SEQ. To achieve this goal, a geeSEBAL algorithm and NEVA model were employed in both stationary and non-stationary conditions. GeeSEBAL was used to automatically estimate ET, allowing for validation against ET station data. Considering that geeSEBAL does not depend on any ground-level measurements as input data, it is expected that this tool will be beneficial for the examination of water balances for worldwide application, as well as for water resource management in areas with limited data [11]. They also mentioned that the purpose of geeSEBAL is to enhance the comprehension of the effects of land cover alterations on ET during the past few decades. The recent version of geeSEBAL utilises Landsat imagery and reanalysis data to calculate the time series of ET_a, demonstrating encouraging outcomes for regional-scale investigations conducted in areas with limited data availability [11].

Changes in water storage are expected to result in changes in precipitation and evapotranspiration patterns, subsequently affecting plant phenology [12,13]. Since the intensity of extremes including extreme precipitation events, extreme evapotranspiration events and extreme deficit of water storage depend on several factors, such as vegetation cover [14], relative humidity, evapotranspiration [15] and topography, identifying the drivers of extremes helps us quantify, predict and project extremes [16]. Given the complexity of heat and energy exchanges between the land and the atmosphere, quantifying ET is regarded as a difficult undertaking [17]. Our capacity to analyse the ET process has substantially increased as a result of the advancement of various remote sensing technologies, particularly the creation and use of multiple surface energy balance (SEB) models [18]. Although, ET cannot be measured directly from satellites [19], it can be calculated using Mapping Evapotranspiration at High Resolution with Internalised Calibration (METRIC) [20] and the Surface Energy Balance Algorithm for Land (SEBAL) [17,21]. The core mechanism of the SEBAL, which is based on choosing endmembers that reflect the extremes of the hot (dry) and cold (wet) pixels, estimates the near-surface temperature gradient (dT) [17,20]. Previously, the process of identifying hot and cold pixels was performed manually, but advancements in technology have made it possible to automate this task. One such technique, known as Calibra-

tion using Inverse Modelling at Extreme Conditions (CIMEC) [22], utilises the Normalised Difference Vegetation Index (NDVI) and Ts percentiles to automatically determine endmembers. In this study, a platform called geeSEBAL (https://github.com/et-brasil/geesebal (accessed on 15 June 2023)) was used. It combines the capabilities of Google Earth Engine (GEE) with the Surface Energy Balance Algorithm for Land (SEBAL) framework [11]. It is an application or tool developed to leverage the GEE platform's application programming interface (API) and serves as a powerful tool for conducting various analyses related to remote sensing and evapotranspiration estimation.

A Bayesian inference framework that supports both non-stationary and stationary estimations was proposed by Cheng et al. [23]. As numerous natural phenomena happen under a non-stationary context, the idea of non-stationarity has been shown to be quite helpful in the field of hydroclimatology for analysing extremes. Their study findings suggested that NEVA calculates extreme return levels and variables effectively. The persistence of hydroclimatic extremes is destructive to the economy, natural ecosystems, agriculture, infrastructures and human health [24–28]. Identifying design extremes at different recurrence intervals and durations can be accomplished by performing a frequency analysis of extremes and looking at changes in the return period of the extremes using NEVA [1]. This model allows us to incorporate shifting extremes in intensity and frequency analysis [23].

Generalised Extreme Value (GEV) distributions and the Log Pearson Type 3 (LP3) are frequently utilised to conduct intensity analyses of hydroclimatic extremes. These statistical distributions are widely used for studying the occurrence and magnitude of extreme events in hydrology and climate research. Previous research used the GEV distribution to create Temperature Duration Frequency (TDF) curves [28,29]. Additionally, the Australian Rainfall and Runoff (ARR) guideline [30] has recommended the use of the GEV distribution for calculating design floods and rainfalls.

The study aimed to achieve the following specific objectives: (1) To evaluate the actual evapotranspiration derived from geeSEBAL by feeding two different climate datasets (ground-based observations and global climate products); (2) to compare the spatiotemporal distribution of the P and ET_o derived from a global climate dataset with the results of the same variables derived from ground-based observation and determine the model accuracy; (3) to evaluate and map the spatiotemporal distribution of water storage derived from a lump water balance for the last 32 years by considering two climate datasets and comparing the results incorporating physical drivers in terms of cause and effect; (4) to analyse the intensity and frequency of rainfall extreme events, evapotranspiration extremes and water storage deficit extremes under both stationary and non-stationary conditions using the GEV model for the estimation of different return levels.

In this study, we propose an integrated framework that combines geeSEBAL, NEVA-GEV and spatial distribution analysis to evaluate the return levels of extremes, including extreme rainfall events, extreme evapotranspiration events and extreme water storage deficit. We believe that the physical disturbance within a catchment alters the underlying process and results in temporal fluctuation in parameter values. As hydroclimatic variables can significantly vary over time, space, and climate zones, it is necessary to employ accurate data with higher spatial resolution for variability analysis [31]. So, we provided the geeSEBAL results by incorporating high quality datasets and considering the physical system drivers and their relationship. The outcomes of the study could be useful in understanding the spatial variation of rainfall, evapotranspiration and water storage by incorporating both stationary and non-stationary assumptions, thereby assisting decision-makers in making informed decisions for disaster preparedness, emergency response, health care services and the selection of appropriate materials for infrastructure development.

2. Materials and Methods

Figure 1 shows the main methods and data sets used in this study. The steps in this study are as follows: (a) deriving ET_a from the geeSEBAL algorithm and WS from a lump water balance, (b) accuracy assessment of P, ET_o and ET_a derived from station

and global climate datasets, (c) spatial analysis of extremes, including P, ET_a and WS and (d) investigating the extreme events analysis using the GEV model.

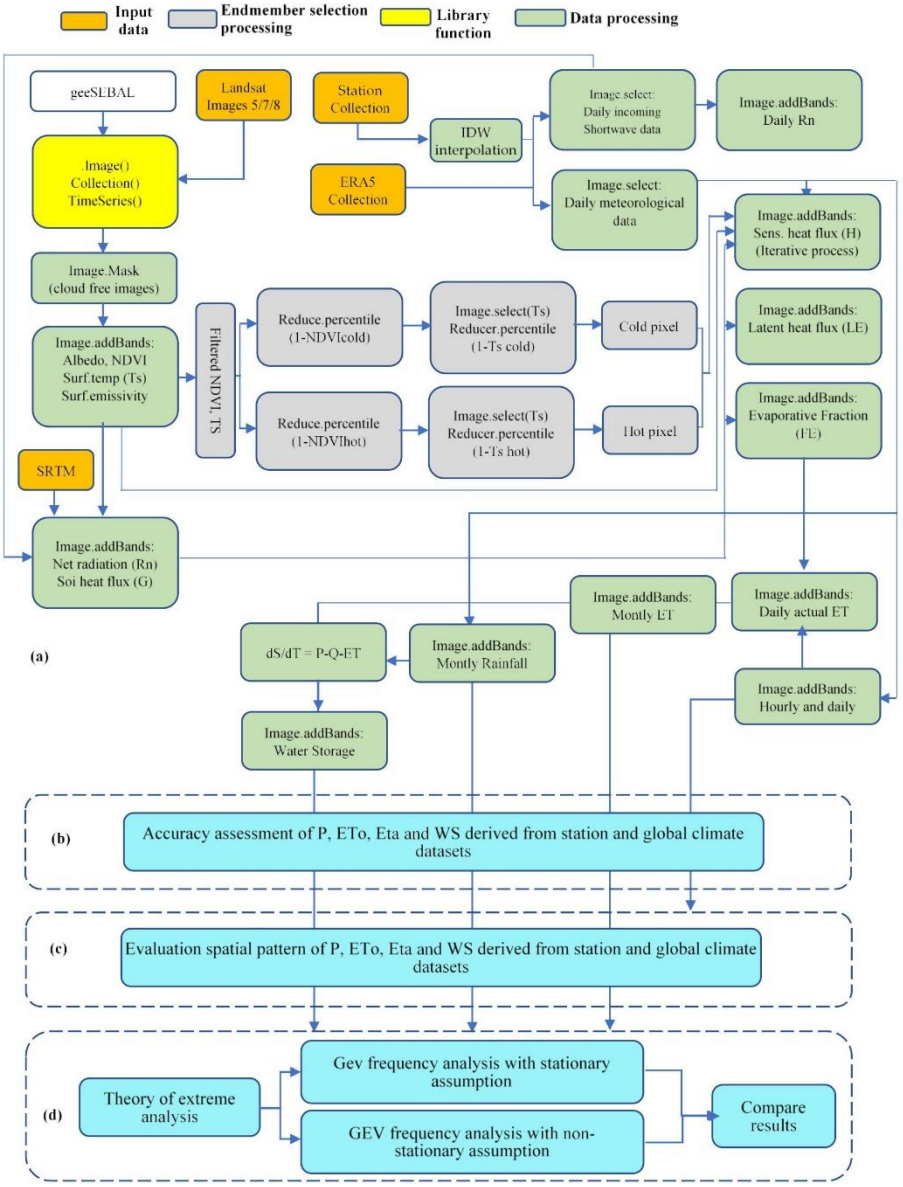

Figure 1. Flowchart of geeSEBAL, GEE and GEV model to estimate extremes. (**a**) geeSEBAL algorithm, (**b**) accuracy assessment of hydrometeorological variables from station and global climate data, (**c**) spatial pattern of hydrometeorological variables from station and global climate data, (**d**) extreme events analysis (Modified [11]).

2.1. Study Region

The Lockyer Catchment is the case study area which is located in SEQ as illustrated in Figure 2. Lockyer Creek is the main stream which runs eastward into the Brisbane River then enters Moreton Bay [32]. The catchment is located east of Toowoomba and west of Brisbane, within the local government boundaries of the Lockyer Valley Regional Council, Somerset Regional Council, Toowoomba Regional Council and Ipswich Regional Council [33]. Recognising its significance, the relevant infrastructure operators and decision-makers, such as the Queensland Department of Environment and Science and Seqwater, acknowledged the importance of this catchment [34]. It covers approximately 3000 km^2, with an average annual rainfall of 1000–2012 mm [35].

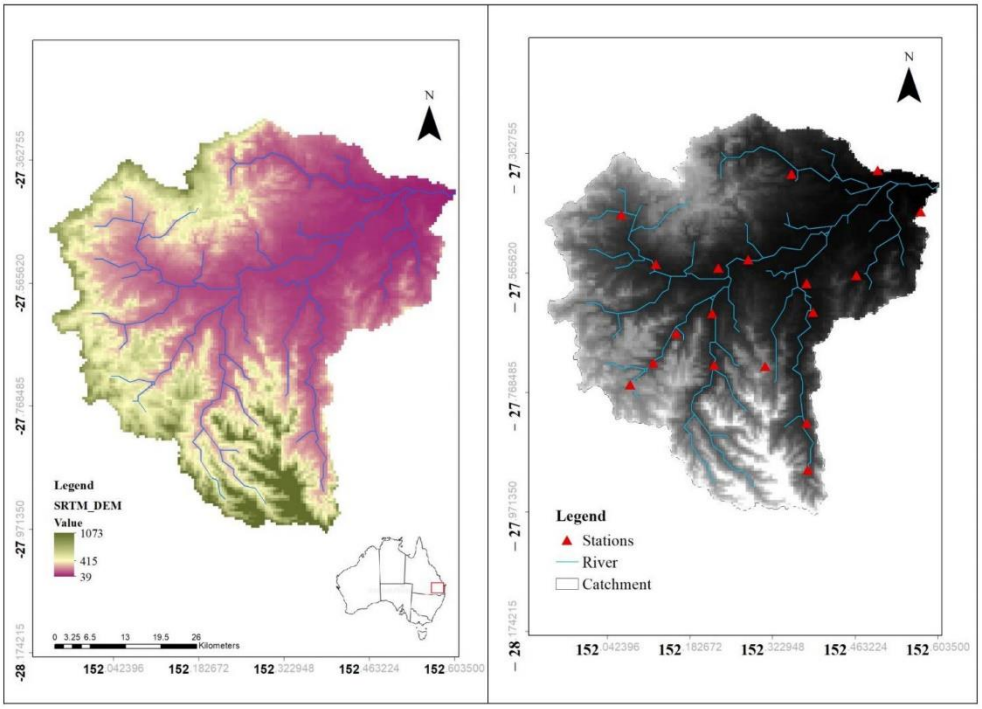

Figure 2. Geographical location of studied area in Australia (**Left**). Hydro-meteorological stations considered along the Lockyer Catchment (**Right**).

However, there is a significant temporal fluctuation, resulting in rivers that are dry for most of the year. The watershed comprises some of Australia's richest farmed areas, with high-value vegetable cultivation and grazing [32]. The northern and southern sections of the Lockyer watershed receive a lot of rain. The majority of the basin received moderate to low rainfall and during Australia's recent droughts and the Lockyer Creek valley was one of the driest catchments in Queensland [36]. Collectively, they drain around 3000 km^2 of land, about a fourth of the Brisbane River's watershed. The Lockyer Catchment, which has a population of over 35,000 people, has considerable environmental, economic and social importance.

In this region, there have been several unique climatic events in recent decades, such as between 1988 and 1989, when there was above average rainfall, and from 2000 to 2008, when there was a catastrophic and prolonged drought. Drought relief measures were

implemented in 2008. However, the region continues to experience reoccurring cycles of drought and flood crises, sometimes impacting the entire country for an extended duration. The frequency of flood events, like the one in 2022, may be misestimated under a stationarity assumption given that previous studies have shown the assumption to no longer be valid. Moreover, it has been observed that the relationship between runoff and rainfall in the Lockyer Catchment is non-stationary [37,38]. Therefore, it is crucial to develop novel methods to estimate non-stationary rainfall extremes, evapotranspiration extremes and water storage deficit to enhance the design and management of hydraulic structures which minimise human and financial losses in the future.

2.2. Observed and Global Climate Dataset

Daily meteorological data including minimum and maximum air temperature (°C), minimum and maximum relative humidity (%), wind speed (m/s), surface solar radiation (MJ/m^2) and hydrological data, such as evapotranspiration (mm) and rainfall (mm), were sourced from two datasets: ground-based observations (Figure 2) and global climate products. The ground-based observations were obtained from SILO, an Australian climate data source (http://www.longpaddock.qld.gov.au/silo (accessed on 15 January 2023)) [39,40] that covers the period from 1990 to 2022. SILO data are the most commonly used and most reliable climate data for environmental studies in Australia [41]. Fourteen SILO meteorological and hydrological stations were applied for this research. First, the Inverse Distance Weighting (IDW) interpolation method was used to interpolate the station data and rasterise the meteorological parameters. To run the geeSEBAL algorithm, daily meteorological ground-based observations and the hourly fifth generation ECMWF reanalysis (ERA5) climate dataset with 9 km spatial resolution were incorporated in GEE and were used separately for running geeSEBAL, as well as estimation of water storage. Land use information was obtained from the Australian government, Geoscience Australia (https://www.ga.gov.au/, accessed on 15 January 2023), for simulation purposes. A Shuttle Radar Topography Mission (SRTM) digital elevation model (DEM) [42] dataset with a grid size of 90 m was used as input for the geeSEBAL algorithm.

2.3. Google Earth Engine Application: The geeSEBAL Algorithm

The initial method created by Bastiaanssen et al. [17] is the foundation for the geeSEBAL [11], which makes the assumption that latent heat flux (*LE*) (W/m^2) can be approximated as a residual of the surface energy balance.

$$LE = R_n - G - H \tag{1}$$

where R_n is the net radiation; G is the soil heat flux (W/m^2); H is the sensible heat flux (W/m^2). Given that both H and the aerodynamic resistance to turbulent heat transport (r_{ah}) are unknown, H was calculated by an iterative procedure.

$$H = \frac{\rho_a \, C_p dT}{r_{ah}} \tag{2}$$

where C_p is the specific heat capacity, r_{ah} aerodynamic resistance to turbulent heat transmission between two heights, dT represents the near-surface temperature difference between two heights ρ_a is air density [17]. A linear connection between T_s and (dT) is provided and cold and hot endmember selection is required to solve the iterative approach. The a and b coefficients are calculated individually for each picture.

$$dT = a + bT_s \tag{3}$$

Comprehensive documentation for the formulation and calibration of the SEBAL algorithm is covered in [17]. GEE infrastructure was used to develop the geeSEBAL algorithm [43], which enables the estimation of evapotranspiration at regional scales by using

meteorological reanalysis data and Landsat imagery [11]. The schematic representation of geeSEBAL is illustrated in Figure 1, highlighting the factors that were considered in the present study. The JavaScript APIs were used to integrate the SEBAL algorithm into GEE [11].

The three primary purposes of the geeSEBAL tool are: (1) Image: derivation of actual evapotranspiration from a particular image (accessible for JavaScript); (2) ImageCollection: batch method to calculate ET_a provided a date range and (3) Timeseries: long-term ET_a time series estimate at user-provided locations. All applications and codes are freely accessible at https://github.com/et-brasil/geesebal (accessed on 15 January 2023). Additionally, the Earth Engine programme (https://etbrasil.org/geesebal, accessed on 15 January 2023) offers a graphical user interface version of geeSEBAL [11,44,45]. For the purpose of running geeSEBAL, a series of Landsat images with the highest data quality were used. We used cloud cover filters using the CFMask method [46], which generates a bitmask to identify each image's pixels for clouds, clouds with shadows, clouds with confidence and pixels for ice and snow. The characteristics of Landsat collections used in this study are included in Table 1.

Table 1. The datasets available in the GEE platform that are used in geeSEBAL.

Product	GEE ID	Resolution	Time Coverage
LANDSAT 8 OLI/TIRS	LANDSAT/LC08/C01/T1_SRLANDSAT/LC08/C01/T1	30 m	Apr/2013–Present
LANDSAT 7 ETM+	LANDSAT/LE07/C01/T1_SRLANDSAT/LE07/C01/T1	30 m	Jan/1999–Present
LANDSAT 5 TM	LANDSAT/LT05/C01/T1_SR LANDSAT/LT05/C01/T1	30 m	Mar/1984–May/2012

The geeSEBAL algorithm was run separately using ERA5 reanalysis data and station data. Advised hot and cold endmembers percentiles were applied to determine the hot and cold pixels. The selection of candidates for the cold endmembers involved identifying densely vegetated areas, whereas sparsely vegetated regions were considered for the hot endmembers. The candidate with the lowest T_s (20%) and greatest NDVI (5%) percentiles was selected to represent the cold end. Conversely, the hot endmember was determined by selecting the candidate with the highest Ts percentile (20%) and the lowest NDVI (10%) percentiles.

Long-term ET_a was generated using the geeSEBAL algorithm, and the gaps between the Landsat images were filled by multiplying a ratio map of the last available simultaneous maps of ET_a and reference evapotranspiration, ET_o, to the new ET_o map [47]. It is vital to consider the non-stationary condition of rainfall and storage (Equation (4)) in a catchment, especially when the relationship between rainfall and runoff is non-stationary. In this equation, P is daily precipitation (mm), q is runoff (mm) 20% of precipitation [30,48], and ET_a is daily actual evapotranspiration (mm) derived from the geeSEBAL algorithm.

$$\frac{dS}{dT} = P - q - ET_a \tag{4}$$

2.4. Assessing Extremes in a Non-Stationary Approach Using GEV Model

A stationary time series is defined as one in which all finite dimensional distributions are time invariant [49]. The stationary assumption may not be valid in relation to changes caused by human and climatic factors, which results in non-stationary situations [3]. The simplifying assumption of stationarity is used to estimate the largest instantaneous extremes, and structures are built with this assumption in mind. It is important to acknowledge that the impacts of climate change are growing, leading to an increase in non-stationary conditions worldwide. The frequency of flood events like the one in 2022 may be misestimated under a stationarity assumption given that previous studies [38] have

shown the assumption to no longer be valid. Therefore, it is critical to take a non-stationary approach to these issues (Figure 1). In order to analyse the non-stationary extremes, the NEVA software package [1] was utilised.

NEVA calculates the extreme value in a Bayesian method using a Differential Evolution Markov Chain technique for global optimisation across the parameter field [1]. Extreme Value Theory (EVT) provides two fundamental distributions for describing extremes: either the peaks-over-threshold approach using the Generalised Pareto Distribution (GPD) [50–52] or the block maxima (or minima) approach using the Generalised Extreme Value (GEV) family of distributions [53]. NEVA typically contains two sections: 1. GEV distribution for yearly maximum analysis (block maxima) and 2. The peak-over-threshold (POT) approach uses the GPD for analysis of extremes over a specific threshold. The GEV method has been applied in this study. The GEV distribution's cumulative distribution function (cdf) is represented using the following equations:

$$F(x) = exp\left\{-\left(1+\varepsilon\left(\frac{x-\mu}{\sigma}\right)\right)^{\frac{-1}{\varepsilon}}\right\} \quad (5)$$

$$\left(1+\varepsilon\left(\frac{x-\mu}{\sigma}\right)\right) > 0 \quad (6)$$

The GEV distribution is incredibly adaptable to simulate the behaviour of many severe occurrences since it just has three parameters $(\mu, \varepsilon, \sigma)$. The location, scale and shape parameters are defined by μ, ε and σ, respectively [52].

The GEV becomes the Gumbel, Fréchet and Weibull distributions, respectively, when $\varepsilon = 0$, $\varepsilon < 0$ and $\varepsilon > 0$, respectively.

In NEVA, the shape and scale parameters are assumed to be constant while the location parameter is considered to represent a linear function of time to accommodate for non-stationary [1].

$$\mu(t) = \mu_1 t + \mu_0 \quad (7)$$

NEVA uses the Mann–Kendall trend test at the user-selected significance level to identify trends and non-stationarity in extremes in data [1]. The Mann–Kendall (MK) statistical test [54] was undertaken to calculate the importance of climatic time series' trends [55–58]. There is no monotonic trend at the specified level of significance according to the null hypothesis (H0) of the MK test. The alternative hypothesis (Ha) in this test shows a monotonic trend over time. More details about Mann–Kendall are documented in [31]. The Bayesian approach employs a generic inference methodology. The Bayes theorem for estimating GEV parameters under the non-stationary assumption can be defined as follows under the assumption that observations are independent of one another [1,52]:

$$p\left(\beta\middle|\vec{y},x\right) \propto p\left(\vec{y}\middle|\beta,x\right)p((\beta|x)) \quad (8)$$

$$p\left(\vec{y}\middle|\beta,x\right) = \prod_{t=1}^{Nt} p(y_t|\beta,x(t)) = \prod_{t=1}^{Nt} p(y_t|\mu(t),\sigma,\varepsilon) \quad (9)$$

For the components, which are β without $x(t)$, the stationarity may be thought of as a specific instance of the aforementioned equation:

$$p\left(\theta\middle|\vec{y}\right) \propto p\left(\vec{y}\middle|\theta\right)\, p(\theta) = \prod_{t=1}^{Nt} p\,(y_t|\theta)\, p(\theta) \quad (10)$$

Thus, according to the non-stationary assumption, $x(t)$ stands for the collection of all covariate values. The derived posterior distributions $p\left(\theta\middle|\vec{y}\right)$ and $p\left(\vec{y}\middle|\beta,x\right)$ reveal the parameters' behaviour under stationarity $\theta = (\mu, \varepsilon, \sigma)$ or non-stationarity $\beta = (\mu_1, \mu_0, \varepsilon, \sigma)$.

3. Results

The research introduces a comprehensive approach by combining geeSEBAL with two climate data sets (global data and station data), NEVA-GEV and spatial distribution analysis. This integrated framework aims to assess the return levels of extreme events, such as heavy rainfall, evapotranspiration and water storage deficit, by taking into account the physical factors and their interactions within the system.

3.1. Station Data and ERA5 Land Reanalysis Feeding into geeSEBAL as Meteorological Inputs

GeeSEBAL was run by ERA5 reanalysis and station data with advised percentiles. The cold (wet) endmember was selected in the area with the highest concentration of vegetation, consisting of the coldest 20% T_s of the top 5% vegetated pixels according to NDVI, and the hot (dry) endmember was chosen in the area with the lowest concentration of vegetation, consisting of the warmest 20% T_s of the lowest 10% NDVI vegetated pixels. To identify the spatial pattern of four parameters among stations and ERA5 reanalysis are displayed in Figures 3 and 4 at Lockyer Catchment. These two figures provide better insight into how rain, ET_o, ET_a and WS are distributed over the catchment for the period of 2000 to 2022. Rainfall follows a similar trend in the upstream and downstream parts of the catchment during these years. The rainfall and ET_a have almost identical trends which indicates the highest rise in the year 2010.

Between December 2010 and January 2011, flooding of historic proportions swept across large areas of Queensland due to prolonged rainfall [59], as illustrated in Figures 3 and 4. More than 78% of the state was declared a disaster zone, affecting 2.5 million people negatively and causing about 33 deaths [59]. The flood events affected approximately 29,000 homes and businesses, with an estimated damage cost of over $5 billion [59]. Interestingly, the estimation of spatial patterns derived from ERA5 land reanalysis are almost identical with station data for rain. Whereas in ET_a, ERA5 reanalysis overestimates the spatial variability compared to station data. Accordingly, water storage for the year 2010 confirms that the whole catchment reached its highest annually. The spatial pattern of figures for ERA5 reanalysis represents the more noticeable variation in the year 2005. The rain and water storage deficit in station data range from (~1200 mm) to (~1500 mm) and from (~250 mm) to (~500 mm), respectively (Figure 3). Similarly, Figure 4 shows the rain and water storage in ERA5, depicting the highest rise (~1500 mm) and (~500 mm) for years 2010 and 2020, respectively, while potential evapotranspiration has a remarkable increase from (~1450 mm) to (~1600 mm) in the year 2020 for both station and ERA5 reanalysis datasets. Water storage for both the station and ERA5 data remain the same, whereas ET_a for the station and ERA5 exhibit variation from approximately 100 mm to 700 mm and from 400 mm to 1000 mm, respectively. ERA5 reanalysis overestimates ET_a in comparison to the station.

So, the relationship between actual evapotranspiration and water storage is similar. Irrigated areas were concentrated alongside the streams and the Gatton area, which is known as the agricultural hub in Southeast Queensland. This also confirms the strong correlation between water storage and irrigated areas. The Lockyer Valley includes some of Australia's richest farmed area, with high-value vegetable cultivation, and, as can be observed, the highest water storage is concentrated in the irrigated areas [32]. So, the relationship between actual evapotranspiration and water storage is similar.

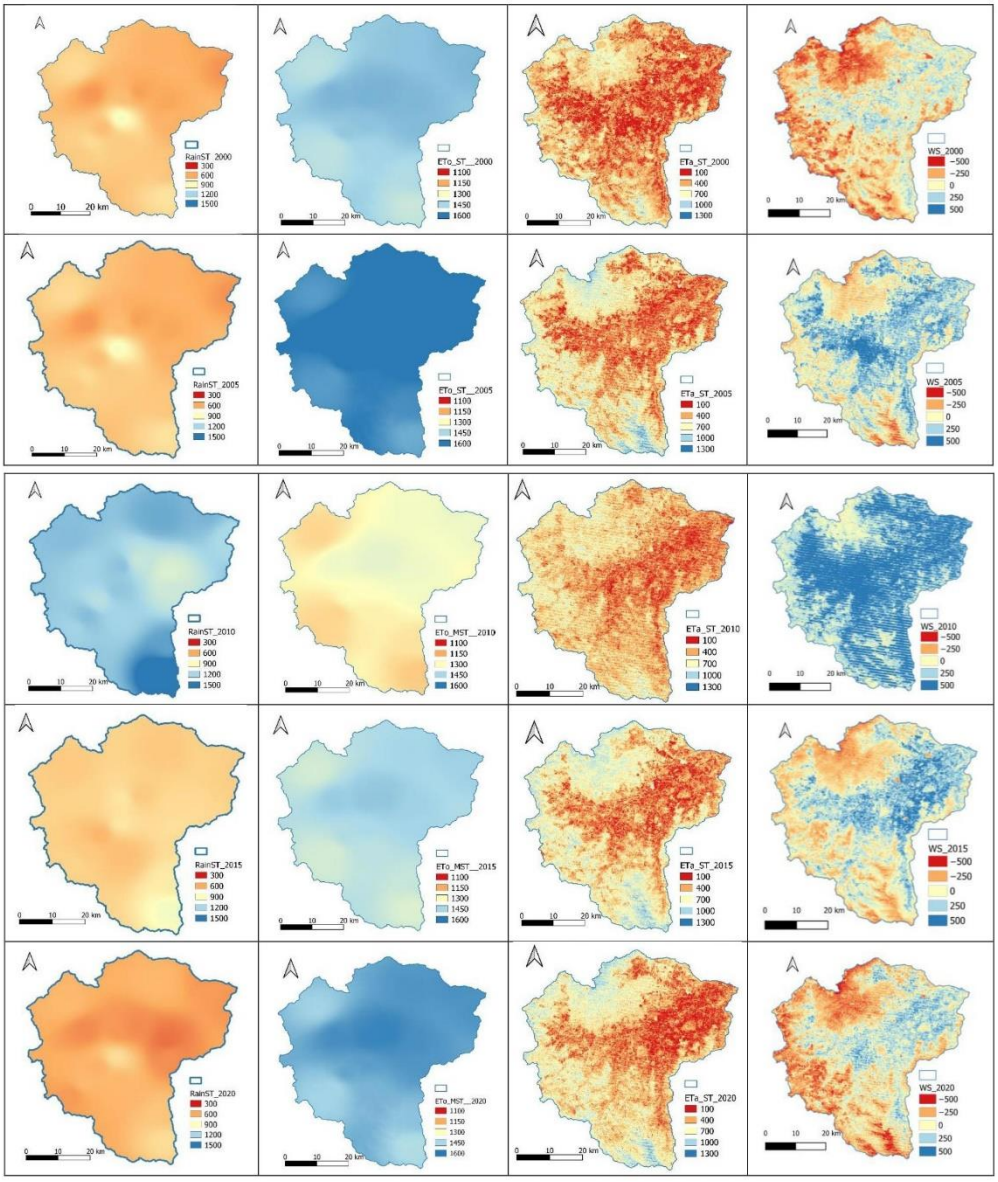

Figure 3. Changes in spatial pattern of hydroclimate parameters (annual cumulative rainfall (column 1), reference evapotranspiration (column 2), actual evapotranspiration (column 3) and water storage deficit (column 4)) from 2000 to 2020 based on geeSEBAL algorithm resulting from station datasets over the Lockyer Catchment.

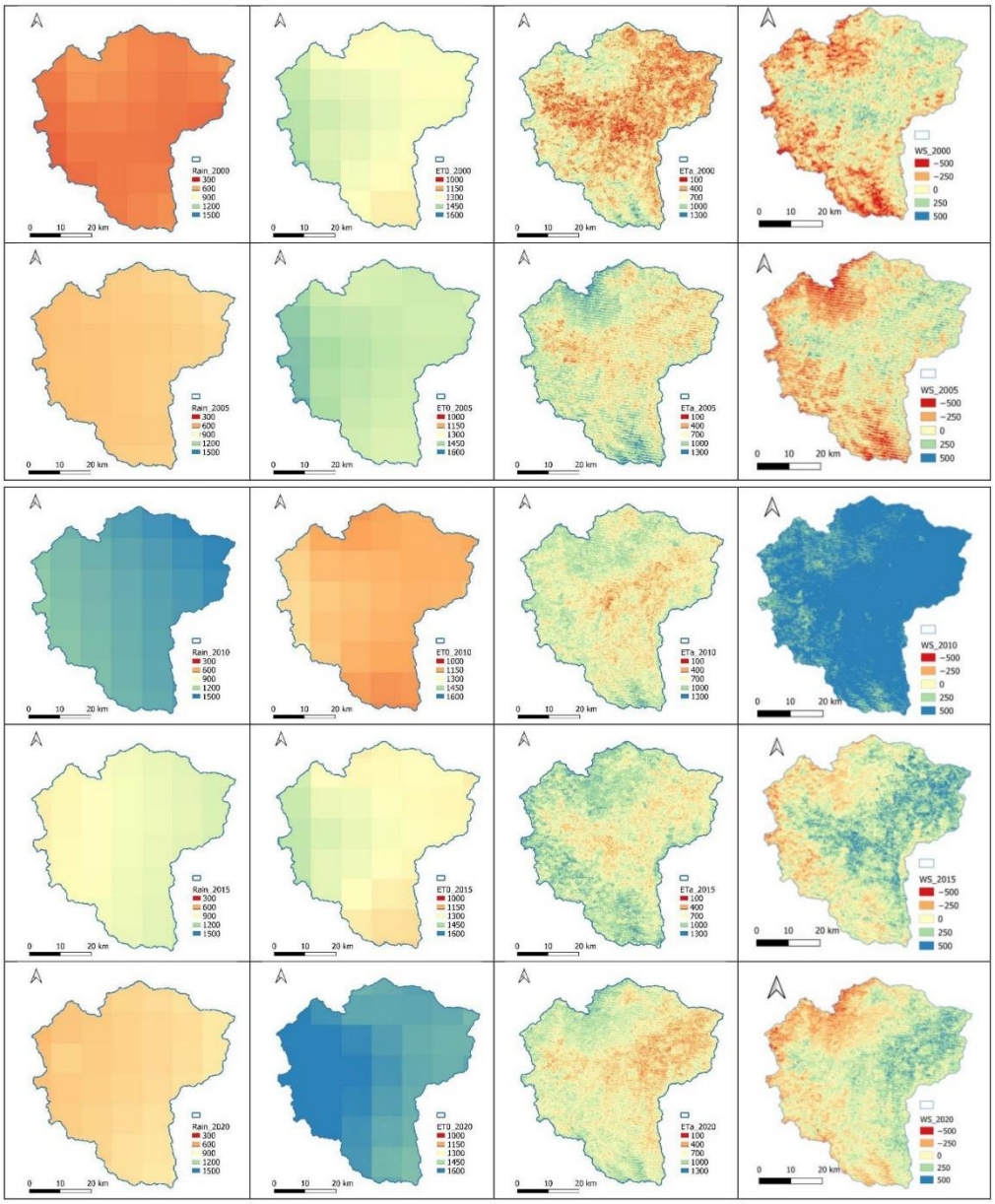

Figure 4. Changes in spatial pattern of hydroclimate parameters (annual cumulative rainfall (column 1), reference evapotranspiration (column 2), actual evapotranspiration (column 3) and water storage deficit (column 4)) from 2000 to 2020 based on geeSEBAL algorithm resulted from ERA5 reanalysis datasets over the Lockyer Catchment.

3.2. Validation of geeSEBAL ET_a and ET_o and Rain across Stations

To determine the model's accuracy, we compared the geeSEBAL algorithm driven by ERA5 reanalysis data and the reported data in the stations. Descriptive statistics results showed reasonable accuracy agreement between geeSEBAL ET_a, gridded ET_o and ERA5 rainfall and stations (Table 2). All the stations presented R^2 and Pearson correlation for rainfall ranging from 0.76 to 0.84 and from 0.87 to 0.92, respectively, and some of the stations' results are presented in Table 2. The minimum RMSE was represented by Whitestone station (37.53 mm) and West Haldon station (38.97 mm) for rainfall. Due to the lack of clear sky images, R^2 values of ET_a were low, ranging from 0.35 to 0.56 for the Upper Tenthill and Townson stations, respectively. Despite the low values of R^2, ET_a presented a similar accuracy to rain and its RMSE, ranging from 45.23 mm (Whitestone) to 58.56 mm (Upper Tenthill). On the other hand, ET_o estimates indicated a high accuracy for the 32 years, ranging from R^2 of 0.97 to 0.94, and Pearson's correlation of 0.97 to 0.96 for Townson and Placid Hills stations, respectively.

Table 2. Statistical comparison of annual cumulative rainfall, actual and potential evapotranspiration derived from geeSEBAL with the gauging station data.

Station	Variable mm	R^2 %	Pearson's Correlation	RMSE mm/Month	Bias	MBias
Gatton	P	0.76	0.87	45.38	1.14	0.16
	ET_a	0.53	0.73	49.96	−34.07	0.15
	ET_o	0.94	0.96	83.73	−71.33	0.28
Placid Hills	P	0.82	0.90	48.35	−4.63	0.16
	ET_a	0.42	0.65	54.34	−38.45	0.13
	ET_o	0.94	0.96	83.15	−69.19	0.28
Thornton	P	0.84	0.92	44.09	−9.04	0.17
	ET_a	0.54	0.73	51.47	−35.77	0.14
	ET_o	0.94	0.97	80.25	−64.27	0.27
Townson	P	0.84	0.92	57.10	−19.70	0.17
	ET_a	0.56	0.75	53.02	−39.15	0.14
	ET_o	0.95	0.97	77.29	−62.01	0.26
Upper Tenthill	P	0.80	0.89	41.93	−0.17	0.16
	ET_a	0.35	0.59	58.56	−45.15	0.12
	ET_o	0.94	0.97	81.23	−65.86	0.28
West Haldon	P	0.82	0.90	38.97	−4.07	0.16
	ET_a	0.51	0.72	49.14	−33.76	0.15
	ET_o	0.95	0.97	73.13	−56.93	0.29
Whitestone	P	0.83	0.91	37.53	3.14	0.16
	ET_a	0.54	0.74	45.23	−30.51	0.15
	ET_o	0.944	0.97	74.33	−62.85	0.28

Figure 5a–u illustrates the nominated stations' Pearson correlation which revealed a strong spatial agreement with ET_o. For all 14 stations, ET_o had remarkable agreement, ranging from 0.65 to 0.97. It also shows a similar relationship for the rain and ET_a, respectively.

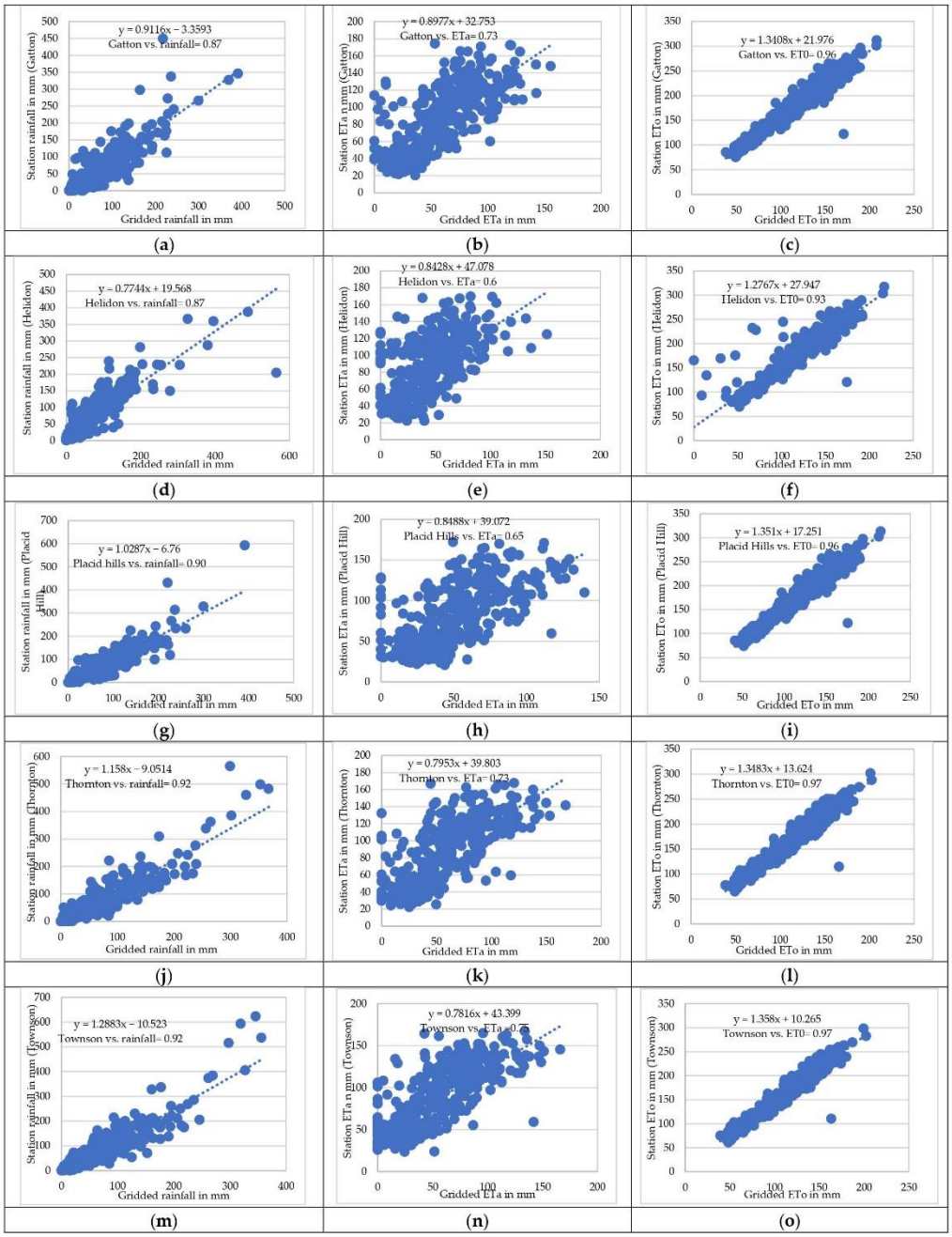

Figure 5. *Cont.*

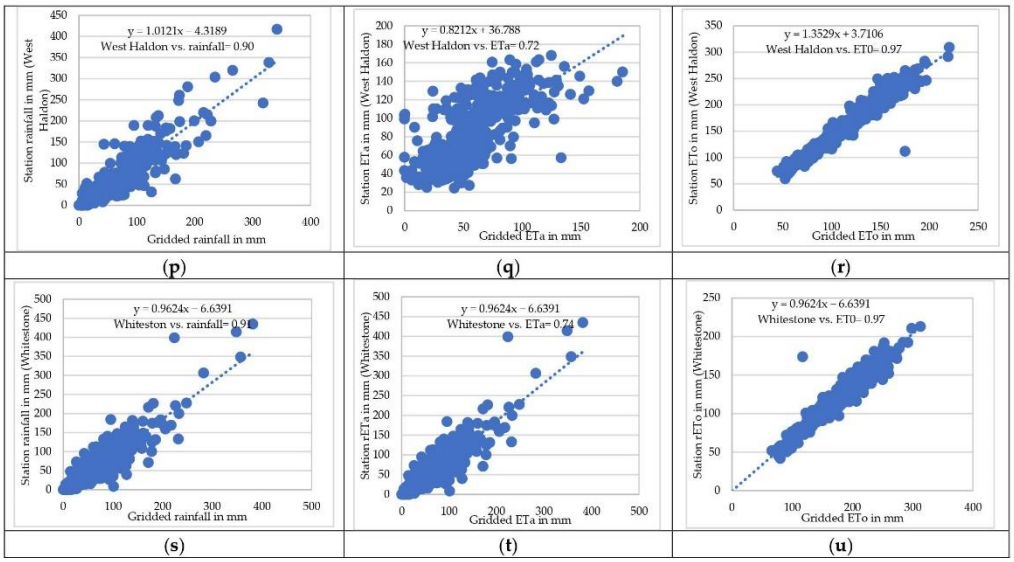

Figure 5. The relationship between monthly cumulative rainfall, reference evapotranspiration and actual evapotranspiration derived from geeSEBAL for the period 1990–2020 with the station datasets (**a**–**u**) in the Lockyer Catchment.

3.3. Results of Trends

The null hypothesis (H0) identified that there is no monotonic trend at the specified significance level (SL) in extremes. The alternative hypothesis (Ha) suggests that the data exhibit a trend at the SL. The SLs of 0.01 (1%), 0.05 (5%) and 0.1 (10%) were investigated in the calculation. The results in Table 3 show that there is a significant trend in the maximum precipitation series for the stations Placid Hills (5% SL) and Townson (1%) and the global climate dataset for Placid Hills (5% SL) and Townson (1% SL). Some stations and the global climate dataset exhibit a trend; therefore, they are in the non-stationary form.

Table 3. Detailed statistical results of trend and step change analysis of rain extremes for gauging stations in Lockyer Catchment.

Test	Statistical Tests	*p*-Value	Test Statistic	Critical Values SL = 0.1	SL = 0.05	SL = 0.01	Test Result
Placid Hills							
Trend detection	Mann–Kendall	0.028	−2.2	1.645	1.960	2.576	H0 rejected at 5%
Global climate dataset corresponding to Placid Hills							
Trend detection	Mann–Kendall	0.011	−2.5	1.645	1.960	2.576	H0 rejected at 5%
Townson							
Trend detection	Mann–Kendall	0.009	−2.62	1.645	1.960	2.576	H0 rejected at 1%
Global climate dataset corresponding to Townson							
Trend detection	Mann–Kendall	0.016	−2.41	1.645	1.960	2.576	H0 rejected at 5%

3.4. Results of Stationary and Non-Stationary Analysis for Rainfall

Studying the non-stationary aspects of the extremes is the goal of this research. Table 4 shows the return levels of rainfall for the stations and global climate data for 14 selected stations in the Lockyer Catchment which are located in the southern part of Queensland. Return levels of extreme were estimated using the NEVA software for the return periods of

10 through 100 years, which are the standard design return periods used in hydrologic studies. The (100-year return period) and (10-year return period) station rainfall in Gatton and Helidon range from 550.98 mm to 312 mm (stationary), from 624.97 mm to 324.47 mm (non-stationary) and from 441.30 mm to 279.35 mm (stationary), from 450.77 mm to 282.12 mm (non-stationary). The return levels of Townson and Placid Hills which are located next to the Gatton agricultural hub of Southeast Queensland are indicated in Table 4. Placid Hills exhibits a variation of design rainfall for (20-year return period) to (50-year return period), from 371.52 mm (stationary) to 387.93 mm (non-stationary), and from 467.35 mm (stationary) to 491.09 mm (non-stationary), respectively. However, for gridded rainfall, Placid Hills indicates the highest variability of (50-year return period) from 354.20 mm (stationary) to 624.46 mm (non-stationary). Moreover, design rainfall of Placid Hills for (20-year return period) ranges from 305.19 (stationary) to 406.05 (non-stationary). According to Table 4, the extreme rainfall events under the non-stationary assumption are higher than the extreme rainfall events under the stationary assumption in both ground-based measurements and global climate data. The results also show that the difference between the maximum rainfall events under the stationary and non-stationary assumptions in the global climate data is generally greater than in the station data for different return periods.

Table 4. The maximum rainfall (mm) in different return periods for different stations in the Lockyer Catchment.

	Rainfall		Rainfall	
Return Period	**Station**		**ERA5 Data**	
Gatton	**Stationary**	**Non-Stationary**	**Stationary**	**Non-Stationary**
10	312.64	324.47	279.35	282.12
20	379.38	402.04	325.41	328.86
50	472.53	520.23	388.93	394.75
100	550.98	624.97	441.30	450.77
Helidon				
10	339.96	336.66	292.61	325.507
20	437.19	436.11	343.12	393.58
50	596.99	606.25	417.67	492.67
100	748.07	765.74	478.62	575.84
Placid Hills				
10	310.52	323.20	267.89	298.30
20	371.52	387.83	305.19	406.05
50	467.35	491.09	354.20	624.46
100	560.60	583.60	390.19	874.67
Townson				
10	434.12	419.51	289.18	303.4
20	528.48	513.25	344.46	365.64
50	670.93	657.57	424.26	460.33
100	796.57	788.64	493.24	544
Whitestone				
10	311.75	325.49	285.94	285.94
20	370.14	390.83	340.92	340.92
50	452.33	479.13	422.21	422.21
100	512.60	546.52	499.93	499.93

Table 4 shows the variation in gridded rainfall data for the 100-year return period from 450.77 mm (non-stationary) to 441.30 mm (stationary) for Gatton and from 575.84 mm (non-stationary) to 478.62 mm (stationary) for Helidon. For the design rainfall in Helidon (gridded data), for a 100-year period, the change between stationary and non-stationary was more noticeable; 97.22 mm compared to 9.45 mm in Gatton. Whereas in Helidon (station data), the difference between stationary and non-stationary indicates less variability, 17.4 mm (100-year period) compared to Gatton, 73.99 mm (100-year period). Of the 14 stations, the GEV distribution rainfall shows that 5 stations' data (Helidon, Gatton, Placid hills, Townson and Whitestone) and 3 gridded data (Helidon, Gatton and Placid hills) represent the non-stationary condition, respectively (Table 4). As Gatton is identified as the agricultural hub in Southeast Queensland, it is important to understand the short, intense rainfall for water resource management. As can be seen from Table 4, Gatton station represents the most remarkable variations in comparison to other stations. Rainfall return levels at high return periods were found to have noticeable variation compared to low return periods. The ERA5 estimates are noticeably lower than the station-based estimates for the region, as shown in Table 4, especially at the 50 and 100-year return periods.

3.5. Results of Stationary and Non-Stationary Analysis for Evapotranspiration

For the management of water resources, a precise estimation of evapotranspiration is necessary. Among the ET algorithms, SEBAL is the most promising methods for estimating evapotranspiration [18]. The GEV distribution evapotranspiration confirmed that, of the 14 stations, 6 stations' data (Helidon, Gatton, Placid hills, Thornton, Townson and Whitestone) and 2 gridded data (Thornton and Whitestone) exhibited the non-stationary condition.

Figures 6 and 7 show the return levels for evapotranspiration derived from the geeSEBAL algorithm for both station and global climate data. According to Figure 6a–e, stations' actual evapotranspiration shows a range of 184.88 mm (stationary) to 169.02 mm (non-stationary) for the 100-year return period and from 169.38 mm (stationary) to 157.86 mm (non-stationary) for the 10-year period in Gatton. Helidon also exhibits variation in ET_a, ranging from 189.76 mm (stationary) to 161.98 mm (non-stationary), from 164.43 mm (stationary) to 153.41 mm (non-stationary) for (100-year period) and (10-year period), respectively. The difference between stationary and non-stationary reaches 27.78 mm in Helidon compared to 13.99 mm in Townson for the 100-year return period. Additionally, this demonstrates that Helidon experiences significant variability compared to other stations. According to Figure 7a-d, ET_a derived from the geeSEBAL algorithm ranges from 171.32 mm (stationary) to 170.62 mm (non-stationary) for the 100-year period and from 149.57 mm (stationary) to 146.22 mm (non-stationary) for the 10-year period in Thornton. The least variation is observed from the 100-year to 10-year return level periods.

3.6. Results of Stationary and Non-Stationary Analysis for Water Storage

Due to a lack of field data for water storage, this variable was assessed based on the satellite-derived images. The return levels of water storage for station and global climate data are shown in Table 5. The 10-year and 100-year return levels' water storage derived using the global climate data varies from 202.44 mm to 224.80 mm and from 95.45 mm to 108.70 mm for stationary and non-stationary, respectively in Gatton. The results of the Gatton station data illustrate no variation between the stationary and non-stationary conditions. Whitestone and Gatton act quite similarly when experiencing non-stationary conditions in the global climate data. The GEV distribution for water storage in Whitestone station varies from 321.33 mm (stationary) to 344.60 mm (non-stationary), from 99.57 mm (stationary) to 106.32 mm (non-stationary) for (100-year period) and (10-year period), respectively, whereas the rest of the stations indicate a lack of variation in the stationary condition.

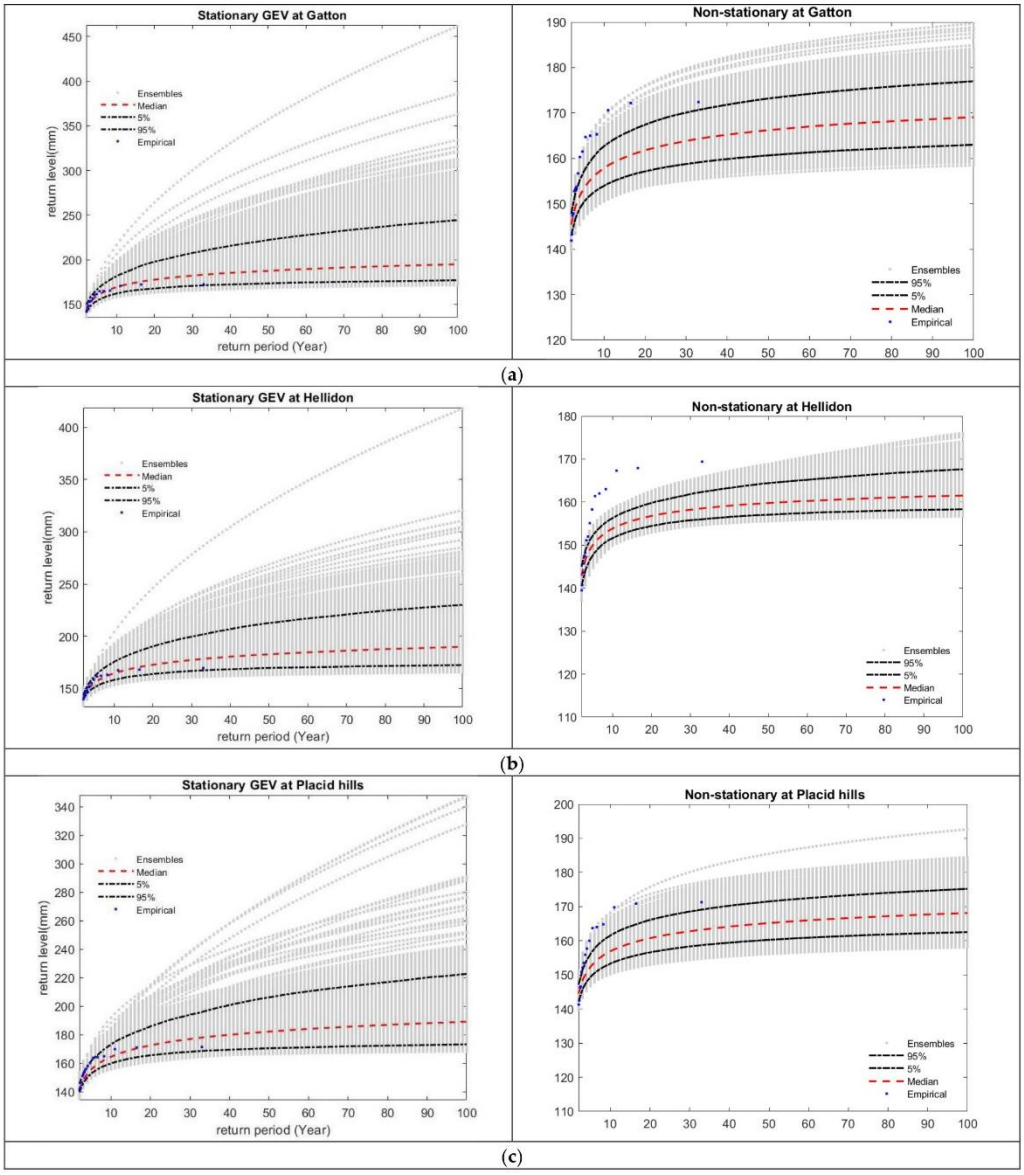

Figure 6. *Cont.*

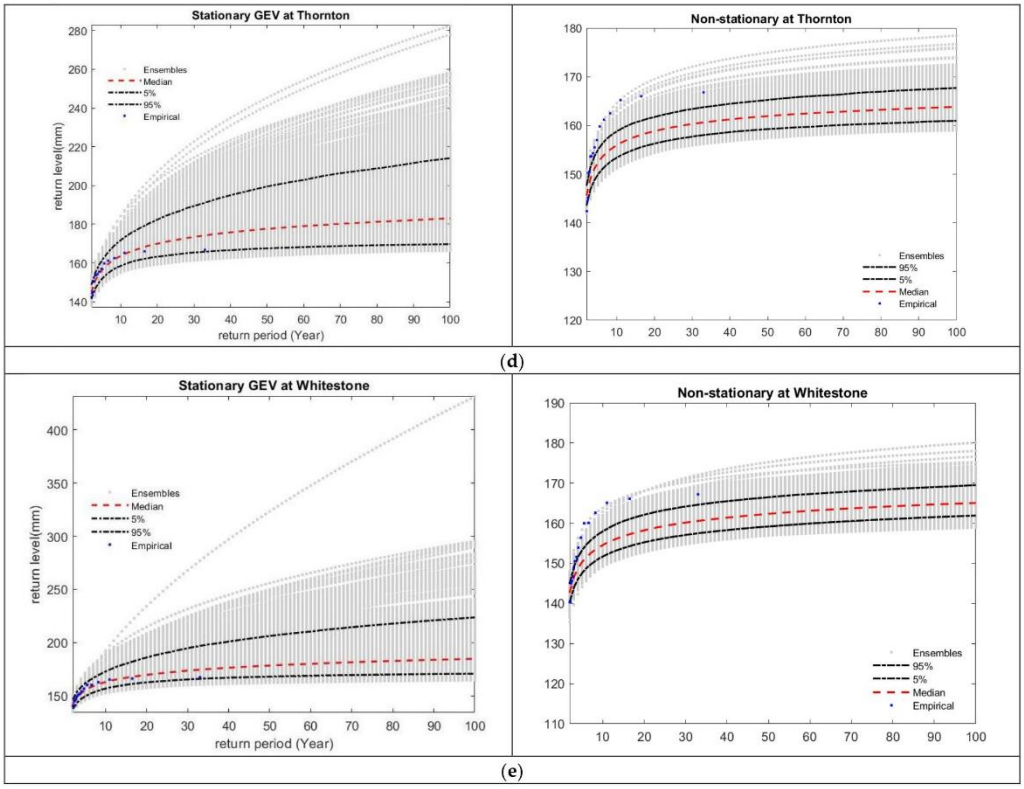

Figure 6. The output of NEVA's non-stationary GEV framework, standard return levels with design exceedance probability for ET_a based on station data (**a**–**e**) (Figure generated using MATLAB).

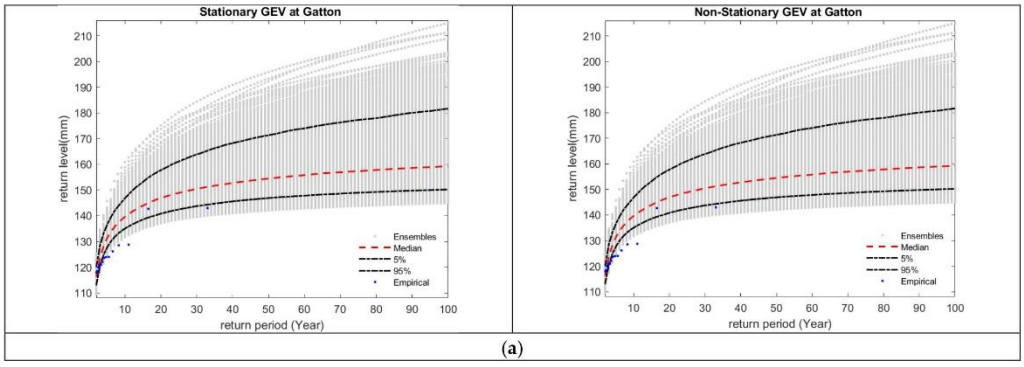

Figure 7. *Cont.*

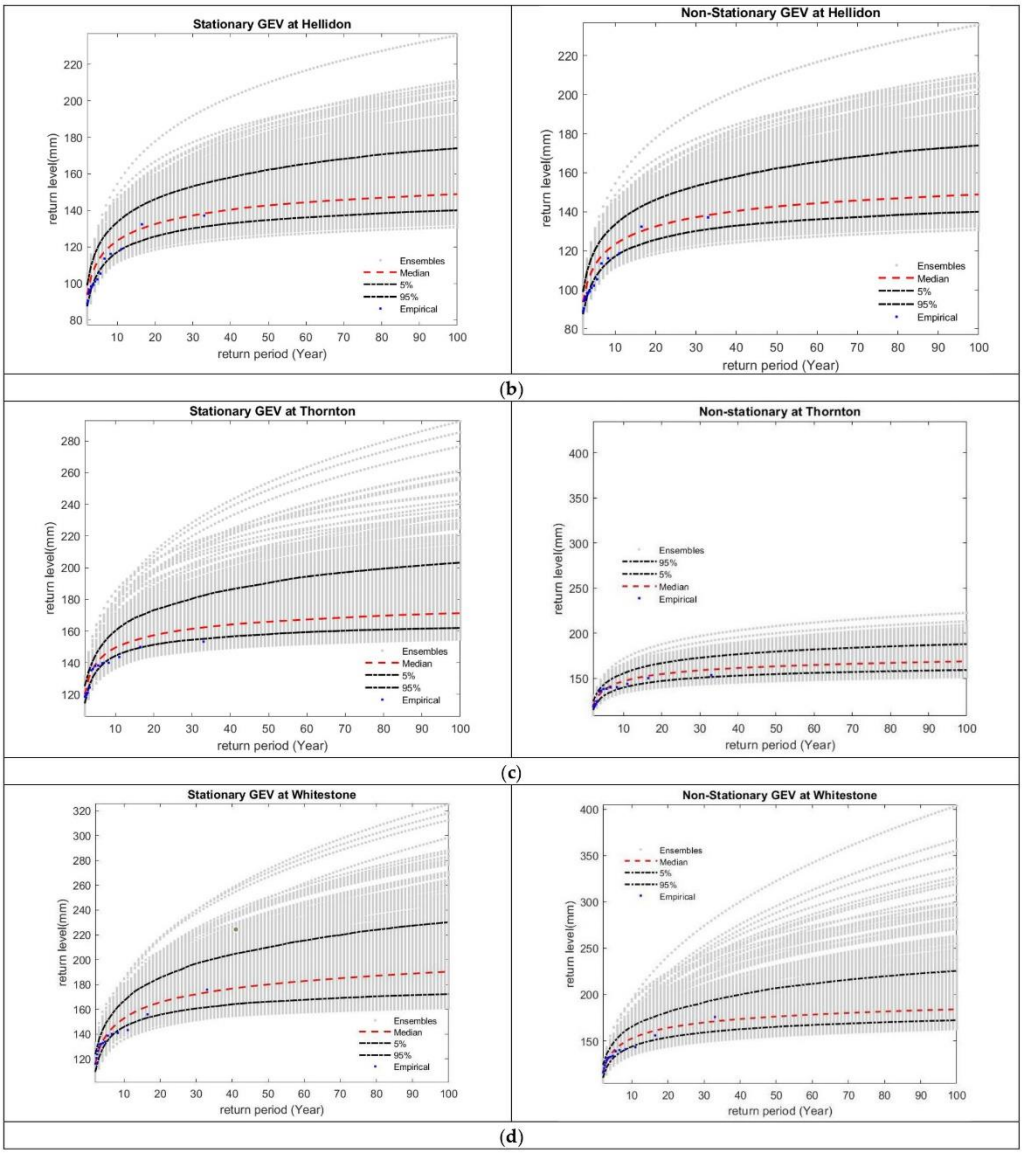

Figure 7. The output of NEVA's non-stationary GEV framework, standard return levels with design exceedance probability for ET_a based on global climate data (**a–d**) (Figure generated using MATLAB).

Table 5. The maximum water storage in different return periods of different stations in the Lockyer Catchment.

	Water Storage		Water Storage	
Return Period	**Based on Station**		**Based on ERA5 Data**	
Gatton	**Stationary**	**Non-Stationary**	**Stationary**	**Non-Stationary**
10	100.71	100.71	95.45	108.70
20	144.89	144.89	126.97	142.55
50	202.65	202.65	168.84	188.3
100	247.64	247.64	202.44	224.80
Helidon				
10	133.93	133.93	132.96	132.96
20	196.26	196.26	156.91	156.91
50	286.70	286.70	195.64	195.64
100	363.34	363.34	224.83	224.83
Placid Hills				
10	120.79	120.79	113.70	113.70
20	179.07	179.07	136.92	136.92
50	255.67	255.67	163.25	158.23
100	316.06	316.06	180.55	176.99
Thornton				
10	165.76	165.76	110.55	110.55
20	233.13	233.13	137.04	137.04
50	328.51	328.51	174.03	174.03
100	415.159	415.159	199.66	199.66
Townson				
10	197.20	197.20	97.80	97.80
20	256.35	256.35	136.77	136.77
50	343.19	343.19	193.38	193.38
100	411.08	411.08	241.17	241.17
Whitestone				
10	99.57	106.32	96.92	96.92
20	156.79	164.97	147.03	147.03
50	244.30	258.30	231.33	231.33
100	321.33	344.60	314.13	314.13

4. Discussion

This research study's results clearly indicate that extreme events including extreme rainfall, extreme evapotranspiration and water storage deficit under the stationary assumption are mostly lower than the extreme events under the non-stationary assumption in both station and global climate datasets. Like previous studies on rainfall IDF [60,61], the annual rainfall extremes, evapotranspiration extremes and water storage extremes are well-described by the GEV distribution. In a previous study, the global-scale models of climate variability were considered in the development of nonstationary TDF curves in Canada [28]. Another study on rainfall IDF shows that adoption of stationary assumption underestimates the design climate extremes [23]. Since rainfall extremes are well-researched

from both the stationary and nonstationary perspectives [62,63], a comparison can easily be made. This study considered stationary and non-stationary assumptions. The reasons for adopting this approach are its easy estimation procedure which is suitable for professional applications. In the majority of instances, the gap between stationary and non-stationary widens as the return period increases as it is highlighted in several studies [1,64]. Numerous studies have been performed around the world to prove the effect of non-stationary on extreme values [65,66]. Moreover, the extreme events in all studied variables and return periods of the global climate data are lower than the extreme events of the ground-based measurements. The spatial patterns derived from ERA5 land reanalysis data closely resemble the station data for water storage and rainfall. In ET_a, ERA5 reanalysis and station were approximately the same. However, the ERA5 land data of some years overestimates the higher spatial variability compared to station data. Therefore, reanalysis data offers satisfactory outcomes for estimating ET_a, providing an intriguing option for assessing spatial and temporal aspects across regional and continental scales.

A common pattern of uncertainty ranging between stationary and non-stationary assumptions is noticed across all stations with varying variables, including extreme rainfall, extreme ET_a and extreme water storage deficit. The findings suggest that extreme rainfall shows a greater disparity between ground-based measurements made under stationary and non-stationary assumptions compared to data obtained from global climate products. The uncertainty range expands from the 10-year period to 100-year period, with the water storage deficit showing less variation between stationary and non-stationary conditions, while rainfall exhibits a sharp variation, and evapotranspiration shows moderate variation. Evapotranspiration and water storage derived from ERA5 land reanalysis data follow the same uncertainty with stations' data. The highest difference between stationary and non-stationary 100-year station rainfall is observed in Thornton (89.25 mm), Gatton (73.99 mm), Whitestone (33.92 mm), Placid Hills (23 mm) and Helidon (17.67 mm), respectively. It is noted that the global climate data tends to underestimate the outcomes in comparison to station data. Overall, this study highlights the importance of considering non-stationary conditions in hydroclimatic analysis and provides valuable insights into the performance of the geeSEBAL algorithm and NEVA methods for estimating and analysing hydrological variables.

5. Conclusions

In this study, the non-stationary and stationary conditions for extreme rainfall, extreme evapotranspiration and water storage deficit were investigated in Southeast Queensland (SEQ), Australia. The geeSEBAL algorithm was used to generate actual evapotranspiration, and the NEVA programme was used to estimate the intensity and frequency of extremes using the GEV distribution. The estimation was likely based on the assumption that the location parameter has a linear relationship with time. The key findings of this study are as follows: (1) The ET_a derived from geeSEBAL by feeding global climate products overestimates ET_a derived from geeSEBAL by feeding station data; (2) the statistical results indicate reasonable accuracy agreement between global climate datasets, P, ET_o and geeSEBAL ET_a and ground-based measurements; (3) the analysis of the spatiotemporal distribution of rainfall is almost identical with two different climate datasets (ground-based observations and global climate products). ET_0 from global climate datasets underestimates the results compared to station data. Interestingly, rainfall and ET_a have shown that the highest rise is in the year 2010, which admits the historical flooding in SEQ; (4) the spatiotemporal distribution of water storage derived from a lump water balance remains the same for both climate datasets; (5) the intensity and frequency of rainfall extremes, evapotranspiration extremes and water storage deficit extremes under the stationary assumption are mostly lower than extreme events under the non-stationary assumption in both ground-based and global climate datasets under different return levels.

This research utilised the geeSEBAL algorithm in the Google Earth Engine (GEE) environment to estimate evapotranspiration (ET) at regional scales using Landsat imagery.

Understanding the dynamics of evapotranspiration (ET) is essential to address the challenges related to freshwater scarcity and increased water demand for agriculture and food production. While the GEV distribution approach was employed to analyse extremes, further investigations into other mechanisms, such as evapotranspiration and water storage, would provide a more comprehensive understanding of the underlying issues. The examination of station data also demonstrated that, even though geeSEBAL primarily relies on reanalysis data for meteorological input, the estimations of ET are similar to those obtained when the algorithm is supplied with real ground-based observations of meteorological conditions. The evaluation of ET_a and water storage deficit demonstrated that the geeSEBAL algorithm has the capability to enhance irrigation management in Gatton, a prominent agricultural centre in the study area. By addressing the rising water needs for food production and water supplies, it also has the ability to lessen the consequences of drought [45]. This research can provide a foundation for future research and facilitate comparisons with existing studies by focusing on advanced statistical analysis. Understanding the statistical properties and characteristics of extreme events is essential for risk assessment and management and for the development of adaptation strategies. From the results, it can be concluded that extreme events under the stationary assumption are lower than extreme events under the non-stationary assumption in both global climate products and ground-based measurements for this region. In this study, the framework used examined the severity and coverage of various variables by analysing their frequency, intensity and duration, thereby exploring their spatiotemporal evolution. This framework can be applied to any geographical area, providing estimations of extreme conditions that are essential for infrastructure planning and design, risk assessment and disaster management. As we only covered the non-stationary conditions in extreme events with NEVA by incorporating the outputs of geeSEBAL, it is recommended that, in future studies, spatial Bayesian Hierarchical Modelling methods and ProNEVA [67] that allow for the incorporation of additional covariates for modelling the spatial variability observed in the GEV parameters are applied.

The outcomes regarding extreme events highlight that failure to account for non-stationary conditions and neglecting trends in extreme events results in inaccuracies when estimating such events. These inaccuracies can lead to errors in infrastructure development and design, causing financial losses and potential harm to human lives. Conducting detailed investigations into the underlying causes of extremes can be interesting for future studies. By quantifying the probabilities of extreme occurrences, decision-makers can make informed choices regarding infrastructure development, resource allocation and emergency planning.

Author Contributions: Conceptualization, Hadis Pakdel, Dev Raj Paudyal, Sreeni Chadalavada, Md Jahangir Alam and Majid Vazifedoust; Methodology, Hadis Pakdel, Dev Raj Paudyal, Sreeni Chadalavada, Md Jahangir Alam and Majid Vazifedoust; Software, Hadis Pakdel and Majid Vazifedoust; Validation, Hadis Pakdel; Formal analysis, Hadis Pakdel and Majid Vazifedoust; Investigation, Hadis Pakdel; Resources, Hadis Pakdel; Data curation, Hadis Pakdel; Writing—original draft preparation, Hadis Pakdel; Writing—review and editing, Dev Raj Paudyal, Sreeni Chadalavada, Md Jahangir Alam and Majid Vazifedoust; Visualization, Hadis Pakdel; Supervision, Dev Raj Paudyal, Sreeni Chadalavada and Md Jahangir Alam; Project administration, Dev Raj Paudyal, Sreeni Chadalavada and Md Jahangir Alam. All authors have read and agreed to the published version of the manuscript.

Funding: This research received no external funding. This research was supported by the Graduate Research School, University of Southern Queensland and this is part of the first author's PhD project entitled "Variability of Extreme Climate Events and Impacts of Future Climate Change on the Streamflow".

Data Availability Statement: The data supporting the findings of this study are available from the first author upon reasonable request.

Acknowledgments: The authors would like to thank the reviewers and the editors who gave valuable time to review the manuscript.

Conflicts of Interest: The authors declare no conflict of interest. Jahangir Alam works at the MDBA; however, this research has no link with the MDBA.

References

1. Cheng, L.; AghaKouchak, A.; Gilleland, E.; Katz, R.W. Non-stationary extreme value analysis in a changing climate. *Clim. Chang.* **2014**, *127*, 353–369. [CrossRef]
2. IPCC. *Climate Change 2007: Synthesis Report. Contribution of Working Groups I, II and III to the Fourth Assessment Report of the Intergovernmental Panel on Climate Change*; Core Writing Team, Pachauri, R.K., Reisinger, A., Eds.; Cambridge University Press: Cambridge, UK, 2007; p. 104.
3. Salas, J.; Obeysekera, J.; Vogel, R. Techniques for assessing water infrastructure for nonstationary extreme events: A review. *Hydrol. Sci. J.* **2018**, *63*, 325–352. [CrossRef]
4. Cooley, D. Extreme value analysis and the study of climate change. *Clim. Chang.* **2009**, *97*, 77–83. [CrossRef]
5. Love, C.A.; Skahill, B.E.; Russell, B.T.; Baggett, J.S.; AghaKouchak, A. An Effective Trend Surface Fitting Framework for Spatial Analysis of Extreme Events. *Geophys. Res. Lett.* **2022**, *49*, e2022GL098132. [CrossRef]
6. Salas, J.D.; Obeysekera, J. Revisiting the concepts of return period and risk for nonstationary hydrologic extreme events. *J. Hydrol. Eng.* **2014**, *19*, 554–568. [CrossRef]
7. Cooley, D. Return periods and return levels under climate change. In *Extremes in a Changing Climate*; AghaKouchak, A., Easterling, D., Hsu, K., Schubert, S., Sorooshian, S., Eds.; Water Science and Technology Library; Springer: Berlin/Heidelberg, Germany, 2013; Volume 65, pp. 97–114.
8. Abbs, D.; McInnes, K.; Rafter, T. The impact of climate change on extreme rainfall and coastal sea levels over south-east Queensland. *Div. Mar. Atmos. Res. Commonw. Sci. Ind. Res. Organ. Aust.* **2007**. Available online: https://www.cmar.csiro.au/e-print/open/2007/abbsdj_c.pdf (accessed on 2 September 2023).
9. Mpelasoka, F.; Hennessy, K.; Jones, R.; Bates, B. Comparison of suitable drought indices for climate change impacts assessment over Australia towards resource management. *Int. J. Climatol. A J. R. Meteorol. Soc.* **2008**, *28*, 1283–1292. [CrossRef]
10. Zhang, H.; Wang, B.; Li Liu, D.; Zhang, M.; Feng, P.; Cheng, L.; Yu, Q.; Eamus, D. Impacts of future climate change on water resource availability of eastern Australia: A case study of the Manning River basin. *J. Hydrol.* **2019**, *573*, 49–59. [CrossRef]
11. Laipelt, L.; Kayser, R.H.B.; Fleischmann, A.S.; Ruhoff, A.; Bastiaanssen, W.; Erickson, T.A.; Melton, F. Long-term monitoring of evapotranspiration using the SEBAL algorithm and Google Earth Engine cloud computing. *ISPRS J. Photogramm. Remote Sens.* **2021**, *178*, 81–96. [CrossRef]
12. Kiem, A.S.; Johnson, F.; Westra, S.; van Dijk, A.; Evans, J.P.; O'Donnell, A.; Rouillard, A.; Barr, C.; Tyler, J.; Thyer, M. Natural hazards in Australia: Droughts. *Clim. Chang.* **2016**, *139*, 37–54. [CrossRef]
13. Van Loon, A.F.; Stahl, K.; Di Baldassarre, G.; Clark, J.; Rangecroft, S.; Wanders, N.; Gleeson, T.; Van Dijk, A.I.; Tallaksen, L.M.; Hannaford, J. Drought in a human-modified world: Reframing drought definitions, understanding, and analysis approaches. *Hydrol. Earth Syst. Sci.* **2016**, *20*, 3631–3650. [CrossRef]
14. Ajami, H.; Sharma, A.; Band, L.E.; Evans, J.P.; Tuteja, N.K.; Amirthanathan, G.E.; Bari, M.A. On the non-stationarity of hydrological response in anthropogenically unaffected catchments: An Australian perspective. *Hydrol. Earth Syst. Sci.* **2017**, *21*, 281–294. [CrossRef]
15. Petheram, C.; Potter, N.; Vaze, J.; Chiew, F.; Zhang, L. Towards better understanding of changes in rainfall-runoff relationships during the recent drought in south-eastern Australia. In Proceedings of the 19th International Congress on Modelling and Simulation, Perth, Australia, 12–16 December 2011; pp. 12–16.
16. IPCC. *Climate Change 2014: Synthesis Report. Contribution of Working Groups I, II and III to the Fifth Assessment Report of the Intergovernmental Panel on Climate Change*; IPCC: Geneva, Switzerland, 2014.
17. Bastiaanssen, W.G.; Menenti, M.; Feddes, R.A.; Holtslag, A.A.M. A remote sensing surface energy balance algorithm for land (SEBAL). 1. Formulation. *J. Hydrol.* **1998**, *212*, 198–212. [CrossRef]
18. Liou, Y.-A.; Kar, S.K. Evapotranspiration estimation with remote sensing and various surface energy balance algorithms—A review. *Energies* **2014**, *7*, 2821–2849. [CrossRef]
19. Gebremichael, M.; Wang, J.; Sammis, T.W. Dependence of remote sensing evapotranspiration algorithm on spatial resolution. *Atmos. Res.* **2010**, *96*, 489–495. [CrossRef]
20. Allen, R.G.; Tasumi, M.; Morse, A.; Trezza, R.; Wright, J.L.; Bastiaanssen, W.; Kramber, W.; Lorite, I.; Robison, C.W. Satellite-based energy balance for mapping evapotranspiration with internalized calibration (METRIC)—Applications. *J. Irrig. Drain. Eng.* **2007**, *133*, 395–406. [CrossRef]
21. Bezerra, B.G.; da Silva, B.B.; dos Santos, C.A.; Bezerra, J.R. Actual evapotranspiration estimation using remote sensing: Comparison of SEBAL and SSEB approaches. *Adv. Remote Sens.* **2015**, *4*, 234. [CrossRef]
22. Allen, R.G.; Burnett, B.; Kramber, W.; Huntington, J.; Kjaersgaard, J.; Kilic, A.; Kelly, C.; Trezza, R. Automated calibration of the METRIC-Landsat evapotranspiration process. *JAWRA J. Am. Water Resour. Assoc.* **2013**, *49*, 563–576. [CrossRef]

23. Cheng, L.; AghaKouchak, A. Nonstationary precipitation intensity-duration-frequency curves for infrastructure design in a changing climate. *Sci. Rep.* **2014**, *4*, 7093. [CrossRef]
24. Jones, B.; Tebaldi, C.; O'Neill, B.C.; Oleson, K.; Gao, J. Avoiding population exposure to heat-related extremes: Demographic change vs climate change. *Clim. Chang.* **2018**, *146*, 423–437. [CrossRef]
25. Khaliq, M.N.; St-Hilaire, A.; Ouarda, T.B.; Bobée, B. Frequency analysis and temporal pattern of occurrences of southern Quebec heatwaves. *Int. J. Climatol. A J. R. Meteorol. Soc.* **2005**, *25*, 485–504. [CrossRef]
26. Rainham, D.G.; Smoyer-Tomic, K.E. The role of air pollution in the relationship between a heat stress index and human mortality in Toronto. *Environ. Res.* **2003**, *93*, 9–19. [CrossRef]
27. Huth, R.; Kyselý, J.; Pokorná, L. A GCM simulation of heat waves, dry spells, and their relationships to circulation. *Clim. Chang.* **2000**, *46*, 29–60. [CrossRef]
28. Ouarda, T.B.; Charron, C. Nonstationary temperature-duration-frequency curves. *Sci. Rep.* **2018**, *8*, 15493. [CrossRef] [PubMed]
29. Mazdiyasni, O.; Sadegh, M.; Chiang, F.; AghaKouchak, A. Heat wave intensity duration frequency curve: A multivariate approach for hazard and attribution analysis. *Sci. Rep.* **2019**, *9*, 11609. [CrossRef] [PubMed]
30. Ball, J.; Babister, M.; Nathan, R.; Weinmann, P.; Weeks, W.; Retallick, M.; Testoni, I. *Australian Rainfall and Runoff-A Guide to Flood Estimation*; Commonwealth of Australia: Canberra, Australia, 2019.
31. Pakdel Khasmakhi, H.; Vazifedoust, M.; Paudyal, D.R.; Chadalavada, S.; Alam, M.J. Google Earth Engine as Multi-Sensor Open-Source Tool for Monitoring Stream Flow in the Transboundary River Basin: Doosti River Dam. *ISPRS Int. J. Geo-Inf.* **2022**, *11*, 535. [CrossRef]
32. Sarker, A.; Ross, H.; Shrestha, K.K. A common-pool resource approach for water quality management: An Australian case study. *Ecol. Econ.* **2008**, *68*, 461–471. [CrossRef]
33. WetlandInfo. Wetland Management Resources in Queensland. Available online: https://wetlandinfo.des.qld.gov.au/wetlands/ (accessed on 6 March 2022).
34. Kiem, A.S.; Vance, T.R.; Tozer, C.R.; Roberts, J.L.; Dalla Pozza, R.; Vitkovsky, J.; Smolders, K.; Curran, M.A. Learning from the past. Using palaeoclimate data to better understand and manage drought in South East Queensland (SEQ), Australia. *J. Hydrol. Reg. Stud.* **2020**, *29*, 100686. [CrossRef]
35. Vance, T.; Roberts, J.; Plummer, C.; Kiem, A.; Van Ommen, T. Interdecadal Pacific variability and eastern Australian megadroughts over the last millennium. *Geophys. Res. Lett.* **2015**, *42*, 129–137. [CrossRef]
36. Lockyer Creek wiki 2022. Available online: https://en.wikipedia.org/wiki/Lockyer_Creek (accessed on 14 May 2022).
37. Cui, T.; Raiber, M.; Pagendam, D.; Gilfedder, M.; Rassam, D. Response of groundwater level and surface-water/groundwater interaction to climate variability: Clarence-Moreton Basin, Australia. *Hydrogeol. J.* **2018**, *26*, 593–614. [CrossRef]
38. Armstrong, M.S.; Kiem, A.S.; Vance, T.R. Comparing instrumental, palaeoclimate, and projected rainfall data: Implications for water resources management and hydrological modelling. *J. Hydrol. Reg. Stud.* **2020**, *31*, 100728. [CrossRef]
39. CSIRO; BOM. *Climate Change in Australia Information for Australia's Natural Resource Management Regions: Technical Report*; CSIRO and Bureau of Meteorology: Canberra, Australia, 2015.
40. Jeffrey, S.J.; Carter, J.O.; Moodie, K.B.; Beswick, A.R. Using spatial interpolation to construct a comprehensive archive of Australian climate data. *Environ. Model. Softw.* **2001**, *16*, 309–330. [CrossRef]
41. Ramezani, M.R.; Yu, B.; Tarakemehzadeh, N. Satellite-derived spatiotemporal data on imperviousness for improved hydrological modelling of urbanised catchments. *J. Hydrol.* **2022**, *612*, 128101. [CrossRef]
42. Mission, N.S.R.T. Shuttle Radar Topography Mission (SRTM) Global. Distributed by OpenTopography. 2013. Available online: https://www.fdsn.org/networks/detail/GH/ (accessed on 15 September 2022).
43. Gorelick, N.; Hancher, M.; Dixon, M.; Ilyushchenko, S.; Thau, D.; Moore, R. Google Earth Engine: Planetary-scale geospatial analysis for everyone. *Remote Sens. Environ.* **2017**, *202*, 18–27. [CrossRef]
44. Kayser, R.H.; Ruhoff, A.; Laipelt, L.; de Mello Kich, E.; Roberti, D.R.; de Arruda Souza, V.; Rubert, G.C.D.; Collischonn, W.; Neale, C.M.U. Assessing geeSEBAL automated calibration and meteorological reanalysis uncertainties to estimate evapotranspiration in subtropical humid climates. *Agric. For. Meteorol.* **2022**, *314*, 108775. [CrossRef]
45. Gonçalves, I.Z.; Ruhoff, A.; Laipelt, L.; Bispo, R.; Hernandez, F.B.T.; Neale, C.M.U.; Teixeira, A.H.d.C.; Marin, F.R. Remote sensing-based evapotranspiration modeling using geeSEBAL for sugarcane irrigation management in Brazil. *Agric. Water Manag.* **2022**, *274*, 107965. [CrossRef]
46. Foga, S.; Scaramuzza, P.L.; Guo, S.; Zhu, Z.; Dilley Jr, R.D.; Beckmann, T.; Schmidt, G.L.; Dwyer, J.L.; Hughes, M.J.; Laue, B. Cloud detection algorithm comparison and validation for operational Landsat data products. *Remote Sens. Environ.* **2017**, *194*, 379–390. [CrossRef]
47. Vazifedoust, M. *Development of an Agricultural Drought Assessment System: Integration of Agrohydrological Modelling, Remote Sensing and Geographical Information*; Wageningen University and Research: Wageningen, The Netherlands, 2007.
48. Carey, B.; Stone, B.; Shilton, P.; Norman, P. Soil Conservation Guidelines for Queensland Chapter 4. In *The Empirical Version of the Rational Method*; Department of Environment and Resource; Queensland Government: Queensland, Australia, 2015.
49. Madsen, H. *Time Series Analysis*; CRC Press: Boca Raton, FL, USA, 2007.
50. Durocher, M.; Burn, D.H.; Ashkar, F. Comparison of estimation methods for a nonstationary Index-Flood Model in flood frequency analysis using peaks over threshold. *Water Resour. Res.* **2019**, *55*, 9398–9416. [CrossRef]

51. Moisello, U. On the use of partial probability weighted moments in the analysis of hydrological extremes. *Hydrol. Process. Int. J.* **2007**, *21*, 1265–1279. [CrossRef]
52. Coles, S.; Bawa, J.; Trenner, L.; Dorazio, P. *An Introduction to Statistical Modeling of Extreme Values*; Springer: Berlin/Heidelberg, Germany, 2001; Volume 208.
53. Morrison, J.E.; Smith, J.A. Stochastic modeling of flood peaks using the generalised extreme value distribution. *Water Resour. Res.* **2002**, *38*, 41-1–41-12. [CrossRef]
54. Mann, H.B. Nonparametric tests against trend. *Econom. J. Econom. Soc.* **1945**, *13*, 245–259. [CrossRef]
55. Xu, C.-y.; Gong, L.; Jiang, T.; Chen, D.; Singh, V. Analysis of spatial distribution and temporal trend of reference evapotranspiration and pan evaporation in Changjiang (Yangtze River) catchment. *J. Hydrol.* **2006**, *327*, 81–93. [CrossRef]
56. Da Silva, R.M.; Santos, C.A.; Moreira, M.; Corte-Real, J.; Silva, V.C.; Medeiros, I.C. Rainfall and river flow trends using Mann–Kendall and Sen's slope estimator statistical tests in the Cobres River basin. *Nat. Hazards* **2015**, *77*, 1205–1221. [CrossRef]
57. Nyikadzino, B.; Chitakira, M.; Muchuru, S. Rainfall and runoff trend analysis in the Limpopo river basin using the Mann Kendall statistic. *Phys. Chem. Earth Parts A/B/C* **2020**, *117*, 102870. [CrossRef]
58. Burkey, J. *A Non-Parametric Monotonic Trend Test Computing Mann-Kendall Tau, Tau-b, and Sen's Slope Written in Mathworks-MATLAB Implemented Using Matrix Rotations*; King County, Department of Natural Resources and Parks, Science and Technical Services section: Seattle, WA, USA, 2006.
59. McGowan, J. A missed opportunity to promote community resilience?–The Queensland Floods Commission of Inquiry. *Aust. J. Public Adm.* **2012**, *71*, 355–363. [CrossRef]
60. Courty, L.G.; Wilby, R.L.; Hillier, J.K.; Slater, L.J. Intensity-duration-frequency curves at the global scale. *Environ. Res. Lett.* **2019**, *14*, 084045. [CrossRef]
61. Papalexiou, S.M.; Koutsoyiannis, D. Battle of extreme value distributions: A global survey on extreme daily rainfall. *Water Resour. Res.* **2013**, *49*, 187–201. [CrossRef]
62. Mondal, A.; Mujumdar, P.P. Modeling non-stationarity in intensity, duration and frequency of extreme rainfall over India. *J. Hydrol.* **2015**, *521*, 217–231. [CrossRef]
63. Westra, S.; Alexander, L.V.; Zwiers, F.W. Global increasing trends in annual maximum daily precipitation. *J. Clim.* **2013**, *26*, 3904–3918. [CrossRef]
64. Sadeghi Loyeh, N.; Massah Bavani, A. Daily maximum runoff frequency analysis under non-stationary conditions due to climate change in the future period: Case study Ghareh Sou Basin. *J. Water Clim. Chang.* **2021**, *12*, 1910–1929. [CrossRef]
65. Serago, J.M.; Vogel, R.M. Parsimonious nonstationary flood frequency analysis. *Adv. Water Resour.* **2018**, *112*, 1–16. [CrossRef]
66. Faulkner, D.; Warren, S.; Spencer, P.; Sharkey, P. Can we still predict the future from the past? Implementing non-stationary flood frequency analysis in the UK. *J. Flood Risk Manag.* **2020**, *13*, e12582. [CrossRef]
67. Ragno, E.; AghaKouchak, A.; Cheng, L.; Sadegh, M. A generalized framework for process-informed nonstationary extreme value analysis. *Adv. Water Resour.* **2019**, *130*, 270–282. [CrossRef]

5.3. Links and implications

This paper focussed on developing a framework to assess non-stationary conditions in extreme hydrometeorological events, specifically extreme rainfall, evapotranspiration, and water storage deficit in Lockyer Catchment in Southeast Queensland, Australia. This study utilises the geeSEBAL platform and NEVA model to analyse spatial and temporal variations in hydrometeorological variables. Through the development of considering non-stationary conditions in extreme event analysis to avoid underestimation of their magnitudes. The ET_a derived from geeSEBAL was evaluated using the highest data quality and using the CFMask method. The NEVA model provided the intensity and frequency of extreme events including extreme precipitation events, extreme evapotranspiration events and extreme water storage deficit events based on the assumption that the location parameter has a linear relationship with time. This framework enabled the achievement of Research Objective 4: *"Analyse the intensity and frequency of rainfall extremes, evapotranspiration extremes and water storage deficit extremes under both stationary and non-stationary conditions using the GEV model for the estimation of different return levels."*

The geeSEBAL model accuracy has been determined by comparing the geeSEBAL algorithm driven by ERA5 reanalysis and the number of fourteen ground-based observations for the period from 1990 to 2022. Spatial-temporal patterns and descriptive statistics results showed reasonable accuracy agreement between geeSEBAL ET_a, gridded ET_o and ERA5 rainfall and 14 stations. The frequency analysis of extreme events derived from 14 stations and gridded satellite data for rainfall, derived from the geeSEBAL algorithm for ET_a and global climate data for water storage for a 100-year period to a 10-year period showed the recurrence interval of return levels of extremes. By examining these extreme events across various periods, researchers can gain insights into the frequency and magnitude of extreme weather and hydrological events, such as intense rainfall, floods, droughts or changes in water storage. This result enabled the achievement of Research Objectives 1 and 4.

The outcome of the framework that will be helpful for adaptation strategies for water management, was provided. This framework can be applied to any catchment around the world for estimating extreme conditions, providing valuable insights for infrastructure planning and design, risk assessment and disaster management.

This research highlighted that the approach highlighted the importance of incorporating a physical system in terms of cause and effect.

This will add the benefit of considering the physical system drivers and their relationship within a catchment in extreme analysis and answer Research Question 4: *"How can the frequency, intensity, and duration of extreme climate events in the catchment be determined?".* The author considers this to be a substantial contribution to the field, offering practical hydrological experts a viable alternative approach to comprehending non-stationary extreme events analysis within a catchment. The second paper provides a foundational understanding of non-stationary conditions in extreme hydrometeorological events, laying the groundwork for the third paper's investigation into the impacts of climate change on flood extremes.

5.4. Conclusions

Chapter 5 of this thesis introduced the second paper published within the scope of this study. This study paper finalised the conducted assessment of hydrometeorological extreme events in this study, and the results could be employed for the modelling and projection of extreme flood events. In Chapter 5, the third research paper is introduced, to establish a framework for the projection of extreme flood events with different return levels under non-stationary conditions.

CHAPTER 6: PAPER 3 – VARIABILITY OF EXTREME CLIMATE EVENTS AND PREDICTION OF LAND COVER CHANGE AND FUTURE CLIMATE CHANGE EFFECTS ON THE STREAMFLOW IN SOUTHEAST QUEENSLAND, AUSTRALIA

6.1. Introduction

The frequency and severity of extremes are changing; thus, it would be necessary to evaluate the impacts of land cover changes, and urbanisation along climate change. A comprehensive approach incorporating the GEV method, GEE, and land cover classification techniques such as SVM and RF proves beneficial for analysing the impact of streamflow. In this research, a novel framework has been created for analysing maximum instantaneous floods in non-stationary catchment conditions in Southeast Queensland by taking into account the physical system in terms of cause and effect.

Various independent variables including the Digital Elevation Model (DEM), population density, slope, road networks, and distance from roads, along with an integrated RF-SVM methodology, are utilised as spatial predictors to forecast their impacts on land cover changes for both near and distant futures. The results indicate that physical factors significantly influence the layout of the landscapes. Results highlight the significant influence of physical factors on landscape arrangement. Evapotranspiration and rainfall projections from eight GCMs under two climate change scenarios (RCP4.5 and RCP8.5) are analysed.

The study employs the hydrological model calibrated with daily streamflow to simulate historical runoff (1990-2010) and project runoff under future scenarios (2020-2065 and 2066-2085) considering land cover percentages. The ProNEVA approach, utilizing Bayesian methods with Differential Evolution Markov Chain technique, evaluates the frequency and magnitude of runoff extremes across parameter space.

The study's conclusions suggest that underestimating flood frequency due to the non-stationary state may increase the danger to the associated hydraulic infrastructure. This framework, transferable to diverse geographical contexts, aids in estimating extreme conditions, informing infrastructure planning, risk assessment, and sustainable water resource management.

6.2. Published paper

Pakdel et al. (2024), “Variability of Extreme Climate Events and Prediction of Land Cover Change and Future Climate Change Effects on the Streamflow in Southeast Queensland, Australia” is published in ISPRS International Journal of Geo-Information (2024), Volume 13, Issue 4.

International Journal of Geo-Information

MDPI

Article

Variability of Extreme Climate Events and Prediction of Land Cover Change and Future Climate Change Effects on the Streamflow in Southeast Queensland, Australia

Hadis Pakdel [1,*], Sreeni Chadalavada [1], Md Jahangir Alam [1,2], Dev Raj Paudyal [3] and Majid Vazifedoust [4]

[1] School of Engineering, The University of Southern Queensland, Springfield Lakes, QLD 4300, Australia; sreeni.chadalavada@unisq.edu.au (S.C.); mdjahangir.alam@unisq.edu.au (M.J.A.)
[2] Murray-Darling Basin Authority (MDBA), Canberra, ACT 2601, Australia
[3] School of Surveying and Built Environment, The University of Southern Queensland, Springfield Lakes, QLD 4300, Australia; devraj.paudyal@unisq.edu.au
[4] Water Engineering Department, University of Guilan, Rasht 4188958643, Iran; vazifedoust@guilan.ac.ir
* Correspondence: hadis.pakdel@unisq.edu.au

Abstract: The severity and frequency of extremes are changing; thus, it is becoming necessary to evaluate the impacts of land cover changes and urbanisation along with climate change. A framework of the Generalised Extreme Value (GEV) method, Google Earth Engine (GEE), and land cover patterns' classification including Random Forest (RF) and Support Vector Machine (SVM) can be useful for streamflow impact analysis. For this study, we developed a unique framework consisting of a hydrological model in line with the Process-informed Nonstationary Extreme Value Analysis (ProNEVA) GEV model and an ensemble of General Circulation Models (GCMs), mapping land cover patterns using classification methods within the GEE platform. We applied these methods in Southeast Queensland (SEQ) to analyse the maximum instantaneous floods in non-stationary catchment conditions, considering the physical system in terms of cause and effect. Independent variables (DEM, population, slope, roads, and distance from roads) and an integrated RF, SVM methodology were utilised as spatial maps to predict their influences on land cover changes for the near and far future. The results indicated that physical factors significantly influence the layout of landscapes. First, the values of projected evapotranspiration and rainfall were extracted from the multi-model ensemble to investigate the eight GCMs under two climate change scenarios (RCP4.5 and RCP8.5). The AWBM hydrological model was calibrated with daily streamflow and applied to generate historical runoff for 1990–2010. Runoff was projected under two scenarios for eight GCMs and by incorporating the percentage of each land cover into the hydrological model for two horizons (2020–2065 and 2066–2085). Following that, the ProNEVA model was used to calculate the frequency and magnitude of runoff extremes across the parameter space. The maximum peak flood differences under the RCP4.5 and RCP8.5 scenarios were 16.90% and 15.18%, respectively. The outcomes of this study suggested that neglecting the non-stationary assumption in flood frequency can lead to underestimating the amounts that can lead to more risks for the related hydraulic structures. This framework is adaptable to various geographical regions to estimate extreme conditions, offering valuable insights for infrastructure design, planning, risk assessment, and the sustainable management of future water resources in the context of long-term water management plans.

Keywords: hydrological extremes; non-stationary; land cover change; climate change; GEV distribution; Google Earth Engine

Citation: Pakdel, H.; Chadalavada, S.; Alam, M.J.; Paudyal, D.R.; Vazifedoust, M. Variability of Extreme Climate Events and Prediction of Land Cover Change and Future Climate Change Effects on the Streamflow in Southeast Queensland, Australia. *ISPRS Int. J. Geo-Inf.* **2024**, *13*, 123. https://doi.org/10.3390/ijgi13040123

Academic Editors: Wolfgang Kainz and Jamal Jokar Arsanjani

Received: 1 February 2024
Revised: 28 March 2024
Accepted: 6 April 2024
Published: 8 April 2024

1. Introduction

The Intergovernmental Panel on Climate Change Assessment Report (IPCC) [1,2] on climate change indicates that climate change will be accompanied by a rise in the frequency, severity, and duration of extreme natural phenomena such as excessive precipitation and

extreme air temperatures in the twenty-first century. The trends suggest that the frequency and intensity of flood events are likely to rise globally due to climate and land use/cover changes attributed largely to urbanisation and anthropogenic activities [2,3]. Ding et al. [4] claimed that one of climate change's most significant implications is the increased frequency and occurrence of severe weather conditions. As hydrological events are more prone to be frequent and extreme, it is becoming increasingly crucial to assess how hydrological events respond to future land use and climate conditions [5]. During extremes, an efficient and economical strategy for achieving situational awareness is essential to enhancing the management of emergency responses. The ability to forecast the occurrence and scale of extreme events is crucial for both infrastructure and emergency management.

Climates are tremendously changeable from year to year at various locations across the world, including Australia, the world's driest inhabited continent, where there is a diverse range of climatic regimes, making it more vulnerable to climate change [6]. According to research [7,8], projected changes in the climate are anticipated to have noticeable effects on the frequency of hydrological elements such as runoff, rainfall, and evapotranspiration (ET) across various regions. Distinguishing between the effects of climate changes and land use changes on observed hydrological shifts is often challenging due to their concurrent occurrence in most regions, with both climate change and land use alterations [8,9]. So, a framework that incorporates land cover patterns and an ensemble of GCMs can be helpful.

Extreme hydrological events have been seen to be significantly influenced by climate change [10] and land cover changes caused by human activities. It is widely acknowledged that climate projections and scenarios, especially concerning extreme events, including extreme precipitation [11] and extreme streamflow, exhibit significant uncertainty across many global regions. Research on hydrological extremes is critically needed, especially for locations where the consequences of climate change are known to be significant [12].

Stationarity was previously believed to make complex statistical studies simpler, as studied by [13]. It offered significant insights into planning, making choices, and comprehending the effects of climate events, assuming a stable climate. Longer data records and a changing environment, however, make assuming stationarity riskier than ever. Under the assumption of a stationary climate, the terms return a level return duration and provide crucial information for decision making, design, and evaluating the effects of outstanding meteorological and climatic events. Traditionally, infrastructure design methods relied on the assumption of constant return levels, assuming that the occurrence of extreme events remains consistent over time [14]. However, it has become evident that the frequency of extreme events is evolving and is anticipated to keep changing in the future [1] Research has also revealed that non-stationarity in hydrological records in certain regions is characterised by increasing or decreasing patterns [13]. Since many extremes include spatial information, the major focus of recent framework advancements has been the challenge of combining spatial information with extreme value analysis strategies [15,16]. Therefore, models capable of accommodating non-stationary climatic and hydrologic extremes are essential [17,18].

Land use/cover changes (LUCC) have been identified as another influential factor for changing hydrological regimes [5]. It should be highlighted that the majority of research on LUCC is based on historical land use statistics [19] and has paid less attention to the linked effects of land cover changes and climate change. Therefore, it is important to estimate future land use scenarios and determine their impacts on extreme hydrological events. In the realm of land cover management and planning, two machine learning algorithm models are employed in Google Earth Engine (GEE): Random Forest (RF) [20] and Support Vector Machine (SVM) [21].

The prolonged presence of extremes poses detrimental impacts on infrastructure, the economy, and human health [22–26]. Applying Nonstationary Extreme Value Analysis (NEVA) [14] grounded in Bayesian inference could identify design extremes at various recurrence durations and intervals by performing a frequency analysis of extremes, observing alterations in the return period [27].

Various statistical distributions, such as Generalized Extreme Value (GEV) distributions [28], find extensive application in the examination of the intensity and frequency of extreme events within climate and hydrology research. Moreover, it has been recommended by the Australian Rainfall and Runoff (ARR) guideline [29] that the GEV distribution be utilized for estimating extreme floods and rainfalls.

Thus, in this research, streamflow is considered based on stationary and non-stationary assumptions. This study assesses the streamflow characteristics in the Lockyer catchment of southeastern Queensland, Australia, to establish return levels. The study aims to develop a methodology and identify the integrated effects of land cover and climate change on extreme streamflow events. The objective of the research is to accomplish the following specific objectives: (1) to explore a methodology that integrates a hydrological model with ensembles of Global Climate Models (GCMs) under Representative Concentration Pathways (RCPs) and projected landcover scenarios along with GEV to improve extremes predictions under the instantaneous impacts of climate change and human activities; (2) applying SVM and RF classification in GEE for projecting future land cover changes; (3) investigating the trend of land cover changes in the basin and projecting these changes with ensembles of GCMs under RCPs for future horizons; (4) performing hydrological simulations for each landcover classification separately under climatic scenarios and landcover changes at baseline and for near and far future horizons; and (5) to apply the ProNEVA model [28], which analyses and compares the return levels of projected streamflow under stationary and non-stationary assumptions and maps the spatiotemporal distribution of extreme events.

More work should be put into adding crucial physical processes to stochastic models, according to [30], who also recommended stochastic-process-based models as a means to bridge the gap between physically based models and statistical models. In this study, we propose an integrated framework for assessing the past and future hydrological consequences of climate change. This framework integrates hydrological models, a machine learning method on the GEE platform, ProNEVA, and climate projections under different scenarios based on the Generalised Extreme Value (GEV) model in stationary and non-stationary conditions [13] and explores the effects of future climate change on the streamflow. Firstly, we presented a technique for obtaining and evaluating the remotely sensed temporal imagery [8] necessary for incorporating land cover into hydrological modelling. Secondly, we assessed the outputs of the GCMs under RCPs projecting the futurist climate simulations that were included in the hydrological model, as recommended by [8,31]. Thirdly, we applied SVM and RF classification in the GEE platform for projecting future land cover changes. Lastly, we applied the ProNEVA model to estimate return levels and assess the frequency and severity of extreme events in streamflow under both assumptions, including non-stationary and stationary. This study's findings will contribute to our knowledge of how severe flood events vary spatially at the catchment level. Investigations into adaptation techniques for handling probable future extremes will be assisted by this new framework for water planners and decision makers.

2. Materials and Methods

The primary techniques and data employed in this investigation are depicted in Figure 1. The procedures outlined in this study are as follows: (a) gaining projected climate variables (rainfall and potential ET) derived from a GCM obtained from the Coupled Model Intercomparison Project Phase 5 (CMIP5) to evaluate climate change impacts on the study area for historical and future periods, (b) calibrating and validating a hydrologic model to analyse the changes in daily inflows that will be used for the streamflow projection, (c) applying SVM and RF classification in GEE for projecting future land cover changes, (d) deriving the runoff coefficient's time series of classes (%) from historical LandSat images and for the near and far future, and (e) evaluating the extremes analysis applying the GEV model.

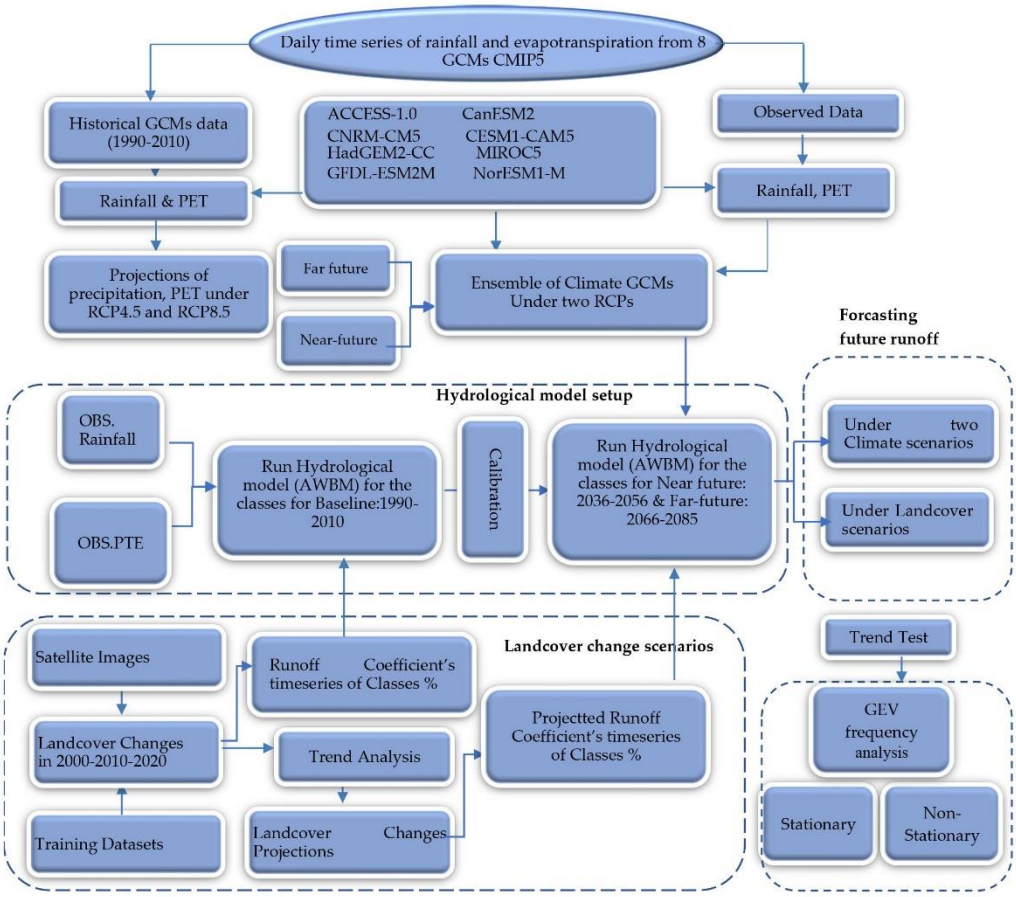

Figure 1. Flowchart of GCMs projections, hydrological model, GEE, and GEV model to estimate streamflow extremes.

2.1. Study Area

The case study region, Lockyer Catchment, is situated in SEQ, as shown in Figure 2. Lockyer Creek, a tributary of Brisbane River, is the primary stream, surrounded by several sub-catchments. The catchment covers an area of 3000 km^2, experiencing an average annual rainfall ranging from 1000 to 2012 mm [32]. The Lockyer catchment includes a range of physical geographic attributes, encompassing the distance of water paths from 0 to 102,815 m, elevations ranging between 30 and 1073 m, basin slopes spanning from 0 to 66 degrees, channel network slopes ranging from 0 to 18 degrees, and a total channel network length of 922,025.285 m. The Lockyer catchment provides significant environmental, economic, and social values and Australia's most fertile agricultural land for the cultivation of highly valuable vegetables [33]. In Australia, floods are one of the frequently occurring disasters that have accounted for substantial amounts of environmental and economic losses in recent years; hence, mitigation of the risks associated with the impacts of these events is necessary [34,35].

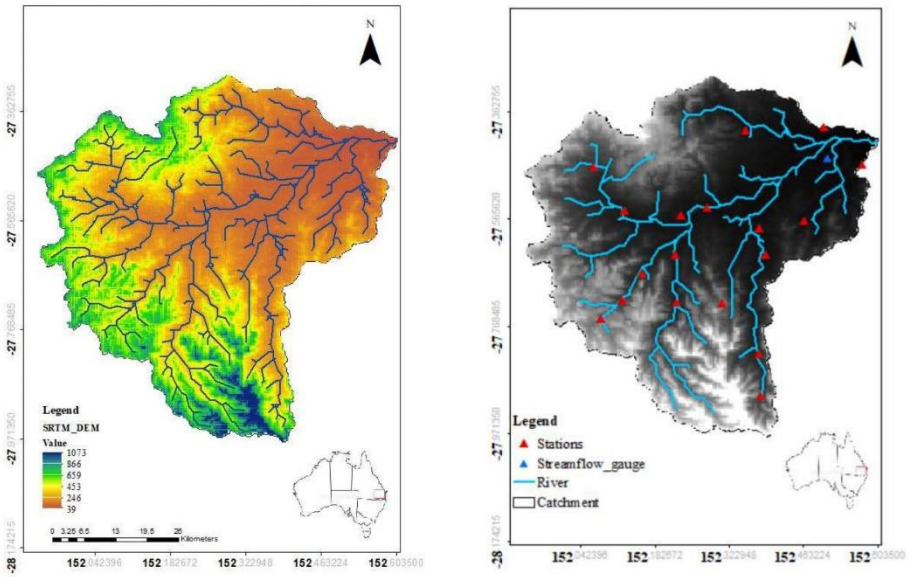

Figure 2. The study's area geographical position in Australia (**Left**) and hydro-meteorological stations are taken into consideration throughout the catchment (**Right**).

There have been a number of exceptional weather occurrences in this area in recent years. For example, in December 2010 and January 2011, continuous rains caused unprecedented levels of flooding to spread throughout significant regions of Queensland [34]. A disaster zone was designated across 78% of the state due to the detrimental impact on 2.5 million people. Over 29,000 houses and businesses were impacted by the floods, which are believed to have caused damage worth over AUD 5 billion [34].

Given that past research has proven the assumption of stationary to be no longer accurate, the frequency of flood occurrences, like the one in February 2022, demonstrates that this assumption is no longer applicable. Furthermore, it has been noted that the connection between runoff and rainfall in this catchment is not constant over time [36,37]. In addition, investigating the impacts of land cover changes and climate change on the streamflow is important. To improve the design and management of hydraulic infrastructure and reduce future human and financial losses, it is imperative to develop unique approaches for estimating non-stationary runoff extremes [13].

2.2. Data Sources: Observed, Remotely Sensed Data and Geospatial Data

Daily hydrological data, including potential evapotranspiration (mm) and rainfall (mm), were retrieved from the stations. The 5 km grid data were achieved through SILO, an Australian climate data source (http://www.longpaddock.qld.gov.au/silo (accessed on 15 January 2023)) [38,39], and cover the period from 1990–2005. Important rainfall sites were selected because of their geographic variety and data quality, which comprised long records with few missing values. Daily streamflow records for 143210B Lockyer Creek at Rifle Range Road station were received from the Queensland Government Water Monitoring Information site (https://water-monitoring.information.qld.gov.au/ (accessed on 15 January 2023)).

The Landsat satellite images (from TM, ETM+, and OLI 1&2 sensors) and ESA global land cover dataset were accessed and used through GEE [40] for conducting the classifications and modelling of changes in land cover and urban growth. Geospatial datasets of road

networks, population density, and the Hydrologically Enforced Digital Elevation Model (DEM-H) product with a 30 m spatial resolution [41] dataset were used as supplementary data inputs during the landcover projection analysis. Since the distance from roads and population density maps were originally in vector format, both maps were first converted into the raster format, resampled to the 30 m spatial resolution, and used for the projection of landcover changes (Table 1).

Table 1. Sources of datasets.

Raster Dataset	Time Coverage	Data Source	Resolution/ Format
Landsat 5 TM	2000–2011	Google Earth Engine (LANDSAT/LT05/C02/T1_L2)	30 m
Landsat 8 OLI	2013–2023	Google Earth Engine (LANDSAT/LT08/C02/T1_L2)	30 m
ESA global land cover	2021	Google Earth Engine (ESA/WorldCover/v100)	10 m
DEM-H: Australian SRTM Hydrologically Enforced Digital Elevation Model	2010	Google Earth Engine (AU/GA/DEM_1SEC/v10/DEM-H)	30 m
Vector Dataset		**Source**	**Data Format**
Roads	2000 and 2023	Queensland Government	Shapefile (.shp)
Distance from roads	2023	Spatial analysis on road network	Shapefile (.shp)
Population	2023	Australian Bureau of Statistics	Shapefile (.shp)

2.3. Classification and Projection of Landcover Changes

To project the landcover changes, first, the main land cover types were classified into six classes (Table 2), and, following ESA global landcover classification [42], discriminated from other features in the Landsat images for the years 2000, 2010, and 2020 using two supervised classification models, including Support Vector Machine (SVM) and Random Forests (RF). The image collection of Landsat images was called for the years 2000, 2010, and 2020 in GEE, separately. The images were filtered based on criteria related to cloud conditions and vegetation cover. The remaining images in each collection were reduced to a single multiband images using median reducers.

Table 2. Land cover classification scheme.

Land Cover Type	Description
Tree cover	Forest and tree cover land
Grassland	Pastures, green spaces, parks, and bushlands
Cropland	Farmland, agricultural
Built-up	Built-up area, residential, commercial, and other infrastructure
Bare/sparse vegetation	Bare soils, sand, rocks, and sparse vegetation
Water Bodies	Lakes, ponds, reservoirs, and rivers

To train the classification models, we mapped the boundaries of more than 200 point features (335) representing six different classes: tree cover, grassland, cropland, built-up, bare soil/sparse vegetation, and water bodies using ESA global landcover and drawing

geometry tools in GEE. The training datasets were split up into groups for training and validation. In total, 70% of the point features were assigned to the training and 30 percent were used in the validation procedure.

The spatial distribution of both the training and validation polygons is illustrated in Figure 3a. After generating the landcovers for the years 2000, 2010, and 2020, the landcover changes were simulated and projected using the SVM and RF approaches in the GEE platform, which is shown in Figure 3b.

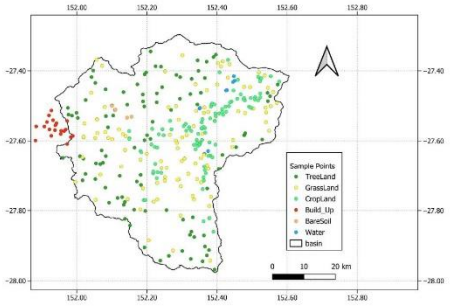

(a)

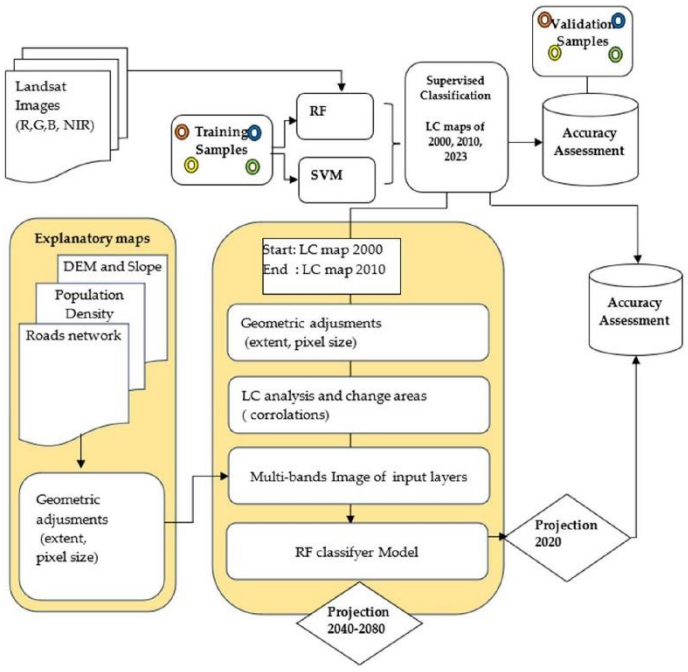

(b)

Figure 3. Land cover changes workflow chart (**a**) and spatial distribution of both training and validation polygons (**b**).

climate-driven fluctuations in observed streamflow and characterising the consequences of precipitation changes. The concept of selecting an appropriate hydrological model has been proven by Jahandideh-Tehrani, et al. [58], as in the Australian region, lumped conceptual hydrological models [59] such as the AWBM are well-suited to use for runoff simulation. The AWBM was created to minimise problems related to physically based hydrological models such as different parameter estimations. For the study catchment, the AWBM model was calibrated at the daily time step. For simulation purposes, calibration (60%) and validation (40%) were employed. The availability of recorded runoff data determined the calibration and validation timeframes for the Lockyer catchment. So, runoff data were used for 1990–2002 (calibration period) and 2003–2010 (for validation period). Daily rainfall, potential ET (PET), and daily runoff were derived from SILO and WMIP throughout the catchment, respectively (Section 2.2).

The AWBM [60] structure and parameters are presented in Table 3. The AWBM is mostly made up of three basic surface storage configurations. The depths of these storage tanks are equal to the C1, C2, and C3 (three surface moisture stores) parameters to create the coefficient of runoff simulation. For each time step, the water balance of each partial region is determined [61]. As demonstrated by [8], in this study, runoff from impermeable surfaces was taken into account by recoding and changing the AWBM. The eight calibrated parameters are adjusted for accuracy in Table 3.

Table 3. Description of parameter values for the AWBM model [60].

Parameter ID	Description	Unit	Default	Minimum	Maximum
A1	Partial area represented by surface storage	-	0.134	0	1
A2		-	0.433	0	1
BFI	Baseflow Index	-	0.35	0	1
C1	Surface storage capacities	mm	7	0	50
C2		mm	70	0	200
C3		mm	250	0	500
Ks	Surface flow recession constant	-	0.90	0	1
Kb	Baseflow recession constant	-	0.90	0	1

To analyse the impacts of climate change on runoff at various sizes, ranging from small locations to huge geographic areas, hydrological models have been widely implemented. The goal of this research is to estimate the effects of climate change on the streamflow in a major catchment (the Lockyer Creek catchment). To accomplish this, a rainfall–runoff model was adjusted and validated before being used to forecast runoff. So, the AWBM was undertaken to assess the impact of climate variability on runoff. The most vital step in climate change research is selecting climate models for future hydro-climatological projections.

The accuracy assessment of the models' validation and calibration was performed based on statistical measurements [62,63], including the correlation coefficient (R^2), Nash-Sutcliffe coefficient (E), Bias, and Root Mean Square Error ($RMSE$), as follows (Equations (1)–(4)):

$$R^2 = \left(\frac{\frac{1\sum_1^n (X_{obs} - X_{obs})(X_{sat} - X_{sat})}{n}}{X_{obs} \times X_{sat}} \right)^2 \quad (1)$$

$$RMSE = \sqrt{\sum_1^n \frac{(X_{sat} - X_{obs})^2}{n}} \quad (2)$$

$$\text{Bias} = \frac{\sum_1^n (X_{sat} - X_{obs})}{n} \quad (3)$$

$$E = 1 - \left(\frac{\frac{1\sum_1^n (Q_{obs} - Q_{sim})^2}{n}}{\frac{1\sum_1^n (Q_{obs} - \overline{Q_{obs}})^2}{n}} \right) \quad (4)$$

In which Q_{obs} and Q_{sim} show the observed and simulated time series, respectively; n is the total number of observations; and $\overline{Qobs}$ is the average of observational values.

2.5. Future Climate Projections and Greenhouse Gas Emissions Scenarios

The Coupled Model Intercomparison Project (CMIP) is the largest intercomparison study and it serves as a baseline for assessing GCMs' capacity to project observed climate changes. In this study, climate change effects on the streamflow in the Lockyer catchment were assessed using eight GCMs of CMIP5. The recently suggested RCPs provide a broader range of possible futures by taking mitigation techniques and land use changes into account [38]. According to the aim of this research study, it is imperative to select appropriate RCP scenarios. RCP 8.5 scenarios [64], which represent high GHG scenarios, have been selected and are currently trending in the same direction, and RCP 4.5 is a depiction of a low-emission scenario and was chosen to analyse less severe situations.

Individual CMIP5 models' capability to predict the Australian climate varies depending on whatever part of the modelling process is studied. These models are the most accurate instruments for predicting the reactions of regional climates in the twenty-first century [65]. Based on the third and fifth stages of the CMIP, Alexander and Arblaster [66] conducted detailed evaluations of anticipated changes in extreme climate events over Australia.

As mentioned in the climate change technical report in Australia [38], the Australian Water Availability Project (AWAP) observed temperature and rainfall data (https://eo-data.csiro.au/projects/awap/ (accessed on 15 January 2023)) were used to create climatic outputs with a resolution of 5 km. In this approach, the model data, whose resolution ranged from 100 to 310 km, were initially applied to the observed data using interpolation on a 5 km grid. In this research, according to the Australian climate change technical report [38], these eight climate models have been suggested for investigating climate change's impacts on SEQ (Table 4).

Table 4. List of eight CMIP5 models used in this research [38].

CMIP5 Model ID	Modelling Centre, Country of Origin, Institution	Ocean Resolution (°LAT × °LON)	Atmospheric Resolution (°LAT × °LON)
ACCESS-1.0	Commonwealth Scientific and Industrial Research Organisation, Partnership between CSIRO and BOM, Australia	1.0 × 1.0	1.9 × 1.2
CNRM-CM5	National Center for Meteorological Research, France	1.0 × 0.8	1.4 × 1.4
CESM1-CAM5	National Center for Atmospheric Research, National Science foundation, United States	1.1 × 0.6	1.2 × 0.9
CanESM2	Canadian Centre for Climate Modeling and Analysis, Canada	1.4 × 0.9	2.8 × 2.8
GFDL-ESM2M	Geophysical Fluid Dynamics Laboratory, United States	1.0 × 1.0	2.5 × 2.0
HadGEM2-CC	MOHC (Met Office Hadley Centre for Climate Science and Services, United Kingdom)	1.0 × 1.0	1.9 × 1.2
MIROC5	Centre for Climate System Research, Japan Atmosphere and the University of Tokyo Ocean Marine-Earth Science and Technology Research Institute	1.6 × 1.4	1.4 × 1.4
NorESM1-M	Norwegian Climate Center (NCC) and University of Bergen, Norway	1.1 × 0.6	2.5 × 1.9

2.6. Assessing Extremes in a Non-Stationary Approach Using the GEV Model

Non-stationary situations arise because the stationary assumption might not be valid for changes brought about by human and climate variables. Even with great progress [14], there is still no complete framework that incorporates the Extreme Value Analysis (EVA) statistical models (Generalised Extreme Value (GEV), Generalised Pareto (GP), and Log-Pearson type III (LP3)) under stationary and non-stationary assumptions (parameters as a function of physical variables or time) [28]. The ProNEVA (https://amir.eng.uci.edu/software.php (accessed on 15 January 2023)) software [28] was employed to examine non-stationary extremes.

With user-defined covariates, which may be time or a physical variable, ProNEVA enables non-stationary studies. The benefit of conducting a stationary analysis with covariates related to the physical aspect lies in the ability to incorporate physical limitations into a statistical model. ProNEVA employs a Bayesian approach to evaluating extremes, utilising a Differential Evolution Markov Chain methodology throughout the parameter value [14]. The essential distributions offered by Extreme Value Theory (EVT) to describe extremes are as follows: the use of Generalised Pareto Distribution (GPD) through the peaks-over-threshold approach [67–69], with the block maxima technique employing the LP3 and GEV family of distributions [70]. Additional details on the GEV distribution have been demonstrated in this article [13].

3. Results

The study establishes a multi-framework by the combination of a hydrological model in line with ProNEVA and an ensemble of GCMs under two RCPs, mapping land cover patterns by implementing the machine learning classification methods in GEE. With consideration for the physical components and how they interact with one another within the system, this integrated approach attempts to evaluate the return levels of flood extremes.

3.1. Spatiotemporal Change Analysis and Land Cover Transition Analysis

When evaluating temporal changes within a collection of land cover categories, the transition matrix is crucial. It showcases the proportions of pixels transitioning from one land cover category to another. Table 5 illustrates the alterations in land cover categories from 2000 to 2085. There is an indication of potential growth in built-up and tree cover areas, from 1971.11 m^2 in 2000 to 12,766.39 m^2 in 2080, and from 172,661.60 m^2 in 2000 to 200,363.23 m^2 in 2080, respectively. The findings of grassland during this period from 2000 to 2080 indicate that grassland values decreased from 102,520.44 m^2 in 2000 to 81,101.62 m^2 in 2020, followed by remarkable decrease to 68,640.10 m^2 in 2060 and by 66,685.44 m^2 in 2080.

Table 5. Evaluation of land cover changes from 2000 to 2080.

Land Cover Classes	2000	2010	2020	2040	2060	2080
	Area in m^2	Area in m^2	Area in m^2	Area in m^2	Area in m^2	Area in m^2
Treeland	172,661.60	191,975.49	188,810.53	202,955.36	202,396.27	200,363.23
Grassland	102,520.44	82,108.81	81,101.62	68,640.10	68,226.88	66,685.44
Cropland	18,844.68	18,383.25	19,151.94	16,865.49	17,086.66	16,796.67
Built-up	1971.11	2963.93	5861.84	8110.32	8868.36	12,766.39
Bare Soil	224.703	338.331	568.422	112.785	108.496	98.39
Water	629.633	1099.02	1357.82	168.116	165.5	142.041

As illustrated in Figure 4 and Table 5, there has been a consistent rise in built-up areas, starting at 1971.11 m^2 in 2010 and increasing to 5861.84 m^2 by 2020. Table 5 also shows a fourfold increase to 8868.36 m^2 in 2060 and sixfold increase to 12,766.39 m^2 in 2080. Evaluating the accuracy of classification methods is vital for understanding their reliability [44]. As shown in Table 6, the results reveal that SVM has a slightly higher

accuracy in the image classification. According to Table 6, the classes of treeland, grassland, and water were classified with a higher accuracy, while the accuracy for built-up and bare soil was slightly lower. The results clearly indicate that RF outperformed SVM in the projection of landcover for the year 2020, yielding 0.71 (OA) and 0.65 (Kappa), which are 23% and 28% higher than those of the SVM model, respectively (Table 6). These results are demonstrated by [71], where RF performs better than SVM. However, for the classification, SVM, in the majority of instances, outperformed RF; for example, for the year 2000, it yielded 0.88 (OA) and 0.85 (Kappa), which are 4% and 5% higher than those of the RF model, respectively.

The classification SVM method in the year 2000 had an Overall Accuracy (OA) of 88%, Kappa of 85%, followed by User's Accuracy (UA) of 100% for cropland and built-up areas, followed by 86% for grassland. It also had a Producer's Accuracy (PA) of 75% for built-up areas and 72% for cropland. The Kappa and OA for the RF method were 80% and 84%, respectively. The UA results for cropland and built-up areas were similar to the SVM method. Grassland and bare soil in terms of UA decreased to 75% and 55%.

The SVM and RF for the year 2010 showed 89% (Kappa) and 91% (OA), and 79% (Kappa) and 82% (OA). In terms of individual class accuracy, the UA indicated 84% (SVM method) and 69% (RF method) for treeland, while the PA was 100% for both methods. The results of the OA (0.84) and Kappa (0.8) were the same in both the SVM and RF models for the year 2020. However, for the individual classification, which contains two classes (grassland and built-up), the SVM model generated a better user's accuracy and producer's accuracy. As can be observed from Table 6, RF outperformed SVM in the projection of landcover for the year 2020, and classified all six classes with a better accuracy than the SVM in terms of the Kappa, OA, and PA. The model incorporates spatial elements like distance from major roads, DEM, and population density to generate a map illustrating changes in land cover, revealing the evolving patterns within the Lockyer catchment (Figure 5).

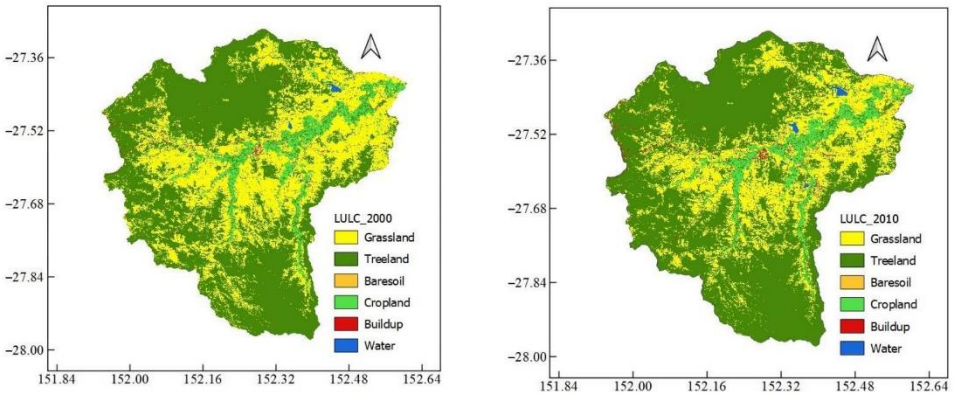

Figure 4. *Cont.*

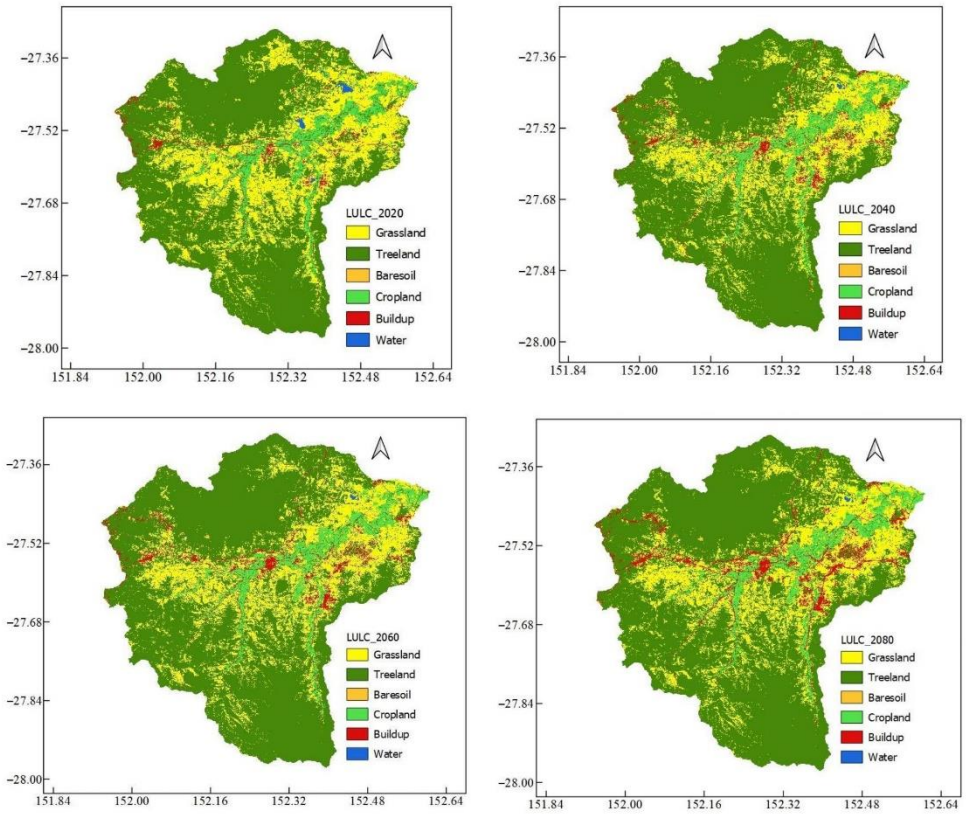

Figure 4. Land cover changes from 2000 to 2080 in the Lockyer catchment.

Table 6. Accuracy assessment of landcover classification and projection using statistical indicators including Kappa coefficient, User's Accuracy (UA), Producer's Accuracy (PA), and Overall Accuracy (OA).

Year	Classification Method	Assessment Index	Landcover Classes					
			TreeLand	GrassLand	CropLand	Built-Up	BareSoil	Water
2000	SVM	UA	0.71	0.86	1	1	0.77	1
		PA	1	1	0.72	0.75	1	1
		Kappa			0.85			
		OA			0.88			
	RF	UA	0.77	0.75	1	1	0.55	1
		PA	1	1	0.8	0.45	1	1
		Kappa			0.8			
		OA			0.84			

Table 6. *Cont.*

Year	Classification Method	Assessment Index	Landcover Classes					
			TreeLand	GrassLand	CropLand	Built-Up	BareSoil	Water
2010	SVM	UA	0.84	0.83	1	1	0.7	1
		PA	1	1	0.87	0.83	0.7	1
		Kappa			0.89			
		OA			0.91			
	RF	UA	0.69	0.88	1	0.85	0.47	1
		PA	1	0.88	0.8	0.58	0.7	1
		Kappa			0.79			
		OA			0.82			
2020	SVM	UA	0.64	0.78	0.88	1	1	1
		PA	1	0.72	0.8	1	0.7	0.71
		Kappa			0.8			
		OA			0.84			
	RF	UA	0.71	0.77	0.94	0.83	1	1
		PA	1	0.68	0.8	1	0.7	0.76
		Kappa			0.8			
		OA			0.84			
Projected 2020 based on 2000–2010	SVM	UA	0.87	0.52	0.86	0.25	0.97	0.98
		PA	0.41	0.38	0.39	0.9	0.07	0.68
		Kappa			0.37			
		OA			0.47			
	RF	UA	0.68	0.48	0.75	0.86	0.86	0.934
		PA	0.89	0.85	0.62	0.51	0.51	0.84
		Kappa			0.65			
		OA			0.71			

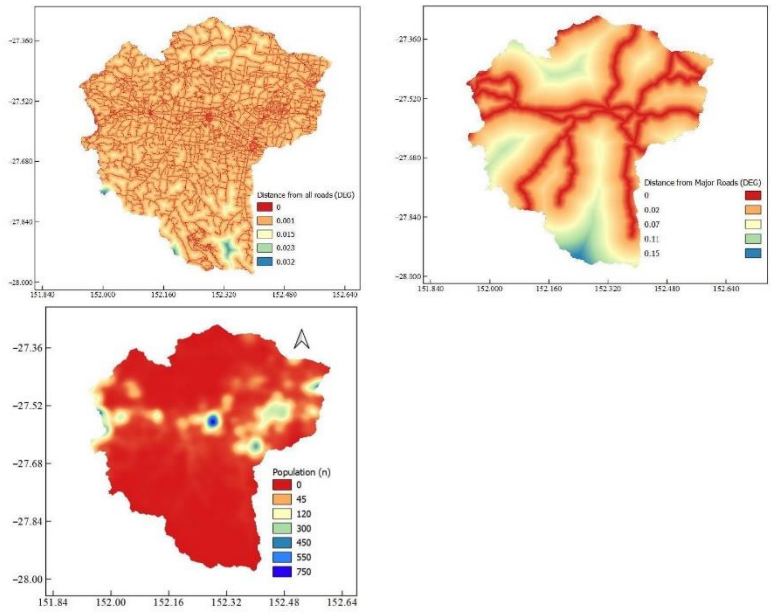

Figure 5. Spatial variables applied to the landcover changes projection in the Lockyer catchment.

3.2. The Performance of Hydrological Model

A comparison between the simulated and observed discharge is used to assess the results of the calibration and validation for the periods of 1990–2002 and 2003–2010, respectively (Figures 6 and 7). The eight calibrated parameters are presented in Table 3. The model's output data were calibrated and validated using the daily streamflow records from the 143210B Lockyer Creek at Rifle Range Road station as the outlet. As illustrated in Figure 2, the Lockyer catchment contains eighteen rainfall-gauging stations. The model utilised inputs consisting of the area's average weighted daily evapotranspiration and rainfall from these 18 gauging stations, along with daily records of discharge from the Rifle Range Road station. The calibration and validation of the hydrologic model were carried out for the periods of 1990–2002 and 2003–2010, respectively. Streamflow data were utilised, allocating 60% for calibration and 40% for validation purposes. According to the results of Table 7 and Figure 6, the findings indicate the model's effective performance and its reliable accuracy in estimating runoff.

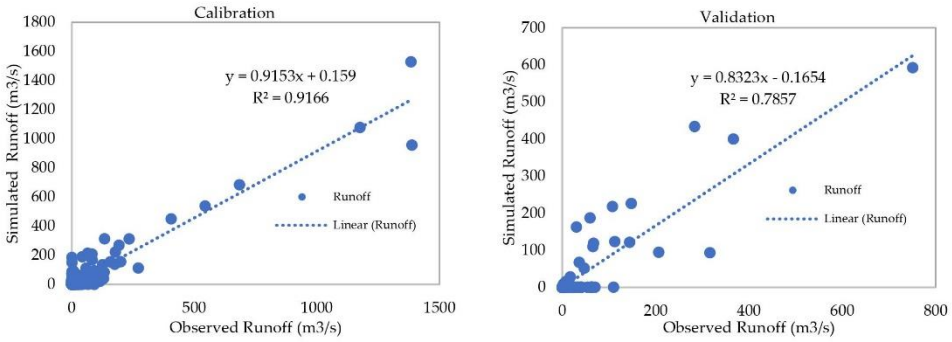

Figure 6. Scatter plot of observed and simulated daily runoff at the Lockyer valley over the calibration (1990–2002) and validation periods (2003–2010).

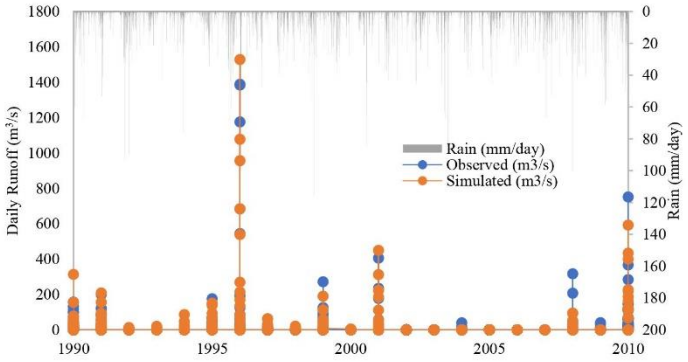

Figure 7. Observed and simulated daily runoff at the Lockyer Valley over the calibration (1990–2002) and validation periods (2003–2010).

Table 7. Daily operational data for the AWBM model during the calibration and validation periods.

	Calibration (1990–2002)	Validation (2003–2010)
R^2	0.92	0.786
Nash	0.89	0.753
RMSE	0.005	0.409
BIAS	0.0004	1.206

Over the calibration, R^2 and Nash were very good, at 92% and 89%, respectively, for the period of 1990–2002. Moreover, PBAIS indicated that the AWBM model performance over the validation period was 1.206 m^3/s (Table 7). Moreover, 78%, and 75% were the calculated R^2 and Nash, respectively, over the validation period. According to Figure 6, there is a good match between the observed and simulated daily discharge in the Lockyer Valley catchment. Figure 6 indicates the model's generally satisfactory performance in simulating flow patterns, and although it slightly underestimates some peak flow instances, it effectively aligns the overall patterns of storm events between the simulations and observed records. Moreover, the accurate simulation of low-flow circumstances further indicates the reliability and competence of the AWBM model in predicting discharge. Ensemble projections depict the long-term average daily inflow at the Rifle Range Road hydrometric station for near and far future periods (2020 to 2086) under the RCP 4.5 and RCP 8.5 scenarios.

3.3. Changes in Projected Streamflow under Climate Change Scenarios

This study assessed changes in runoff factors using two climate change scenarios (RCP 4.5 and RCP 8.5) based on the combined average of eight GCMs. According to Figure 8, a decline in runoff of the ensemble of climate models was generally noticed in the far future (2066–2085) compared to the near future (2020–2065) for almost all months. In February, there was a greater variability in streamflow alterations for both RCP 4.5 and RCP 8.5, suggesting increased uncertainty in the predictions for the two future periods, as indicated by [62]. It can be concluded that the decline in streamflow will likely slow down in the far future compared to the near future, particularly between June and September.

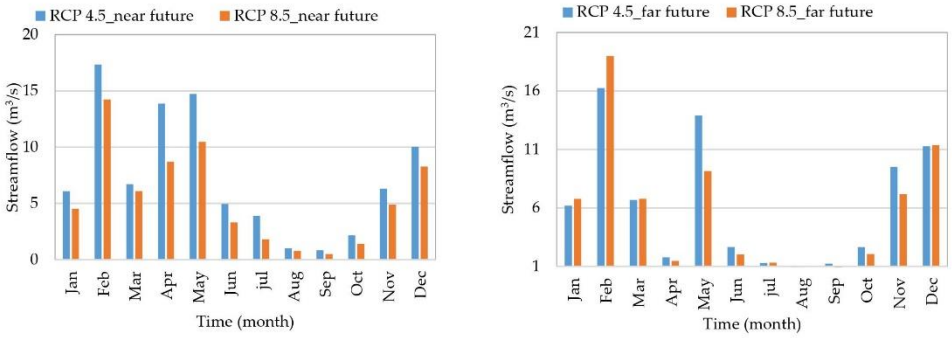

Figure 8. Ensemble projections of long-term average daily inflow at Lockyer Creek at Rifle Range Road station for near future (2020–2065) and far future (2066–2085) periods under RCP 4.5 and RCP 8.5.

Runoff was projected to decline in January and February by 16% in the near future and 18% in the far future. Figure 8 illustrates that the significant increase in projected runoff in February is mostly caused by the increase in projected rainfall. Also, the RCP 8.5 scenario consistently showed lower projected streamflow compared to RCP 4.5 throughout each month. February displayed the greatest span of long-term average daily streamflow

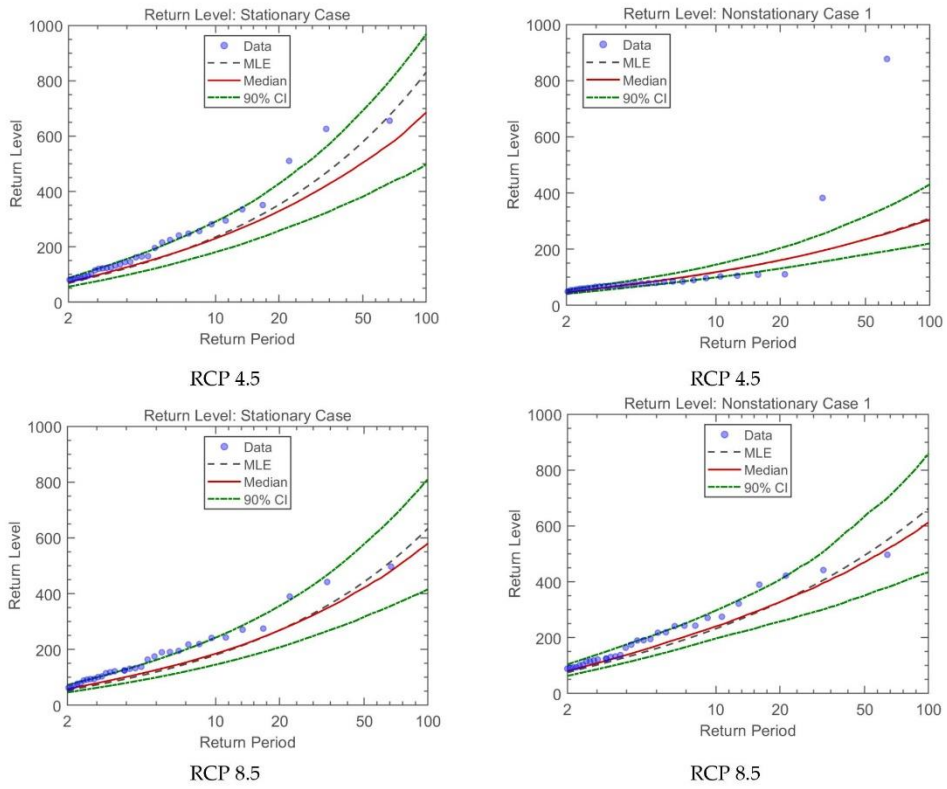

Figure 9. NEVA's non-stationary GEV framework output, standard return levels with the likelihood of design exceedance for flood for future periods (2020–2086) under stationary and non-stationary assumption. (Figure generated using MATLAB R2020b).

4. Discussion

Simple regression models are examined by scholars for modelling changes in the mean, variance, and skewness and combining such non-stationary moments with various pdfs to update design events, given historical research [12,73]. The increasing concern regarding climate change brought on by a rise in greenhouse gas concentrations in the environment is another factor contributing to the growing emphasis on non-stationarity [1,74]. So, in this research, ProNEVA offers parameter estimation, uncertainty quantification, and a comprehensive assessment that allows for a non-stationary analysis using user-defined variables, which can be time or a physical variable. The advantage of performing a stationary analysis with physically related covariates lies in the possibility of imposing physical constraints on a statistical model [28].

In this research, both the non-stationary and stationary conditions for maximum instantaneous flood were investigated. The purpose of this study was to look at the non-stationary possibilities of the Lockyer catchment's maximum instantaneous flood in the future. To achieve this aim, we developed a multi-framework by integrating a hydrological model, SVM and RF classifications in the GEE platform, an ensemble of GCMs under two RCPs, and the ProNEVA model, for the aim of evaluating the impacts of climate change on floods, streamflow, and water supply in both stationary and non-stationary conditions. SVM and RF classifications in the GEE platform were used to estimate the projected land

cover changes in the future period and, by assuming a linear relationship between the location parameter and time, the ProNEVA model was applied to assess the magnitude and frequency of extreme floods utilising the GEV distribution.

According to the ARR guideline, [29] states that the GEV distribution should be applied for the purpose of designing floods and rainfalls. Earlier research on extremes [13,75,76] aligns closely with the characteristics outlined in the GEV distribution. Even with notable progress [77], there lacks an all-encompassing structure that integrates the commonly employed EVA statistical models, specifically, GEV, GP, and LP3, accounting for both stationary and non-stationary assumptions (where parameters vary with time or specific covariates) [28]. This research examines both the ProNEVA and land cover classification approaches to account for the cause-and-effect dynamics within the physical system. The model incorporates spatial factors like DEM, distance from road, and population density along with the SVM and RF classification models to produce a map illustrating land cover changes.

ProNEVA [28] incorporates the underlying physical drivers triggering extreme events, serving as a crucial instrument for quantifying the probability of extreme occurrences in a particular area or timeframe. This study investigates both ProNEVA and land cover classification to comprehensively address the cause-and-effect dynamics within the physical system. Since our focus was solely on non-stationary conditions in extreme events, using ProNEVA with a time covariant by incorporating the outputs of the ensemble of GCMs under different scenarios from the hydrological model and GEE classification approach, it is recommended that, in future studies, ProNEVA allows for the incorporation of the physical drivers as additional covariates for flood frequency analysis and modelling.

A script was coded using GEE to compute the percentage of area change per year, generating a transition matrix demonstrating the pixel shifts between different land covers. This approach was chosen due to its straightforward estimation process, which is well-suited for practical use. Enhancing the lumped conceptual hydrological model projection involves integrating various land covers by recognizing distinct land cover types and understanding how these types affect the model parameters, guided by the land cover classification map. This integration considers the influences of different land covers on evapotranspiration processes. The outcomes distinctly demonstrate that the inclusion of each land cover within the hydrological model leads to improved accuracy in the model's results. Studies have consistently emphasised the disparity between stationary and non-stationary when incorporating the non-stationary condition [13,28,75]. Therefore, using the classification method through GEE presents an appealing option for assessing spatial and temporal aspects across regional and continental scales. The maximum instantaneous flood in the non-stationary assumption generally shows greater values compared to the maximum peak floods in the stationary assumption in both the RCP 4.5 and RCP 8.5 scenarios for different return levels. Generally, the range of uncertainty between stationary and non-stationary conditions tends to widen from 50 year to 75 year return level periods. Under the RCP 8.5 scenario, there is comparatively less variation between stationary and non-stationary conditions, whereas RCP 4.5 demonstrates a more pronounced difference. The outcomes of the trend analysis on future periods' maximum peak flood data reveal a growing disparity in the maximum instantaneous flood between stationary and non-stationary assumptions. This suggests that the increasing difference may be a compelling reason to analyse extremes with non-stationary conditions. Moreover, exploring the variability of the scale parameter over time, both linearly and non-linearly, is possible. Analysing the impact of simultaneously incorporating non-stationarity assumptions in both scale and shape parameters on the outcomes is also a potential area of investigation for future studies.

5. Conclusions

The outputs from this study can be utilised in risk assessments and for devising adaptation strategies for state government authorities and local councils. This framework

applies to diverse geographic regions, delivering vital information about extreme events such as floods necessary for risk evaluation, infrastructure design, and disaster response. Examining the non-stationary assumption in extreme flood events analysis presents a novel concern in the Lockyer catchment. Given the presence of water reservoirs, urban and rural zones, and cultivable lands in this area, forecasting the return period values for extreme floods in future periods becomes crucial, which will assist water planners, decision makers, and local communities in constructing water systems and managing resources by activating emergency response operations.

ProNEVA outcomes, when considering the physical drivers, highlight that disregarding the non-stationary condition and trends in extreme flood data leads to inaccuracies in estimating these floods across various return periods, often resulting in underestimations. This leads to flaws in the construction of hydraulic infrastructure and results in human and financial losses. Through the quantification of the likelihood of extreme events, decision makers can make well-informed decisions related to infrastructure development, resource allocation, and emergency planning. The findings of this study will assist water planners in exploring potential adaptation strategies while considering expected future alterations. It should be noted that the effectiveness of future land cover projections and hydrological simulations depends on the accuracy of the input data and assumptions made in the modelling process.

There are natural constraints that limit the accuracy of future projections, including uncertainties associated with climate projections and scenarios. The study recommends using a multi-framework approach that integrates both physical system understanding and statistical methods to gain a deeper understanding of non-stationary assumptions in extreme events at the catchment scale. The research could lead to future studies that incorporate comprehensive uncertainty analysis techniques to assess model predictions' reliability under various climate change scenarios. Furthermore, investigating innovative techniques for capturing and integrating non-stationary trends in hydrological processes could improve model predictability and facilitate more robust decision making.

Author Contributions: Conceptualization, Hadis Pakdel, Sreeni Chadalavada, Md Jahangir Alam, Dev Raj Paudyal and Majid Vazifedoust; methodology, Hadis Pakdel, Sreeni Chadalavada, Md Jahangir Alam, Dev Raj Paudyal and Majid Vazifedoust; software, Hadis Pakdel and Majid Vazifedoust; validation, Hadis Pakdel; formal analysis, Hadis Pakdel; investigation, Hadis Pakdel; resources, Hadis Pakdel; data curation, Hadis Pakdel; writing—original draft preparation, Hadis Pakdel; writing—review and editing, Sreeni Chadalavada, Dev Raj Paudyal, Md Jahangir Alam and Majid Vazifedoust; visualization, Hadis Pakdel; supervision, Sreeni Chadalavada and Dev Raj Paudyal; project administration, Sreeni Chadalavada, Md Jahangir Alam and Dev Raj Paudyal. All authors have read and agreed to the published version of the manuscript.

Funding: This research received no external funding.

Data Availability Statement: The data supporting the findings of this study are available from the first author upon reasonable request.

Acknowledgments: This research has been supported by the Graduate Research School, University of Southern Queensland and this is part of the first author's PhD project entitled "Variability of Extreme Climate Events and Impacts of Future Climate Change on the Streamflow".

Conflicts of Interest: The authors declare no conflicts of interest. Jahangir Alam works at the MDBA, however this research has no links with the MDBA.

References

1. IPCC. *Climate Change 2007: Synthesis Report. Contribution of Working Groups I, II and III to the Fourth Assessment Report of the Intergovernmental Panel on Climate Change*; Core Writing Team, Pachauri, R.K., Reisinger, A., Eds.; Cambridge University Press: Cambridge, UK, 2007; p. 104.
2. IPCC. *Climate Change 2014: Synthesis Report. Contribution of Working Groups I, II and III to the Fifth Assessment Report of the Intergovernmental Panel on Climate Change*; Cambridge University Press: Cambridge, UK, 2014.

3. Wang, J.; Hu, C.; Ma, B.; Mu, X. Rapid urbanization impact on the hydrological processes in Zhengzhou, China. *Water* **2020**, *12*, 1870. [CrossRef]
4. Ding, Y.; Zhang, Y.; Song, J. Changes in Weather and Climate Extreme Events and Their Association with the Global Warming. *Meteorol. Mon.* **2002**, *28*, 3–7.
5. Wang, Q.; Xu, Y.; Wang, Y.; Zhang, Y.; Xiang, J.; Xu, Y.; Wang, J. Individual and combined impacts of future land-use and climate conditions on extreme hydrological events in a representative basin of the Yangtze River Delta, China. *Atmos. Res.* **2020**, *236*, 104805. [CrossRef]
6. Head, L.; Adams, M.; McGregor, H.V.; Toole, S. Climate change and Australia. *Wiley Interdiscip. Rev. Clim. Change* **2014**, *5*, 175–197. [CrossRef]
7. Al-Safi, H.I.J.; Sarukkalige, P.R. Assessment of future climate change impacts on hydrological behavior of Richmond River Catchment. *Water Sci. Eng.* **2017**, *10*, 197–208. [CrossRef]
8. Ramezani, M.R.; Helfer, F.; Yu, B. Individual and combined impacts of urbanization and climate change on catchment runoff in Southeast Queensland, Australia. *Sci. Total Environ.* **2023**, *861*, 160528. [CrossRef] [PubMed]
9. Lamichhane, S.; Shakya, N.M. Integrated assessment of climate change and land use change impacts on hydrology in the Kathmandu Valley watershed, Central Nepal. *Water* **2019**, *11*, 2059. [CrossRef]
10. Meaurio, M.; Zabaleta, A.; Boithias, L.; Epelde, A.M.; Sauvage, S.; Sánchez-Pérez, J.-M.; Srinivasan, R.; Antiguedad, I. Assessing the hydrological response from an ensemble of CMIP5 climate projections in the transition zone of the Atlantic region (Bay of Biscay). *J. Hydrol.* **2017**, *548*, 46–62. [CrossRef]
11. Bloschl, G.; Montanari, A. Climate change impacts—Throwing the dice? *Hydrol. Process. Int. J.* **2010**, *24*, 374–381. [CrossRef]
12. Salas, J.; Obeysekera, J.; Vogel, R. Techniques for assessing water infrastructure for nonstationary extreme events: A review. *Hydrol. Sci. J.* **2018**, *63*, 325–352. [CrossRef]
13. Pakdel, H.; Paudyal, D.R.; Chadalavada, S.; Alam, M.J.; Vazifedoust, M. A Multi-Framework of Google Earth Engine and GEV for Spatial Analysis of Extremes in Non-Stationary Condition in Southeast Queensland, Australia. *ISPRS Int. J. Geo-Inf.* **2023**, *12*, 370. [CrossRef]
14. Cheng, L.; AghaKouchak, A.; Gilleland, E.; Katz, R.W. Non-stationary extreme value analysis in a changing climate. *Clim. Change* **2014**, *127*, 353–369. [CrossRef]
15. Cooley, D. Extreme value analysis and the study of climate change. *Clim. Change* **2009**, *97*, 77–83. [CrossRef]
16. Love, C.A.; Skahill, B.E.; Russell, B.T.; Baggett, J.S.; AghaKouchak, A. An Effective Trend Surface Fitting Framework for Spatial Analysis of Extreme Events. *Geophys. Res. Lett.* **2022**, *49*, e2022GL098132. [CrossRef]
17. Salas, J.D.; Obeysekera, J. Revisiting the concepts of return period and risk for nonstationary hydrologic extreme events. *J. Hydrol. Eng.* **2014**, *19*, 554–568. [CrossRef]
18. Cooley, D. Return periods and return levels under climate change. In *Extremes in a Changing Climate*; AghaKouchak, A., Easterling, D., Hsu, K., Schubert, S., Sorooshian, S., Eds.; Water Science and Technology Library; Springer: Dordrecht, The Netherlands, 2013; Volume 65, pp. 97–114.
19. Burn, D.H.; Sharif, M.; Zhang, K. Detection of trends in hydrological extremes for Canadian watersheds. *Hydrol. Process.* **2010**, *24*, 1781–1790. [CrossRef]
20. Gislason, P.O.; Benediktsson, J.A.; Sveinsson, J.R. Random forests for land cover classification. *Pattern Recognit. Lett.* **2006**, *27*, 294–300. [CrossRef]
21. Gualtieri, J.A.; Cromp, R.F. Support vector machines for hyperspectral remote sensing classification. In Proceedings of the 27th AIPR Workshop: Advances in Computer-Assisted Recognition, Washington, DC, USA, 14–16 October 1998; pp. 221–232.
22. Jones, B.; Tebaldi, C.; O'Neill, B.C.; Oleson, K.; Gao, J. Avoiding population exposure to heat-related extremes: Demographic change vs climate change. *Clim. Change* **2018**, *146*, 423–437. [CrossRef]
23. Khaliq, M.N.; St-Hilaire, A.; Ouarda, T.B.; Bobée, B. Frequency analysis and temporal pattern of occurrences of southern Quebec heatwaves. *Int. J. Climatol. A J. R. Meteorol. Soc.* **2005**, *25*, 485–504. [CrossRef]
24. Rainham, D.G.; Smoyer-Tomic, K.E. The role of air pollution in the relationship between a heat stress index and human mortality in Toronto. *Environ. Res.* **2003**, *93*, 9–19. [CrossRef] [PubMed]
25. Huth, R.; Kyselý, J.; Pokorná, L. A GCM simulation of heat waves, dry spells, and their relationships to circulation. *Clim. Change* **2000**, *46*, 29–60. [CrossRef]
26. Ouarda, T.B.; Charron, C. Nonstationary temperature-duration-frequency curves. *Sci. Rep.* **2018**, *8*, 15493. [CrossRef] [PubMed]
27. Cheng, L.; AghaKouchak, A. Nonstationary precipitation intensity-duration-frequency curves for infrastructure design in a changing climate. *Sci. Rep.* **2014**, *4*, 7093. [CrossRef] [PubMed]
28. Ragno, E.; AghaKouchak, A.; Cheng, L.; Sadegh, M. A generalized framework for process-informed nonstationary extreme value analysis. *Adv. Water Resour.* **2019**, *130*, 270–282. [CrossRef]
29. Ball, J.; Babister, M.; Nathan, R.; Weinmann, P.; Weeks, W.; Retallick, M.; Testoni, I. *Australian Rainfall and Runoff—A Guide to Flood Estimation*; Open Publications of UTS Scholars: Ultimo, NSW, Australia, 2019.
30. Montanari, A.; Koutsoyiannis, D. Modeling and mitigating natural hazards: Stationarity is immortal! *Water Resour. Res.* **2014**, *50*, 9748–9756. [CrossRef]
31. Usman, M.; Ndehedehe, C.E.; Farah, H.; Manzanas, R. Impacts of climate change on the streamflow of a large river basin in the Australian tropics using optimally selected climate model outputs. *J. Clean. Prod.* **2021**, *315*, 128091. [CrossRef]

32. Vance, T.; Roberts, J.; Plummer, C.; Kiem, A.; Van Ommen, T. Interdecadal Pacific variability and eastern Australian megadroughts over the last millennium. *Geophys. Res. Lett.* **2015**, *42*, 129–137. [CrossRef]
33. Sarker, A.; Ross, H.; Shrestha, K.K. A common-pool resource approach for water quality management: An Australian case study. *Ecol. Econ.* **2008**, *68*, 461–471. [CrossRef]
34. Enquiry, Q.F.C. *Interim Report, 1 August 2011*; Queensland Floods Commission of Inquiry: Brisbane, Australia, 2011. Available online: http://www.floodcommission.qld.gov.au/publications/interim-report (accessed on 16 April 2022).
35. Van den Honert, R.C.; McAneney, J. The 2011 Brisbane floods: Causes, impacts and implications. *Water* **2011**, *3*, 1149–1173. [CrossRef]
36. Cui, T.; Raiber, M.; Pagendam, D.; Gilfedder, M.; Rassam, D. Response of groundwater level and surface-water/groundwater interaction to climate variability: Clarence-Moreton Basin, Australia. *Hydrogeol. J.* **2018**, *26*, 593–614. [CrossRef]
37. Armstrong, M.S.; Kiem, A.S.; Vance, T.R. Comparing instrumental, palaeoclimate, and projected rainfall data: Implications for water resources management and hydrological modelling. *J. Hydrol. Reg. Stud.* **2020**, *31*, 100728. [CrossRef]
38. CSIRO; BOM. *Climate Change in Australia Information for Australia's Natural Resource Management Regions: Technical Report*; CSIRO and Bureau of Meteorology: Canberra, Australia, 2015.
39. Jeffrey, S.J.; Carter, J.O.; Moodie, K.B.; Beswick, A.R. Using spatial interpolation to construct a comprehensive archive of Australian climate data. *Environ. Model. Softw.* **2001**, *16*, 309–330. [CrossRef]
40. Pakdel, H.; Vazifedoust, M.; Paudyal, D.R.; Chadalavada, S.; Alam, M.J. Google Earth Engine as Multi-Sensor Open-Source Tool for Monitoring Stream Flow in the Transboundary River Basin: Doosti River Dam. *ISPRS Int. J. Geo-Inf.* **2022**, *11*, 535. [CrossRef]
41. Mission, N.S.R.T. Shuttle Radar Topography Mission (SRTM) Global. Distributed by OpenTopography. Available online: https://www.fdsn.org/networks/detail/GH/ (accessed on 15 September 2022).
42. Zanaga, D.; Van De Kerchove, R.; Daems, D.; De Keersmaecker, W.; Brockmann, C.; Kirches, G.; Wevers, J.; Cartus, O.; Santoro, M.; Fritz, S. ESA WorldCover 10 m 2021 v200. 2022. Available online: https://pure.iiasa.ac.at/18478 (accessed on 16 April 2022).
43. Cortes, C.; Vapnik, V. Support-vector networks. *Mach. Learn.* **1995**, *20*, 273–297. [CrossRef]
44. Esmaeili, P.; Vazifedoust, M.; Rahmani, M.; Pakdel, H. A simple rule-based algorithm in Google Earth Engine for operational discrimination of rice paddies in Sefidroud Irrigation Network. *Arab. J. Geosci.* **2023**, *16*, 649. [CrossRef]
45. Pal, M.; Mather, P.M. Support vector machines for classification in remote sensing. *Int. J. Remote Sens.* **2005**, *26*, 1007–1011. [CrossRef]
46. Xie, G.; Niculescu, S. Mapping and monitoring of land cover/land use (LCLU) changes in the crozon peninsula (Brittany, France) from 2007 to 2018 by machine learning algorithms (support vector machine, random forest, and convolutional neural network) and by post-classification comparison (PCC). *Remote Sens.* **2021**, *13*, 3899. [CrossRef]
47. Briem, G.J.; Benediktsson, J.A.; Sveinsson, J.R. Multiple classifiers applied to multisource remote sensing data. *IEEE Trans. Geosci. Remote Sens.* **2002**, *40*, 2291–2299. [CrossRef]
48. Iqbal, M.S.; Dahri, Z.H.; Querner, E.P.; Khan, A.; Hofstra, N. Impact of climate change on flood frequency and intensity in the Kabul River Basin. *Geosciences* **2018**, *8*, 114. [CrossRef]
49. Zhou, Q.; Leng, G.; Huang, M. Impacts of future climate change on urban flood volumes in Hohhot in northern China: Benefits of climate change mitigation and adaptations. *Hydrol. Earth Syst. Sci.* **2018**, *22*, 305–316. [CrossRef]
50. Cui, T.; Yang, T.; Xu, C.-Y.; Shao, Q.; Wang, X.; Li, Z. Assessment of the impact of climate change on flow regime at multiple temporal scales and potential ecological implications in an alpine river. *Stoch. Environ. Res. Risk Assess.* **2018**, *32*, 1849–1866. [CrossRef]
51. Melsen, L.A.; Addor, N.; Mizukami, N.; Newman, A.J.; Torfs, P.J.; Clark, M.P.; Uijlenhoet, R.; Teuling, A.J. Mapping (dis) agreement in hydrologic projections. *Hydrol. Earth Syst. Sci.* **2018**, *22*, 1775–1791. [CrossRef]
52. Boughton, W. A hydrograph-based model for estimating the water yield of ungauged catchments. In Proceedings of the Hydrology and Water Resources Symposium, Newcastle, IEAust, Newcastle, Australia, 30 June–2 July 1993.
53. Boughton, W. The Australian water balance model. *Environ. Model. Softw.* **2004**, *19*, 943–956. [CrossRef]
54. Boughton, W.C. An Australian water balance model for semiarid watersheds. *J. Soil Water Conserv.* **1995**, *50*, 454–457.
55. Boughton, W. Calibrations of a daily rainfall-runoff model with poor quality data. *Environ. Model. Softw.* **2006**, *21*, 1114–1128. [CrossRef]
56. Boughton, W. Effect of data length on rainfall–runoff modelling. *Environ. Model. Softw.* **2007**, *22*, 406–413. [CrossRef]
57. Yu, B.; Zhu, Z. A comparative assessment of AWBM and SimHyd for forested watersheds. *Hydrol. Sci. J.* **2015**, *60*, 1200–1212. [CrossRef]
58. Jahandideh-Tehrani, M.; Zhang, H.; Helfer, F.; Yu, Y. Review of climate change impacts on predicted river streamflow in tropical rivers. *Environ. Monit. Assess.* **2019**, *191*, 752. [CrossRef] [PubMed]
59. Petheram, C.; Rustomji, P.; McVicar, T.R.; Cai, W.; Chiew, F.H.; Vleeshouwer, J.; Van Niel, T.G.; Li, L.; Cresswell, R.G.; Donohue, R.J. Estimating the impact of projected climate change on runoff across the tropical savannas and semiarid rangelands of northern Australia. *J. Hydrometeorol.* **2012**, *13*, 483–503. [CrossRef]
60. Podger, G. *Rainfall Runoff Library User Guide*; Cooperative Research Centre for Catchment Hydrology: Clayton, Australia, 2004.
61. Esmaeili-Gisavandani, H.; Lotfirad, M.; Sofla, M.S.D.; Ashrafzadeh, A. Improving the performance of rainfall-runoff models using the gene expression programming approach. *J. Water Clim. Change* **2021**, *12*, 3308–3329. [CrossRef]

62. Tehrani, M.J.; Helfer, F.; Jenkins, G. Impacts of climate change and sea level rise on catchment management: A multi-model ensemble analysis of the Nerang River catchment, Australia. *Sci. Total Environ.* **2021**, *777*, 146223. [CrossRef]
63. Pakdel, H.; Vazifedoust, M.; Marofi, S.; Tizro, A.T. Simulation of river discharge in ungauged catchments by forcing GLDAS products to a hydrological model (a case study: Polroud basin, Iran). *Water Supply* **2020**, *20*, 277–286. [CrossRef]
64. Eccles, R.; Zhang, H.; Hamilton, D.; Trancoso, R.; Syktus, J. Impacts of climate change on streamflow and floodplain inundation in a coastal subtropical catchment. *Adv. Water Resour.* **2021**, *147*, 103825. [CrossRef]
65. Kirono, D.G.; Round, V.; Heady, C.; Chiew, F.H.; Osbrough, S. Drought projections for Australia: Updated results and analysis of model simulations. *Weather Clim. Extrem.* **2020**, *30*, 100280. [CrossRef]
66. Alexander, L.V.; Arblaster, J.M. Historical and projected trends in temperature and precipitation extremes in Australia in observations and CMIP5. *Weather Clim. Extrem.* **2017**, *15*, 34–56. [CrossRef]
67. Durocher, M.; Burn, D.H.; Ashkar, F. Comparison of estimation methods for a nonstationary Index-Flood Model in flood frequency analysis using peaks over threshold. *Water Resour. Res.* **2019**, *55*, 9398–9416. [CrossRef]
68. Moisello, U. On the use of partial probability weighted moments in the analysis of hydrological extremes. *Hydrol. Process. Int. J.* **2007**, *21*, 1265–1279. [CrossRef]
69. Coles, S.; Bawa, J.; Trenner, L.; Dorazio, P. *An Introduction to Statistical Modeling of Extreme Values*; Springer: London, UK, 2001; Volume 208.
70. Morrison, J.E.; Smith, J.A. Stochastic modeling of flood peaks using the generalised extreme value distribution. *Water Resour. Res.* **2002**, *38*, 41-1–41-12. [CrossRef]
71. Adugna, T.; Xu, W.; Fan, J. Comparison of random forest and support vector machine classifiers for regional land cover mapping using coarse resolution FY-3C images. *Remote Sens.* **2022**, *14*, 574. [CrossRef]
72. Sadeghi Loyeh, N.; Massah Bavani, A. Daily maximum runoff frequency analysis under non-stationary conditions due to climate change in the future period: Case study Ghareh Sou Basin. *J. Water Clim. Change* **2021**, *12*, 1910–1929. [CrossRef]
73. Obeysekera, J.; Salas, J.D. Quantifying the uncertainty of design floods under nonstationary conditions. *J. Hydrol. Eng.* **2014**, *19*, 1438–1446. [CrossRef]
74. IPCC. Summary for Policymakers. In *Climate Change 2021: The Physical Science Basis. Contribution of Working Group I to the Sixth Assessment Report of the Intergovernmental Panel on Climate Change*; Masson-Delmotte, V., Zhai, P., Pirani, A., Connors, S.L., Péan, C., Berger, S., Caud, N., Chen, Y., Goldfarb, L., Gomis, M.I., et al., Eds.; IPCC: Geneva, Switzerland, 2021; *In Press*.
75. Lima, C.H.; Lall, U.; Troy, T.J.; Devineni, N. A climate informed model for nonstationary flood risk prediction: Application to Negro River at Manaus, Amazonia. *J. Hydrol.* **2015**, *522*, 594–602. [CrossRef]
76. Gilleland, E.; Katz, R.W. New software to analyze how extremes change over time. *Eos Trans. Am. Geophys. Union* **2011**, *92*, 13–14. [CrossRef]
77. Sarhadi, A.; Soulis, E.D. Time-varying extreme rainfall intensity-duration-frequency curves in a changing climate. *Geophys. Res. Lett.* **2017**, *44*, 2454–2463. [CrossRef]

6.3. Links and implications

This paper marks the conclusion of the research by utilising the hydrometeorological extreme results generated in paper 2 and continuing it through the hydrological model's calibration and projection of an ensemble of GCMs to estimate flood extremes in the past. Subsequently, projecting the flood extremes in the near and far future period. This paper achieved Research Objectives 2, 3 and 4: *"To evaluate the impacts of land cover changes and urbanisation by applying SVM and RF classification along with climate change,","Perform the hydrological simulations for each landcover classification separately under ensembles of GCMs under different RCPs and landcover changes in the baseline and the near and far future horizons*," and *"Analyse the intensity and frequency of projected streamflow extreme events, under both stationary and non-stationary conditions using the GEV model."*

To achieve these objectives, a multi-framework was developed by integrating the hydrological model, SVM and RF classifications in the GEE platform, an ensemble of GCMs under two scenarios, and the ProNEVA model, to evaluate the impact of climate change on floods, streamflow, and water supply.
The SVM and RF classification in the GEE platform was applied to estimate the projected land cover changes in the future period and by assuming that the location parameter has a linear relationship with time, the ProNEVA model was applied to assess the magnitude and frequency of extreme flood utilising the GEV distribution. ProNEVA (Ragno et al., 2019) incorporates the underlying physical drivers triggering extreme events, serving as crucial instruments for quantifying the probability of extreme occurrences in a particular area or timeframe.

This research examines both ProNEVA and landcover classification to account for the physical system in terms of cause and effect. This research covers non-stationary conditions in extreme events with ProNEVA with time covariant by incorporating the outputs of the ensemble of GCMs under different scenarios from the hydrological model and GEE classification approach. It is recommended that, in future studies, ProNEVA allow for the incorporation of physical drivers as additional covariates for modelling floods.

6.4. Conclusion

Chapter 5 of this dissertation introduced the third research paper crafted within the scope of this study. This paper discussed flood extremes in various scenarios using multiple GCMs and projected changes in land cover under non-stationary conditions in future periods.

CHAPTER 7: PAPER 4 – EXTREME TEMPERATURES AND TEMPERATURE-DURATION-FREQUENCY (TDF) RELATIONSHIP IN VARYING CLIMATIC ZONES ACROSS AUSTRALIA

7.1. Introduction

The climate is undergoing significant change, leading to shifts in the frequency and severity of extreme temperatures. This dynamic climate landscape necessitates the development of robust tools to predict and understand these temperature extremes for various applications, including infrastructure design, urban planning, and environmental management.

The escalating frequency and duration of these events underscore the urgency to better comprehend their variability and potential impacts. TDF curves offer a systematic approach to exploring the relationship between extreme temperatures, duration, and recurrence levels. By analysing historical temperature data through TDF curves, researchers can discern trends, identify step changes, and assess the spatial variability of extreme temperatures across different regions.

This study focuses on investigating the presence of trends and step changes in extreme temperatures across nine locations in Australia. Utilising a GEV distribution and employing Monte Carlo Bayesian inference techniques, the frequency analysis of annual maximum temperatures for durations ranging from one to 15 days was conducted. The findings revealed rising trends and step changes in several cities, highlighting the spatial heterogeneity of extreme temperature patterns across the continent.

Understanding the characteristics of extreme temperatures and the development of TDF curves offer practical insights for various sectors, including healthcare, agriculture, infrastructure management, and natural disaster preparedness. By integrating TDF curves into decision-making processes, stakeholders can enhance risk assessment, optimising infrastructure design, and improve public health interventions in response to extreme temperature events.

While previous studies have explored similar concepts in different geographic contexts, this research contributes to the developing field of TDF curve development in Australia.

By applying robust statistical methodologies and considering both stationary and non-stationary assumptions, this study provides a comprehensive analysis of extreme temperature variability, laying the groundwork for future investigations and informed decision-making.

In conclusion, the development of TDF curves represents a crucial step towards enhancing our understanding of extreme temperatures and their impacts on society and the environment. By leveraging these curves; policymakers, planners, and stakeholders can effectively mitigate risks, adapt to changing climate conditions, and foster resilience in the face of evolving temperature extremes.

7.2. Submitted paper

Chowdhury et al. (2024), “Extreme Temperatures and Temperature-Duration-Frequency (TDF) Relationship in Varying Climatic Zones Across Australia” is submitted to Urban Climate Journal.

Extreme Temperatures and Temperature-Duration-Frequency (TDF) Relationship in Varying Climatic Zones Across Australia

Rezaul Chowdhury [†], Sreenivasulu Chadalavada [a, *], Hadis Pakdel[a], Kevin McDougall[a]

[a] School of Engineering, The University of Southern Queensland, Springfield Lakes QLD 4300, Australia; Sreeni.Chadalavada@unisq.edu.au; Hadis.Pakdel@unisq.edu.au; Kevin.McDougall@unisq.edu.au

* Correspondence: Sreeni.Chadalavada@unisq.edu.au

Abstract: The frequency and severity of extreme temperatures are changing and therefore, the necessity for the development of the concept of design temperatures has emerged. The maximum or minimum design temperature at a location can be considered as reliable predictors of temperture extremmes to support the design of infrastructure, urban planning and environmental impacts of changing temperature. These design tempertures in the form of temperature-duration-frequency (TDF) curves can be utilized to better understand the variability of extreme temperatures with respect to duration and recurrence levels. This study explored the presence/absence of trend and step change in extreme temperatures for nine locations across Australia. Frequency analysis of annual maximum temperatures from 1 to 15-day durations was performed using a generalized extreme value (GEV) distribution under stationary and non-stationary conditions, where the parameters were estimated using the Monte Carlo Bayesian inference approach. Rising trend and step change were observed in Hobart, Adelaide, Perth, Darwin, Alice Springs, Sydney and Melbourne, but not identified in Cairns and Brisbane. Lower variability in design temperatures was found in Cairns and Brisbane, as well as in Darwin and Alice Springs. In contrast, high variability was observed in Sydney and Melbourne, and high design temperatures are reflected in Adelaide and Perth. The approach followed in this study can be applied to any location for TDF curves development and can be utilised to support health risk management of heatwaves, design of infrastructures where temperature related changes may impact the environment and preparedness for natural hazards like droughts and bushfires.

Keywords: Temperature Extremes; Risk Assessment; Temperature-Duration-Frequency curves, design temperature

1. Introduction

A rise of global average temperature from 2°C to more than 4°C is predicted by 2100 (Brown and Caldeira, 2017; Raftery et al., 2017). This rise of temperature increases the frequency of hot days and nights and prolongs temperature extremes (Steffen et al., 2014). Prolonged temperature extremes above a threshold level are typically known as a heatwave (Mazdiyasni and AghaKouchak, 2015). In Australia, a heatwave is defined as three or more consecutive days of extreme temperatures, relative to the local climate condition ((BoM), 2012; Nairn and Fawcett, 2011). A temperature threshold can be determined either based on a percentile of each month's daily temperatures or based on a fixed value (Meehl and Tebaldi, 2004). Persistent temperature extremes or heatwaves are detrimental to public health, agriculture, natural ecosystems, infrastructures, energy sectors and economic activities (Huth et al., 2000; Jones et al., 2018; Khaliq et al., 2005; Ouarda and Charron, 2018; Rainham and Smoyer-Tomic, 2003; Zampieri et al., 2017). Heat stress is the direct health impact of prolonged temperature extremes. Prolonged temperature extremes increase mortality rates (Mazdiyasni et al., 2017) and risk of natural hazards like bushfires (Koutsias et al., 2012). Particularly, urban residents are more susceptible to extreme temperatures (Khaliq et al., 2005). In the past, the European (in 2003) and Russian (in 2010) heatwaves caused more than 70,000 and 56,000 deaths, respectively (Beniston, 2004; Grumm, 2011).

The Australian annual mean temperature has increased by more than 1°C since 1910, and the rate of very hot days has been increasing since the 1990s ((BoM), 2020). An increased frequency and length of temperature extremes was observed from 1971 to 2008 across the country (Steffen et al., 2014) and a further increase is predicted (Cowan et al., 2014). Since 1900, the number of deaths in Australia due to heatwaves exceeds all other natural hazards (Coates et al., 2014). Increased hospital admissions (Hondula and Barnett, 2014; Nitschke et al., 2011) and mortality rates among women and the elderly (Tong et al., 2012) are associated with extreme temperatures. Exposure to extreme temperature causes substantial economic loss, due to lower labour productivity and less

human performance (Zander et al., 2015; Zander et al., 2019). Apart from health impacts, infrastructure and utilities such as electricity transmission networks and transport systems are substantially affected by heatwaves (Steffen et al., 2014). The economic loss from the 2009 heatwaves in southeast Australia was estimated to be AU$800 million, which was largely caused by power outages and transport disruptions (Chhetri et al., 2012). In terms of natural hazards, a vast region of Australia is susceptible to drought and bushfires with both hazards being exacerbated by prolonged temperature extremes. Furthermore, the risk of fire hazards is expected to increase with the projected rise of extreme temperatures (Lucas et al., 2007). While these curves may not directly explain the underlying causes or analyze the physical system, they serve as valuable tools for understanding the probability of extreme temperature events and identifying the frequency and magnitude of these extremes. The practical significance of TDF curves for extreme temperatures lies in their ability to undertake risk assessment, infrastructure design, and decision-making processes. By incorporating these curves into planning and design, we can plan to manage risk to infrastructure, human exposure to extreme heat events and manage the impacts our natural environment to these events..

Frequency analysis of temperature extremes and the development of temperature-duration-frequency (TDF) curves are useful in determining design temperatures at various recurrence intervals and durations. To the best of our knowledge, TDF curves have not yet been developed in Australia, but a small number of studies have been carried out in North America. Kharin and Zwiers (2000) performed frequency analysis of temperature extremes, but the duration of the extremes was not considered in their study. Motivated by rainfall intensity-duration-frequency (IDF) curves, Ouarda and Charron (2018) developed a method for nonstationary TDF curves in Canada using frequency analysis of the annual maximum temperature series. Very recently, Mazdiyasni et al. (2019) developed heatwave IDF curves for different cities located in the United States. They applied a multivariate copula function to relate heatwave duration and intensity and considered mean daily temperature series, instead of annual maximum series. Both studies performed frequency analysis of heatwaves for durations ranging from one to ten days. The Generalised Extreme Value (GEV) and Log Pearson Type 3 (LP3) distributions are often used for frequency analysis of hydroclimatic extremes. Previous studies applied the GEV distribution for the development of TDF curves (Mazdiyasni et al., 2019; Ouarda and Charron, 2018). The Australian Rainfall and Runoff (ARR) (Ball et al., 2019) guideline has also recommended the GEV distribution for estimating design rainfalls and floods. In terms of parameter estimation, both stationary and nonstationary approaches were applied in previous studies (Ouarda and Charron, 2018). The nonstationary approach was adopted on the basis that climate change alters hydroclimatic extremes (Cheng and AghaKouchak, 2014).

Understanding the characteristics of temperature extremes, design temperatures and TDF curves are useful for different sectors of the community including healthcare, agriculture, natural disaster management, infrastructure and energy production. Similar to design rainfall and flood information, design temperatures can be useful in the planning and risk assessment across many areas. Therefore, this study explores the characteristics of extreme temperatures at several major cities in Australia (Table 1) based on the Australian Climate Observations Reference Network–Surface Air Temperature (ACORN-SAT) to develop TDF curves. It applies robust statistical techniques for characterizing extreme temperatures and applies GEV distribution for frequency analysis. The TDF curves are developed for durations ranging from one to fifteen days, and for different annual exceedance probability (AEP) levels. The outcomes of the study could be useful in understanding the spatial variation of design temperatures, selection of appropriate materials for infrastructures, appropriate preparedness for natural hazards, health care services and for public awareness.

Table 1. Details of ACORN-SAT stations used in the study

Site no.	Site name	Latitude	Longitude	Elevation (m)	Study period	Missing data (%)
31011	Cairns	16.87 °S	145.75 °E	2	1910-2017	0.34%
40842	Brisbane Airport	27.39 °S	153.13 °E	5	1949-2016	0.1%
66062	Sydney	33.86 °S	151.21 °E	39	1910-2017	0.08%
86338	Melbourne	37.83 °S	144.98 °E	8	1910-2018	0.01%
94029	Hobart	42.89 °S	147.33 °E	51	1918-2018	0.12%
23090	Adelaide (Kent Town)	34.92 °S	138.62 °E	48	1910-2018	0.17%
09021	Perth Airport	31.93 °S	115.98 °E	15	1910-2018	0.028%
14015	Darwin Airport	12.42 °S	130.89 °E	30	1910-2018	0.786%
15590	Alice Springs Airport	23.80 °S	133.89 °E	546	1910-2018	0.275%

2. Materials and Methods

2.1. Study region

The Australian Climate Observations Reference Network – Surface Air Temperature (ACORN-SAT) dataset of the Australian Bureau of Meteorology provides daily maximum temperature in degree Celsius (°C), which has been developed in order to monitor climate variability and change in the country (Trewin, 2018). For frequency analysis, it is necessary that time series data are free from trends/jumps caused by equipment drift and logistics problems like change of equipment, station location and sampling frequency (Ouarda and Charron, 2018). The ACORN-SAT data are adjusted, homogenised and peer reviewed. The first and the current version of ACORN-SAT data was published in 2011 and 2018, respectively. Australian summer season extends from December to February, but in many years the maximum daily temperatures were observed in other months (October or March, for example). Therefore, temperature extremes data were extracted for each water year (October to September). The details of stations used in this study are provided in Table 1, which show that the missing data is comparatively very low (less than 1%), and no attempt was taken in this study to fill these missing values.

It should be noted that nominated stations consists of the high quality homogenised and validated data from Australia's Bureau of Meteorology (BOM). The BOM has adopted a rigorous process to validate its historic temperature records to ensure that any changes in temperature readings are not due to local or human impacts. The issue of heat islands and urbanisation have been addressed through the quality assurance and data validation process undertaken by the BOM. Additionally, the location of the recording stations at these major centres is usually in areas of open space and grassland (such as airports) and located away from the urban centres (usually 15-20km from the city centres) where the impact of heat islands may be highest. The data homogenisation utilises the mean temperature increases across the chosen stations to correlate closely with the overall analysis across all of Australia and reflect Australia wide trends. It should be highlighted that stations selected are major cities in different climatic zones around Australia. The distribution and availability of high quality and long-term data climatic data is often limited to major centres where most of the Australian population is concentrated. Therefore, the choice of stations was base both on climatic zones and availability of high-quality long-term data (Figure 1).

The annual maximum temperature series have been estimated for one to fifteen days of durations. Duration is defined as a run of consecutive days of highest average daily maximum temperatures. A *D-day* duration of temperature extremes is the largest average of *D*-consecutive days of daily maximum temperatures. The extreme temperature time series of *D-day* duration can be denoted by T_D. For year n, $\boldsymbol{T_{D_n}}$ is the largest value of average daily maximum temperatures observed consistently for any *D-day* duration during the year (October to September). When the duration is more than 1 day, a moving average method having a window of width D>1 day (D = 2, 3, 4, … ,15) was used. The concept was previously applied in several relevant studies (Javelle et al., 2002; Khaliq et al., 2005; Ouarda and Charron, 2018), in particular the concept is well adopted in rainfall IDF curves development, where frequency analysis of time-averaged rainfall intensities is performed at various durations (Hosking and Wallis, 1993; Ouarda et al., 2001).

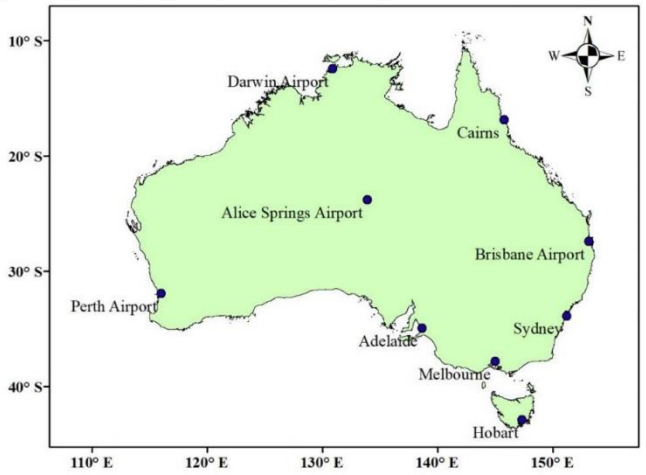

Figure 1. The locations of meteorological stations in geographical locations of Australia.

2.2. Analysis of trend and step change

The temperature extremes data series were analysed for the presence of trends and step change or jump. Three statistical tests were performed to confirm the presence or absence of trends. They were the Spearman rank correlation test (Dahmen and Hall, 1990; Siegel and Castellan), the Mann–Kendall test (Kendall, 1948) and the linear regression test. Both Mann-Kendall and Spearman tests are rank-based non-parametric tests and the linear regression test is one of the most common tests for trend (Kundzewicz et al., 2000). These tests were previously applied in several trend studies (Chowdhury and Beecham, 2010; Chowdhury et al., 2015; Khaliq et al., 2005; Pakdel et al., 2022).

Step changes in data series were tested by using four statistical tests. The Mann-Whitney or Rank-sum test, is a rank-based test, that detects the point of change in the mean between two independent sample groups (Chiew and McMahon, 1993; Kundzewicz et al., 2000; Ouarda et al., 2001). The cumulative sum (CUSUM), which is also a rank-based test, compares the successive observations with the median of the time series (Chiew and McMahon, 1993). The cumulative deviation test (Buishand, 1982) is based on the rescaled cumulative sum of the deviations from the mean of the series and it is used to detect a change point towards the centre of the time series. The Student's t-test (Snedecor and Cochran, 1989), a parametric test, and the Worsley likelihood ratio test (Worsley, 1979) were used for testing whether two samples have different means. To perform these step change tests, the time series were divided into two non-overlapping subsamples of approximately equal length.

2.3. Probability distribution

The GEV distribution has been applied for frequency distribution of annual maximum series of extreme temperature (TD). The GEV distribution is recommended for Australian hydro-climatological conditions (Ball et al., 2019) and it has been widely applied for frequency analysis of flood peaks and natural extreme events including heatwaves (Bauer, 1996; Courty et al., 2019; Hosking et al., 1985; Khaliq et al., 2005; Mazdiyasni et al., 2019; Morrison and Smith, 2002; Ouarda and Charron, 2018; Stedinger and Lu, 1995). The cumulative distribution function (cdf) of GEV distribution can be written as (Courty et al., 2019):

$$F(T) = \begin{cases} \exp\left[-\left(\frac{T-\mu}{\sigma}\right)^{1/\kappa}\right], & \kappa \neq 0 \\ \exp\left[\exp\left(-\frac{T-\mu}{\sigma}\right)\right], & \kappa = 0 \end{cases} \quad (1)$$

where T is the temperature variable, and μ, σ and κ are the location, scale and shape parameter, respectively. When the shape parameter $\kappa = 0$, $\kappa < 0$ and $\kappa > 0$, the GEV simplifies to the Gumbel, Fréchet and Weibull distribution, respectively. The quantile function of the GEV distribution can be written as:

$$T(D,p) = \mu_D + \sigma_D y \quad (2)$$

where, D is temporal duration, p is annual exceedance probability (AEP), and y is expressed in terms of p as:

$$y = \frac{1}{\kappa}\{1 - [-\ln(1-p)]^{\kappa}\} \quad (3)$$

Therefore, the quantile functions can be written as:

$$T_D(p) = \begin{cases} \mu + \frac{\sigma}{k}\left(1 - [-\ln(1-p)]^{k}\right), & k \neq 0 \\ \mu - \sigma \ln[-\ln(1-p)] \quad , & k = 0 \end{cases} \quad (4)$$

For a given value of AEP (p), the quantile estimates TD(p) can be obtained by substituting estimated values of the parameters to the quantile function.

2.4. GEV parameter estimation

The Monte Carlo Bayesian inference of the extreme value analysis package TUFLOW Flike (TUFLOW Flike 5.0.300.0, http://flike.tuflow.com/) was used for parameter estimation (Kuczera, 1999). The TUFLOW Flike software starts the search for the most probable parameters by setting the shape parameter $\kappa = 0$ and uses the Gumbel method-of-moments estimates of the location (μ) and scale (σ) parameters fitted to the temperature extreme data. It involves two search algorithms, global and quasi-Newton, to locate the model parameters which maximise the posterior density. The global search algorithm was applied in this study. The shape parameter was initially assigned a value 0 ($\kappa = 0$) so the distribution became Gumbel. No prior information was assumed, and 99,000 parameter samples were generated in the Bayesian inference method. The chi-squared test statistic (Snedecor and Cochran, 1989) was used for the goodness of the fit test. Results show that the GEV distribution fits well within the annual maximum temperature series at 5% significance level.

A general inference method is followed in the Bayesian approach. The approach uses a probability distribution to describe what is known about the parameters. The posterior probability density of the parameters β given the data T can be expressed as (Kuczera, 1999):

$$\xi(\boldsymbol{\beta}|\boldsymbol{T}) \propto \boldsymbol{f}(\boldsymbol{T}|\boldsymbol{\beta})\xi(\boldsymbol{\beta}) \quad (5)$$

where ξ(β) is the prior probability density of the parameters and $\boldsymbol{f}(\boldsymbol{T}|\boldsymbol{\beta})$ is the sampling distribution of the data for a chosen probability distribution and parameters β. For an annual maximum series data length of n years, say, Q = {q1, q2,….qn), the sampling distribution of Q can be defined as the joint probability density function (pdf) of n data:

$$\boldsymbol{f}(\boldsymbol{Q}|\boldsymbol{\beta}) = \boldsymbol{f}(\boldsymbol{q_1}, \boldsymbol{q_2}, \dots, \boldsymbol{q_n}|\boldsymbol{\beta}) = \prod_{i=1}^{n} \boldsymbol{f}(\boldsymbol{q_i}|\boldsymbol{\beta}) \quad (6)$$

where $\boldsymbol{f}(\boldsymbol{q}|\boldsymbol{\beta})$ is the pdf of the frequency model (GEV, for example), q is statistically independent data and β is a vector of parameters. The Bayesian distribution of q explicitly accounts for parameter uncertainty. The expected exceedance probability of q exceeding qp can be defined as:

$$\boldsymbol{P}(\boldsymbol{q} > \boldsymbol{q_p}|\boldsymbol{T}) = \int_{\beta} \boldsymbol{P}(\boldsymbol{q} > \boldsymbol{q_p}|\boldsymbol{\beta})\xi(\boldsymbol{\beta}|\boldsymbol{T})\, \boldsymbol{d\beta} \quad (7)$$

where $\boldsymbol{P}(\boldsymbol{q} > \boldsymbol{q_p}|\boldsymbol{\beta})$ is the probability of q exceeding qp given that β is the true parameter vector. Applying the Monte Carlo technique (random sampling from a probability distribution), the expected exceedance probability for qp can be written as:

$$\boldsymbol{P}(\boldsymbol{q} > \boldsymbol{q_p}|\boldsymbol{T}) = \int_{\beta} \boldsymbol{P}(\boldsymbol{q} > \boldsymbol{q_p}|\boldsymbol{\beta}) \frac{\xi(\boldsymbol{\beta}|\boldsymbol{T})}{\boldsymbol{I}(\boldsymbol{\beta})} \boldsymbol{I}(\boldsymbol{\beta})\, \boldsymbol{d\beta} \quad (8)$$

where $\boldsymbol{I}(\boldsymbol{\beta})$ is the importance pdf. Sampling of N independent and identically distributed samples from $\boldsymbol{I}(\boldsymbol{\beta})$ yield {β1, β2, …, βN}, therefore Eq. 8 can be written as:

$$\boldsymbol{P}(\boldsymbol{q} > \boldsymbol{q_p}|\boldsymbol{T}) = (\sum_{i=1}^{N} \boldsymbol{P}(\boldsymbol{q} > \boldsymbol{q_p}|\boldsymbol{\beta_i})\boldsymbol{w_i}) / \sum_{i=1}^{N} \boldsymbol{w_i} \quad (9)$$

where, $\boldsymbol{w_i} = \frac{\xi(\boldsymbol{\beta}|\boldsymbol{T})}{\boldsymbol{I}(\boldsymbol{\beta})}$ is the weight.

The Monte Carlo sampling generates a sequence of parameters and their normalised weights $\{\boldsymbol{\beta_i}, \boldsymbol{p_i}, \boldsymbol{i} = \boldsymbol{1, 2, \dots, N}\}$, where the normalised weight $\boldsymbol{p_i} = \boldsymbol{w_i} / \sum_{j=1}^{n} \boldsymbol{w_j}$. Sampling from N values of $\boldsymbol{\beta_i}$ according to the probability $\boldsymbol{p_i}$ yields samples drawn from $\xi(\boldsymbol{\beta}|\boldsymbol{T})$. The quantile $\boldsymbol{q_p}(\beta)$ can be defined as P[q > $\boldsymbol{q_p}$(β)] = p, where p is AEP. After ranking of N quentiles {qp(βi), i = 1,…,N}, the upper and lower confidence levels are the quantiles whose exceedance probabilities are the closest to α/2 and (1- α/2), respectively, where α is the significance level. The 10% and 90% confidence levels are considered in this study.

2.4. GEV parameter estimation

For all stations and durations, design extreme temperatures have been estimated for different AEPs using the quantile equation (Eq. 2) and estimated GEV parameters. Stationary TDF curves have been developed by plotting design temperatures and AEPs at the vertical and horizontal axis respectively. The logarithm (log10) scale is used for the horizontal axis. While the design temperatures were estimated from 1 in 1-year AEP to 1 in 100000-year AEPs, the TDF curves were plotted for 1 in 2-year to 1 in 100-year AEPs in Figures 5 to 13. Each curve represents a duration (one to fifteen days).

3. Results

3.1. Trend and step change

The null hypothesis (H_o) was defined as the absence of trend and step change in temperature extremes. The H_o was rejected when the test statistic value was higher than the critical value at a significance level (SL). Three SLs were considered, 0.01 (1%), 0.05 (5%) and 0.1 (10%). Table 2 shows the detailed statistical tests results for a station (Perth airport, 1-day duration). The 1-day annual maximum temperature series including 5-year moving average line for the same station is plotted in Figure A. 1. For step change analysis, the time series were divided into two equal sub-series, and the mean and median values were calculated for each sub-series. As an example, the mean (and median) extreme temperatures for Perth during 1910-1964 and 1965-2018 period were estimated to be 41.28°C (41.1°C) and 42.06°C (41.95°C), respectively.

Table 2. Detailed statistical results of trend and step change analysis of 1-day temperature extremes for Perth airport (site no. 09021)

Test	Statistical tests	Test statistic	Critical values			Test result
			SL = 0.1	SL = 0.05	SL = 0.01	
Trend detection	Mann-Kendall	2.603	1.645	1.960	2.576	Ho rejected at 1%
	Spearman's Rho	2.840	1.645	1.960	2.576	Ho rejected at 1%
	Linear regression	2.523	1.661	1.984	2.626	Ho rejected at 5%
Step change	CUSUM	17.000	12.737	14.199	17.018	Ho rejected at 5%

	Cumulative deviation	1.464	1.170	1.291	1.551	Ho rejected at 5%
	Worsley likelihood	3.098	2.869	3.159	3.790	Ho rejected at 10%
	Rank Sum	2.748	1.645	1.960	2.576	Ho rejected at 1%
	Student's t	2.061	1.661	1.984	2.626	Ho rejected at 5%

Table 3 shows the outcomes of trend and step change analysis for all stations and durations. The presence of a statistically significant increasing trend and step change (H_o rejected) is denoted by red (1% SL), brown (5% SL) and yellow (10% SL) cell colours. A green cell colour denotes the absence of a statistically significant trend or step change (H_o accepted) in the data. Five locations (Hobart, Adelaide, Perth, Darwin and Alice Springs) exhibit the existence of significant trend and step change in the observed temperature extremes for all durations. Among them, Adelaide, Perth and Darwin are located in the south, west and north of Australia, respectively. Alice Springs is positioned in the middle of the country and Hobart is located on the island of Tasmania (south of mainland Australia). Cairns, which is located in the north-east region, does not exhibit the presence of a significant trend for any of the durations explored. A significant step change was also absent in Cairns, except that the CUSUM test predicted a step change for longer durations (9 to 15 days). For Brisbane, which is also located in the same region, a significant trend at 5% SL was not identified for any duration, however at 10% SL a trend was observed for 3- to 5-day durations. Except for 3 to 5-day durations, a significant step change at 5% SL was not identified for Brisbane. Hence, temperature extremes at Cairns and Brisbane, which are in the north-eastern state of Queensland, do not exhibit existence of significant trend and shift.

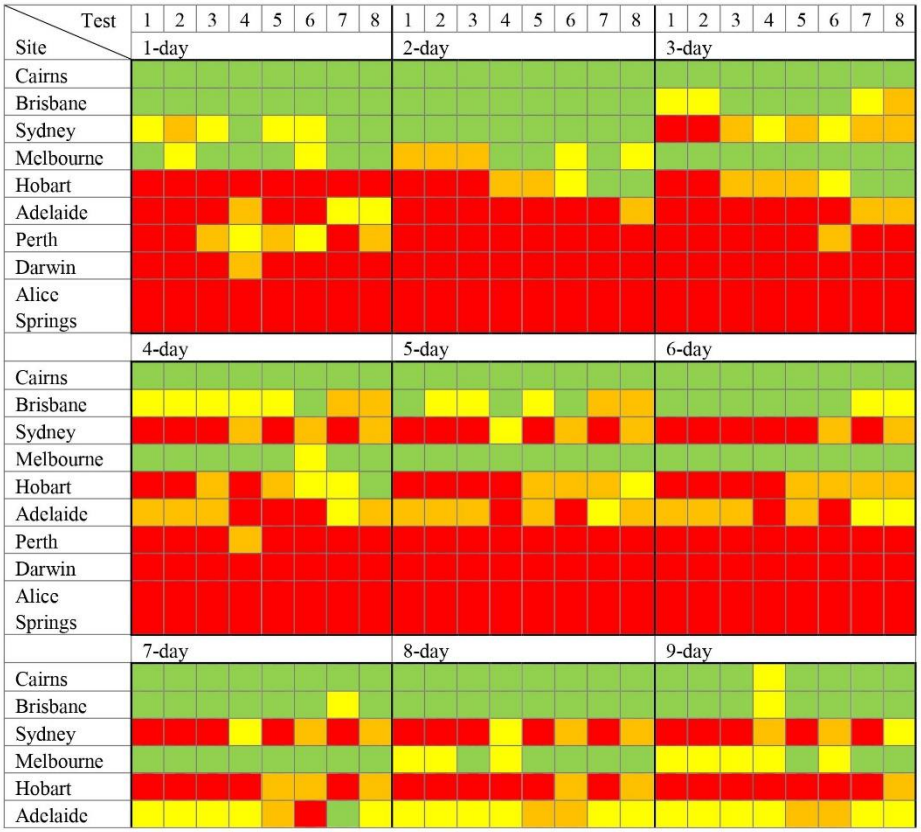

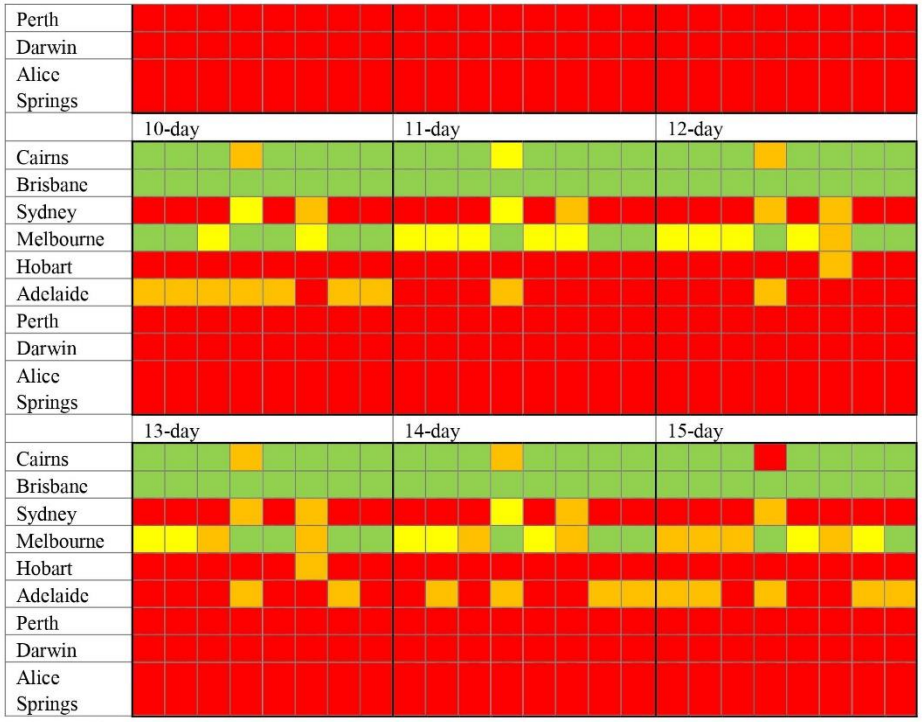

Table 3. Color diagram of statistical test results for trend and step change analysis of temperature extremes for all duration. Statistical tests are denoted by numbers, where 1 (Mann-Kendall), 2 (Spearman), 3 (linear regression), 4 (cumulative sum), 5 (cumulative deviation), 6 (Worsley likelihood), 7 (Rank sum) and 8 (Student's t). Tests 1 to 3, and 4 to 8 are used for trend and step change analysis, respectively. Cell colors indicate statistical significance levels, where red, brown, and yellow represents 1%, 5%, and 10% significance levels, respectively. Green cells indicate statistically nonsignificant outcomes.

Sydney, located in the southeast region, demonstrates the presence of a statistically significant trend and step change in extreme temperatures for 3- to 15-day durations. Interestingly, while the 1-day duration reveals the existence of a statistically significant trend (5% SL) and step change (10% SL), the 2-day duration did not show a significant trend. Whereas for Melbourne, also located in the southeast region, a statistically significant trend (5% SL) was detected for 2-day and 13- to 15-day durations, but not for 1-day and 3- to 12-day duration temperature extremes. However, a trend at 10% SL was observed for durations from 8- to 12-day. A statistically significant step change at 5% SL was only observed for prolonged durations (12- to 15-day) in Melbourne. Results from Sydney and Melbourne stations reveal that the trend and step change in extreme temperatures in the southeast region of Australia exhibit variability across the durations.

3.2. GEV distribution parameters

The GEV distribution (Pakdel et al., 2023) was found to fit well within the temperature extremes for all stations and durations. Distribution parameters were estimated using the Bayesian inference method. Figure 2 displays the spatial-temporal variability of location, scale, and shape parameters, respectively. Overall, the location parameter (μ), which specifies the centre of the distribution, decreases with the increase of duration for all stations. However, the decrease is remarkable for Perth, Adelaide, Melbourne, Sydney, and Hobart. A significant drop in the location parameter value was observed from 1-day to 7-day duration, thereafter the drop was not noticeable. For other stations (Alice Springs, Darwin, Cairns and Brisbane), a change (decrease) of location parameter with duration was not evident, which indicates less spatio-temporal variability of extreme temperatures. The maximum and minimum value of μ was observed in Alice Springs and Hobart, respectively.

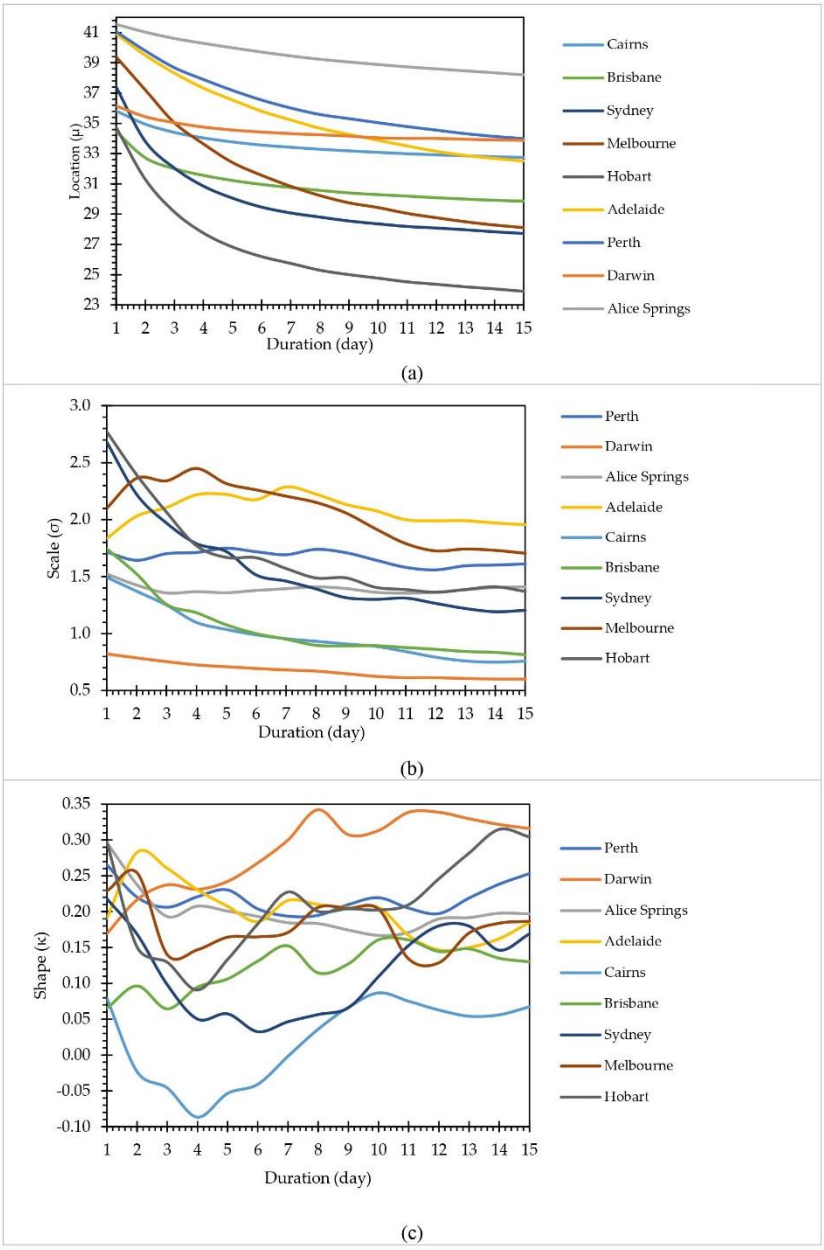

Figure 2. Spatial -temporal variation of (a) location parameter (μ), (b) scale parameter (σ), (c) shape parameter (κ).

Spatial variation of scale parameter (σ) can be clearly observed in Figure 2 (b). Interestingly, the value of σ and its temporal variation pattern are almost identical for Hobart and Sydney, Cairns and Brisbane and for Melbourne and Adelaide. Comparatively, less temporal variability was observed for Alice Springs, Perth, and Darwin. The

scale parameter defines the deviation around μ and its large value indicates the presence of variability in the data series. For 1-day duration temperature extremes, Sydney and Hobart station exhibited the maximum variability, but the σ value decreased rapidly from 1-day to 7-day duration. For all other durations, the maximum value of σ was observed for Adelaide and Melbourne stations, which represents the existence of high variability in extreme temperatures, whereas the minimum σ value was identified for Darwin for all durations indicating the existence of less variability of Darwin's extreme temperatures.

The variability of the shape parameter (κ), which indicates the tail behaviour of the distribution, is shown in Figure 2 (c). Except for Cairns for the 2- to 6-day duration, a positive skewness was observed for all stations and for all durations. Comparatively, a smaller temporal variability of κ was observed for Alice Springs and Perth. The κ value exhibited a decreasing trend from 1- to 3- or 4-day durations for Cairns, Sydney, Hobart, Perth and Alice Springs, but an increasing trend was observed for Darwin. Temperature extremes for Cairns exhibited the minimum κ value among all the stations, whereas the maximum κ value was identified for Darwin from the 4-day duration.

While previous studies (Courty et al., 2019) on rainfall IDF using the GEV distribution observed scaling properties of stationary GEV parameters with rainfall duration, this study shows that scaling of stationary GEV parameters with temperature duration was absent, particularly for the scale and shape parameters. Therefore, it can be postulated that the distribution parameters should be estimated for each duration of interest.

3.3. Temperature-Duration-Frequency (TDF) curves

The quantile function (Eq.2) was used to estimate design temperatures for various durations and AEPs. The TDF curves were developed by plotting design temperatures against the AEP for each of 1- and 15-day duration. Each line in the TDF curves represents a duration (D) distributed from 1-D (1-day) to 15-D (15-day). The 10% and 90% confidence level (CL) estimates of design temperatures are only shown for 1-day duration. The general relation of TDF curves is that design temperature increases with recurrence interval and is inversely related to duration (increases at short duration).

Figures 3 and 4 show the TDF curves for Cairns and Brisbane, respectively, which are located in the northeast region of Australia. The 1% and 99% AEP design temperatures in Cairns vary from 36°C (15-day) to 42°C (1-day), and from 32°C (15-day) to 34.5°C (1-day), respectively. Design temperatures in Cairns vary in a narrow range, which indicates the existence of less variability in extreme temperatures. Figure 3 (b) depicts non-stationary assumptions based on 5 and 95% posterior probability intervals of the ensemble. The 1% AEP (100-year return period) and 99% AEP (1-year return period) design temperatures in Cairns vary from 36°C (15-day) to 42°C (1-day), and from 33.5°C (15-day) to 36.7°C (1-day). For the design temperatures in Cairns, for a 1-year period, the difference between the non-stationary 36.7°C (1-day) and stationary 34.5°C (1-day) temperature was approximately 2.2°C. Whereas in Brisbane (Figure 4 (a)), design temperatures vary from 33°C (15-day) to 42°C (1-day) for 1% AEP and from 29°C (15-day) to 32°C (1-day) for 99% AEP. Changes of design temperatures between 1- to 3-day duration were more noticeable in Brisbane. Figure 4 (b) exhibits temperatures in non-stationary analysis vary from 30.5°C (15-day) to 35.5°C (1-day) for 99% AEP (1-year return period). The difference between the non-stationary 30.5°C (15-day) and stationary 29°C (15-day) temperature is approximately 1.5°C. In other words, a stationary assumption will underestimate the extreme temperature (Cheng and AghaKouchak, 2014). The uncertainty range (difference between 90% and 10% CL) reaches more than 2°C from 2% AEP and from 20% AEP for Cairns and Brisbane, respectively. This also confirms the existence of high variability of temperature extremes in Brisbane.

The TDF curves for Sydney and Melbourne, which are in the southeast of Australia, are shown in Figures 5 and 6. Sydney exhibits a variation of design temperatures from 32°C (15-day) to 45°C (1-day) for 1% AEP and from 26°C (15-day) to 33°C (1-day) for 99% AEP. On the other hand, Melbourne exhibits a variation from 25°C (15-day) to 38°C (1-day) and from 25°C (15-day) to 36°C (1-day), respectively. According to Figures 5 (b), temperatures in a non-stationary condition for Sydney vary from 27°C (15-day) to 39°C (1-day) for 99% AEP (1-year return period). Melbourne, as identified in Figures 6 (b) represents a variation from 33°C (15-day) to 45°C (1-day) for 1% AEP (100-year return period) and from 29°C (15-day) to 40.8°C (1-day) for 99% AEP (1-year return period). Design temperatures in Melbourne, for 99% AEP and 1% AEP, show that the difference between the non-stationary and stationary temperatures have a high variability that is approximately 14°C and 12°C (1-day), and 8°C and 4°C (15-day) respectively. The concept of non-stationary has proven to be a valuable tool for understanding extremes in hydro climatology since natural phenomena occurred in non-stationary conditions. As stationary assumptions underestimate extremes such as floods and drought, planners and decision-makers can

consider non-stationary assumptions for planning, and construction of hydraulic structures. Design temperature at high AEP levels (low recurrence interval, frequently observed) for Melbourne was found to vary more considerably between the durations which indicates the presence of high temporal variability of temperature extremes. Both Sydney and Melbourne stations exhibit a high variation in design temperatures from 1- to 7-day duration. In terms of the uncertainty range, both stations behave quite similarly – with the range reaching more than 2°C from 2% AEP.

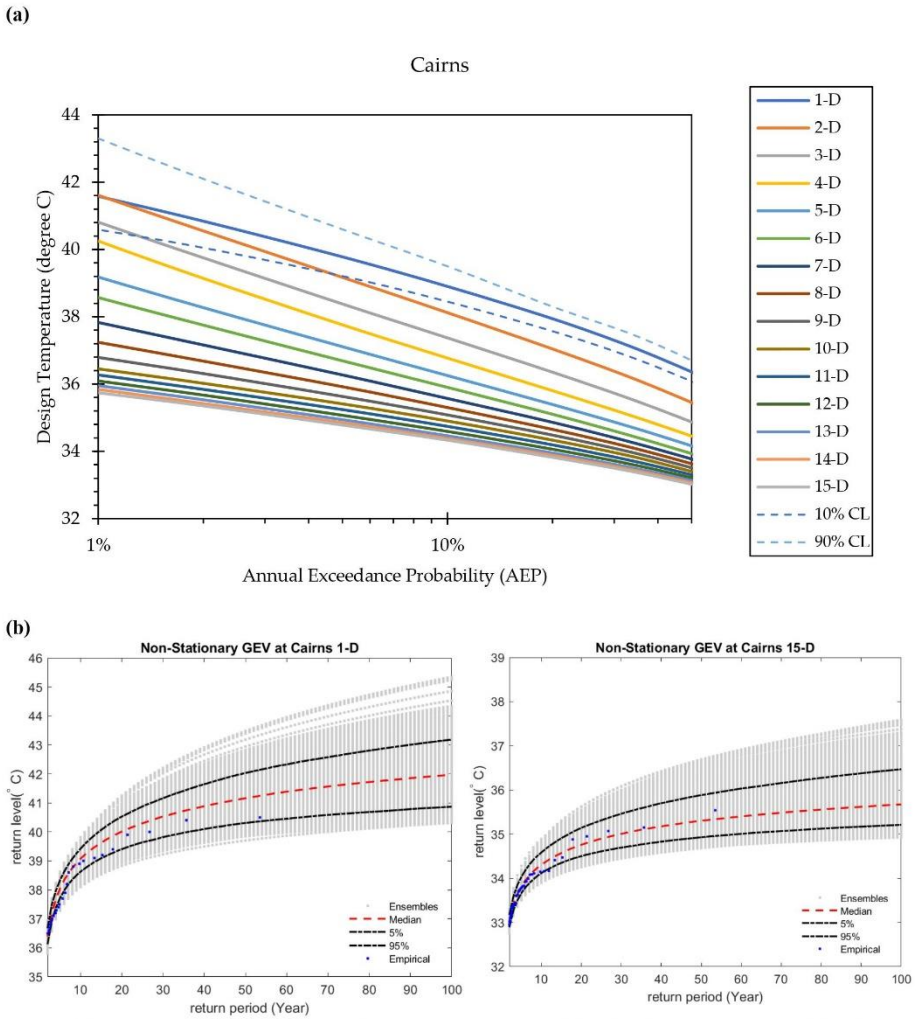

Figure 3. (a)TDF curves for Cairns (D is day and CL is confidence level plotted for 1-D) (b) the output of NEVA's non-stationary GEV framework, standard return levels with design exceedance probability (figure generated using MATLAB)

The TDF curves for Hobart, located south of mainland Australia, and for Adelaide, located in South Australia, are shown in Figures A. 2 and A. 3, respectively. Design temperature at 1% AEP varies from 27.5°C (15-day) to 41.5°C (1-day) and from 38.5°C (15-day) to 46.5°C (1-day) for Hobart and Adelaide, respectively, whereas the low recurrence interval design temperatures at 99% AEP varies from 21°C (15-day) to 29°C (1-day), and from

29°C (15-day) to 37.5°C (1-day), respectively. This clearly shows the existence of higher design temperatures for mainland South Australia compared to the island of Tasmania. The variation of design temperatures with duration is more noticeable for Hobart than Adelaide. Interestingly, design temperatures for Perth (Figure A. 4), which is located in the southwest region of Australia, are almost identical to Adelaide. The uncertainty range reaches to over 2 °C from 2% AEP and from 5% AEP for Adelaide and Hobart, respectively. Whereas in Perth, this starts from 0.5% AEP, indicating the existence of less variability in design temperatures. According to the Figures A. 2 (b) and A. 3 (b), the low recurrence interval design temperatures in the non-stationary condition at 99% AEP (1-year period) varies from 22.5°C (15-day) to 33°C (1-day), and from 33°C (15-day) to 42°C (1-day) for Hobart and Adelaide, respectively. Design temperatures in Hobart and Adelaide, for 99% AEP, the difference between the non-stationary and stationary temperatures is approximately 4°C and 4.5°C (1-day), and 1.5°C and 4°C (15-day) respectively. Moreover, in Perth at the low recurrence interval design temperatures at 99% AEP varies from 3°C (15-day) to 5°C (1-day).

The design temperatures of Darwin, which is in the northern region of Australia, exhibit a lower variability with frequency and duration (Figure A. 5). The high recurrence interval (1% AEP) design temperature for Darwin varies from about 35 °C (15-day) to 39 °C (1-day), whereas the low recurrence level (99% AEP) temperature in the stationary and non-stationary conditions vary from 33 °C to 35.5 °C, and 34.5 °C to 38.5 °C (Figure A. 4 (b)). Alice Springs, which is located in the central part of Australia, also exhibits less variability in design temperatures with duration and frequency (Figure A. 6). For Alice Springs, the 1% AEP 1-day and 15-day design temperatures are estimated to be 45 °C and 43 °C respectively, whereas they are 38.5 °C and 36 °C for 99% AEP. This clearly shows the presence of lower variability in design temperatures across the recurrence interval and duration for both Darwin and Alice Springs stations. The uncertainty range also exhibits the existence of low variability for both stations. The range reaches to more than 2 °C from 0.01% AEP and 0.2% AEP, respectively. Alice Springs, in the non-stationary condition at the low recurrence interval design temperatures at 99% AEP, varies from 41 °C (1-day) to 39°C (15-day) (Figure A. 6 (b)).

For all stations, a general behavior of uncertainty range is observed. The uncertainty range decreases from 100% AEP to 80% AEP, and then less variation is noticed until 20% AEP, thereafter a sharp increase is observed from 10% AEP to more rare frequencies. It is mostly likely that higher uncertainty is expected in high recurrence interval extremes. The highest uncertainty range for 1% AEP 1-day design temperature is observed for Brisbane (5.63°C), followed by Cairns (2.71°C), Sydney (2.45 °C) and Hobart (2.3 °C). For other stations, the range was found to be less than 2 °C. The lowest uncertainty range was observed for Darwin (0.83 °C), which is logical considering the existence of less variability in design temperatures across duration and recurrence interval.

(a)

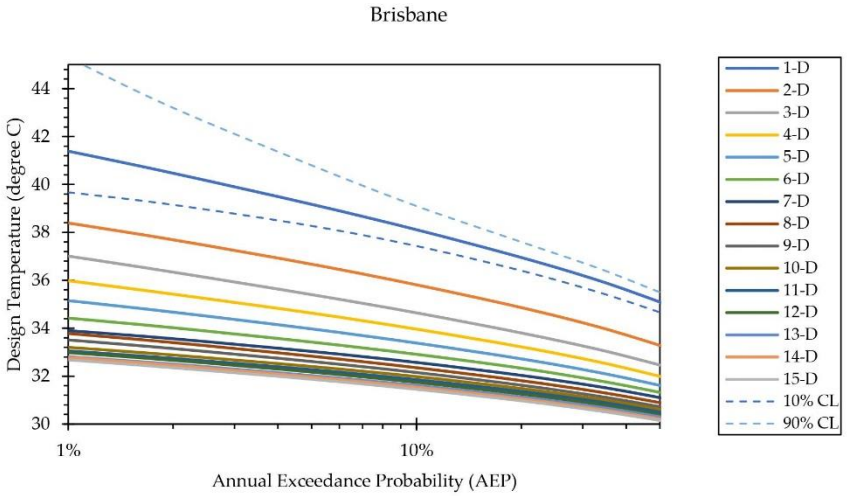

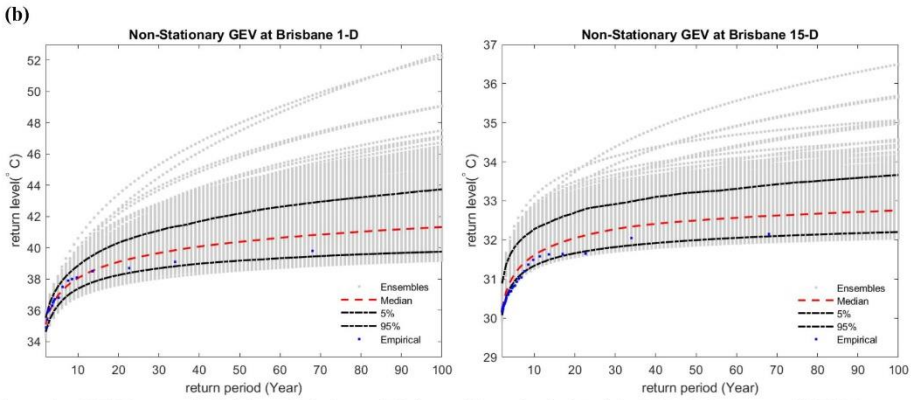

Figure 4. (a) TDF curves for Brisbane (D is day and CL is confidence level plotted for 1-D) (b) the output of NEVA's non-stationary GEV framework, standard return levels with design exceedance probability (figure generated using MATLAB)

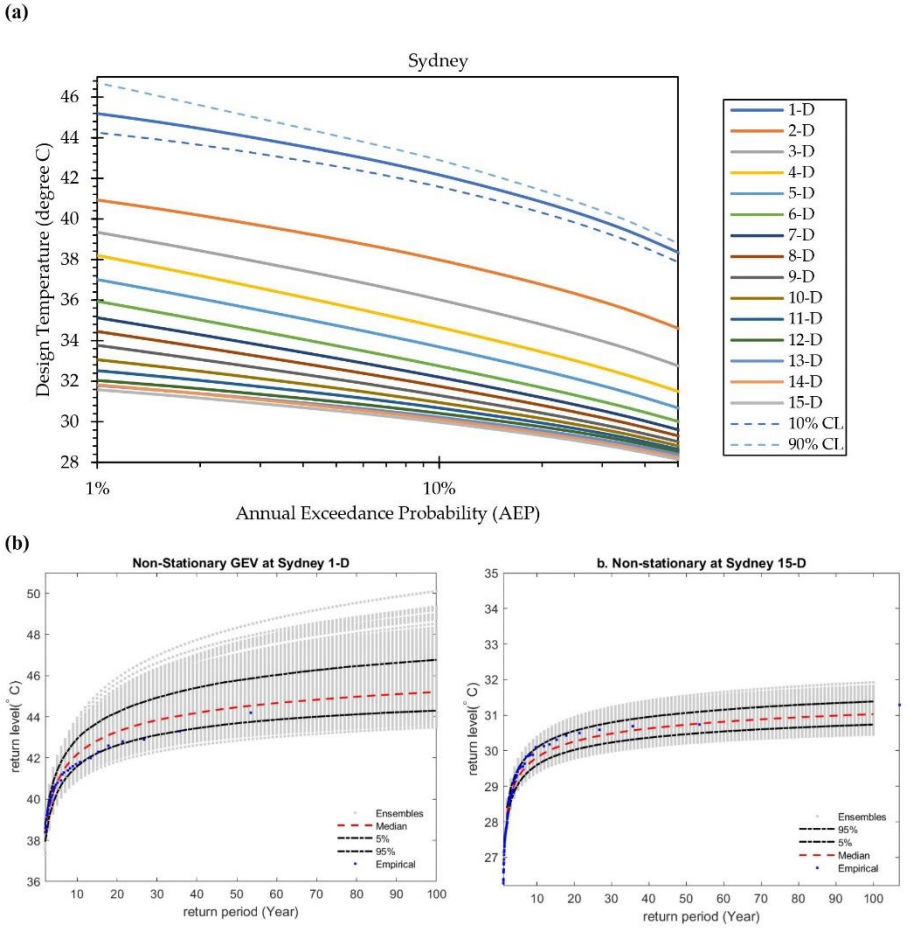

Figure 5. (a) TDF curves for Sydney (D is day and CL is confidence level plotted for 1-D) (b) the output of NEVA's non-stationary GEV framework, standard return levels with design exceedance probability (figure generated using MATLAB)

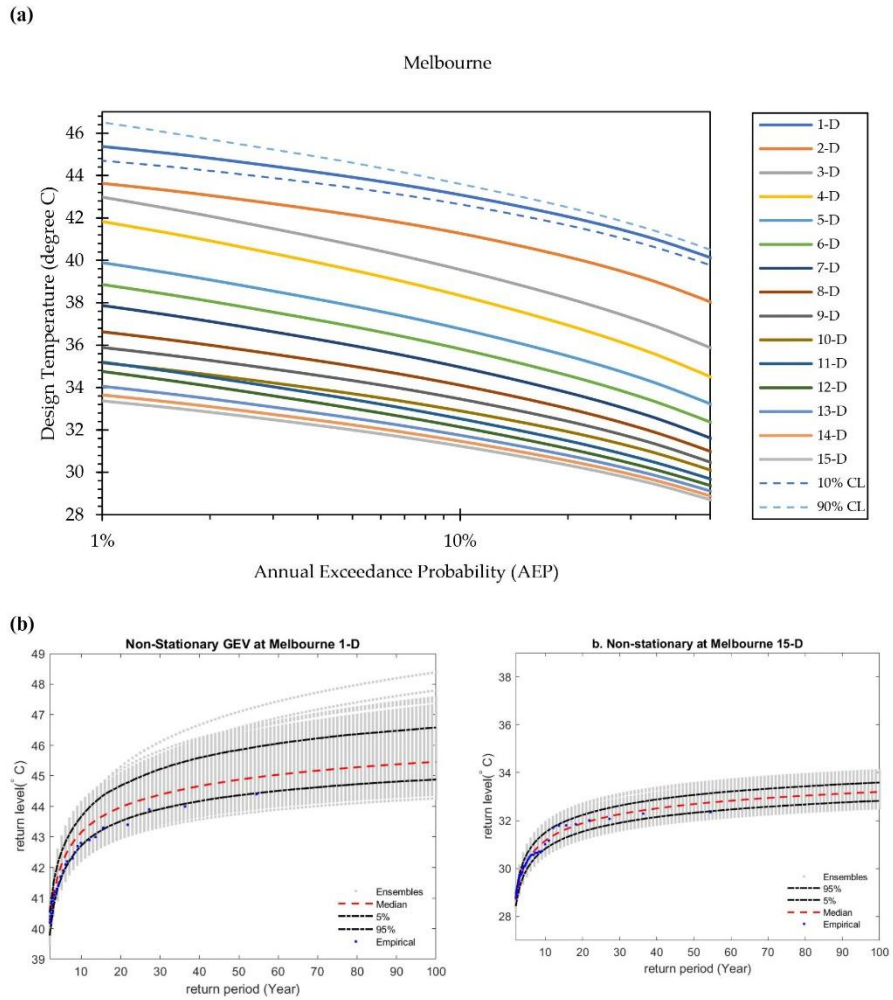

Figure 6. (a) TDF curves for Melbourne (D is day and CL is confidence level plotted for 1-D) (b) the output of NEVA's non-stationary GEV framework, standard return levels with design exceedance probability (figure generated using MATLAB)

4. Discussion

While the development of TDF curves is a comparatively new addition to scientific research, their analysis follows a concept well-established for rainfall IDF curve development. Both TDF and rainfall IDF curves are developed by using climate extremes (extreme temperature and rainfall, respectively). Like previous studies on rainfall IDF (Courty et al., 2019; Papalexiou and Koutsoyiannis, 2013), the annual maximum temperature extremes are well-described by the GEV distribution. Unlike the GEV parameters for rainfall IDF (Courty et al., 2019), a robust scaling relationship with duration is not identified in this study (Figure 2). Generally, a high value of location parameter (μ) indicates a more intense overall distribution and the presence of high temperature extremes in the data series, whereas a higher scale parameter (σ) confirms the presence of more extreme events in the tail of the

distribution. This study shows that μ estimates exhibit a decreasing tendency towards longer duration, but σ and particularly the shape parameter (κ), show a high degree of variability indicating an absence of the scaling property. The latter two parameters are influenced by the less probable extremes in the data series.

Several factors influence the characteristics of extreme temperatures. Previous studies support that an increase of mean temperature changes the variability, frequency, duration and intensity of temperature extremes (Coumou and Rahmstorf, 2012; Im et al., 2018; Im et al., 2017; Perkins et al., 2012). The large-scale climate variability modes (El-Niño Southern Oscillation ENSO, for example) also influence the characteristics of extreme temperatures (Ouarda and Charron, 2018). Several studies explored the teleconnection between large-scale climate variability models and hydro-climatological variables, including extreme temperatures (Chowdhury and Beecham, 2010; Loikith and Broccoli, 2014). In Australia, the El Niño phenomenon decreases average rainfall, but increases average temperature and frequency of extreme temperatures (Alexander et al., 2009; Arblaster and Alexander, 2012; Kenyon and Hegerl, 2008; Min et al., 2013).

The high degree of variability of TDF curves represents Australia's high spatial variability of climate conditions. A tropical/sub-tropical climate exists in the north and northeast region, where Darwin, Cairns and Brisbane stations are located. The ENSO and Madden-Julian Oscillation (MJO) phenomena influence the climate in this zone. The El-Niño phenomenon causes a rise of temperature and prevailing dry conditions with occurrence of droughts in the eastern Australian region. Five stations, Sydney, Melbourne, Hobart, Adelaide and Perth, fall in the temperate climate zone in the south, southeast and southwest regions of Australia. In addition to ENSO, the sub-tropical ridge (a high-pressure belt) and the Southern Annular Mode (SAM) phenomena affect the climate in this region. The Alice Springs station falls in an arid or desert climate zone. The climate is influenced by the Indian Ocean Dipole (IOD), a positive IOD phenomenon is associated with warm temperatures in this zone.

As shown in Table 3, temperature extremes in some stations (Hobart, Adelaide, Perth, Darwin and Alice Springs) exhibit a statistically significant trend and step change and their climate is influenced by some global climate variability indices (discussed in the previous paragraphs). Consequently, adoption of a stationary assumption (temperature extremes will not significantly vary over time) for TDF curves development may not reflect the influence of the wider global climate extremes. In a previous study, the global-scale modes of climate variability were considered in the development of nonstationary TDF curves in Canada (Ouarda and Charron, 2018). Another study on rainfall IDF shows that adoption of stationary assumption underestimates the design climate extremes (Cheng and AghaKouchak, 2014). Since rainfall IDF curves are well-researched from both the stationary and nonstationary perspectives, a comparison can easily be made. This study considered stationary and non-stationary assumptions. The reasons for adopting this approach are its easy estimation procedure which is suitable for professional applications, and the method is similar to the current practice of rainfall IDF curves in Australia. In the current practice, stationary IDF data are increased by a factor (a fixed percent value) in order to consider the influence of climate change and variability conditions. Cheng and AghaKouchak (2014) provided a Bayesian inference framework for stationary and non-stationary estimates. The results of their study indicated that NEVA software can estimate extreme variables and the return levels. The concept of non-stationary has proven to be a valuable tool for extremes, hydro climatology since natural phenomenon occurred in non-stationary conditions (Cheng et al., 2014; Pakdel et al., 2023). As a result, utilising non-stationary data, new methods for analysing the frequency of extremes should be developed. As stationary assumptions underestimate the extremes such as temperature, thus, the planner and decision-makers can consider non-stationary assumption for planning and construction of hydraulic structures.

Information of design temperatures in the form of TDF curves could be useful in different sectors such as human health, ecosystem assessment and infrastructure management. The human body operates at about 37°C temperature and it is comfortable within a narrow range of conditions. If the temperature increases to 38°C for several hours, heat exhaustion can occur which impairs the mental and physical capacity of humans (Berry et al., 2010; Parsons, 2007). An excessively high temperature for a short period can also be very dangerous. Parsons (2007) reported that a 42°C core temperature for a few hours can cause heat stroke and death. Therefore, cooling as well as heating requirements and thermal design will be more effective if the design temperatures at different frequency and durations are known. For infrastructure design, the Australian Building Codes Board divided the whole country into eight National Construction Code (NCC) climate zones. Cairns and Brisbane fall in Zone 1 and 2, respectively. Zone 1 represents high humidity summer and warm winter, whereas Zone 2 is characterized by warm humid summer and mild winter. Sydney and Melbourne both fall in Zone 6, which represents a mild temperate climate. Hobart falls in Zone 7 (cool temperate climate), whereas Adelaide and Perth fall in Zone 5

(warm temperate climate). Darwin and Alice Springs fall in Zone 1 and 3, respectively. While Zone 3 is characterised by hot dry summers and a warm winter climate, Zone 1 represents a hot humid summer and a warm winter climate. Each of these NCC climate zones are spatially homogeneous and do not represent the spatial variability of design temperatures. Therefore, TDF data can potentially be utilised for design of infrastructures, where temperature related changes are inevitable such as electrical grids and power plants.

5. Conclusions

This study investigated the extreme temperature under stationary and non-stationary assumptions. Hydrological processes rely heavily on stationarity over time, however for hydrology, the validity of the stationarity of long term temperature data may become more problematic as climatic and human effects create non stationary conditions (Salas et al., 2018). Thus, in this research, extreme temperature was considered across a sample of Australian sites based on a non-stationary assumption. The location parameter (μ) was considered to have a linear connection to time. Nine geographical distributed stations were investigated in this study using the GEV distribution with Bayesian inference for parameter estimation. The GEV distribution statistically fits well within the annual maximum temperature at different durations. However, it may be possible that a different distribution (Log Pearson, for example) and different parameter estimation techniques (L-moments, for example) could also fit the frequency distribution. To the best of our knowledge, TDF curves have not yet been established in Australia. The method used in this study is applicable to any location for the development of TDF curves and can be used to support decision making in areas such as health risk management of heatwaves, the design of infrastructure where temperature-related changes may impact the infrastructure, and for readiness for natural hazards like bushfires and droughts. In future studies, an increased number of stations could help explore the more detailed spatial variability of design temperatures across Australia and could be useful in developing homogeneous regions having similar design temperatures.

The regional frequency analysis may be useful for determining temperature quantiles at locations where reliable long term and high-quality data is limited. Furthermore, it is feasible to look at non-linear and linear variations of the scale and shape parameter over time. This research can provide a foundation for future research and facilitate comparisons with existing studies by focusing on advanced statistical analysis. Once the TDF curves are established, they can be used as inputs for further investigations, such as assessing the vulnerability of different bioregions, evaluating the effectiveness of adaptation measures, or estimating potential damages and losses. Moreover, the impact on our natural environments (flora, fauna, and eco-systems), agriculture and different land use pattern effects on the temperature can be addressed. Conducting detailed investigations into the underlying causes of extreme temperatures can be interesting for future studies. Lastly, through the quantification of the probabilities of extreme temperature occurrences, decision-makers can make informed choices regarding infrastructure development, environmental management, resource allocation, and emergency planning.

Author Contributions: Conceptualization, Rezaul Chowdhury, Sreeni Chadalavada, Hadis Pakdel and Kevin McDougall; Methodology, Rezaul Chowdhury, Sreeni Chadalavada, Hadis Pakdel; Software, Rezaul Chowdhury, Sreeni Chadalavada, Hadis Pakdel; Validation, Rezaul Chowdhury, Sreeni Chadalavada, Hadis Pakdel and Kevin McDougall; Formal analysis, Rezaul Chowdhury, Sreeni Chadalavada, Hadis Pakdel and Kevin McDougall; Investigation, Rezaul Chowdhury; Resources, Rezaul Chowdhury; Data curation, Rezaul Chowdhury; Writing—review and editing Rezaul Chowdhury, Kevin McDougall Sreeni Chadalavada, and Hadis Pakdel; Visualization, Rezaul Chowdhury, Sreeni Chadalavada, Hadis Pakdel; Supervision, Rezaul Chowdhury, Sreeni Chadalavada and Kevin McDougall; Project administration, Rezaul Chowdhury, Sreeni Chadalavada and Kevin McDougall. All authors have read and agreed to the published version of the manuscript.

Funding: This research received no external funding.

Conflicts of Interest: The authors declare no conflict of interest.

Data Availability Statement: The data supporting the findings of this study are available from the first author upon reasonable request.

References

(BoM), B.o.M., 2012. Annual Climate Report 2012.

(BoM), B.o.M., 2020. Long-term temperature record: Australian climate observations reference network - surface air temperature.

Alexander, L.V., Uotila, P., Nicholls, N., 2009. Influence of sea surface temperature variability on global temperature and precipitation extremes. Journal of Geophysical Research: Atmospheres 114.

Arblaster, J.M., Alexander, L.V., 2012. The impact of the El Niño - Southern Oscillation on maximum temperature extremes. Geophysical Research Letters 39.

Ball, J., Babister, M., Nathan, R., Weinmann, P., Weeks, W., Retallick, M., Testoni, I., 2019. Australian Rainfall and Runoff-A guide to flood estimation. Commonwealth of Australia.

Bauer, E., 1996. Characteristic frequency distributions of remotely sensed in situ and modelled wind speeds. International Journal of Climatology 16, 1087-1102.

Beniston, M., 2004. The 2003 heat wave in Europe: A shape of things to come? An analysis based on Swiss climatological data and model simulations. Geophysical research letters 31.

Berry, H.L., Bowen, K., Kjellstrom, T., 2010. Climate change and mental health: a causal pathways framework. International journal of public health 55, 123-132.

Brown, P.T., Caldeira, K., 2017. Greater future global warming inferred from Earth's recent energy budget. Nature 552, 45-50.

Buishand, T.A., 1982. Some methods for testing the homogeneity of rainfall records. Journal of hydrology 58, 11-27.

Cheng, L., AghaKouchak, A., 2014. Nonstationary precipitation intensity-duration-frequency curves for infrastructure design in a changing climate. Scientific reports 4, 1-6. DOI: 10.1038/srep07093.

Cheng, L., AghaKouchak, A., Gilleland, E., Katz, R.W., 2014. Non-stationary extreme value analysis in a changing climate. Climatic change 127, 353-369.

Chhetri, P., Hashemi, A., Basic, F., Manzoni, A., Jayatilleke, G., 2012. Bushfire, heat wave and flooding case studies from Australia. Report from the International Panel of the Weather project funded by the European Commission's 7th framework programme.

Chiew, F., McMahon, T., 1993. Detection of trend or change in annual flow of Australian rivers. International Journal of Climatology 13, 643-653.

Chowdhury, R., Beecham, S., 2010. Australian rainfall trends and their relation to the southern oscillation index. Hydrological Processes: An International Journal 24, 504-514.

Chowdhury, R.K., Beecham, S., Boland, J., Piantadosi, J., 2015. Understanding South Australian rainfall trends and step changes. International Journal of Climatology 35, 348-360.

Coates, L., Haynes, K., O'brien, J., McAneney, J., De Oliveira, F.D., 2014. Exploring 167 years of vulnerability: An examination of extreme heat events in Australia 1844–2010. Environmental Science & Policy 42, 33-44.

Coumou, D., Rahmstorf, S., 2012. A decade of weather extremes. Nature climate change 2, 491-496.

Courty, L.G., Wilby, R.L., Hillier, J.K., Slater, L.J., 2019. Intensity-duration-frequency curves at the global scale. Environmental Research Letters 14, 084045.

Cowan, T., Purich, A., Perkins, S., Pezza, A., Boschat, G., Sadler, K., 2014. More frequent, longer, and hotter heat waves for Australia in the twenty-first century. Journal of Climate 27, 5851-5871.

Dahmen, E., Hall, M.J., 1990. Screening of hydrological data: tests for stationarity and relative consistency. ILRI.

Grumm, R.H., 2011. The central European and Russian heat event of July–August 2010. Bulletin of the American Meteorological Society 92, 1285-1296.

Hondula, D.M., Barnett, A.G., 2014. Heat-related morbidity in Brisbane, Australia: spatial variation and area-level predictors. Environmental health perspectives 122, 831-836.

Hosking, J., Wallis, J., 1993. Some statistics useful in regional frequency analysis. Water resources research 29, 271-281.

Hosking, J., Wallis, J.R., Wood, E.F., 1985. An appraisal of the regional flood frequency procedure in the UK Flood Studies Report. Hydrological Sciences Journal 30, 85-109.

Huth, R., Kyselý, J., Pokorná, L., 2000. A GCM simulation of heat waves, dry spells, and their relationships to circulation. Climatic Change 46, 29-60.
Im, E.-S., Kang, S., Eltahir, E.A., 2018. Projections of rising heat stress over the western Maritime Continent from dynamically downscaled climate simulations. Global and Planetary Change 165, 160-172.
Im, E.-S., Pal, J.S., Eltahir, E.A., 2017. Deadly heat waves projected in the densely populated agricultural regions of South Asia. Science advances 3, e1603322.
Javelle, P., Ouarda, T.B., Lang, M., Bobée, B., Galéa, G., Grésillon, J.-M., 2002. Development of regional flood-duration–frequency curves based on the index-flood method. Journal of Hydrology 258, 249-259.
Jones, B., Tebaldi, C., O'Neill, B.C., Oleson, K., Gao, J., 2018. Avoiding population exposure to heat-related extremes: demographic change vs climate change. Climatic change 146, 423-437.
Kendall, M.G., 1948. Rank correlation methods.
Kenyon, J., Hegerl, G.C., 2008. Influence of modes of climate variability on global temperature extremes. Journal of Climate 21, 3872-3889.
Khaliq, M.N., St - Hilaire, A., Ouarda, T.B., Bobée, B., 2005. Frequency analysis and temporal pattern of occurrences of southern Quebec heatwaves. International Journal of Climatology: A Journal of the Royal Meteorological Society 25, 485-504.
Kharin, V.V., Zwiers, F.W., 2000. Changes in the extremes in an ensemble of transient climate simulations with a coupled atmosphere–ocean GCM. Journal of climate 13, 3760-3788.
Koutsias, N., Arianoutsou, M., Kallimanis, A.S., Mallinis, G., Halley, J.M., Dimopoulos, P., 2012. Where did the fires burn in Peloponnisos, Greece the summer of 2007? Evidence for a synergy of fuel and weather. Agricultural and Forest Meteorology 156, 41-53.
Kuczera, G., 1999. Comprehensive at - site flood frequency analysis using Monte Carlo Bayesian inference. Water resources research 35, 1551-1557.
Kundzewicz, Z., Robson, A., International Workshop on Detecting Changes in Hydrological Data , W., Organization, W.M., Hydrology, I.o., Mondiale, O.M., Data, W.C., Programme, M., Ecology, C.f., Hydrology, Unesco, 2000. Detecting Trend and Other Changes in Hydrological Data. World Meteorological Organization.
Loikith, P.C., Broccoli, A.J., 2014. The influence of recurrent modes of climate variability on the occurrence of winter and summer extreme temperatures over North America. Journal of climate 27, 1600-1618.
Lucas, C., Hennessy, K., Mills, G., Bathols, J., 2007. Bushfire weather in southeast Australia: recent trends and projected climate change impacts.
Mazdiyasni, O., AghaKouchak, A., 2015. Substantial increase in concurrent droughts and heatwaves in the United States. Proceedings of the National Academy of Sciences 112, 11484-11489.
Mazdiyasni, O., AghaKouchak, A., Davis, S.J., Madadgar, S., Mehran, A., Ragno, E., Sadegh, M., Sengupta, A., Ghosh, S., Dhanya, C., 2017. Increasing probability of mortality during Indian heat waves. Science advances 3, e1700066.
Mazdiyasni, O., Sadegh, M., Chiang, F., AghaKouchak, A., 2019. Heat wave intensity duration frequency curve: A multivariate approach for hazard and attribution analysis. Scientific reports 9, 1-8.
Meehl, G.A., Tebaldi, C., 2004. More intense, more frequent, and longer lasting heat waves in the 21st century. Science 305, 994-997.
Min, S.K., Cai, W., Whetton, P., 2013. Influence of climate variability on seasonal extremes over Australia. Journal of Geophysical Research: Atmospheres 118, 643-654.
Morrison, J.E., Smith, J.A., 2002. Stochastic modeling of flood peaks using the generalized extreme value distribution. Water resources research 38, 41-41-41-12.
Nairn, J., Fawcett, R., 2011. Defining heatwaves: heatwave defined as a heat-impact event servicing all. Europe 220, 224.
Nitschke, M., Tucker, G.R., Hansen, A.L., Williams, S., Zhang, Y., Bi, P., 2011. Impact of two recent extreme heat episodes on morbidity and mortality in Adelaide, South Australia: a case-series analysis. Environmental Health 10, 1-9.

Ouarda, T.B., Charron, C., 2018. Nonstationary temperature-duration-frequency curves. Scientific reports 8, 1-8.
Ouarda, T.B., Girard, C., Cavadias, G.S., Bobée, B., 2001. Regional flood frequency estimation with canonical correlation analysis. Journal of hydrology 254, 157-173.
Pakdel, H., Paudyal, D.R., Chadalavada, S., Alam, M.J., Vazifedoust, M., 2023. A Multi-Framework of Google Earth Engine and GEV for Spatial Analysis of Extremes in Non-Stationary Condition in Southeast Queensland, Australia. ISPRS International Journal of Geo-Information 12, 370.
Pakdel, H., Vazifedoust, M., Paudyal, D.R., Chadalavada, S., Alam, M.J., 2022. Google Earth Engine as Multi-Sensor Open-Source Tool for Monitoring Stream Flow in the Transboundary River Basin: Doosti River Dam. ISPRS International Journal of Geo-Information 11, 535.
Papalexiou, S.M., Koutsoyiannis, D., 2013. Battle of extreme value distributions: A global survey on extreme daily rainfall. Water Resources Research 49, 187-201.
Parsons, K., 2007. Human thermal environments: the effects of hot, moderate, and cold environments on human health, comfort and performance. CRC press.
Perkins, S., Alexander, L., Nairn, J., 2012. Increasing frequency, intensity and duration of observed global heatwaves and warm spells. Geophysical Research Letters 39.
Raftery, A.E., Zimmer, A., Frierson, D.M., Startz, R., Liu, P., 2017. Less than 2 C warming by 2100 unlikely. Nature climate change 7, 637-641.
Rainham, D.G., Smoyer-Tomic, K.E., 2003. The role of air pollution in the relationship between a heat stress index and human mortality in Toronto. Environmental research 93, 9-19.
Salas, J., Obeysekera, J., Vogel, R., 2018. Techniques for assessing water infrastructure for nonstationary extreme events: a review. Hydrological Sciences Journal 63, 325-352. https://doi.org/310.1080/02626667.02622018.01426858.
Siegel, S.C., Castellan, J., NJ (1988). Nonparametric statistics for the behavioural sciences. New York, McGraw-Hill.
Snedecor, G.W., Cochran, W.G., 1989. Statistical Methods, eight edition. Iowa state University press, Ames, Iowa 1191.
Stedinger, J., Lu, L.-H., 1995. Appraisal of regional and index flood quantile estimators. Stochastic hydrology and hydraulics 9, 49-75.
Steffen, W., Hughes, L., Perkins, S., 2014. Heatwaves: hotter, longer, more often.
Tong, S., Wang, X.Y., Guo, Y., 2012. Assessing the short-term effects of heatwaves on mortality and morbidity in Brisbane, Australia: comparison of case-crossover and time series analyses. PloS one 7, e37500.
Trewin, B., 2018. The Australian Climate Observations Reference Network-Surface Air Temperature (ACORNSAT) Version 2. Bureau of Meteorology.
Worsley, K., 1979. On the likelihood ratio test for a shift in location of normal populations. Journal of the American Statistical Association 74, 365-367.
Zampieri, M., Ceglar, A., Dentener, F., Toreti, A., 2017. Wheat yield loss attributable to heat waves, drought and water excess at the global, national and subnational scales. Environmental Research Letters 12, 064008.
Zander, K.K., Botzen, W.J., Oppermann, E., Kjellstrom, T., Garnett, S.T., 2015. Heat stress causes substantial labour productivity loss in Australia. Nature climate change 5, 647-651.
Zander, K.K., Moss, S., Garnett, S.T., 2019. Climate change–related heat stress and subjective well-being in Australia. Weather, climate, and society 11, 505-520.

Supplementary Materials:

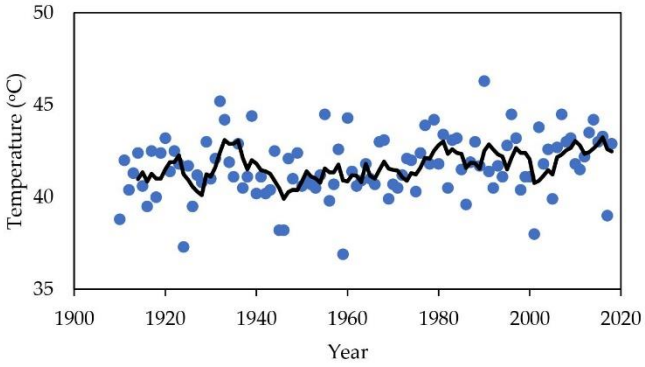

Figure A. 1. Time series plot of 1-day temperature extreme for the Perth airport station (site no. 09021), blue dots represent 1-day annual maximum temperature, and their 5-year moving average is represented by solid black line. Average temperature during 1910-1964 and 1965-2018 periods are 41.28°C and 42.06°C.

(a)

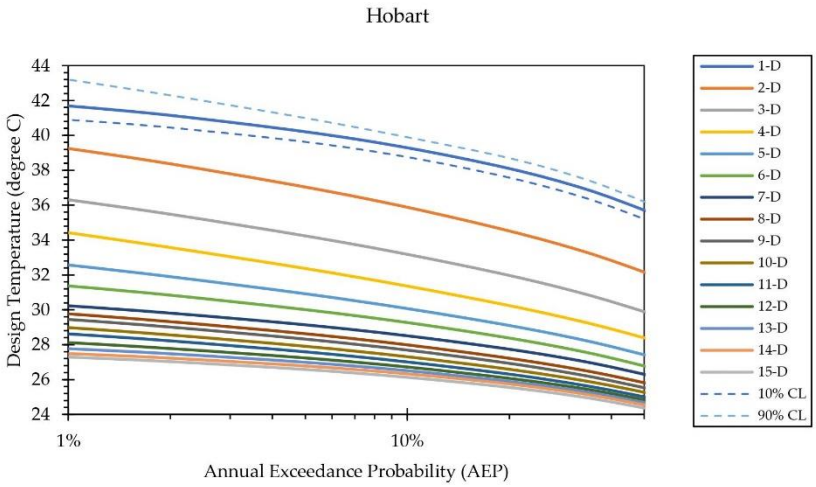

(b)

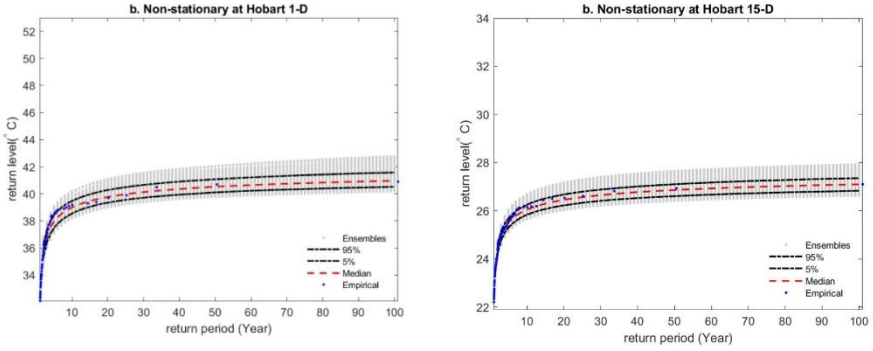

Figure A. 2. (a) TDF curves for Hobart (D is day and CL is confidence level plotted for 1-D) b) the output of NEVA's non-stationary GEV framework, standard return levels with design exceedance probability (figure generated using MATLAB)

(a)

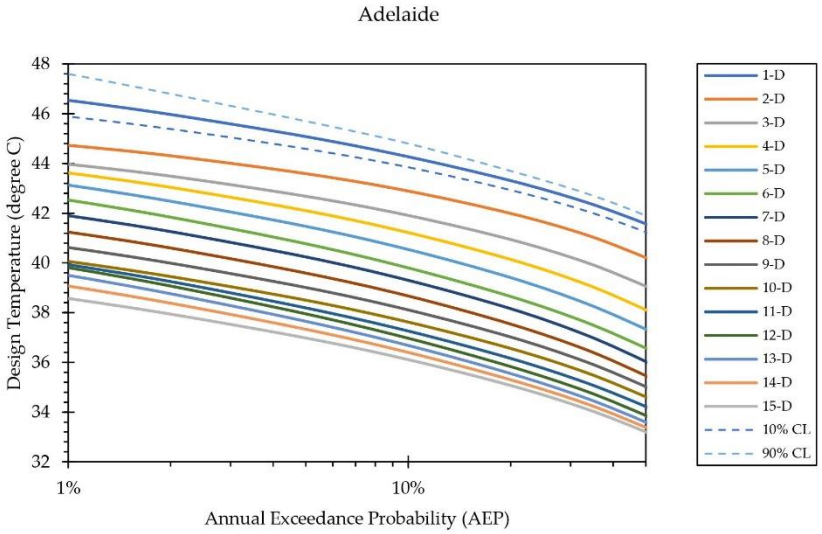

(b)

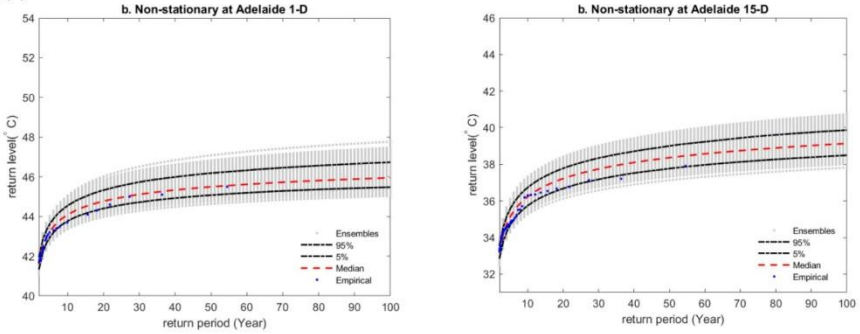

Figure A. 3. (a) TDF curves for Adelaide (D is day and CL is confidence level plotted for 1-D) b) the output of NEVA's non-stationary GEV framework, standard return levels with design exceedance probability (figure generated using MATLAB)

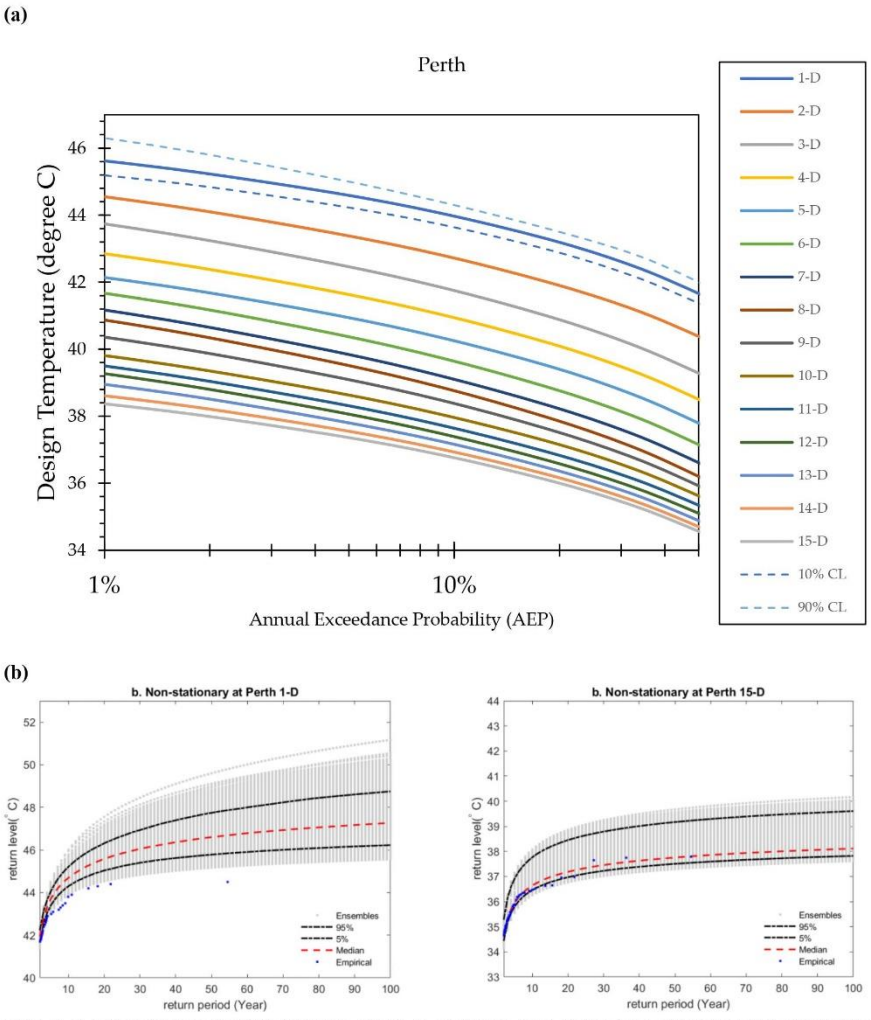

Figure A. 4. (a) TDF curves for Perth (D is day and CL is confidence level plotted for 1-D) b) the output of NEVA's non-stationary GEV framework, standard return levels with design exceedance probability (figure generated using MATLAB)

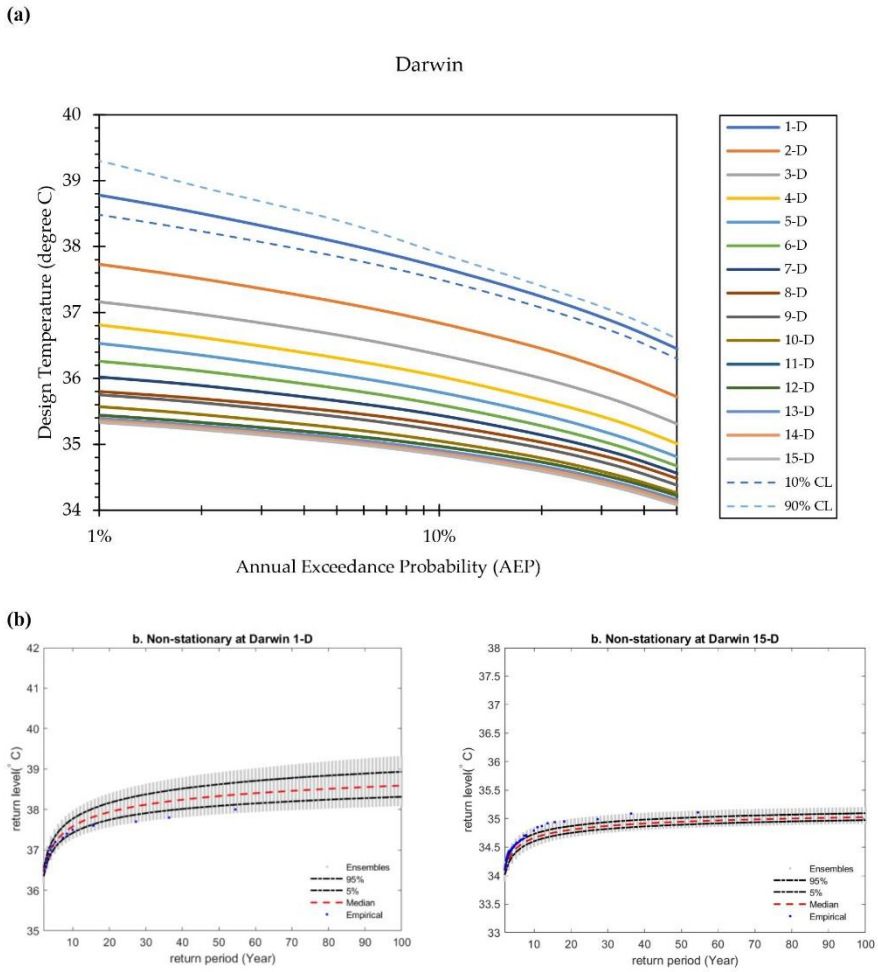

Figure A. 5. (a) TDF curves for Darwin (D is day and CL is confidence level plotted for 1-D) b) the output of NEVA's non-stationary GEV framework, standard return levels with design exceedance probability (figure generated using MATLAB)

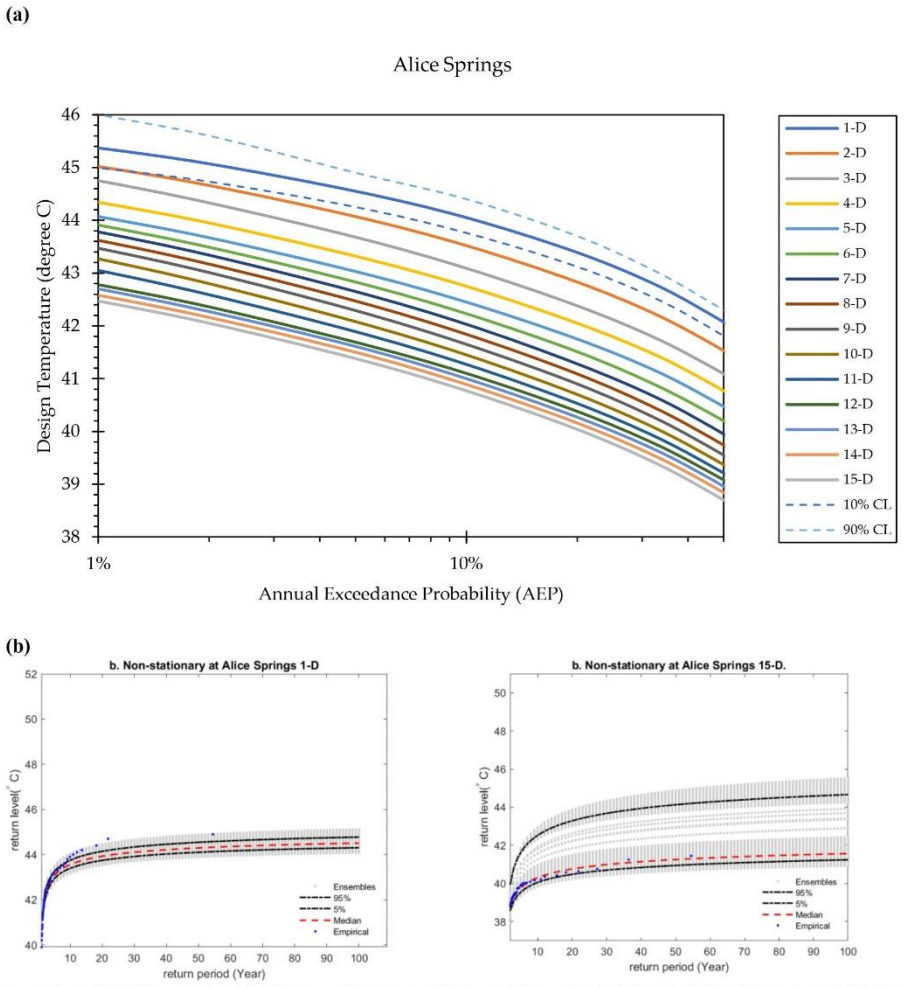

685 **Figure A. 6.** (a) TDF curves for Alice Springs (D is day and CL is confidence level plotted for 1-D) b) the output of NEVA's
686 non-stationary GEV framework, standard return levels with design exceedance probability (figure generated using MATLAB)
687

7.3. Links and implications

This paper aligns with papers 2 and 3 to generate the extreme temperature using TDF curves and GEV distributions in the whole of Australia. This paper provides the concept of design temperatures, which serve as reliable indicators of extreme temperature events that are crucial for planning and decision-making processes. Extreme temperature events, whether heatwaves or cold spells, pose significant risks to human health, agriculture, ecosystems, and infrastructure. This paper achieved Research Objective 4: *"Analyse the intensity and frequency of extreme events, under both stationary and non-stationary conditions using the GEV model."*

To achieve these objectives, this research developed annual maximum temperature extremes and durations from 1 to 15 days across Australia using GEV distributions. Through the utilisation of TDF curves to analyse past temperature records, researchers can detect trends, recognise abrupt shifts, and evaluate the geographical diversity of extreme temperatures across various areas. Detecting the trends was the main focus of the first paper and it applied to the second, third and fourth papers before determining the non-stationary assumptions.

This paper consequently follows the aim of the third paper on infrastructure design and management. The second paper discusses the significance of design temperatures for infrastructure planning in relation to temperature-related changes. These implications suggest potential synergies in addressing infrastructure challenges related to both water and temperature extremes. It is suggested that future research explores the underlying causes of extreme temperatures and assesses the effectiveness of adaptation measures.

7.4. Conclusion

Chapter 6 of this dissertation introduced the fourth research paper crafted within the scope of this study. This paper discussed extreme temperatures under different return levels. In Chapter 7, additional analysis is offered on the conducted research, addressing the initial research inquiries from Chapter 1, and drawing conclusive remarks while suggesting potential avenues for future research.

CHAPTER 8: DISCUSSION AND CONCLUSION

8.1. Introduction

This thesis has evaluated the non-stationary scenarios of maximum instantaneous flood and rainfall extremes under climate change and landcover change scenarios in the Lockyer Valley catchment in SEQ, Australia in the future period. The thesis demonstrated the comprehensive methodology for evaluating landcover and climate change's long-term hydrological consequences. The research showed that the land cover classification, hydrological model, and ensemble of GCMs under different RCPs along with the GEV model shows the uncertainty bounds between stationary and non-stationary tend to widen in the highest return period. According to the ARR guideline (Ball et al., 2019), the GEV distribution should be applied for designing systems that account for floods and rainfall. Under the RCP 8.5 scenario, there is comparatively less variation between stationary and non-stationary conditions, whereas RCP 4.5 demonstrates a more pronounced difference. This research showed that extreme analysis of future periods' maximum peak flood data reveals a growing disparity in the maximum instantaneous flood between stationary and non-stationary assumptions. This suggests that the increasing difference may be a compelling reason to analyse extreme with non-stationary conditions. The following sections summarise the main conclusions of this thesis concerning the research topics, how it has advanced knowledge in the subject, and potential prospects for future study.

8.2. Assess and map hydro-climatological trends and their impacts on surface water using GEE. Develop a framework for extreme hydrometeorological events.

Papers 1 and 2 of this research developed a spatial pattern method in the GEE platform and proved that using multi-sensor satellite data, particularly from platforms like GEE, to analyse hydroclimatic trends which aligns with validating the trend analysis before applying extreme analysis. Understanding hydroclimatic variability for water resource management was directly determined through the trend analysis. The necessity of extremes in non-stationary assumptions is to determine the trends of variables.

The first paper provides insights into long-term trends and spatial patterns. Consequently, the second paper delves into trend analysis, extreme events and non-stationary conditions, enhancing our understanding of the dynamic nature of

hydroclimatic systems. The comparison of ETa, ETo, and ERA5 rainfall data with station records indicates generally good agreement. ETa showed moderate Pearson correlations ranging from 0.59 to 0.75 and reasonable RMSE values. ETo exhibited strong correlations of 0.96–0.97 but higher RMSE values ranging from 73.13 to 87.73 mm. Rainfall demonstrated solid correlations and RMSE values. Analysis of rainfall data from Gatton revealed differences in uncertainty bounds between stationary and non-stationary conditions, with global climate datasets underestimating this disparity compared to station data by approximately 9.47 mm (73.99 mm for station data versus 64.52 mm for global climate datasets). The variation between stationary and non-stationary conditions was least pronounced in water storage, more significant in rainfall, and moderate in evapotranspiration.

8.3. Develop a framework for assessing extreme events and land cover impacts using SVM and RF in GEE. Perform hydrological simulations under GCM ensembles, RCPs, and land cover changes.

Paper 3 of this research developed a framework for evaluating past and future extreme floods under climate change and land cover scenarios. The proposed framework combines hydrological modelling, land cover projections using machine learning techniques, climate projections and RCPs, ProNEVA model accounting for both stationary and non-stationary conditions. Through this integrated methodology, this paper aims to investigate the changes of future climate change on streamflow patterns.

It is widely acknowledged that climate GCMs and scenarios, especially concerning extreme events including extreme precipitation (Bloschl & Montanari, 2010), and extreme streamflow show significant uncertainty.

Research on hydrological extremes is critically needed, especially for the locations where the consequences of climate change are known to be significant (Salas et al., 2018).

In analysing extremes, it's crucial to consider both real (physical) and perceived (statistical) processes. Montanari and Koutsoyiannis (2014) emphasised the importance of incorporating relevant physical mechanisms into stochastic models. They advocated for the development of stochastic-process-based models as a means to reconcile the gap between physically-driven models lacking statistical components

and statistical models devoid of physical insights. The temporal shifts have been assessed among various land cover categories using a transition matrix, which delineated the proportions of pixels transitioning between different categories. The model incorporates spatial elements like distance from major roads, DEM, and population density to generate future maps depicting changes in land cover, revealing the evolving patterns within the Lockyer Catchment.

Undertaking changes in runoff factors using two climate change scenarios (RCP4.5 and RCP 8.5) based on the multi GCMs. The results clearly indicate that a decline in runoff of the ensemble of climate models is generally noticed in the far future (2066-2085) compared to the near future (2020-2065) almost for all months. In February, there is greater variability in streamflow alterations for both RCP 4.5 and RCP 8.5, suggesting increased uncertainty in the predictions for the two future periods as indicated by (Tehrani et al., 2021). It can be concluded that the decline in streamflow will likely slow down in the far future compared to the near future, particularly between June and September.

8.4. Determine extreme climate events in the catchment. Assess the effectiveness of GEV models in overcoming climatic model limitations for evaluating extremes.

Papers 2 and 3 of this research provided NEVA and ProNEVA models to derive different return levels of extreme events. Paper 4 evaluated annual maximum temperature extremes using NEVA GEV and TDF curves for frequency analysis of annual maximum temperatures from 1 to 15-day durations. Return levels of rainfall, evapotranspiration and water storage for the stations and global climate data for 14 selected stations in the Lockyer Catchment were evaluated.

Return levels of extreme events including temperature were estimated using the NEVA software for the return periods of 10 through 100 years, which are the standard design return periods used in hydrologic studies. For flood extremes, the non-stationary conditions of the flood were investigated under two climate scenarios projected from the averaged ensemble of eight GCMs under two scenarios RCP 4.5 and RCP 8.5 during future periods for 66 years.

The results indicated that the highest floods in the stationary assumption generally appear smaller compared to the maximum sudden floods in the non-stationary assumption across both scenarios. As the return period extends, shows

a decline most of the time. Additionally, the findings indicate the contrast between the peak sudden flood assuming stationary versus non-stationary conditions in both scenarios for the period 2020 to 2086. The difference between non-stationary and stationary in RCP 4.5 is greater than RCP 8.5 in all return periods. Peak flood return levels at low return level periods were indicated to have noticeable variation compared to high return periods.

8.5. Contribution to knowledge

This research contributed significantly to our understanding of flood extremes and the impact it has on the non-stationary assumption. Firstly, GeeSEBAL was employed to automatically estimate ET, facilitating validation against ET station data. Given its independence from ground-level measurements as input, GeeSEBAL is anticipated to be advantageous for analysing water balances globally and for managing water resources in data-scarce regions (Laipelt et al., 2021).

The authors also emphasised that the aim of GeeSEBAL is to deepen understanding of the impact of land cover changes on ET over recent decades. The latest iteration of GeeSEBAL utilises Landsat imagery and reanalysis data to compute ETa time series, showing promising results for regional-scale investigations in areas with limited data availability (Laipelt et al., 2021).
By incorporating non-stationary conditions in extreme events frequency analysis using the ProNEVA model, the study highlights the importance of accounting for changing environmental factors over time. This enhances the accuracy of flood magnitude estimation and helps mitigate risks associated with hydraulic infrastructure and human settlements.

The utilisation of Support Vector Machine (SVM) and Random Forest (RF) classification techniques in conjunction with the Google Earth Engine (GEE) platform enables the mapping of land cover patterns and estimation of future changes. This innovative approach enhances the spatial resolution and accuracy of land cover analysis, providing valuable insights for water resource management and infrastructure planning. The results highlight the significance of considering non-stationary conditions in extreme flood frequency analysis, as neglecting this aspect can lead to underestimation of flood magnitudes and increased risks for hydraulic structures. Through the incorporation of TDF curves in decision-making, stakeholders

can improve risk evaluation, refine infrastructure planning, and enhance public health strategies during extreme temperature occurrences. While previous investigations have delved into related themes across various regions, this study adds to the evolving domain of TDF curve formulation within Australia. The framework developed in this study provides valuable insights for infrastructure planning, risk assessment, and sustainable water resource management.

8.6. Future research direction

This study should serve as a foundation for the use of multi-framework by considering both physical system and statistical approaches to comprehend the non-stationary assumption in extremes in the catchment scale. The following is expected to be the next research direction that this study will lead to.

1) Future studies could incorporate comprehensive uncertainty analysis techniques to assess the robustness and reliability of model predictions under different climate change scenarios.

2) Applying a non-stationary model for the Lockyer Catchment by considering the assumptions that the scale and shape parameters have linear functions with time. This adjustment will enhance the modelling approach, improving the capture of flood variations over time and increasing prediction accuracy and reliability.

3) Exploring alternative statistical models beyond the GEV model to capture non-stationary behaviour in extreme event distributions.

4) Incorporating hydraulic modelling techniques, to assess the hydraulic performance of dams under various scenarios, including extreme flood events and reservoir operation conditions.

5) Evaluate the effectiveness of existing dam infrastructure and spillway designs in mitigating hydraulic risks and identify potential vulnerabilities or areas for improvement.

6) Undertaking a similar developed framework to other geographic regions with different climatic, hydrological, and land cover characteristics could provide valuable insights into regional variations in flood risk and vulnerability.

REFERENCES

Note that the references provided cover Chapters 1, 2, 3 and 8, along with the introductory and concluding segments of the other chapters. References for the papers featured in Chapters 4 through to Chapter 7 are integrated within the reference sections of those respective papers.

Abbs, D, McInnes, K & Rafter, T 2007, 'The impact of climate change on extreme rainfall and coastal sea levels over south-east Queensland', Div. of Marine and Atmospheric Research, Commonwealth Scientific and Industrial Research Organisation, Australia.

Al-Safi, HIJ & Sarukkalige, PR 2017, 'Assessment of future climate change impacts on hydrological behavior of Richmond River Catchment', Water Science and Engineering, vol. 10, no. 3, pp. 197-208.

Alexander, LV & Arblaster, JM 2017, 'Historical and projected trends in temperature and precipitation extremes in Australia in observations and CMIP5', Weather and Climate Extremes, vol. 15, pp. 34-56.

Allen, RG, Burnett, B, Kramber, W, Huntington, J, Kjaersgaard, J, Kilic, A, Kelly, C & Trezza, R 2013, 'Automated calibration of the METRIC-Landsat evapotranspiration process', JAWRA Journal of the American Water Resources Association, vol. 49, no. 3, pp. 563-76.

Allen, RG, Tasumi, M, Morse, A, Trezza, R, Wright, JL, Bastiaanssen, W, Kramber, W, Lorite, I & Robison, CW 2007, 'Satellite-based energy balance for mapping evapotranspiration with internalized calibration (METRIC)—Applications', Journal of Irrigation and Drainage Engineering, vol. 133, no. 4, pp. 395-406.

Armstrong, MS, Kiem, AS & Vance, TR 2020, 'Comparing instrumental, palaeoclimate, and projected rainfall data: Implications for water resources management and hydrological modelling', Journal of Hydrology: Regional Studies, vol. 31, p. 100728.

Ball, J, Babister, M, Nathan, R, Weinmann, P, Weeks, W, Retallick, M & Testoni, I 2019, Australian Rainfall and Runoff-A guide to flood estimation, Commonwealth of Australia, 1925297071, <http://arr.ga.gov.au/arr-guideline>.

Banerjee, A, Chen, R, E. Meadows, M, Singh, R, Mal, S & Sengupta, D 2020, 'An analysis of long-term rainfall trends and variability in the uttarakhand himalaya using Google Earth Engine', Remote Sensing, vol. 12, no. 4, p. 709. doi:10.3390/rs12040709.

Bastiaanssen, WG & al., e 1998, 'A remote sensing surface energy balance algorithm for land (SEBAL). 1. Formulation', Journal of Hydrology, vol. 212, pp. 198-212.

Bloschl, G & Montanari, A 2010, 'Climate change impacts—throwing the dice?', Hydrological Processes: An International Journal, vol. 24, no. 3, pp. 374-81.

Boughton, W 1993, 'A hydrograph-based model for estimating the water yield of ungauged catchments', Hydrology and Water Resources Symposium, Newcastle, IEAust, 1993.

Boughton, W 2004, 'The Australian water balance model', Environmental Modelling & Software, vol. 19, no. 10, pp. 943-56.

Boughton, W 2006, 'Calibrations of a daily rainfall-runoff model with poor quality data', Environmental Modelling & Software, vol. 21, no. 8, pp. 1114-28.

Boughton, W 2007, 'Effect of data length on rainfall–runoff modelling', Environmental Modelling & Software, vol. 22, no. 3, pp. 406-13.

Boughton, WC 1995, 'An Australian water balance model for semiarid watersheds', Journal of soil and water conservation, vol. 50, no. 5, pp. 454-7.

Briem, GJ, Benediktsson, JA & Sveinsson, JR 2002, 'Multiple classifiers applied to multisource remote sensing data', IEEE transactions on geoscience and remote sensing, vol. 40, no. 10, pp. 2291-9.

Burkey, J 2006, 'A non-parametric monotonic trend test computing Mann-Kendall Tau, Tau-b, and Sen's slope written in Mathworks-MATLAB implemented using matrix rotations', King Country, Department of Natural Resources and Parks, Science and Technical Services Section, Seattle.

Burn, DH, Sharif, M & Zhang, K 2010, 'Detection of trends in hydrological extremes for Canadian watersheds', Hydrological Processes, vol. 24, no. 13, pp. 1781-90.

Cheng, L & AghaKouchak, A 2014, 'Nonstationary precipitation intensity-duration-frequency curves for infrastructure design in a changing climate', Scientific reports, vol. 4, no. 1, pp. 1-6. DOI: 10.1038/srep07093.

Cheng, L, AghaKouchak, A, Gilleland, E & Katz, RW 2014, 'Non-stationary extreme value analysis in a changing climate', Climatic Change, vol. 127, no. 2, pp. 353-69.

Chiew, FH 2006, 'Estimation of rainfall elasticity of streamflow in Australia', Hydrological Sciences Journal, vol. 51, no. 4, pp. 613-25.

Coles, S, Bawa, J, Trenner, L & Dorazio, P 2001, An introduction to statistical modeling of extreme values, vol. 208, Springer.

Cooley, D 2009, 'Extreme value analysis and the study of climate change', Climatic Change, vol. 97, no. 1, pp. 77-83.

Cooley, D 2013, 'Return periods and return levels under climate change', in Extremes in a changing climate, In: AghaKouchak, A., Easterling, D., Hsu, K., Schubert, S., Sorooshian, S. (eds) Extremes in a Changing Climate. Water Science and Technology Library, Springer, vol. 65, pp. 97-114.

Cortes, C & Vapnik, V 1995, 'Support-vector networks', Machine learning, vol. 20, pp. 273-97.

CSIRO & BOM 2015, Climate change in Australia information for Australia's natural resource management regions: Technical report, CSIRO and Bureau of Meteorology Australia.

Cui, T, Raiber, M, Pagendam, D, Gilfedder, M & Rassam, D 2018, 'Response of groundwater level and surface-water/groundwater interaction to climate variability: Clarence-Moreton Basin, Australia', Hydrogeology journal, vol. 26, no. 2, pp. 593-614.

Da Silva, RM, Santos, CA, Moreira, M, Corte-Real, J, Silva, VC & Medeiros, IC 2015, 'Rainfall and river flow trends using Mann–Kendall and Sen's slope estimator statistical tests in the Cobres River basin', Natural Hazards, vol. 77, no. 2, pp. 1205-21.

Debele, S, Strupczewski, W & Bogdanowicz, E 2017, 'A comparison of three approaches to non-stationary flood frequency analysis', Acta Geophysica, vol. 65, no. 4, pp. 863-83.

Durocher, M, Burn, DH & Ashkar, F 2019, 'Comparison of estimation methods for a nonstationary Index-Flood Model in flood frequency analysis using peaks over threshold', Water Resources Research, vol. 55, no. 11, pp. 9398-416.

Engeland, K, Hisdal, H & Frigessi, A 2004, 'Practical extreme value modelling of hydrological floods and droughts: a case study', Extremes, vol. 7, no. 1, pp. 5-30.

Esmaeili-Gisavandani, H, Lotfirad, M, Sofla, MSD & Ashrafzadeh, A 2021, 'Improving the performance of rainfall-runoff models using the gene expression programming approach', Journal of Water and Climate Change, vol. 12, no. 7, pp. 3308-29.

Esmaeili, P, Vazifedoust, M, Rahmani, M & Pakdel, H 2023, 'A simple rule-based algorithm in Google Earth Engine for operational discrimination of rice paddies in Sefidroud Irrigation Network', Arabian Journal of Geosciences, vol. 16, no. 12, p. 649.

Foga, S, Scaramuzza, PL, Guo, S, Zhu, Z, Dilley Jr, RD, Beckmann, T, Schmidt, GL, Dwyer, JL, Hughes, MJ & Laue, B 2017, 'Cloud detection algorithm comparison and validation for operational Landsat data products', Remote Sensing of Environment, vol. 194, pp. 379-90.

Fu, G, Charles, SP & Chiew, FH 2007, 'A two-parameter climate elasticity of streamflow index to assess climate change effects on annual streamflow', Water Resources Research, vol. 43, no. 11.

Gislason, PO, Benediktsson, JA & Sveinsson, JR 2006, 'Random forests for land cover classification', Pattern recognition letters, vol. 27, no. 4, pp. 294-300.

Gonçalves, IZ, Ruhoff, A, Laipelt, L, Bispo, R, Hernandez, FBT, Neale, CMU, Teixeira, AHdC & Marin, FR 2022, 'Remote sensing-based evapotranspiration modeling using geeSEBAL for sugarcane irrigation management in Brazil', Agricultural water management, vol. 274, p. 107965.

Gorelick, N, Hancher, M, Dixon, M, Ilyushchenko, S, Thau, D & Moore, R 2017, 'Google Earth Engine: Planetary-scale geospatial analysis for everyone', Remote Sensing of Environment, vol. 202, pp. 18-27. https://doi.org/10.1016/j.rse.2017.06.031.

Gosling, SN & Arnell, NW 2011, 'Simulating current global river runoff with a global hydrological model: model revisions, validation, and sensitivity analysis', Hydrological Processes, vol. 25, no. 7, pp. 1129-45.

Gualtieri, JA & Cromp, RF 1999, 'Support vector machines for hyperspectral remote sensing classification', 27th AIPR workshop: Advances in computer-assisted recognition, SPIE, pp. 221-32.

Haddeland, I, Clark, DB, Franssen, W, Ludwig, F, Voß, F, Arnell, NW, Bertrand, N, Best, M, Folwell, S & Gerten, D 2011, 'Multimodel estimate of the global terrestrial water balance: setup and first results', Journal of hydrometeorology, vol. 12, no. 5, pp. 869-84.

Hagemann, S, Chen, C, Clark, DB, Folwell, S, Gosling, SN, Haddeland, I, Hanasaki, N, Heinke, J, Ludwig, F & Voss, F 2013, 'Climate change impact on available water resources obtained using multiple global climate and hydrology models', Earth System Dynamics, vol. 4, no. 1, pp. 129-44.

Head, L, Adams, M, McGregor, HV & Toole, S 2014, 'Climate change and Australia', Wiley Interdisciplinary Reviews: Climate Change, vol. 5, no. 2, pp. 175-97.

Huth, R, Kyselý, J & Pokorná, L 2000, 'A GCM simulation of heat waves, dry spells, and their relationships to circulation', Climatic Change, vol. 46, no. 1, pp. 29-60.

IPCC 2007, 'Climate Change 2007: Synthesis Report. Contribution of Working Groups I, II and III to the Fourth Assessment Report of the Intergovernmental Panel on Climate Change [Core Writing Team, Pachauri, R.K and Reisinger, A. (eds.)]', Cambridge University Press, Cambridge, pp 104.

IPCC 2021, 'Summary for Policymakers. In: Climate Change 2021: The Physical Science Basis. Contribution of Working Group I to the Sixth Assessment Report of the Intergovernmental Panel on Climate Change [Masson-Delmotte, V., P. Zhai, A. Pirani, S.L. Connors, C. Péan, S. Berger, N. Caud, Y. Chen, L. Goldfarb, M.I. Gomis, M. Huang, K. Leitzell, E. Lonnoy, J.B.R. Matthews, T.K. Maycock, T. Waterfield, O. Yelekçi, R. Yu, and B. Zhou (eds.)]. In Press.', IPCC: Geneva, Switzerland.

Jahandideh-Tehrani, M, Zhang, H, Helfer, F & Yu, Y 2019, 'Review of climate change impacts on predicted river streamflow in tropical rivers', Environmental monitoring and assessment, vol. 191, no. 12, pp. 1-23.

Jeffrey, SJ, Carter, JO, Moodie, KB & Beswick, AR 2001, 'Using spatial interpolation to construct a comprehensive archive of Australian climate data', Environmental Modelling & Software, vol. 16, no. 4, pp. 309-30.

Jones, B, Tebaldi, C, O'Neill, BC, Oleson, K & Gao, J 2018, 'Avoiding population exposure to heat-related extremes: demographic change vs climate change', Climatic Change, vol. 146, no. 3, pp. 423-37.

Kayser, RH, Ruhoff, A, Laipelt, L, de Mello Kich, E, Roberti, DR, de Arruda Souza, V, Rubert, GCD, Collischonn, W & Neale, CMU 2022, 'Assessing geeSEBAL automated calibration and meteorological reanalysis uncertainties to estimate evapotranspiration in subtropical humid climates', Agricultural and forest meteorology, vol. 314, p. 108775.

Kendall, M 1975, Rank correlation methods,4th ed. Charles Griffin: London, UK,.

Khaliq, MN, St-Hilaire, A, Ouarda, TB & Bobée, B 2005, 'Frequency analysis and temporal pattern of occurrences of southern Quebec heatwaves', International Journal of Climatology: A Journal of the Royal Meteorological Society, vol. 25, no. 4, pp. 485-504.

Kiem, AS, Vance, TR, Tozer, CR, Roberts, JL, Dalla Pozza, R, Vitkovsky, J, Smolders, K & Curran, MA 2020, 'Learning from the past. Using palaeoclimate data to better understand and manage drought in South East Queensland (SEQ), Australia', Journal of Hydrology: Regional Studies, vol. 29, p. 100686.

Kirono, DG, Round, V, Heady, C, Chiew, FH & Osbrough, S 2020, 'Drought projections for Australia: Updated results and analysis of model simulations', Weather and Climate Extremes, vol. 30, p. 100280.

Laipelt, L, Kayser, RHB, Fleischmann, AS, Ruhoff, A, Bastiaanssen, W, Erickson, TA & Melton, F 2021, 'Long-term monitoring of evapotranspiration using the SEBAL algorithm and Google Earth Engine cloud computing', ISPRS Journal of Photogrammetry and Remote Sensing, vol. 178, pp. 81-96.

Lamichhane, S & Shakya, NM 2019, 'Integrated assessment of climate change and land use change impacts on hydrology in the Kathmandu Valley watershed, Central Nepal', Water, vol. 11, no. 10, p. 2059.

Lockyer Creek wiki 2022, <https://en.wikipedia.org/wiki/Lockyer_Creek>>.

Love, CA, Skahill, BE, Russell, BT, Baggett, JS & AghaKouchak, A 2022, 'An Effective Trend Surface Fitting Framework for Spatial Analysis of Extreme Events', Geophysical Research Letters, vol. 49, no. 11, p. e2022GL098132.

Mann, HB 1945, 'Nonparametric tests against trend', Econometrica: Journal of the econometric society, vol. 13, pp. 245-59.

Mazdiyasni, O, Sadegh, M, Chiang, F & AghaKouchak, A 2019, 'Heat wave intensity duration frequency curve: A multivariate approach for hazard and attribution analysis', Scientific reports, vol. 9, no. 1, pp. 1-8.

Meaurio, M, Zabaleta, A, Boithias, L, Epelde, AM, Sauvage, S, Sánchez-Pérez, J-M, Srinivasan, R & Antiguedad, I 2017, 'Assessing the hydrological response from an ensemble of CMIP5 climate projections in the transition zone of the Atlantic region (Bay of Biscay)', Journal of Hydrology, vol. 548, pp. 46-62.

Mission, NSRT 2013, 'Shuttle Radar Topography Mission (SRTM) Global. Distributed by OpenTopography', URL: https://www. fdsn. org/networks/detail/GH/, doi: doi. org/10.5069/G9445JDF.

Moisello, U 2007, 'On the use of partial probability weighted moments in the analysis of hydrological extremes', Hydrological Processes: An International Journal, vol. 21, no. 10, pp. 1265-79.

Montanari, A & Koutsoyiannis, D 2014, 'Modeling and mitigating natural hazards: Stationarity is immortal!', Water Resources Research, vol. 50, no. 12, pp. 9748-56.

Morrison, JE & Smith, JA 2002, 'Stochastic modeling of flood peaks using the generalised extreme value distribution', Water Resources Research, vol. 38, no. 12, pp. 41-1--12.

Nyikadzino, B, Chitakira, M & Muchuru, S 2020, 'Rainfall and runoff trend analysis in the Limpopo river basin using the Mann Kendall statistic', Physics and Chemistry of the Earth, Parts A/B/C, vol. 117, p. 102870.

Obeysekera, J & Salas, JD 2014, 'Quantifying the uncertainty of design floods under nonstationary conditions', Journal of Hydrologic Engineering, vol. 19, no. 7, pp. 1438-46.

Ouarda, TB & Charron, C 2018, 'Nonstationary temperature-duration-frequency curves', Scientific reports, vol. 8, no. 1, pp. 1-8.

Pakdel, H, Vazifedoust, M, Paudyal, DR, Chadalavada, S & Alam, MJ 2022, 'Google Earth Engine as Multi-Sensor Open-Source Tool for Monitoring Stream Flow in the Transboundary River Basin: Doosti River Dam', ISPRS International Journal of Geo-Information, vol. 11, no. 11, p. 535.

Pakdel, H, Paudyal, DR, Chadalavada, S, Alam, MJ & Vazifedoust, M 2023, 'A Multi-Framework of Google Earth Engine and GEV for Spatial Analysis of Extremes in Non-Stationary Condition in Southeast Queensland, Australia', ISPRS International Journal of Geo-Information, vol. 12, no. 9, p. 370.

Pal, M & Mather, PM 2005, 'Support vector machines for classification in remote sensing', International Journal of Remote Sensing, vol. 26, no. 5, pp. 1007-11.

Petheram, C, Rustomji, P, McVicar, TR, Cai, W, Chiew, FH, Vleeshouwer, J, Van Niel, TG, Li, L, Cresswell, RG & Donohue, RJ 2012, 'Estimating the impact of projected climate

change on runoff across the tropical savannas and semiarid rangelands of northern Australia', Journal of hydrometeorology, vol. 13, no. 2, pp. 483-503.

Ragno, E, AghaKouchak, A, Cheng, L & Sadegh, M 2019, 'A generalized framework for process-informed nonstationary extreme value analysis', Advances in water Resources, vol. 130, pp. 270-82.

Rainham, DG & Smoyer-Tomic, KE 2003, 'The role of air pollution in the relationship between a heat stress index and human mortality in Toronto', Environmental Research, vol. 93, no. 1, pp. 9-19.

Ramezani, MR, Yu, B & Tarakemehzadeh, N 2022, 'Satellite-derived spatiotemporal data on imperviousness for improved hydrological modelling of urbanised catchments', Journal of Hydrology, vol. 612, p. 128101.

Ramezani, MR, Helfer, F & Yu, B 2023, 'Individual and combined impacts of urbanization and climate change on catchment runoff in Southeast Queensland, Australia', Science of the Total Environment, vol. 861, p. 160528.

Salas, J, Obeysekera, J & Vogel, R 2018, 'Techniques for assessing water infrastructure for nonstationary extreme events: a review', Hydrological Sciences Journal, vol. 63, no. 3, pp. 325-52. https://doi.org/10.1080/02626667.2018.1426858.

Salas, JD & Obeysekera, J 2014, 'Revisiting the concepts of return period and risk for nonstationary hydrologic extreme events', Journal of Hydrologic Engineering, vol. 19, no. 3, pp. 554-68.

Salinas, JL, Castellarin, A, Viglione, A, Kohnova, S & Kjeldsen, T 2014, 'Regional parent flood frequency distributions in Europe–Part 1: Is the GEV model suitable as a pan-European parent?', Hydrology and Earth System Sciences, vol. 18, no. 11, pp. 4381-9.

Sarker, A, Ross, H & Shrestha, KK 2008, 'A common-pool resource approach for water quality management: An Australian case study', Ecological economics, vol. 68, no. 1-2, pp. 461-71.

Strupczewski, WG, Kochanek, K, Markiewicz, I, Bogdanowicz, E, Weglarczyk, S & Singh, VP 2011, 'On the tails of distributions of annual peak flow', Hydrology Research, vol. 42, no. 2-3, pp. 171-92.

Tabari, H, Marofi, S, Aeini, A, Talaee, PH & Mohammadi, K 2011, 'Trend analysis of reference evapotranspiration in the western half of Iran', Agricultural and forest meteorology, vol. 151, no. 2, pp. 128-36. https://doi.org/10.1016/j.agrformet.2010.09.009.

Tehrani, MJ, Helfer, F & Jenkins, G 2021, 'Impacts of climate change and sea level rise on catchment management: A multi-model ensemble analysis of the Nerang River catchment, Australia', Science of the Total Environment, vol. 777, p. 146223.

Thompson, J, Green, A, Kingston, D & Gosling, S 2013, 'Assessment of uncertainty in river flow projections for the Mekong River using multiple GCMs and hydrological models', Journal of Hydrology, vol. 486, pp. 1-30.

Trewin, B 2018, The Australian Climate Observations Reference Network-Surface Air Temperature (ACORNSAT) Version 2, Bureau of Meteorology.

Van Dijk, AI, Beck, HE, Crosbie, RS, de Jeu, RA, Liu, YY, Podger, GM, Timbal, B & Viney, NR 2013, 'The Millennium Drought in southeast Australia (2001–2009): Natural and

human causes and implications for water resources, ecosystems, economy, and society', Water Resources Research, vol. 49, no. 2, pp. 1040-57.

Vance, T, Roberts, J, Plummer, C, Kiem, A & Van Ommen, T 2015, 'Interdecadal Pacific variability and eastern Australian megadroughts over the last millennium', Geophysical Research Letters, vol. 42, no. 1, pp. 129-37.

Wang, Q, Xu, Y, Wang, Y, Zhang, Y, Xiang, J, Xu, Y & Wang, J 2020, 'Individual and combined impacts of future land-use and climate conditions on extreme hydrological events in a representative basin of the Yangtze River Delta, China', Atmospheric Research, vol. 236, p. 104805.

Wasko, C, Westra, S, Nathan, R, Pepler, A, Raupach, T, Dowdy, A, Johnson, F, Ho, M, McInnes, K & Jakob, D 2023, 'A systematic review of climate change science relevant to Australian design flood estimation', Hydrology and Earth System Sciences Discussions, vol. 2023, pp. 1-48.

WetlandInfo 2022, Wetland management resources in Queensland, Department of Environment and Science, Queensland, viewed 6 March 2022, <https://wetlandinfo.des.qld.gov.au/wetlands/>.

Xie, G & Niculescu, S 2021, 'Mapping and monitoring of land cover/land use (LCLU) changes in the crozon peninsula (Brittany, France) from 2007 to 2018 by machine learning algorithms (support vector machine, random forest, and convolutional neural network) and by post-classification comparison (PCC)', Remote Sensing, vol. 13, no. 19, p. 3899.

Xu, C-y, Gong, L, Jiang, T, Chen, D & Singh, V 2006, 'Analysis of spatial distribution and temporal trend of reference evapotranspiration and pan evaporation in Changjiang (Yangtze River) catchment', Journal of Hydrology, vol. 327, no. 1-2, pp. 81-93.

Yu, B & Zhu, Z 2015, 'A comparative assessment of AWBM and SimHyd for forested watersheds', Hydrological Sciences Journal, vol. 60, no. 7-8, pp. 1200-12.

Zanaga, D, Van De Kerchove, R, Daems, D, De Keersmaecker, W, Brockmann, C, Kirches, G, Wevers, J, Cartus, O, Santoro, M & Fritz, S 2022, 'ESA WorldCover 10 m 2021 v200'.

Zolghadr-Asli, B, Bozorg-Haddad, O, Sarzaeim, P & Chu, X 2019, 'Investigating the variability of GCMs' simulations using time series analysis', Journal of Water and Climate Change, vol. 10, no. 3, pp. 449-63. doi: 10.2166/wcc.018.099.